QinetiQ

A Generic Model of 1-60 GHz Radio Propagation through Vegetation - Final Report

QINETIQ/KI/COM/CR020196/1.0

Copy ___ of 22

Cover + xvi + 134 pages
May 2002

NC Rogers, A Seville, J Richter, D Ndzi, N Savage, RFS Caldeirinha
AK Shukla, MO Al-Nuaimi, K Craig, E Vilar and J Austin

Customer Information	
Customer Reference Number	AY3880
Project Title	Propagation loss through vegetation.
Company Name	Radiocommunications Agency
Customer Contact	Dave Eden
Contract Number	AY3880/510005719
Milestone Number	9
Date Due (dd/mm/yyyy)	May 2002

This Document was produced by QinetiQ for the UK Radiocommunications Agency
Under Order/Contract reference AY3880/510005719

List of contents

List of contents iii

Authorisation vi

Record of changes vii

Abstract viii

Executive summary ix

List of Tables xi

List of Figures xii

Acronyms and Abbreviations xv

1 Introduction 1

1.1 Contractual matters 1

1.2 Purpose 1

1.3 Scope 1

1.4 Structure 1

2 Overview of Existing Vegetation Attenuation Models 2

2.1 Introduction 2

2.2 Empirical Models 2

2.3 Semi-Empirical Models 3

2.4 Theoretical (Analytical) Models 3

2.5 Depolarisation 4

2.6 Conclusions 4

3 A Generic Model of Propagation through Vegetation 5

3.1 Rationale 5

3.2 Design of Measurement to highlight individual effects 5

3.3 General structure 6

3.4 Ground Reflection model element 6

3.5 Diffraction model element 8

3.6 The RET Engine 13

3.7 Combination of model elements 31

3.8 Method of application 33
3.9 Model Validation 39
3.10 Discussion 41

4 Analysis of Wideband Measurements 46
4.1 Introduction 46
4.2 Case Studies 49
4.3 Discussion 74

5 Conclusions 78
5.1 Existing Models of 1-60GHz Propagation through Vegetation 78
5.2 The New Generic model 78
5.3 Model Performance 78
5.4 Wideband Channel Characteristics 79

6 Recommendations 80

7 Acknowledgements 81

8 References 82

A Contributions to the International Telecommunication Union (ITU-R) 86
A.1 Contents 86

B A Review of Existing Vegetation Attenuation Models 106
B.1 Background 106
B.2 Overview of Empirical Models 107
B.3 The Modified Exponential Decay Model (MED) 108
B.4 The ITU-R Model and its Derivatives 109
B.5 Semi-Empirical Models 109
B.6 Non Zero Gradient Model 110
B.7 Dual Gradient Model 110
B.8 Performance of models based on Measured Data 112
B.9 Analytical (theoretical) Modelling 113
B.10 Geometrical and Uniform Theories of Diffraction (GTD/UTD) 113
B.11 The Radiative Energy Transfer Theory 114
B.12 Full wave solutions 117
B.13 Physical Optics 117
B.14 Other Prediction Models for Vegetation Attenuation 118

B.15 Depolarisation 120
B.16 Conclusion 121
B.17 References for Section B 121

C The Measurements Database 125
C.1 Introduction 125
C.2 Format of the measurements database 125
C.3 Vegetation Geometry file format 129
C.4 Instructions for adding measurements to complement the database 130
C.5 Calculation of Signal Maxima, Minima and Noise Floor Attenuation 132

Distribution list 134

Report documentation page 135

Authorisation

Prepared by	Dr. Neil Rogers
Title	Principal Investigator
Signature	
Date	
Location	D714, QinetiQ Ltd., Malvern Technology Centre, St. Andrews Rd., Malvern, Worcs., WR14 3PS.
Authorised by	Nigel Smith
Title	Manager - Advanced Communications Technology Business Group
Signature	
Date	

Principal authors

Names	Neil C. Rogers, Anil K. Shukla
Location	QinetiQ Ltd., Malvern Technology Centre, St. Andrews Rd., Malvern, Worcs., WR14 3PS.
Names	Andy Seville, Ken Craig
Location	Rutherford Appleton Laboratory
Names	Jürgen Richter, Rafael F.S. Caldeirinha, Miqdad O. Al-Nuaimi
Location	University of Glamorgan
Names	David Ndzi, Nick Savage, Enric Vilar, John Austin
Location	University of Portsmouth

Record of changes

Issue	Date	Detail of Changes
0.a	23/01/02	Document framework and template
0.b	13/4/02	Draft of main sections (omitting Section 3 and Appendix C)
0.c	19/04/02	Draft incorporating Section 3, and Appendices B and C
0.d	1/5/02	Draft incorporating revisions following meeting with RA
0.e	10/5/02	Draft issued to RA for comments
0.f	13/5/02	Draft incorporating extra subsections at end of Section 3
1.0	31/5/02	First Issue

Abstract

This is the final report of a 15-month project to develop a generic model of 1-60 GHz narrowband radio signal attenuation in vegetation. The report provides a summary of previous modelling of millimetre-wave propagation through vegetation. The new generic model, which combines edge diffraction, ground reflection and a direct (through vegetation) signal (modelled using Radiative Energy Transfer (RET) theory) is described. RET is used to predict the attenuation *vs.* foliage depth using parameters to describe the absorption and scatter cross-section, albedo, and scatter function of the vegetation.

The generic model is based on measurements made at twelve locations in England, including eight different species of trees, both in-leaf and out-of-leaf. A wide variety of geometries were included in the measurements, including propagation through single trees, lines of trees, and dense woodland. The vegetation density and structure was characterised by computerised analysis of hemispherical-aperture photographs of the canopy, together with measurements of tree spacing, heights and leaf dimensions. A variety of antenna beamwidths, heights, and angular geometries were measured. Narrowband measurements were made between 2 and 18 GHz (at 0.5 GHz intervals) and wideband measurements (up to 120 MHz bandwidth) were made at 1.3, 2.2, 11.2, 37.5 and 61.5 GHz. The wideband measurements were made to inform the analysis process (for example, to identify multipath components). Several case studies of the wideband data have been performed.

The model is ideally suited to micro- and picocellular radio service planning, and with the aid of databases of forest dimensions, locations and tree types, the model may be used on a macrocellular scale.

Executive summary

Introduction

This is the final report of contract AY3880/510005719 between the UK Radiocommunications Agency (RA) (the customer) and a QinetiQ-led consortium comprised of QinetiQ, the Rutherford Appleton Laboratory (RAL), and the Universities of Portsmouth and Glamorgan.

Propagation algorithms that determine path loss and broadcast signal coverage are essential for planning wireless networks for cellular mobile, and for designing fixed terrestrial and satellite communication services. The demand for increased data rates and greater bandwidths has required systems to use radio frequencies in the microwave and millimetre-wave bands. Vegetation obstructing or close to the line-of-sight propagation path causes radiowave absorption, scattering, diffraction and depolarisation.

Existing propagation models (reviewed in Appendix B) contain few parameters relating to the vegetation medium, path geometry, system configuration and seasonal effects. To overcome these limiting factors and predict the attenuation of narrowband radio signals at 1-60 GHz for a full range of propagation geometries and vegetation characteristics appropriate to vegetation common in the UK, a generic model was developed. The model has been developed through a campaign of measurements, algorithm development, and preliminary wideband data analysis.

Measurements

Measurements were made at twelve locations in England, including eight species of trees, both in-leaf and out-of-leaf. A wide variety of vegetation geometries were included in the measurements, (e.g. single trees, lines of trees, and dense woodland). The vegetation density and structure was characterised by computerised analysis of hemispherical-aperture photographs of the canopy, together with measurements of tree spacing, heights and leaf dimensions. A variety of antenna beamwidths, heights, and angular geometries were also used. Narrowband measurements were made between 2 and 18 GHz (at 0.5 GHz intervals) and wideband measurements were made with 31 MHz bandwidth at 1.3, 2.0, 11.2 GHz and with 120MHz bandwidth at 2.2, 2.4, 37.5 and 61.5 GHz. A complete set of measurements, with photographs, plans and other details of the experimental arrangements is available on a CD-ROM from the Radiocommunications Agency.

The Generic Model

The generic model combines the effects of three individual propagation modes: diffraction from the side and top of the foliage, ground reflection and direct (through vegetation) propagation. The extent of the vegetation is modelled as rectangular hexahedrons (boxes). Diffraction is modelled using up to two "knife edges", in accordance with ITU-R Recommendation 526. Ground reflection is modelled according to ITU-R Rec. 527. The direct (through vegetation) ray is modelled using the theory of Radiative Energy Transfer (RET) which accounts for both scattering and absorption.

RET predicts the attenuation *vs.* foliage depth using parameters to describe the absorption and scatter cross-sections, albedo, and scatter function (phase function) of the vegetation. For this contract, these parameters have been determined empirically for each vegetation type by fitting RET curves to the measurements in an iterative manner. The database of RET parameters is presently limited to a small number of representative species and for a limited number of frequencies. RET parameters are obtained for other species and frequencies by interpolation to frequency and the vegetation characteristics (i.e. average leaf area and percentage visible sky or Leaf Area Index (LAI)).

Preliminary Wideband Measurements

The wideband measurements demonstrate the relative importance of various modes of propagation (e.g. direct, scattered, diffracted or reflected rays) and quantify the loss of coherency of the waveforms with increasing depth of vegetation. Series of 128 channel impulse responses were recorded over 4.29s periods and superposed to give the Delay Power Spectrum, from which is calculated the delay spread and the frequency correlation function from which the coherency bandwidth is calculated. Preliminary analysis shows variations with radio wavelength compared to the leaf sizes. Early indications show that when the trees were out of leaf, the attenuation due to leaf absorption was eliminated but the secondary multipath component was stronger, thus reducing the coherency bandwidth. Trees in leaf show a strong diffraction component around the canopy edges and the leaves are found to attenuate the ground reflected ray strongly. An analysis of wideband measurements from the RAL site showed that measurements that formed the basis of the current ITU-R Recommendation may have been affected by reflections from lampposts and passing vehicles.

Conclusion and Recommendations

The generic model presented in this report is ideally suited to micro- and picocellular radio service planning. With the aid of databases of forest dimensions, locations and tree types, the model may be applied on a macrocellular scale.

The key recommendations are as follows:

- Develop a wideband (>100MHz) and dynamic model of propagation in vegetation;
- Investigate vegetation-induced scatter and reflection characteristics for interference prediction;
- Establish a relationship between RET model parameters and differing UK vegetation types;
- Extend the databases to include under-represented species and higher frequencies;
- Assess the effects of depolarisation of planar radio waves in vegetation.

List of Tables

Table 3-1 Fitted values of α with frequency / species 36
Table 3-2 Fitted values of β with frequency / species 36
Table 3-3 Fitted values of albedo with frequency / species 37
Table 3-4 Fitted values of σ_τ with frequency / species 37
Table 4-1 1GHz delay spread and excess attenuation for selected foliage depths 75
Table 4-2 2GHz delay spread and excess attenuation for selected foliage depths 75
Table 4-3 11GHz delay spread and excess attenuation for selected foliage depths 76

List of Figures

Figure 3-1 Consideration of three modes of propagation through and around vegetation 5
Figure 3-2 Generic Vegetation Model Development 6
Figure 3-3 Measured height gain for line of sight signal 7
Figure 3-4 Comparison of height gain measurement with 2-ray model 7
Figure 3-5 Edge diffracted components 8
Figure 3-6 Measured attenuation as a function of height, compared with prediction at 2GHz 8
Figure 3-7 Measured attenuation as a function of height, compared with prediction at 6GHz 9
Figure 3-8 Measured attenuation as a function of height, compared with prediction at 10GHz 9
Figure 3-9 Measured attenuation as a function of height, compared with prediction at 14GHz 10
Figure 3-10 Measured attenuation as a function of height, compared with prediction at 18GHz 10
Figure 3-11 Geometry for side edge diffraction at Mound site 11
Figure 3-12 Measured attenuation as a function of vegetation depth, cf prediction at 2GHz 12
Figure 3-13 Measured attenuation as a function of vegetation depth, cf prediction at 6GHz 12
Figure 3-14 Measured attenuation as a function of vegetation depth, cf prediction at 10GHz 12
Figure 3-15 Measured attenuation as a function of vegetation depth, cf. prediction at 14GHz 13
Figure 3-16 Measured attenuation as a function of vegetation depth, cf. prediction at 18GHz 13
Figure 3-17 Scattering from a homogeneous random medium of scatterers *ds* 14
Figure 3-18 Excess attenuation due to vegetation using RET, individual contributions and sum using Equation 3-7 18
Figure 3-19 The scatter function with varying parameters α and β 20
Figure 3-20 Influence of parameter α on the RET attenuation curve 21
Figure 3-21 Influence of parameter β on the RET attenuation curve 22
Figure 3-22 Influence of albedo W on the RET attenuation curve 22
Figure 3-23 Measurement and best fit RET attenuation curve for Silver Maple at Twyning Nursery at 11 GHz in leaf 23
Figure 3-24 Measurement and best fit RET attenuation curve for Silver Maple at Twyning Nursery at 11 GHz out of leaf 24
Figure 3-25 Measurement and best fit RET attenuation curve for Common Lime at Twyning Nursery at 1.3 GHz in leaf 24
Figure 3-26 Measurement and best fit RET attenuation curve for Common Lime at Twyning Nursery at 1.3 GHz out of leaf 25
Figure 3-27 RET geometry for normal incidence ($\theta_P = 0^o$) and for small transmitter elevation 25
Figure 3-28 RET geometry for large transmitter elevation 26
Figure 3-29 Vertical excess attenuation curve for $\Delta\gamma_R = 10^o$, $\theta_P = 45^o$, $\theta_R = 45^o$ 28
Figure 3-30 Vertical excess attenuation curve for $\Delta\gamma_R = 10^o$, $\theta_P = 45^o$, $\theta_R = 90^o$ 28
Figure 3-31 Vertical excess attenuation curve for $\Delta\gamma_R = 10^o$, $\theta_P = 45^o$, $\theta_R = 0^o$ 29
Figure 3-32 Vertical excess attenuation curve for $\Delta\gamma_R = 120^o$, $\theta_P = 45^o$, $\theta_R = 45^o$ 29
Figure 3-33 Vertical excess attenuation curve for $\Delta\gamma_R = 120^o$, $\theta_P = 45^o$, $\theta_R = 90^o$ 30
Figure 3-34 Vertical excess attenuation curve for $\Delta\gamma_R = 120^o$, $\theta_P = 45^o$, $\theta_R = 0^o$ 30
Figure 3-35 Geometry for dominant ground reflection beneath a raised canopy 31
Figure 3-36 Geometry for combination of direct and ground reflected rays through a thin screen 32
Figure 3-37 Signal variability as a function of vegetation depth 33
Figure 3-38 Geometry for Top Diffracted wave 33
Figure 3-39 Geometry for edge diffracted wave 34
Figure 3-40 Geometry for ground reflected wave 35

Figure 3-41 Geometry for London Plane measurement 39
Figure 3-42 Modelled components compared with full measurement record 40
Figure 3-43 Modelled components compared with full measurement record 40
Figure 3-44 Comparison of Generic model fit to data with ITU-R Rec. 833-3 41
Figure 3-45 Received power as a function of time through 4m of Sycamore (in leaf) 42
Figure 3-46 Received power as a function of time through 42m of Sycamore (in leaf) 43
Figure 3-47 Received power as a function of time through 4m of Sycamore (out of leaf) 43
Figure 3-48 Received power as a function of time through 42m of Sycamore (out leaf) 43
Figure 3-49 Received power as a function of time through 5.2m of Silver Maple (in leaf) 44
Figure 3-50 Received power as a function of time through 41.1m of Silver Maple (in leaf) 44
Figure 3-51 Received power as a function of time through 4.9m of London Plane (in leaf) 44
Figure 3-52 Received power as a function of time through 41.7m of London Plane (in leaf) 45
Figure 4-1 Wideband 1.3GHz, 2GHz and 11.647GHz Transmitter 46
Figure 4-2 Wideband 1.3GHz, 2GHz and 11.647GHz Receiver 47
Figure 4-3 Multipath Signal Component Estimation using the SVDP Algorithm 48
Figure 4-4 (a) Example of the Evolution of Impulse Response with Time and (b) Single Snapshot of the Estimated Impulse Response at any Site 49
Figure 4-5 London Plane (a) Picture of Experimental Set-up. (b) Measurement Geometry 50
Figure 4-6 Excess attenuation as a Function of Foliage Depth (London Plane) , In-Leaf 51
Figure 4-7 Excess attenuation as a Function of Foliage Depth (London Plane), Out-of-Leaf 51
Figure 4-8 Delay Spread as a Function of Foliage Depth (London Plane), In-Leaf 52
Figure 4-9 Delay Spread as a Function of Foliage Depth (London Plane), Out-of-Leaf 53
Figure 4-10 1.3GHz London Plane In-leaf at 50.1m (foliage depth 28.7m) 54
Figure 4-11 1.3GHz London Plane Out-of-leaf at 50.1m (foliage depth 28.7m) 54
Figure 4-12 2GHz London Plane In-leaf at 50.1m (foliage depth 28.7m) 55
Figure 4-13 2GHz London Plane Out-of-leaf at 50.1m (foliage depth 28.7m) 55
Figure 4-14 11GHz London Plane In-leaf at 50.1m (foliage depth 28.7m) 56
Figure 4-15 11GHz London Plane Out-of-leaf at 50.1m (foliage depth 28.7m) 56
Figure 4-16 (a) Picture of the row of Silver Maple, (b) Measurement Geometry 57
Figure 4-17 Excess attenuation as a Function of Foliage Depth (Silver Maple), In-Leaf 58
Figure 4-18 Excess attenuation as a Function of Foliage Depth (Silver Maple), Out-of-Leaf 59
Figure 4-19 Delay Spread as a Function of Foliage Depth (Silver Maple), In-Leaf 60
Figure 4-20 Delay Spread as a Function of Foliage Depth (Silver Maple), Out-of-Leaf 60
Figure 4-21 1.3GHz Silver Maple In-Leaf at 31.7m (foliage depth 18.2m) 61
Figure 4-22 1.3GHz Silver Maple Out-of-Leaf at 31.7m (foliage depth 18.2m) 61
Figure 4-23 2GHz Silver Maple In-Leaf at 31.7m (foliage depth 18.2m) 62
Figure 4-24 2GHz Silver Maple Out-of-Leaf at 31.7m (foliage depth 18.2m) 62
Figure 4-25 11GHz Silver Maple In-Leaf at 31.7m (foliage depth 18.2m) 63
Figure 4-26 11GHz Silver Maple Out-of-Leaf at 31.7m (foliage depth 18.2m) 63
Figure 4-27 Common Lime (a) Picture of Measurement Set-up (b) Measurement Geometry 64
Figure 4-28 Excess attenuation as a Function of Foliage Depth (Common Lime), In-Leaf 65
Figure 4-29 Excess attenuation as a Function of Foliage Depth (Common Lime), Out-of-leaf 65
Figure 4-30 Delay Spread as a Function of Foliage Depth (Common Lime), In-Leaf 66
Figure 4-31 Delay Spread as a Function of Foliage Depth (Common Lime), Out-of-Leaf 66
Figure 4-32 1.3GHz Common Lime In-Leaf at 28m (foliage depth 21m) 67
Figure 4-33 1.3GHz Common Lime Out-of-Leaf at 28m (foliage depth 21m) 67
Figure 4-34 2GHz Common Lime In-Leaf at 28m (foliage depth 21m) 68
Figure 4-35 2GHz Common Lime Out-of-Leaf at 28m (foliage depth 21m) 68

Figure 4-36 11GHz Common Lime In-Leaf at 28m (foliage depth 21m) 68
Figure 4-37 11GHz Common Lime Out-of-Leaf at 28m (foliage depth 21m) 69
Figure 4-38 Fermi Avenue (a) Picture of Measurement Set-up (b) Measurement Geometry 70
Figure 4-39 Excess attenuation as a Function of Foliage Depth (Fermi Avenue) 71
Figure 4-40 Delay Spread as a Function of Foliage Depth (Fermi Avenue) 71
Figure 4-41 1.3GHz Fermi Avenue at 90.9m (foliage depth 49m) 72
Figure 4-42 2GHz Fermi Avenue at 90.9m (foliage depth 49m) 72
Figure 4-43 11GHz Fermi Avenue at 90.9m (foliage depth 49m) 73
Figure 4-44 Sycamore (a) Picture of Measurement Set-up (b) Measurement Geometry 73
Figure 4-45 Sycamore 2GHz Estimated Impulse Response (a) With Wind (b) Without Wind 74
Figure 4-46 Sycamore 11GHz Estimated Impulse Response (a) With Wind (b) Without Wind 74

Acronyms and Abbreviations

BER	Bit Error Rate
CCIR	International Radio Consultative Committee
COST	European Co-operation in the field of Scientific and Technical research
CPAR	Centre for RF Propagation and Atmospheric Research, (QinetiQ, Malvern)
DCS	Digital Cellular System
DERA	Defence Evaluation and Research Agency
DG	Dual Gradient
DPS	Delay Power Spectrum
FCF	Frequency Correlation Function
FFT	Fast Fourier Transform
FITU-R	Fitted ITU-R model (University of Glamorgan)
GIS	Geographical Information System
GSM	Groupe Spéciale Mobile
GTD	Geometrical Theory of Diffraction
ITU-R	International Telecommunication Union – Radiocommunications
LAI	Leaf Area Index
LOS	Line of Sight
MED	Modified Exponential Model
MTSRG	Microwave Telecommunications Systems Research Group (Portsmouth University)
ns	nanosecond
NZG	Non-Zero Gradient
PC	Personal Computer
PF	Phase Function
PO	Physical Optics
RA	Radiocommunications Agency
RAL	Rutherford Appleton Laboratory
Rec.	Recommendation
Rep.	Report
RET	Radiative Energy Transfer (theory)
RF	Radio Frequency
RMS	Root-Mean-Square
RP&SD	Radio Propagation and System Design (group), (University of Glamorgan)
Rx	Receiver
SAR	Synthetic Aperture Radar
SVDP	Singular Value Decomposition – Prony
TF	Transfer Function
Tx	Transmitter
UHF	Ultra-High Frequency (300-3000 MHz)
UTD	Uniform Theory of Diffraction
VHF	Very High Frequency (30-300 MHz)
VV	Vertical-to-Vertical (polarisation)
XPD	Cross Polar Discrimination

This page is intentionally blank

1 Introduction

1.1 Contractual matters

1.1.1 This Final Report forms Milestone deliverable number 9 as defined in contract number AY3880/510005719 between the UK Radiocommunications Agency (RA) (the Customer) and QinetiQ ltd. (the contractor). The contractor previously traded under the name DERA (Defence Evaluation and Research Agency).

1.1.2 QinetiQ placed sub-contracts with the Rutherford Appleton Laboratory (RAL), and the Universities of Glamorgan and Portsmouth. QinetiQ and the sub-contracting institutions contributed to the project in approximately equal measure, operating as a consortium.

1.2 Purpose

1.2.1 The aim of the research presented in this report was to study the effects of millimetre wavelength radiowaves propagating through vegetation and to develop a generic model of signal attenuation for narrowband systems. This was achieved through a combination of an extensive measurement campaign and deterministic modelling.

1.3 Scope

1.3.1 This report describes the generic model of narrowband attenuation of 1-60GHz radio propagation through vegetation. Case studies of wideband measurements are presented but wideband characteristics do not form part of the generic model. Appendices to this report contain ITU-R recommendations resulting from the research and a literature review of previous related research. The database of measurements is described in an appendix and this database is available separately upon request from the RA.

1.4 Structure

1.4.1 Section 2 serves as an introduction to the topic of radio propagation through vegetation and provides an overview of this subject. The generic model of narrowband attenuation of 1-60GHz signals through vegetation is presented in Section 3. Section 4 presents a detailed analysis of the wideband characteristics of the channel on a case-by-case basis. The report ends with conclusions and recommendations.

1.4.2 Suggestions for changes and additions to the ITU-R recommendations are summarised in Appendix A and a review of literature pertaining to millimetric radio propagation through vegetation is presented in Appendix B. Appendix C provides a full description of the database of experimental measurements database produced during this research, together with instructions for adding additional measurements to the database.

2 Overview of Existing Vegetation Attenuation Models

2.1 Introduction

2.1.1 Wireless links are revolutionising personal and telecommunication services with overall growth in cellular mobile, fixed terrestrial and satellite communication markets. Increased capacities and wider bandwidths require system designers to consider frequencies at higher bands e.g. microwave and millimetric frequencies.

2.1.2 The larger number of users, especially mobile users, has resulted in network planners increasing system capacity by locating transmission antennas at heights lower than surrounding trees and buildings [Graham, 1998]. Propagation algorithms that determine path loss and signal coverage are critical for successful wireless network planning and deployment.

2.1.3 Trees singly or in a group can be found in cells of land mobile systems as well as in fixed access systems. The trees act as obstacles in the radio path causing both absorption and scatter of radio signals. The scattering and absorption need to be accounted for in radio planning tools to improve their accuracy, with improved co-ordination of radio links and optimum use of the radio spectrum.

2.1.4 Analytical studies based on experimental measurements [Caldeirinha, 2001a] showed that the effects of trees singly or as a group in the radio path of a point-to-point link influenced the received signal level as follows:

i) Directly by providing an additional (excess) attenuation to that of free space;

ii) Indirectly by scattering which resulted in lateral contributions to the received signal;

iii) Through depolarisation of the incident wave. This represented another significant factor in frequency reuse planning and spectrum utilisation [Al-Nuaimi, Hammoudeh,1994a], [Al-Nuaimi, Stephens,1998], [Al-Nuaimi, Hammoudeh, 1993a].

2.1.5 Propagation effects on terrestrial communication systems in the microwave and millimetre wave frequency bands have been investigated in recent years. Measurements available in the literature up to 1982 are summarised in Weissberger's report [Weissberger, 1982], which covers both prediction models and measurement data, reviews fifty reports, journal articles and texts.

2.1.6 Empirical, semi-empirical and analytical models are available in the literature, mainly aimed at characterising the effects of vegetation on propagation and the prediction of excess attenuation. These models are outlined here with a more detailed description given in Appendix B.

2.2 Empirical Models

2.2.1 The main advantage of these models lies in the simplicity of the mathematical expressions, describing them, leading to their straightforward application. They have however many drawbacks, not least of which are their strict dependence on specific measured data and their

failure to relate to the physical processes involved. Dependence on parameters for these models, e.g. frequency, incident angles and path length through vegetation, is usually determined through regression curves fitted to measured data.

2.2.2 Within this category of models, the following are found in the literature: The Modified Exponential Model (MED) [Weissberger, 1982]**,** the ITU-R Model [Stephens, 1998] and its Derivatives, the COST 235 [COST 235, 1996] and the Fitted ITU-R.

2.3 Semi-Empirical Models

2.3.1 These modes are usually simple to apply. They were formulated [Seville, 1997], [Paulsen, Seville, 2000] to give best fits to measured data. Although they do not consider the physical processes underlying propagation in vegetation, they are based on knowledge of the qualitative behaviour of absorption and scatter in homogenous scattering media. These models are relatively new and have been formulated using measured data mostly obtained recently. Two models are included here:

i. The Non Zero Gradient (NZG) Model;
ii. the Dual Gradient (DG) Model.

2.3.2 The DG Model considers the specific geometry and includes a parameter referred to as the illumination width. This gives a measure of the common volume of vegetation contained by the beam widths of the transmit and receive antennas. One of the drawbacks of the DG model lies in the inclusion of an inverse relationship between excess attenuation and the signal frequency. This appears to contradict other models as well as the observed behaviour of measured attenuation data.

2.4 Theoretical (Analytical) Models

2.4.1 In contrast to the above models, analytical models offer an insight into the physical processes involved in radiowave propagation through vegetation. However they invariably require the use of numerical analysis methods to provide solutions to the intractable mathematical formulations [Caldeirinha, Al-Nuaimi, 2000]. Under this category, we have included

i. Geometrical and Uniform Theory of Diffraction (GTD/UTD) [Matschek, Linot, 1999], [Li, Yeo, 1998], [Sachs, Wyatt, 1968], [Tamir, 1967];
ii. The Radiative Energy Transfer Theory (RET) [Al-Nuaimi, Hammoudeh, 1994a], [Johnson, Schwering, 1985], [Ishimaru, 1978];
iii. Full Wave Solutions [Ishimaru, 1978], [Schwering, Espeland, 1988], [Al-Nuaimi, Hammoudeh, 1994b], [Hiu, Sarabandi, 2000], [Didascalu et al, 2000];
iv. Physical Optics [Torrico, Betroni,1998].

2.4.2 Out of these, the RET has been found to offer a highly effective vegetation attenuation and scatter model which can be applied in a variety of radio path geometries and frequencies above 1GHz. The RET model requires, relatively speaking, a few parameters which can be determined from measurements. The model itself requires the evaluation and solution of a number of equations, which, when compared to those involved in empirical models, appear

to be quite complex. However because the RET considers the physical processes involved in propagation through vegetation, solutions obtained from the model are expected to yield more accurate results for the attenuation and scatter components of the propagating signal.

2.5 Depolarisation

2.5.1 Depolarisation of the incident signal arises when it encounters a scattering medium such as vegetation. Models are available for predicting depolarisation from backscattered signals such as those encountered in remote sensing. However little research on the prediction of a signal depolarised as a result of passing through a volume of vegetation, has been reported in the literature. Caldeirinha [Caldeirinha, 2001] showed that a re-radiated signal from a single tree was strongly influenced by depolarisation even in the direction of propagation of the incident wave. The extent of depolarisation depends strongly on wavelength and the tree structure. The change in the polarisation state reported in [Caldeirinha, 2001a], was shown to vary from a well defined elliptical polarisation, in the forward region to random (almost total depolarisation) in back and side scattering regions. In the latter regions, the cross polar component shows considerable enhancement relative to its level in free space. Enhancement of the cross polar component is also significant in the forward region, which is accompanied by a consequent reduction in the co-polar component. As a result, considerable reduction in cross polar discrimination (XPD), occurs.

2.6 Conclusions

2.6.1 Prediction models which estimate the excess attenuation due to vegetation are critical to mobile and terrestrial radio service providers for not only planning radio networks but also for optimising spectrum utilisation by accurately predicting cell coverage, and minimising intercell interference.

2.6.2 A number of propagation prediction models are available and these have been summarised in this section. Further details are included in Appendix B. The models can be used to provide estimates of the excess attenuation at specified frequency bands. The models, although simple, contain few parameters relating to the vegetation medium, path geometry and seasonal effects on the radio system performance.

2.6.3 Disadvantages of these models stem from their limited applicability because in their formulation and validation, they were based on a limited number of site geometries and relatively few measurements.

2.6.4 The applicability of the models may be extended through consideration of further measurements carried out for a variety of vegetation media, path geometries and frequencies. A generic attenuation model with appropriate parameters, based on knowledge and understanding of the propagation modes arising in vegetation, is clearly both valuable and necessary for radio system planning.

3 A Generic Model of Propagation through Vegetation

3.1 Rationale

3.1.1 This project concentrated on the results of previous work [ITU-R], which suggested that there are several possible mechanisms of propagation associated with vegetation. A series of measurements were made to resolve individual propagation modes through, around and underneath the vegetation foliage, as depicted in Figure 3-1.

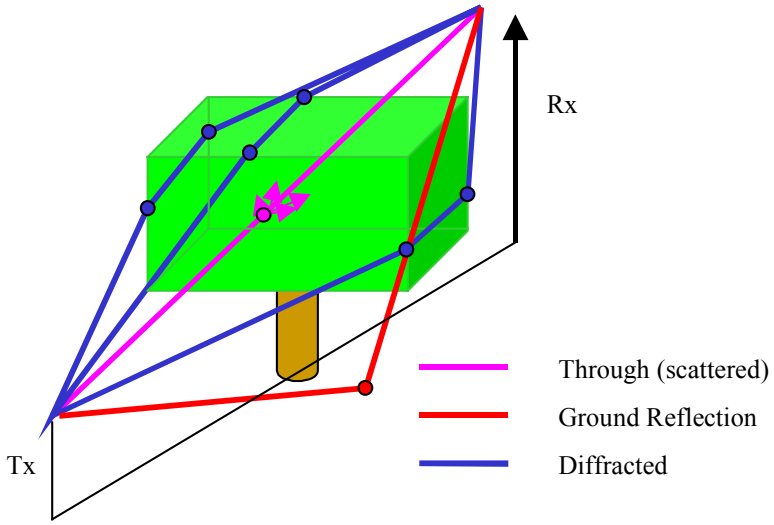

Figure 3-1 Consideration of three modes of propagation through and around vegetation

3.1.2 Where possible, each component was to be modelled using simple method, such that the final model could be easily implemented. The scattered component was modelled using the theory of Radiative Energy Transfer, as this is a fully deterministic model which may be used by fitting the model parameters to the specific measurement geometries and then expanded to provide results for more generic cases.

3.2 Design of Measurement to highlight individual effects

3.2.1 Measurements of the top-diffracted and ground-reflected components were made by varying the receiver height, for various depths of vegetation. Comparisons were then made between predictions of the diffracted and ground reflected components for the given measurement geometry and the actual attenuation measured.

3.2.2 The predicted edge diffracted attenuation was also compared with the measured attenuation, in order to determine in which locations the measured signal was limited by an edge-diffracted component.

3.2.3 The requirements of RET in terms of parameter fitting were a series of measurements:

a. As a function of depth through the vegetation, for several frequencies and species.
b. Phase function measurements, to determine the nature of the scatter function of the vegetation at each frequency and for several tree species.

3.2.4 The general rationale for the development of the generic vegetation model is depicted in Figure 3-2.

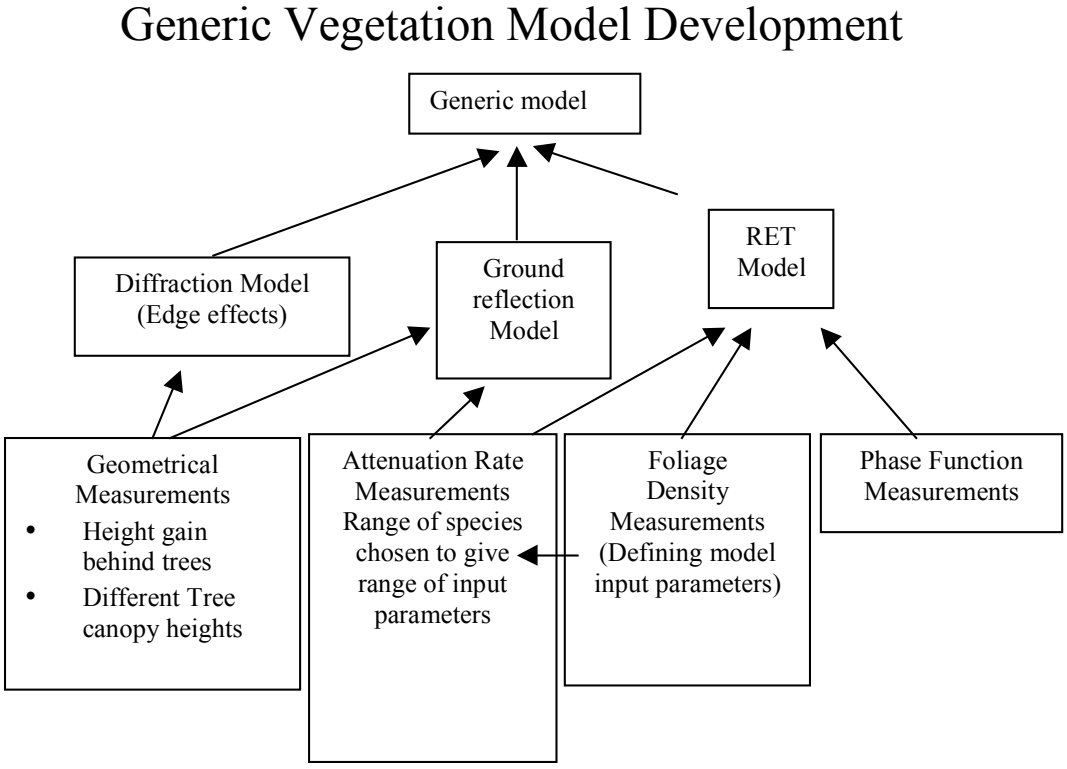

Figure 3-2 Generic Vegetation Model Development

3.3 General structure

3.3.1 The following sections (3.4 - 3.6) cover the development of the appropriate model for each of these mechanisms: the ground reflected mode, the edge-diffracted mode and the through vegetation or scattered mode. Section 3.7 discusses the arguments for the method of combination for each of these components. The method of application is presented in section 3.8 as a series of steps used to predict the total attenuation experienced by a signal propagating through / around / under a volume of vegetation. Section 3.9 reports on the testings of the model. Section 3.10 gives a discussion of the model limitations and recommendations for future work.

3.4 Ground Reflection model element

3.4.1 Several measurements were made for the case of a group of Sycamore trees (*Acer pseudoplatanus L.*) illuminated from a wide beamwidth antenna at a distance of 100m or so, over a frequency range from 2-18GHz. The receive antenna was raised from a height of 5m above the local ground level in 2m steps to a maximum height of 19m. The height of the trees was roughly 17m, and these measurements were made for several depths of vegetation. Figure 3-3 shows the measured attenuation for several frequencies, as a function of the receiver height, for the case of the receiver being placed in clear view of the transmitter.

3.4.2 One can see that the measured signal varies dramatically with height. This is due to the interference between the direct ray from transmitter to receiver, and that reflected by the earth's surface.

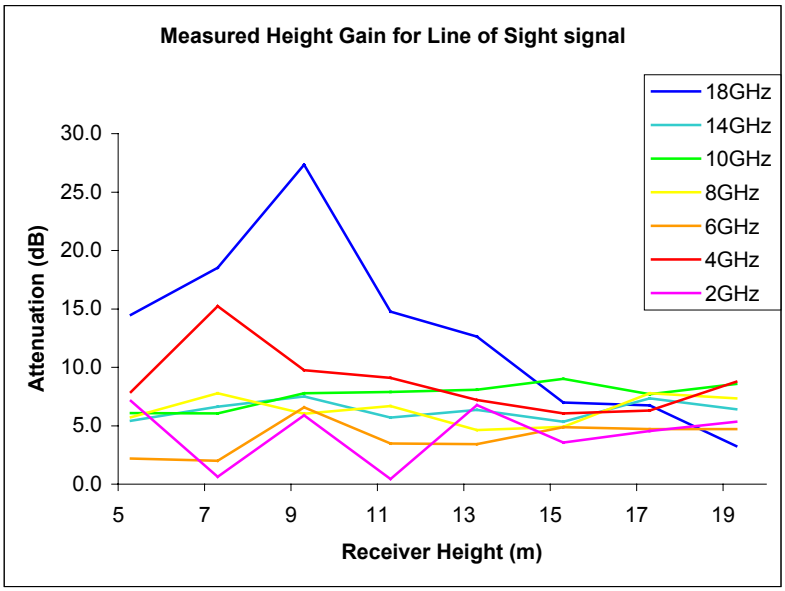

Figure 3-3 Measured height gain for line of sight signal

3.4.3 Comparison of measurements with a 2-Ray model

3.4.3.1 The measurement for the case of the receiver in a clear line of sight position showed a significant variability with receiver height. This is shown in Figure 3-4 compared with the attenuation predicted using a 2-Ray model.

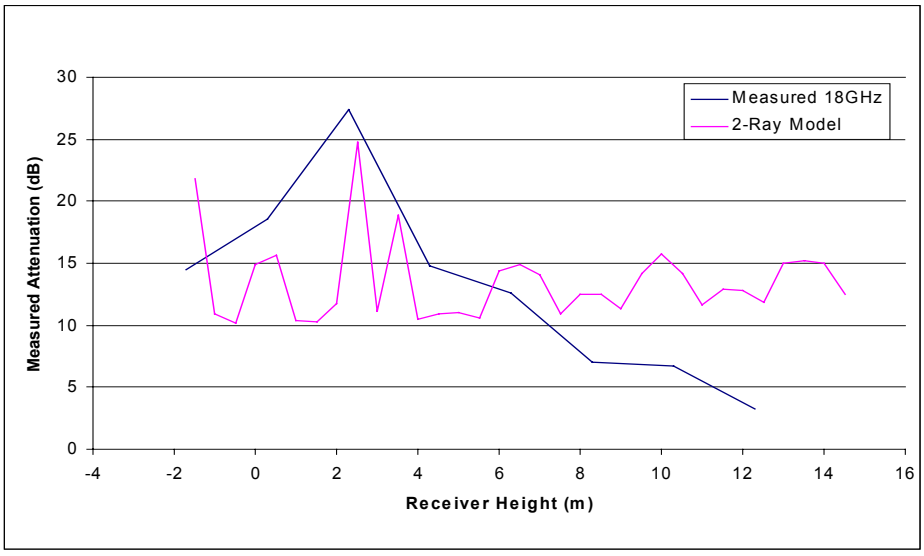

Figure 3-4 Comparison of height gain measurement with 2-ray model

3.4.4 The reflected signal was modelled by a complex summation of a direct and a ground reflected wave. The relative phase of the two waves was determined by the total path length difference. The complex reflection coefficient was obtained using the formulae given in CCIR Rep. 1008-1 with values of the permittivity and conductance assumed to be those of medium dry ground as plotted in ITU-R Rec. 527. The model does not precisely locate the peak in height, and this may be due to the fact that the relative position of the ground and receivers have not been modelled precisely enough. However, the model does approximate the range of signal attenuation variability, which indicates the ratio of the two ray amplitudes is of the right order.

3.5 Diffraction model element

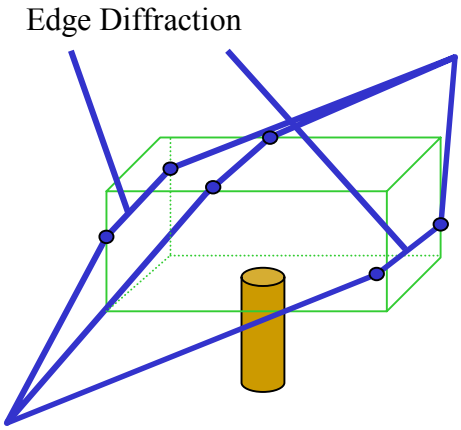

Figure 3-5 Edge diffracted components

3.5.1 Comparison of ITU-R Rec. 526 prediction with measurements for top edge diffraction

3.5.1.1 A comparison of the measured attenuation as a function of height was made with the predicted diffracted component, using the method outlined in ITU-R Recommendation 526, for double isolated knife-edges. Figure 3-6 - Figure 3-10 show the results of these comparisons for 5 different frequencies, with the measured values for different vegetation depths plotted as single points, and the diffraction loss due to propagation over the treetops (predicted by ITU-R Rec. 526) plotted as a series of lines. Each series is plotted in a different colour corresponding to the depth of the vegetation in metres.

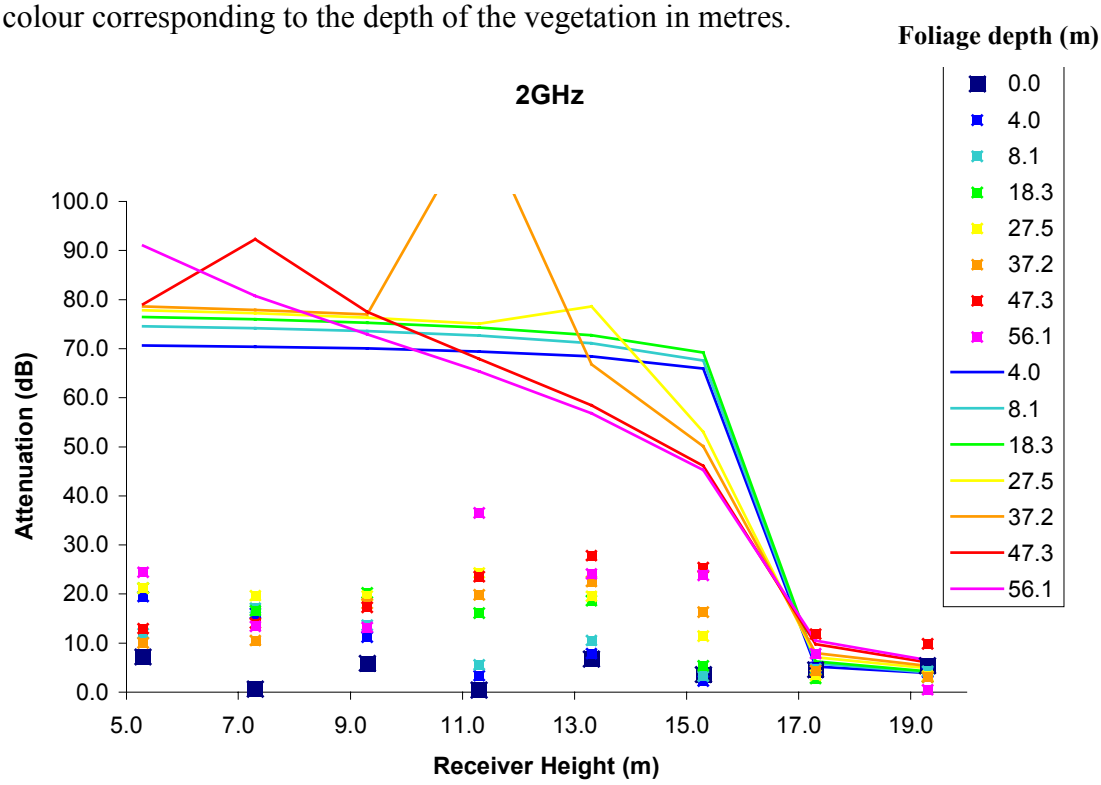

Figure 3-6 Measured attenuation as a function of height, compared with prediction at 2GHz

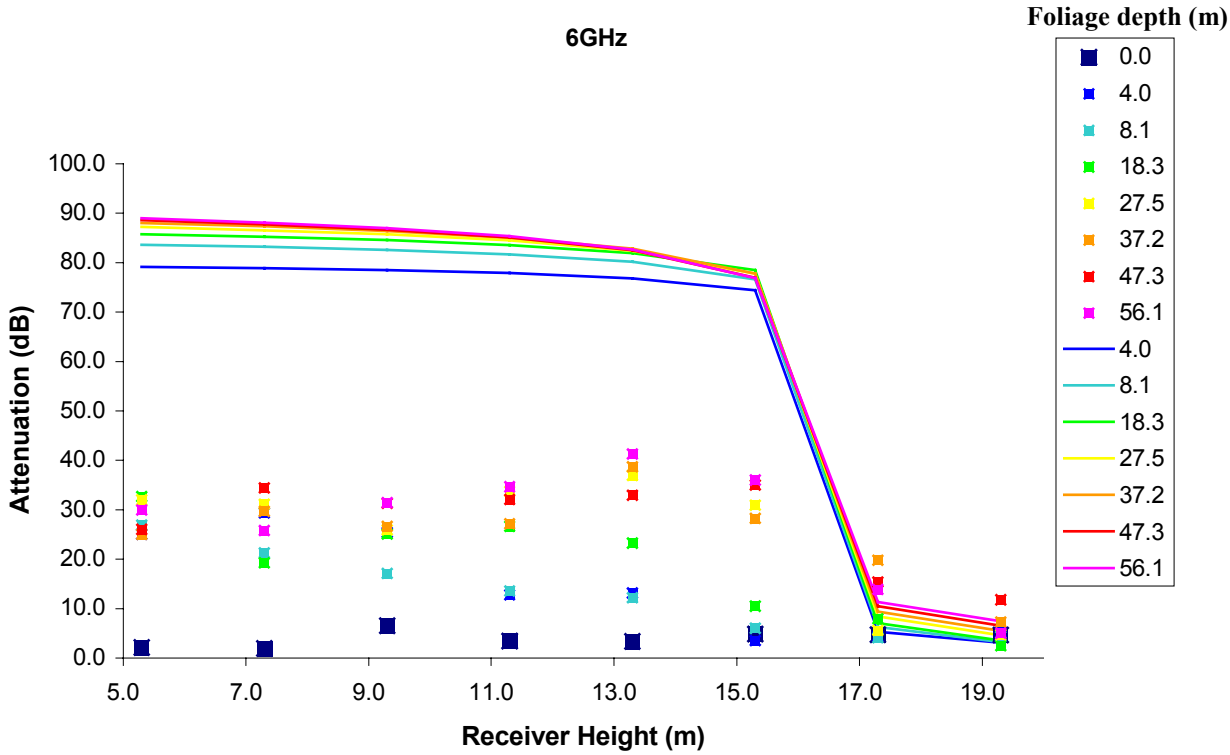

Figure 3-7 Measured attenuation as a function of height, compared with prediction at 6GHz

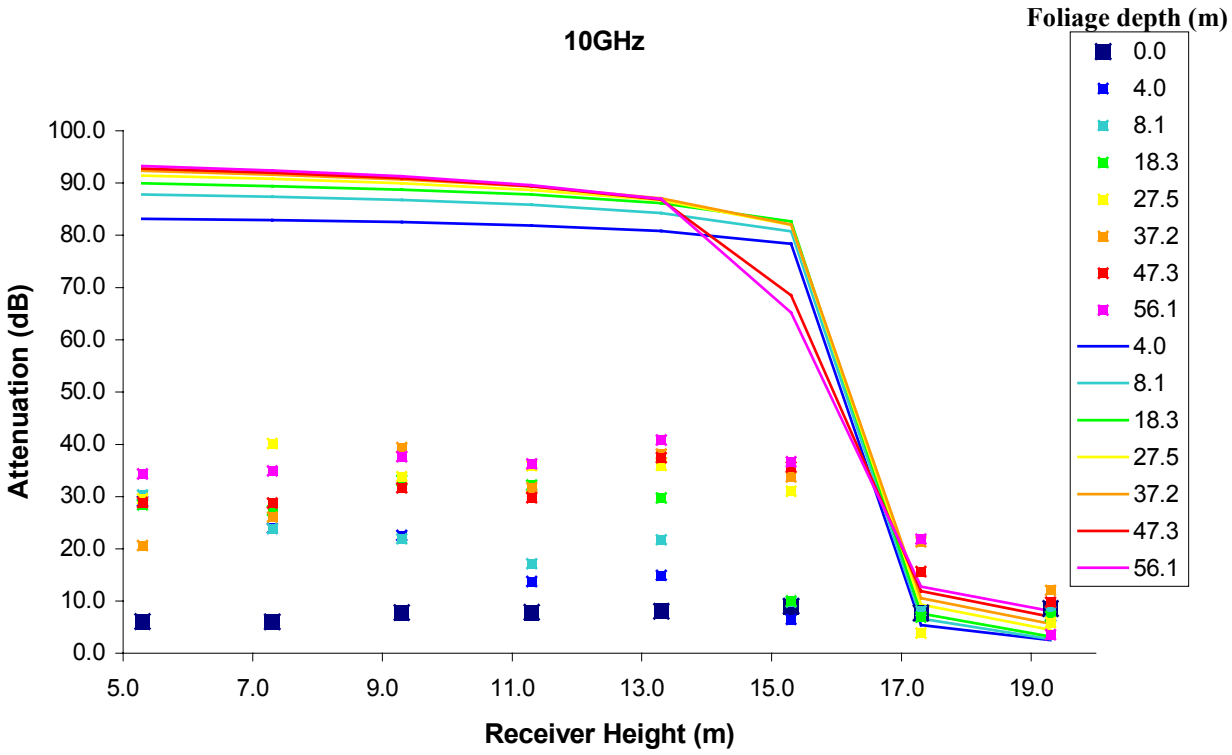

Figure 3-8 Measured attenuation as a function of height, compared with prediction at 10GHz

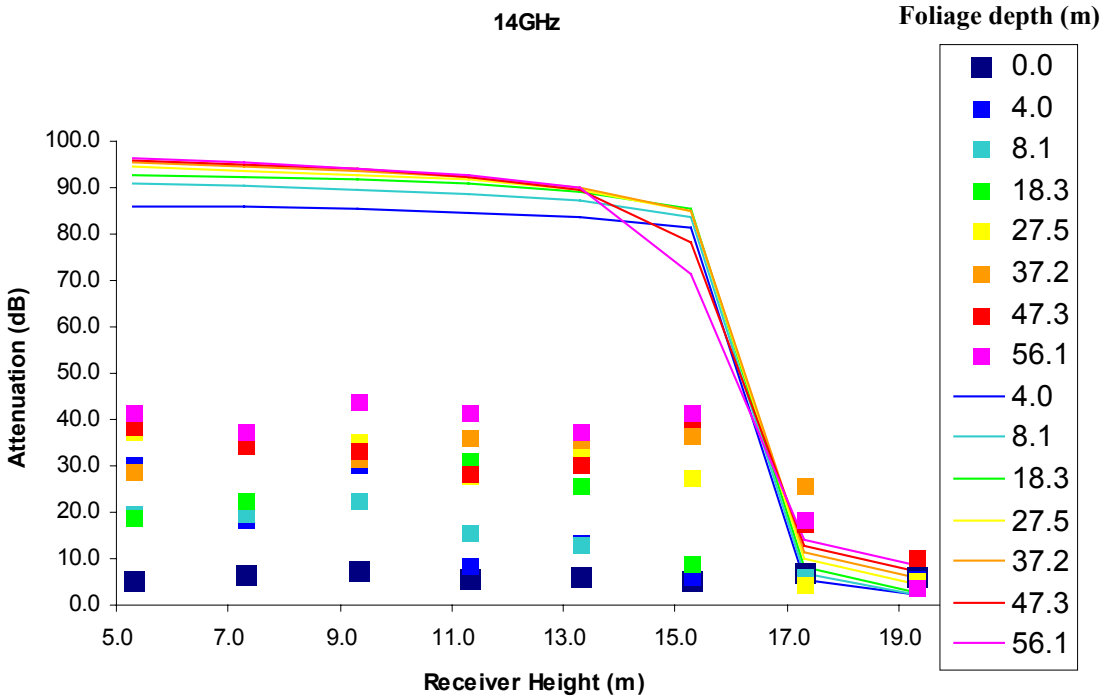

Figure 3-9 Measured attenuation as a function of height, compared with prediction at 14GHz

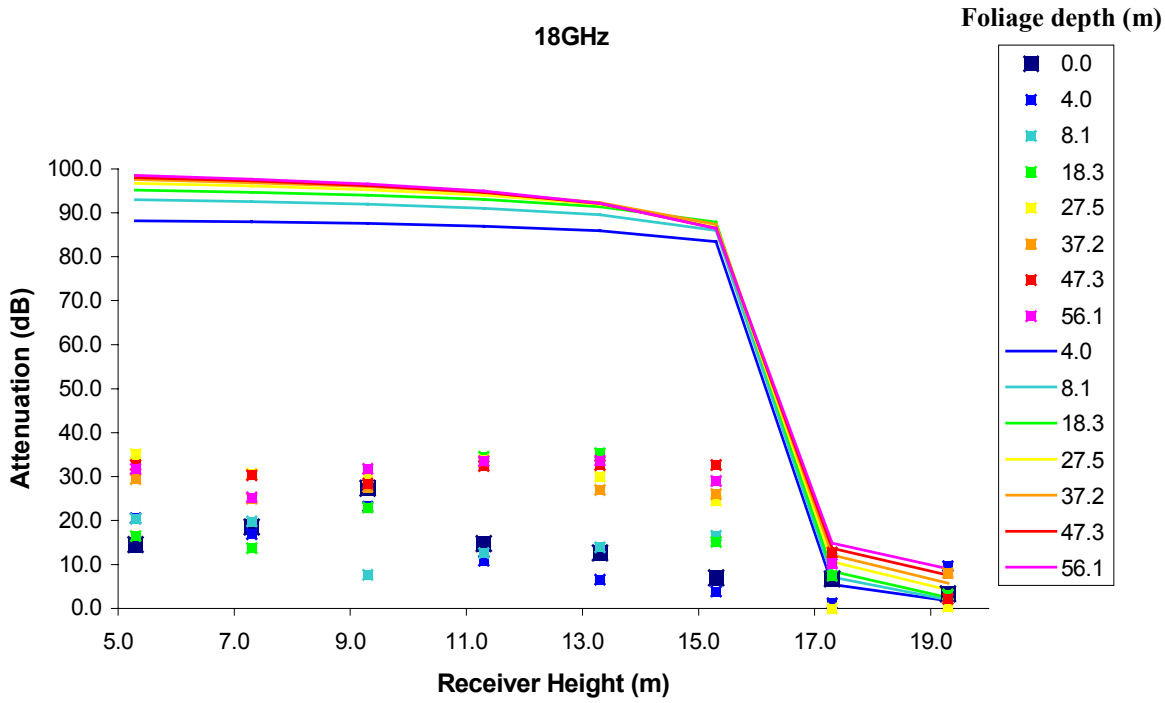

Figure 3-10 Measured attenuation as a function of height, compared with prediction at 18GHz

3.5.1.2 One can see that the predicted values are all much greater than the measured values for all but the receiver heights which the path cleared the tree tops (and was therefore line of sight). This would suggest that at the lower receiver heights, the measured attenuation could not be due to the top-diffracted component.

3.5.2 Comparison of ITU-R Rec. 526 prediction with measurements for side edge diffraction

3.5.2.1 A similar comparison was made with the predicted edge-diffracted for the measurements made at various vegetation depths. The geometry for these measurements is shown in Figure 3-11, along with the assumed diffraction angles.

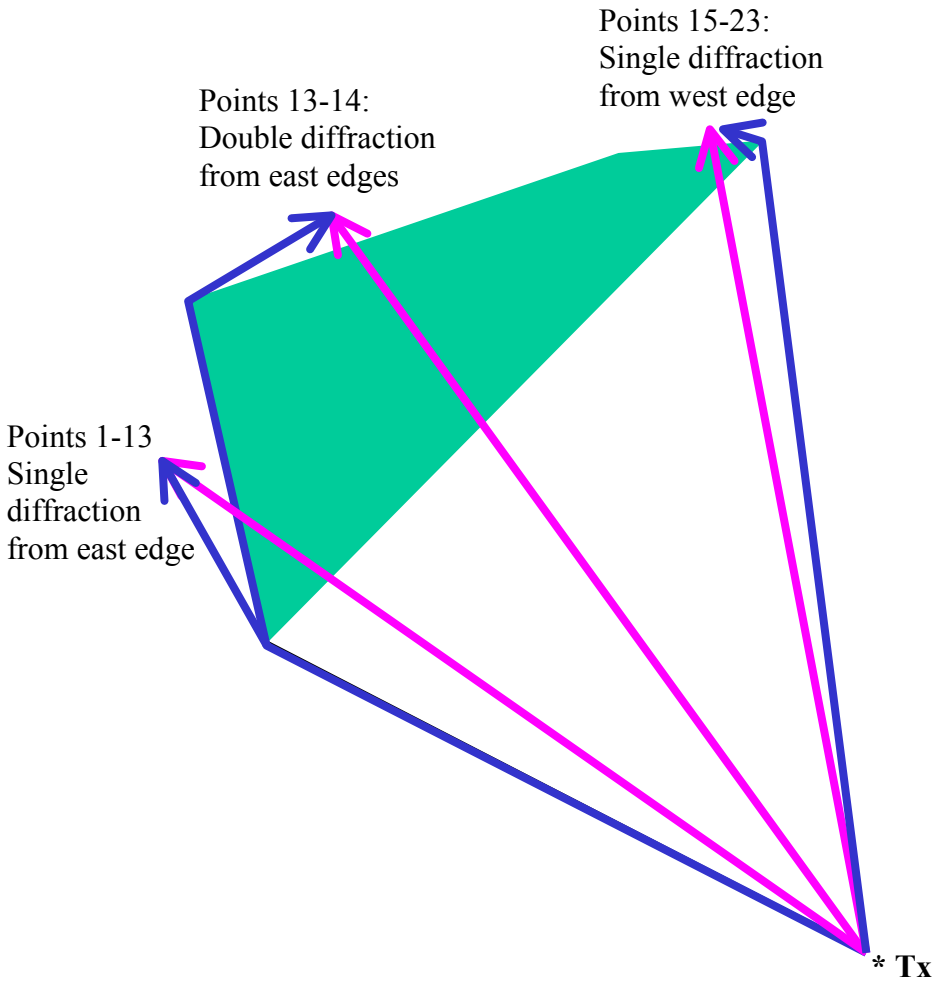

Figure 3-11 Geometry for side edge diffraction at Mound site

3.5.2.2 The measured vegetation attenuation at each height is plotted as a function of vegetation depth in Figure 3-12 - Figure 3-16, for the first eight measurement locations. Each solid line represents the measured attenuation for a given receiver height given in the plot legend (in metres above the local ground level). Also plotted as a dashed line is the predicted diffraction loss for the case of a single knife-edge diffraction point assumed to be at the eastern tip of the vegetation.

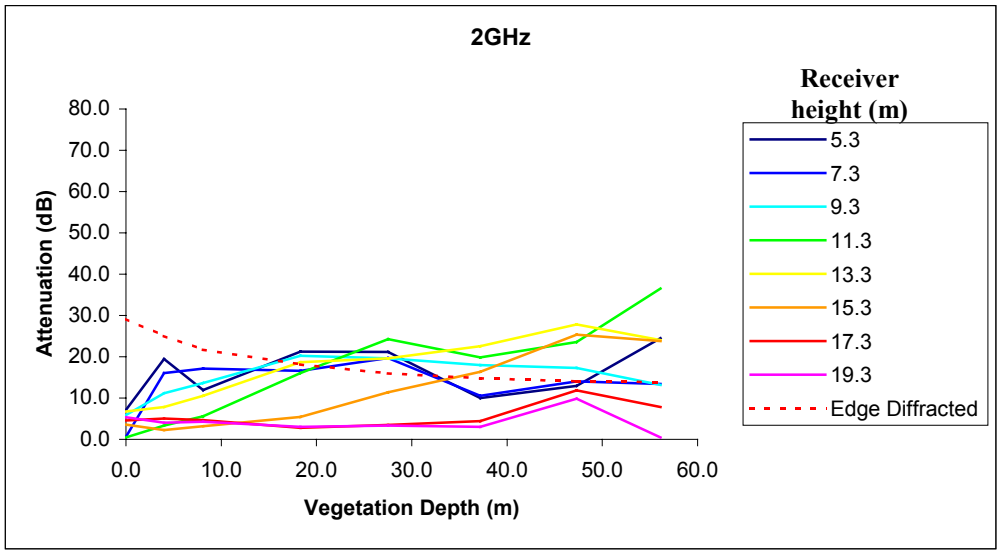

Figure 3-12 Measured attenuation as a function of vegetation depth, cf prediction at 2GHz

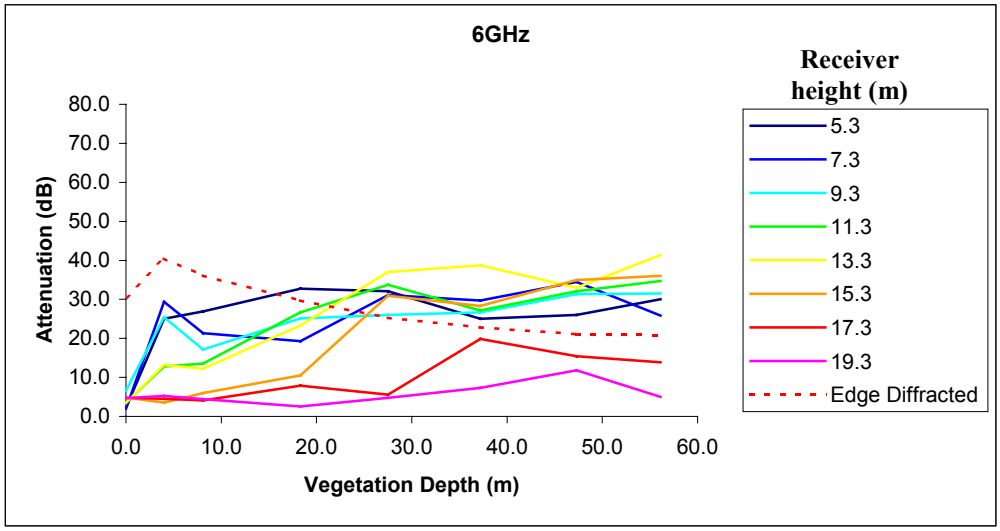

Figure 3-13 Measured attenuation as a function of vegetation depth, cf prediction at 6GHz

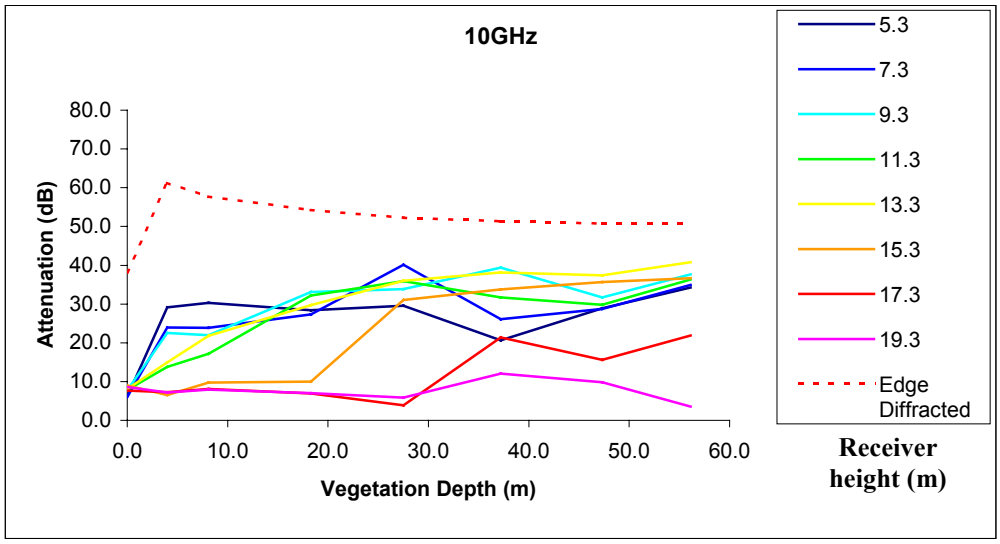

Figure 3-14 Measured attenuation as a function of vegetation depth, cf prediction at 10GHz

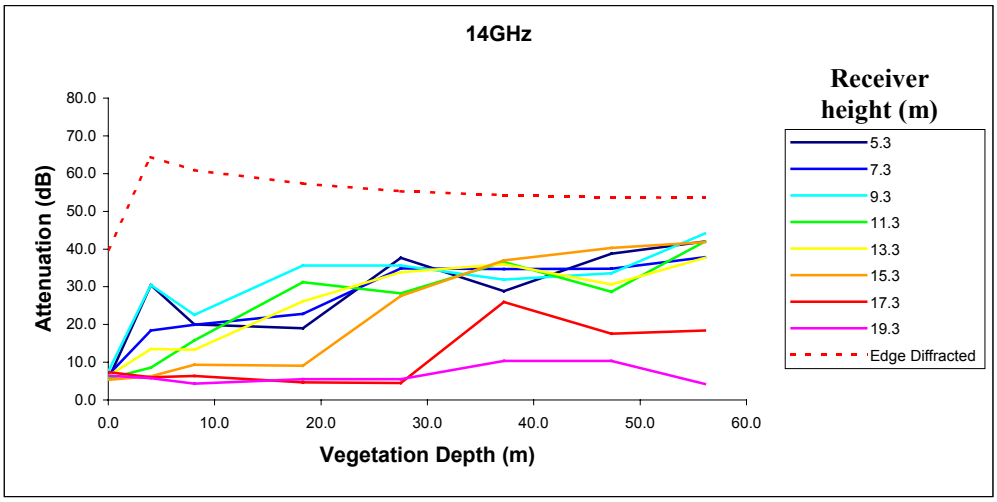

Figure 3-15 Measured attenuation as a function of vegetation depth, cf. prediction at 14GHz

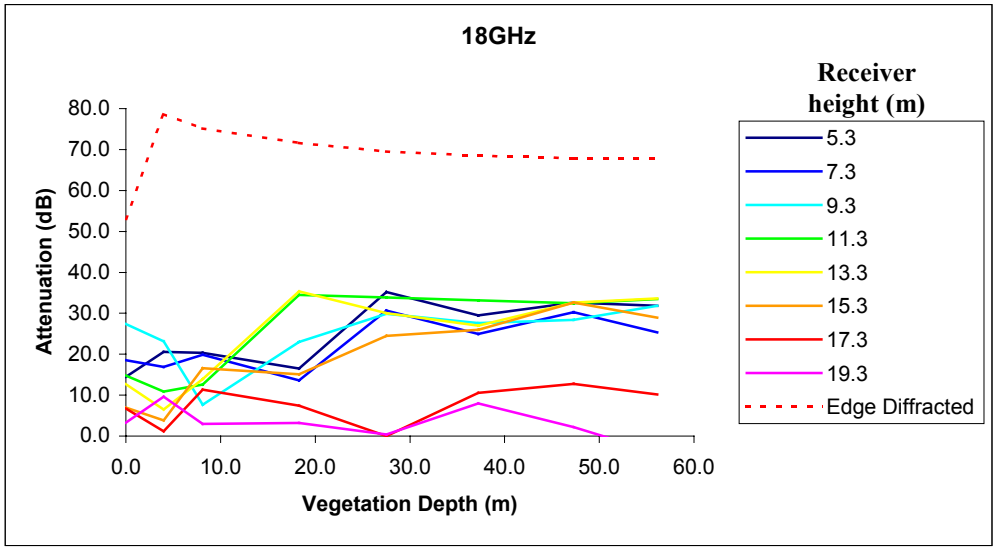

Figure 3-16 Measured attenuation as a function of vegetation depth, cf. prediction at 18GHz

3.5.2.3 One can see that for the lower frequencies, the predicted diffraction loss falls below the level of the measured attenuation, which suggests that for these locations and frequencies, the measured attenuation may be limited by the diffracted component.

3.6 The RET Engine

3.6.1.1 The RET engine utilises the Radiative Energy Transfer Theory [Johnson, Schwering, 1985] to estimate the attenuation and scatter of vegetation on radiowave propagation. The RET equation requires four input parameters to calculate the excess vegetation attenuation and scatter at a given vegetation depth. These parameters vary according to plant species, leaf size and foliage density, foliation state and radiowave frequency. The parameters have to be determined experimentally in the first instance. Where trends emerge from these measurements it will be possible to interpolate for instance over a frequency range not specifically covered in the initial experiments or make prediction about changes in the RET parameters with season. The RET parameters utilised in the RET program have been derived using the excess attenuation curves as functions of vegetation depth. These curves

should be understood as forming an initial representative cross-section database of commonly encountered plant species. It is intended that this database will be expanded, as more measurement data becomes available.

3.6.1.2 Sections 3.6.2 - 3.6.4 summarise the main steps of the theoretical derivation of the RET model and its parameters as detailed in [Johnson, Schwering, 1985].

3.6.1.3 Section 3.6.5 - 3.6.8 describes how the RET parameters presented in this project have been derived by an iterative curve fitting process from the experimental program data.

3.6.1.4 Section 3.8.4 outlines how to implement the RET engine.

3.6.2 The Radiative Energy Transfer Theory

3.6.2.1 The RET models the vegetation medium as a statistically homogeneous random medium of scatterers ds which is characterised by the absorption cross section per unit volume σ_a, the scatter cross-section per unit volume σ_s and the scatter function of the medium $p(\hat{s},\hat{s}')$. As shown in [Johnson, Schwering, 1985] the model considers a plane wave incident from an air half space upon the planar interface of a vegetation half space. The basic equation of the Radiative Energy Transfer theory is expressed in terms of the specific intensity I and is given in Equation 3-1.

$$s.\nabla I(\hat{r},\hat{s}) + (\sigma_A + \sigma_s) I(\hat{r},\hat{s}) = \frac{\sigma_s}{4\pi} \int_{4\pi} p(\hat{s},\hat{s}') I(\hat{r},\hat{s}') d\Omega' \qquad \textit{Equation 3-1}$$

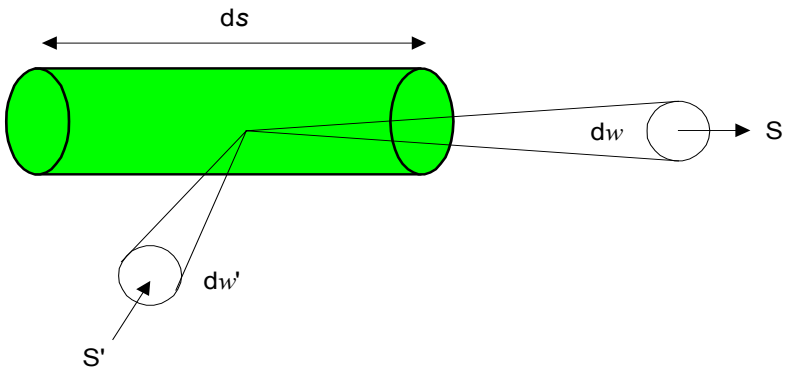

Figure 3-17 Scattering from a homogeneous random medium of scatterers ds

3.6.2.2 Each scatterer is assumed to have a directional scatter profile, or phase function. As the constituents of the tree are large relative to the wavelength at micro- and millimetre wave frequencies, the scatter function is assumed to consist of a strongly scattering forward lobe, which can be assumed to be Gaussian of width, β, with an isotropic background level. The forward lobe takes the form in Equation 3-2,

$$f(\theta) = \left(\frac{2}{\beta}\right)^2 e^{-(\theta/\beta)^2} \qquad \textit{Equation 3-2}$$

where $\theta = \cos^{-1}(\hat{s},\hat{s}')$ and β is the beamwidth of the forward lobe.

3.6.2.3 The scattering pattern is given by Equation 3-3, where α is the ratio of the forward scattered power to the total scattered power. The behaviour of the scattering pattern with varying α and β is discussed in Section 3.6.7.

$$p(\theta) = \alpha f(\theta) + (1 - \alpha) \qquad \textit{Equation 3-3}$$

3.6.2.4 The parameters σ_a, σ_s, α and β are specific to a vegetation medium and may be estimated for the medium under study by comparison of experimental and predicted results [Al-Nuaimi, Stephens, 1994a], [Stephens, Al-Nuaimi, 1995]. The relative magnitudes of σ_a and σ_s are described in terms of the albedo W which is given in Equation 3-4.

$$W = \frac{\sigma_s}{(\sigma_s + \sigma_a)} \qquad \textit{Equation 3-4}$$

3.6.3 Solution for the Transport Equation

3.6.3.1 For the solution of the transport equation (Equation 3-1) the specific intensity at a given point within the vegetation medium, I , is divided into two parts:

$$I(z,\theta) = I_{ri}(z,\theta) + I_d(z,\theta) \qquad \textit{Equation 3-5}$$

where z is the distance into the medium

3.6.3.2 This represents the sum of a coherent component, I_{ri} , which is reduced in intensity due to absorption and scatter of the incident wave, and an incoherent (diffuse) component, I_d, due to the scattered wave. It is also convenient to split I_d into two parts: I_1 and I_2. I_1 is determined primarily by the forward lobe of the scatter function and I_2 by scattering into the isotropic background, so that:

$$I = I_{ri} + I_1 + I_2 \qquad \textit{Equation 3-6}$$

3.6.3.3 The resulting equation simplifies considerably for normal incidence of the direction of propagation of the incident signal to the air-vegetation interface and for aligned transmitter and receiver antennas. Furthermore, considering the radiation pattern of the receiver antenna the resulting equation for the excess attenuation due to vegetation is given by:

$$\frac{P_R}{P_{\max}} = e^{-\tau} \qquad (I_{ri})$$

$$\left.\begin{aligned} &+\frac{\Delta\gamma_R^2}{4}\cdot\{[e^{-\hat{\tau}} - e^{-\tau}]\cdot\overline{q}_M \\ &+e^{-\tau}\cdot\sum_{m=1}^{M}\frac{1}{m!}(\alpha W\tau)^m\ [\overline{q}_m - \overline{q}_M]\} \end{aligned}\right\} \quad (I_1) \quad \textit{Equation 3-7}$$

$$+\frac{\Delta\gamma_R^2}{2}\cdot\{-e^{-\hat{\tau}}\cdot\frac{1}{P_N} + \sum_{k=\frac{N+1}{2}}^{N}[A_k e^{-\frac{\hat{\tau}}{s_k}}\cdot\sum_{n=0}^{N}\frac{1}{1-\frac{\mu_n}{s_k}}]\} \qquad (I_2)$$

where P_R is the received power by the receiving antenna with its gain pattern and $P_{\max}$ is the received signal strength received in the absence of vegetation. $\Delta\gamma_R$ is the beamwidth of the receiving antenna, and *m* is the order of the term I_1. The term I_1 is more accurately evaluated for higher values of *m*, however it will not change significantly for *m* > 10. N in I_2 has to be an odd number larger than 1. A compromise has to be found between accuracy and computing time. Large values for N will increase computing time dramatically. Reasonable values were found to be: $11 < N < 21$.

3.6.3.4 The following relations also apply:

$$\tau = (\sigma_a + \sigma_s)\cdot z = \sigma_\tau \cdot z$$

τ defines the optical density and z is the distance in metres

$$\overline{q}_m = \frac{4}{\Delta\gamma_R^2 + m\beta^2}$$

$$\mu_n = -\cos(\frac{n\pi}{N})$$

Equation 3-8

$$P_n = \sin^2(\frac{\pi}{2N}) \qquad \text{for } n = 0, N$$

$$P_n = \sin(\frac{\pi}{N})\cdot\sin(\frac{n\pi}{N}) \qquad \text{for } n = 1,2,...,N-1$$

$$\hat{\tau} = (1-\alpha W)\tau$$

$$\hat{W} = \frac{(1-\alpha)W}{1-\alpha W} \qquad \hat{W} \text{ is refered to as the reduced albedo}$$

3.6.3.5 The first line on the RHS of Equation 3-7 represents I_{ri}, which is usually referred to as the *'first'* term [Johnson, Schwering, 1985], whereas the sum of the second and third line give I_1, referred to as the *'second'* term. These appear in explicit form. The fourth line represents the *'third'* term I_2 of the RET equation [Johnson, Schwering, 1985], which contains the attenuation coefficients s_k and the amplitude factors A_k. These need to be determined numerically using the following expressions:

3.6.3.6 The attenuation coefficients s_k are determined by the characteristic equation:

$$\frac{\hat{W}}{2} \cdot \sum_{n=0}^{N} \frac{P_n}{1 - \frac{\mu_n}{s}} = 1$$

Equation 3-9

3.6.3.7 The LHS of Equation 3-9 will equal 1 for values of s, which represent the roots of this equation. It will yield $N + 1$ roots, for which the following applies:

$$s_{0,\ldots,\frac{N}{2}} = -s_{N,\ldots,\frac{N+1}{2}}$$

3.6.3.8 The amplitude factors A_k are determined by a system of linear equations given by:

$$\sum_{k=\frac{N+1}{2}}^{N} \frac{A_k}{1 - \frac{\mu_n}{s_k}} = \frac{\delta_n}{P_N} \qquad \text{for} \qquad n = \frac{N+1}{2} \;\ldots\; N$$

Equation 3-10

3.6.3.9 The linear system of equations can be written in matrix form $A \cdot B = C$ as follows:

$$\begin{bmatrix} A_{\frac{N+1}{2}} \\ \vdots \\ A_N \end{bmatrix} \cdot \begin{bmatrix} b_{\frac{N+2}{2},\frac{N+2}{2}} & \cdots & b_{\frac{N+2}{2},N} \\ \vdots & & \vdots \\ b_{N,\frac{N+2}{2}} & \cdots & b_{N,N} \end{bmatrix} = \frac{\delta_n}{P_N}$$

where:

$$b_{n,k} = \frac{1}{1 + \frac{\mu_n}{s_k}} \qquad \text{with} \quad k,n = \frac{N+1}{2} \;\ldots\; N$$

Equation 3-11

$$\delta_n = 0 \quad \text{for} \quad n \neq N$$

and

$$\delta_n = 1 \quad \text{for} \quad n = N$$

3.6.3.10 This system of equations can be solved for coefficients A_k using for example Gaussian elimination.

3.6.3.11 When using antenna beamwidths in these equations, it has to be taken into account that the antenna gain beamwidth and the scatter function beamwidth in Equation 3-7 have been assumed to be Gaussian. Using a Gaussian shape, the main lobe of the power radiation pattern is reduced by 1/e. The resulting beamwidth of the Gaussian pattern is related to the 3 dB beamwidth by $\Delta\gamma_R = 0.6 \cdot \Delta\gamma_{3db}$.

3.6.4 Numerical Evaluation of the RET equation

3.6.4.1 It is useful to illustrate the effects of the individual contributions of the 3 terms I_{ri}, I_1 and I_2 on the overall attenuation curve (Equation 3-7). Figure 3-18 shows each contribution as well as the resulting attenuation curve in dB vs the optical density τ. The graphs are evaluated for the case correspoding to $\alpha = 0.5$, $\beta = 6°$, $W = 0.95$ and $\Delta\gamma_R = 1.2°$.

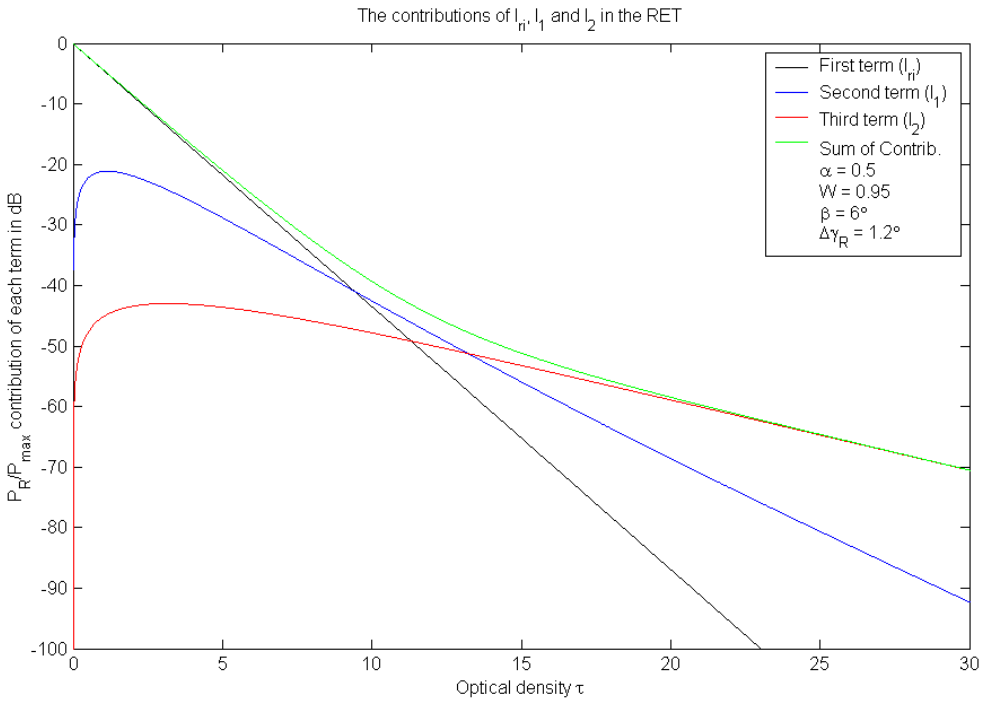

Figure 3-18 Excess attenuation due to vegetation using RET, individual contributions and sum using Equation 3-7

3.6.4.2 The graphs show the relative contributions of I_{ri}, I_1 and I_2 at varying vegetation depth, indicated by the optical density $\tau = \sigma_\tau z$. Due to the different physical basis of the three distinct terms I_{ri}, I_1 and I_2, three different areas can be identified:

i) For small τ the 1st term (I_{ri}) is dominant, indicating a mainly coherent signal propagating in the forward direction which, on a dB scale, declines linearly with optical density.

ii) In an intermediate region, in the example shown in Figure 3-18 between $\tau = 3$ and $\tau = 13$, the 2nd term (I_1) is significant. The general behaviour of I_1 is as follows: For small distances into the scatter medium the first part of the sum in I_1 dominates, letting I_1 increase linearly with τ. As τ increases, I_1 reaches a maximum and then decreases again because of the exponential factor $\exp(-\tau)$. The higher order terms (m) become significant. This results in slowing the attenuation rate and in broadening the beam of the forward scattering signal.

iii) After $\tau = 13$, the 3rd term (I_2) begins to have a significant influence and from around $\tau = 21$ becomes the only significant contribution in the example shown in Figure 3-18. The general behaviour of I_2 is as follows: As τ increases, I_2 first increases linearly with distance, since I_2 is generated by the isotropic scattering of the coherent field components I_{ri} in this region, but then reaches a maximum and decreases again because of absorption by the medium.

3.6.4.3 The behaviour of the components I_{ri}, I_1 and I_2 lead to the following overall behaviour of the excess attenuation curve as a function of distance into the scattering medium.

3.6.4.4 The attenuation curve decreases linearly at a relatively high rate initially as we move away from the air vegetation interface. As the distance increases the attenuation rate decreases significantly due to the effect of the scatter in the medium in the example of Figure 3-18, this occurs at about $\tau = 10$. As the depth increases further, the attenuation rate reduces further as the received signal becomes predominantly affected by the isotropic scatter. From then on, the attenuation curve becomes dominated by the term I_2, which continues to decline with τ, but at a much lower rate.

3.6.5 Numerical evaluation of the scatter (or phase) function

3.6.5.1 The phase (or scatter) function described in Equation 3-2 and Equation 3-3 represents the scatter pattern of the vegetation medium. While in the predominantly coherent region of the vegetation (relatively small optical density τ), where I_{ri} is the dominant mode of propagation through vegetation, the phase function is characterised by a narrow mainly coherent forward lobe and an isotropic backscatter region. The beamwidth of the forward lobe is given by β, whereas α is the ratio of the forward scattered power to the total scattered power. For the curve fitting process described in Section 3.6.8 it is important that α and β can be varied independently from each other and therefore determined separately by the iterative algorithm. Figure 3-19 shows that varying the beamwidth does not affect the level of the isotropic backscatter region, whereas changing α does not alter the beamwidth of the forward lobe. The two quantities can therefore be considered separately.

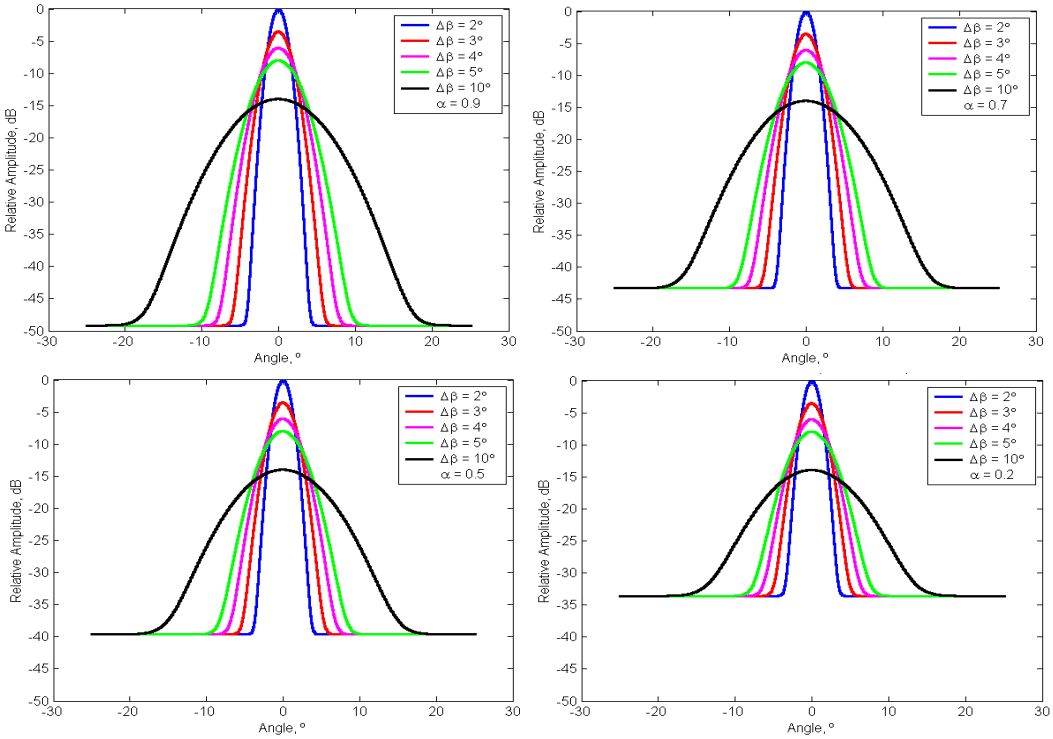

Figure 3-19 The scatter function with varying parameters α and β

3.6.6 The Iterative Determination of the RET parameters from Measured Data

3.6.6.1 In the previous section it was shown that the RET model uses the input parameters β, α, σ_τ and W to determine the excess attenuation as function of depth into vegetation. Parameters α and β can be derived from measuring the phase function of the vegetation medium. A separate document reproduced in Appendix A describes in more detail how these measurements can be conducted. The phase function measurement needs to be carried out at the same experiment sites as attenuation measurements, ideally at one or two trees depth into the vegetation. With α and β determined, attenuation curves for a range of albedos W need to be produced. The initial slope of the measured attenuation curve with depth yields the parameter σ_τ, as shown in Equation 3-12 - Equation 3-14. W can subsequently be determined using best fit with measured depth data.

3.6.6.2 The parameter σ_τ is determined as follows:

3.6.6.3 The first term I_{ri} of the RET equation describes the initial slope of the attenuation function with distance z in metres.

$$P = P_0 \cdot e^{-\sigma_\tau z} \qquad \text{Equation 3-12}$$

3.6.6.4 Where P is the measured signal power inside the vegetation and P_0 is the power received at the incident air-vegetation interface. The RET describes excess attenuation due to vegetation, so that the signal decay, due to free space loss, is not included in P.

3.6.6.5 If the attenuation curve is displayed in dB, Equation 3-12 can be written as:

$$10 \cdot \log \frac{P}{P_0} = -10 \cdot \log(\sigma_\tau z \log e) \qquad \text{Equation 3-13}$$

3.6.6.6 The initial slope of the graph (dB/m) is given by:

$$\frac{\Delta A}{\Delta d} = -4.43 \cdot \sigma_\tau \qquad \text{Equation 3-14}$$

where $A = 10 \cdot \log \frac{P}{P_0}$ is the attenuation in dB.

3.6.6.7 However, for the measurement scenarios presented in this work, no phase function measurements were available. Therefore an iterative curve fitting algorithm has been developed that produces RET attenuation curves over a wide range of input parameters α, β and W. The curve fitting also includes a small number of different σ_τ values to establish the best fit with the measurement data.

3.6.7 Influence of the RET parameters on the attenuation curve

3.6.7.1 In order to illustrate the behaviour of the attenuation curve for varying RET input parameters three simulation results are presented here. The initial slope variation can readily be appreciated so that it does not need to be illustrated here.

3.6.7.2 Figure 3-20 shows the influence of the parameter α on the attenuation curve. It can be observed that varying α changes the final slope of the graph, i.e. the final attenuation rate and also alters the position of the changeover points at which the initial linear slope of the graph reduces to significantly smaller values.

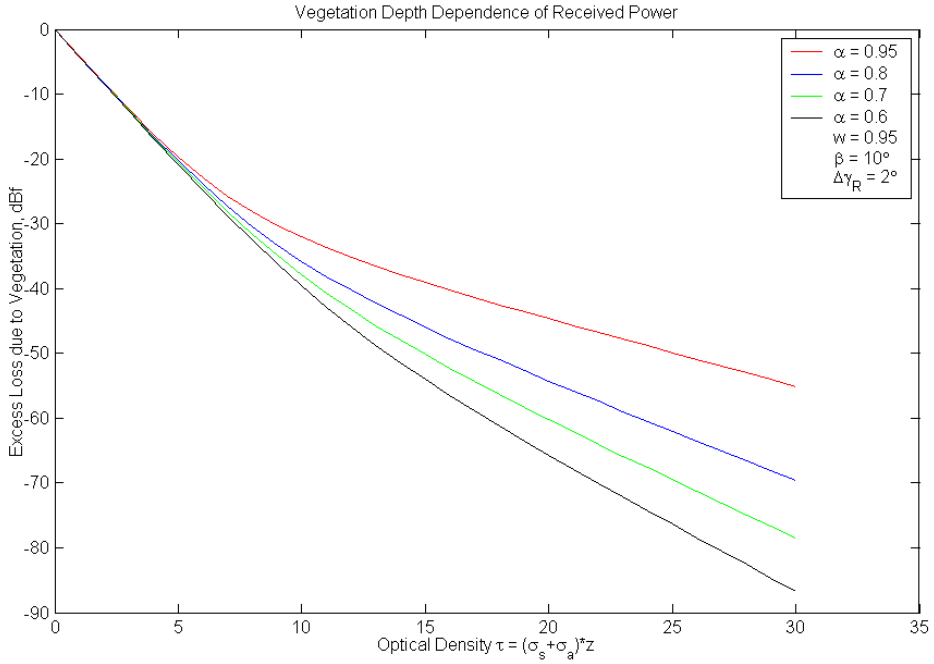

Figure 3-20 Influence of parameter α on the RET attenuation curve

3.6.7.3 Figure 3-21 shows the influence of parameter β on the RET attenuation curve. The parameter β strongly influences the location of the change over points but does not have significant influence on the final attenuation rate of the graph.

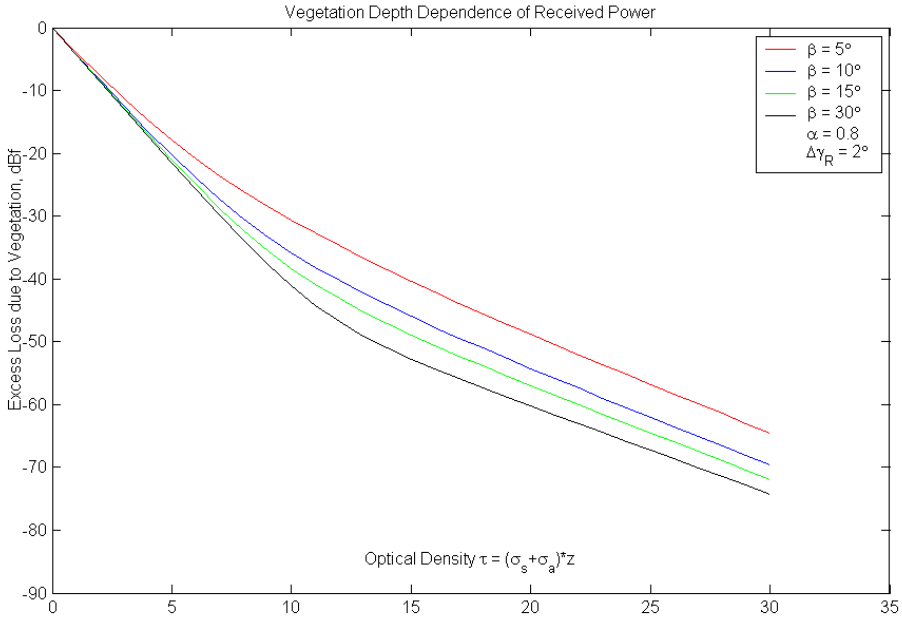

Figure 3-21 Influence of parameter β on the RET attenuation curve

3.6.7.4 Figure 3-22 shows the influence of albedo W on the RET attenuation curve. Here it can be seen that the albedo influences the final attenuation rate but not the change over points.

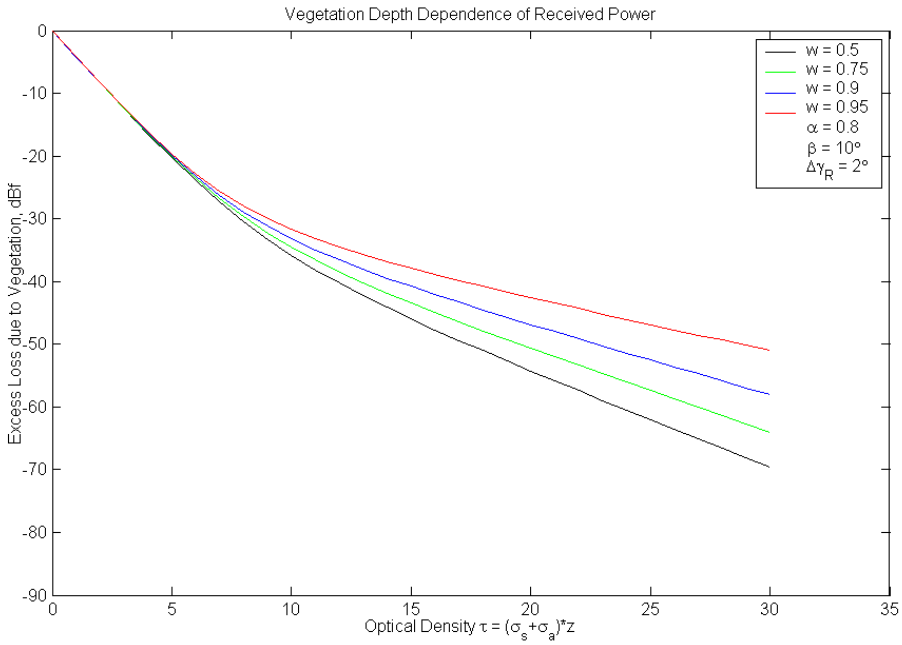

Figure 3-22 Influence of albedo W on the RET attenuation curve

3.6.8 Examples of fitted curves

3.6.8.1 The iterative curve fitting algorithm developed finds the best fit from numerous RET attenuation curves generated by using a wide range of RET parameters for each set of experimental data. A minimum least errors fit determines the best fit and establishes the parameters.

3.6.8.2 The first example in Figure 3-23 shows the best fit RET attenuation curve and measurement data obtained for a line of Silver Maple trees at the Twyning Nursery site using 11 GHz during summer (foliated state). The second example in Figure 3-24 shows the best fit RET attenuation curve and measurement data obtained at the same site and the same frequency in winter (out of leaf) conditions. Figure 3-25 and Figure 3-26 show similar graphs for Common Lime trees at the same nursery in and out of leaf respectively at a frequency of 1.3 GHz.

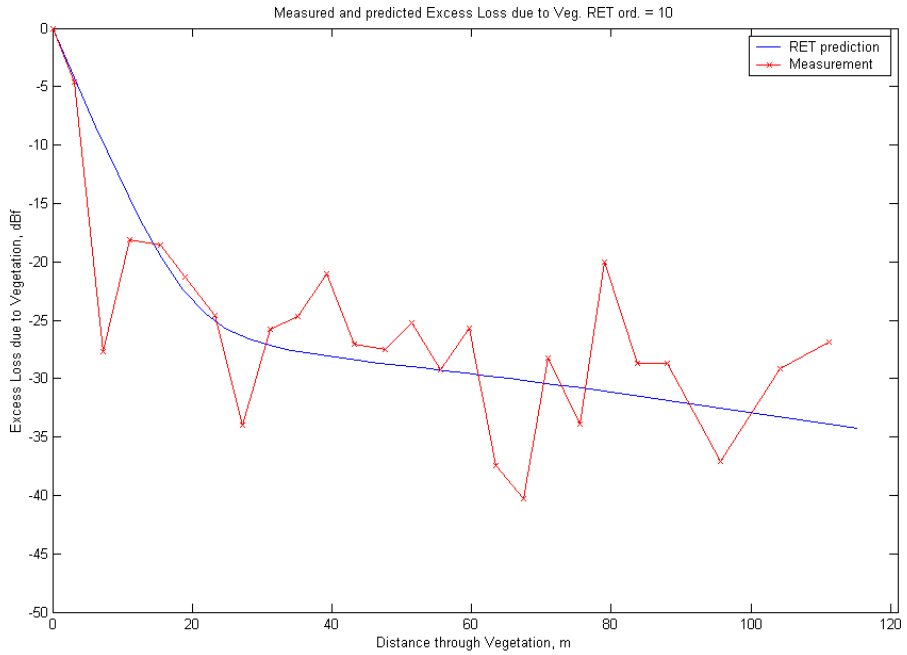

Figure 3-23 Measurement and best fit RET attenuation curve for Silver Maple at Twyning Nursery at 11 GHz in leaf

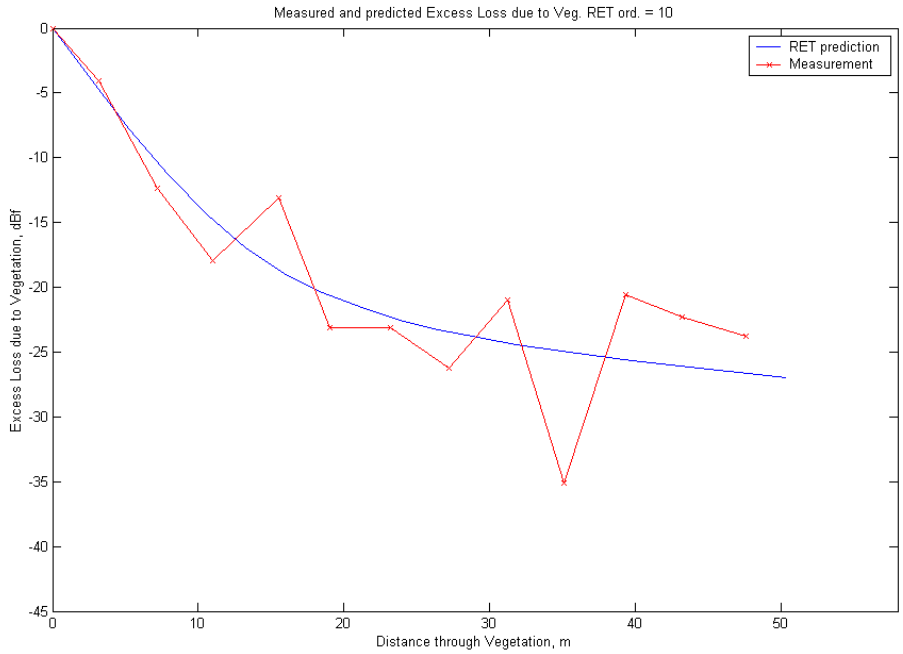

Figure 3-24 Measurement and best fit RET attenuation curve for Silver Maple at Twyning Nursery at 11 GHz out of leaf

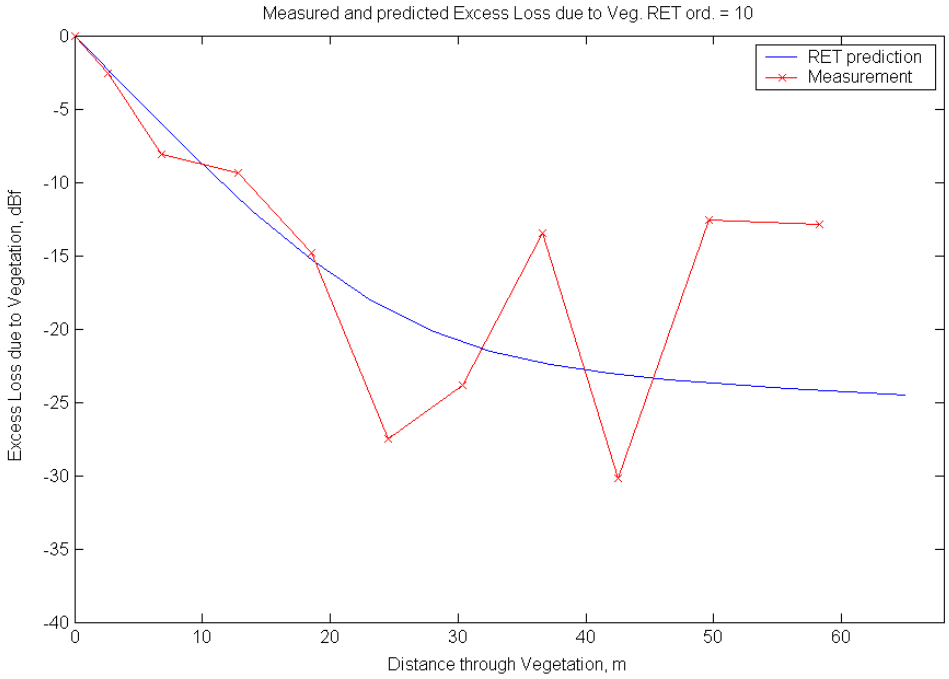

Figure 3-25 Measurement and best fit RET attenuation curve for Common Lime at Twyning Nursery at 1.3 GHz in leaf

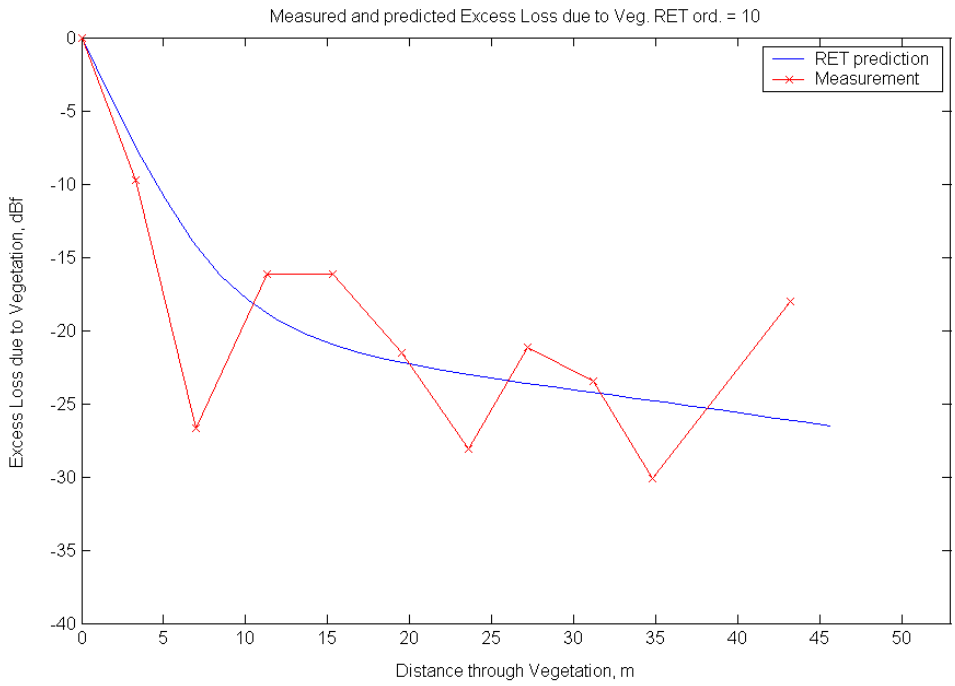

Figure 3-26 Measurement and best fit RET attenuation curve for Common Lime at Twyning Nursery at 1.3 GHz out of leaf

3.6.9 RET prediction for transmitter above canopy

3.6.9.1 The co-ordinate system for the RET predictions in the previous sections has been defined as shown in Figure 3-39.

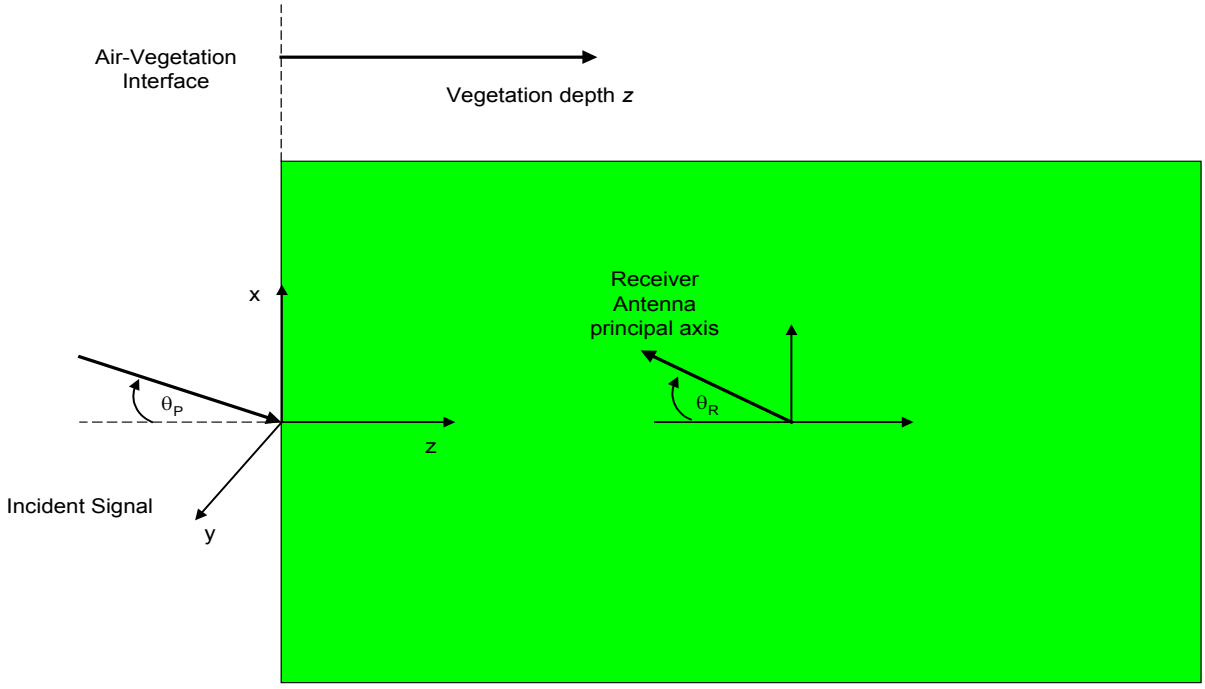

Figure 3-27 RET geometry for normal incidence (θ_P = 0°) and for small transmitter elevation

3.6.9.2 The cases shown previously have been conducted for normal incidence ($\theta_P = 0$) of the signal propagating from the transmitter towards the air-vegetation interface. For elevated transmitter positions two different approaches need to be used.

i. For small transmitter elevations the same co-ordinate system as before can be used and the RET equation can be extended to allow oblique incident signals, as shown in Figure 3-27.
ii. For larger transmitter elevations it is more practical to rotate the whole co-ordinate system and use the RET equation with its extension for oblique incidence as outlined in Figure 3-28. The vegetation depth *z* now is the distance from the canopy top down into the vegetation.

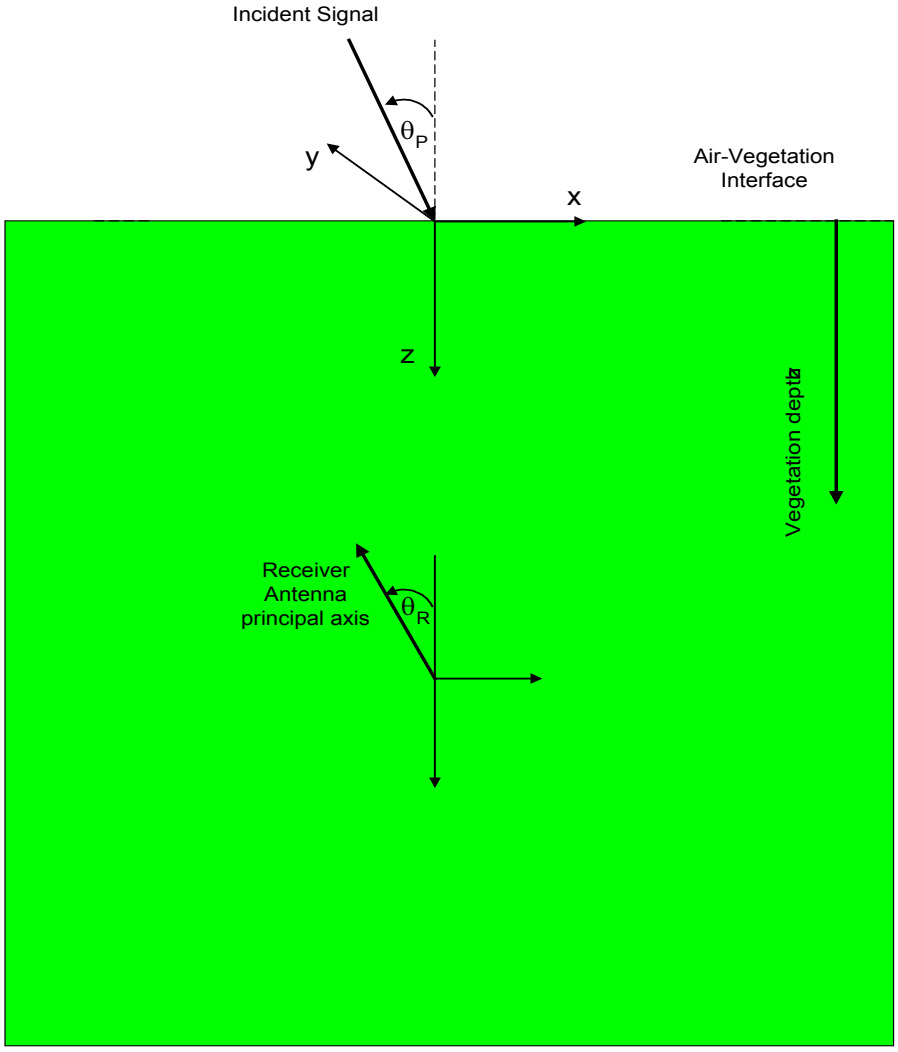

Figure 3-28 RET geometry for large transmitter elevation

3.6.9.3 The RET equation including oblique incidence θ_P and elevation angle θ_R of the receiving antenna is:

$$\frac{P_R}{P_{\max}} = e^{\{-(\frac{\gamma_{RP}}{\Delta\gamma_R})^2 - \tau\}} \qquad (I_{\mathrm{ri}})$$

$$+\frac{\Delta\gamma_R^2}{4}\cdot\{[e^{-\frac{\hat{\tau}}{\mu_P}} - e^{-\frac{\tau}{\mu_P}}]\cdot\overline{q}_M(\gamma_{RP})$$

$$+e^{-\frac{\tau}{\mu_P}}\cdot\sum_{m=1}^{M}\frac{1}{m!}(\alpha W\tau)^m\ [\overline{q}_m(\gamma_{RP}) - \overline{q}_M(\gamma_{RP})]\} \qquad (I_1)$$

$$+\frac{\Delta\gamma_R^2}{2}\cdot\{-e^{-\frac{\hat{\tau}}{\mu_P}}\cdot\frac{F_j(\mu_R)}{P_j} + \sum_{k=\frac{N+1}{2}}^{N}[A_k e^{-\frac{\hat{\tau}}{s_k}}\cdot\sum_{n=0}^{N}\frac{F_n(\mu_R)}{1-\frac{\mu_n}{s_k}}]\} \qquad (I_2)$$

Equation 3-15

with

$$\overline{q}_m(\gamma_{PR}) = \frac{4}{\Delta\gamma_R^2 + m\beta^2}\ e^{-\frac{\gamma_{PR}^2}{\Delta\gamma_R^2 + m\beta^2}}$$

and

$$\gamma_{PR} = \cos^{-1}(\sqrt{(1-\mu_P^2)(1-\mu_R^2)} + \mu_P\mu_R)$$

Equation 3-16

$$\mu_P = \cos(\theta_P)$$

$$\mu_R = \cos(\theta_R)$$

3.6.9.4 Using the geometry shown in Figure 3-28 and Equation 3-15 the excess attenuation curve for vertical vegetation depth from the top of the canopy can be calculated. The orientation of the receiver antenna, especially when using narrow beamwidth antennas, will change the excess attenuation curve significantly.

3.6.9.5 Example simulations for several cases illustrating this will be shown in Figure 3-29 to Figure 3-34. The antenna patterns used in all 6 examples are Gaussian. The incident signal in all 6 examples propagates towards the normal of the air-vegetation interface at an angle θ_p = 45º. The examples show three different orientations of the principal axis of the receiving antenna. One case shows the angle of the principal axis of the receiving antenna with the normal being the same as the direction of the incident signal, i.e. θ_R = 45º. This case is shown in Figure 3-29 and Figure 3-32. In the second case the principal axis of the receiving antenna is aligned horizontally, which following the geometry shown in Figure 3-28 corresponds to θ_R = 90º. This case is shown in Figure 3-30 and Figure 3-33. The final case is the one of the principal axis of the receiving antenna being aligned vertically, which corresponds to θ_R = 0º. The first three examples in Figure 3-29 to Figure 3-31 show the attenuation curves for a receiver antenna 3dB beamwidth of $\Delta\gamma_{R3dB}$ = 10º. This means that the coherent part of signal propagating through the vegetation will only be within the 3dB beamwidth of the antenna when θ_R = 45º. It can clearly be seen that this is the only case where small attentions can be observed at small optical densities τ. The signal received for

θ_R = 0º and θ_R = 90º will be mainly due to scattered signal within the vegetation, therefore large attentions are observed at small vegetation depth in those cases. The last three examples in Figure 3-32 to Figure 3-34 have been conducted for a receiver antenna 3 dB beamwidth of $\Delta\gamma_{R3dB}$ = 120º. It can clearly be seen that due to coherent signal contributions within the 3 dB beamwidth of the receiving antenna, the attenuation rate is low at small optical densities τ.

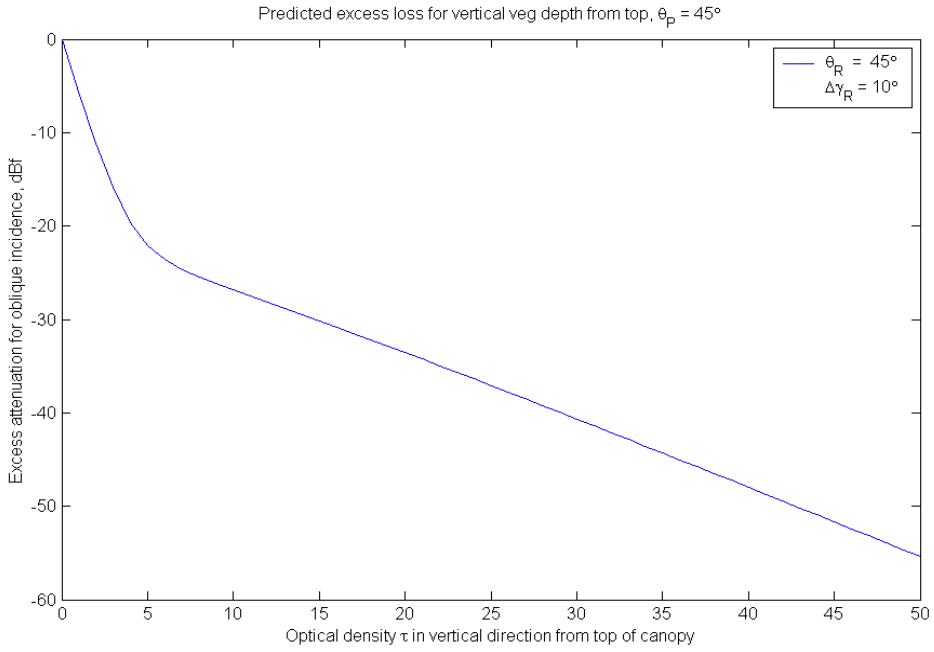

Figure 3-29 Vertical excess attenuation curve for $\Delta\gamma_R$ = 10º, θ_P = 45º, θ_R = 45º

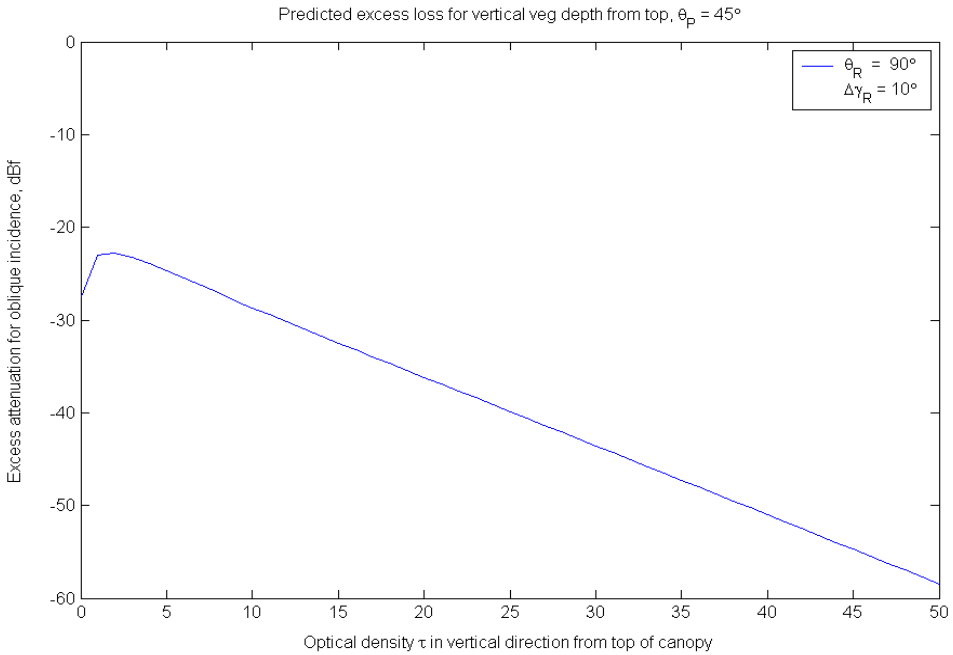

Figure 3-30 Vertical excess attenuation curve for $\Delta\gamma_R$ = 10º, θ_P = 45º, θ_R = 90º

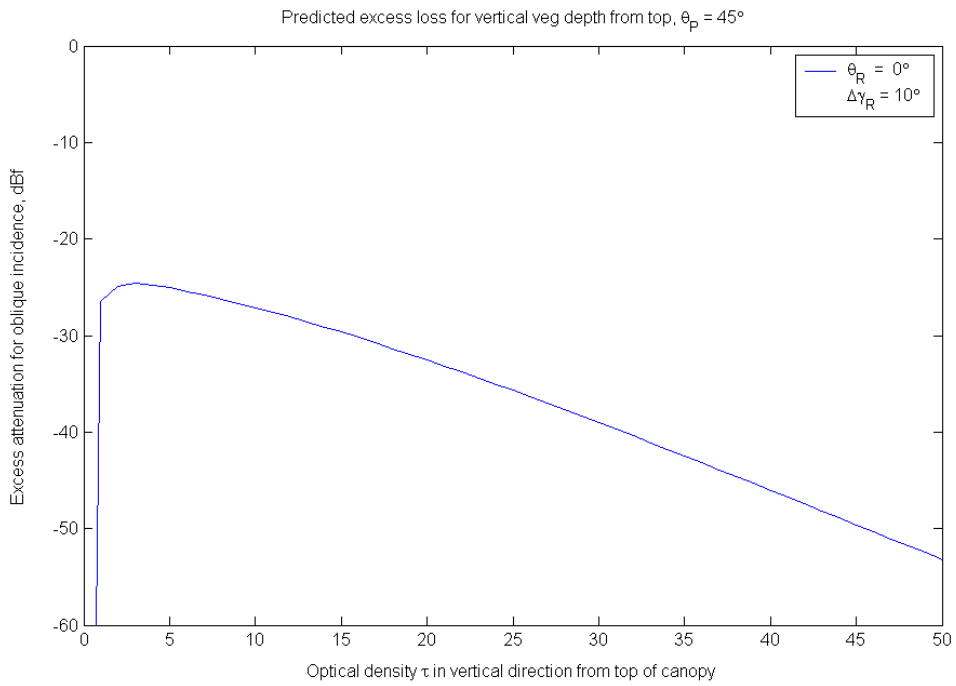

Figure 3-31 Vertical excess attenuation curve for $\Delta\gamma_R = 10°$, $\theta_P = 45°$, $\theta_R = 0°$

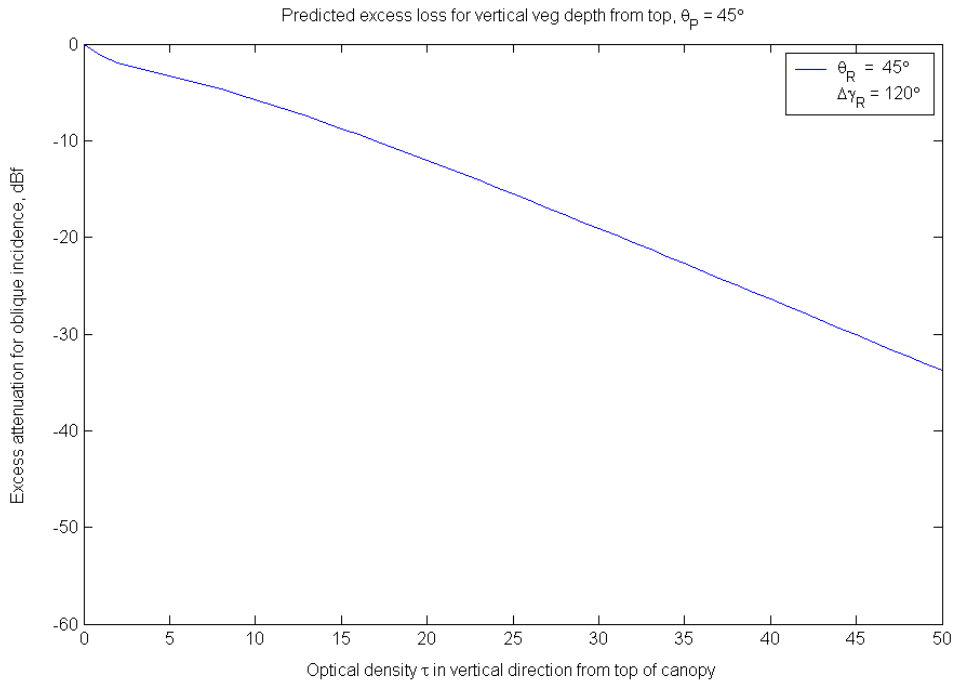

Figure 3-32 Vertical excess attenuation curve for $\Delta\gamma_R = 120°$, $\theta_P = 45°$, $\theta_R = 45°$

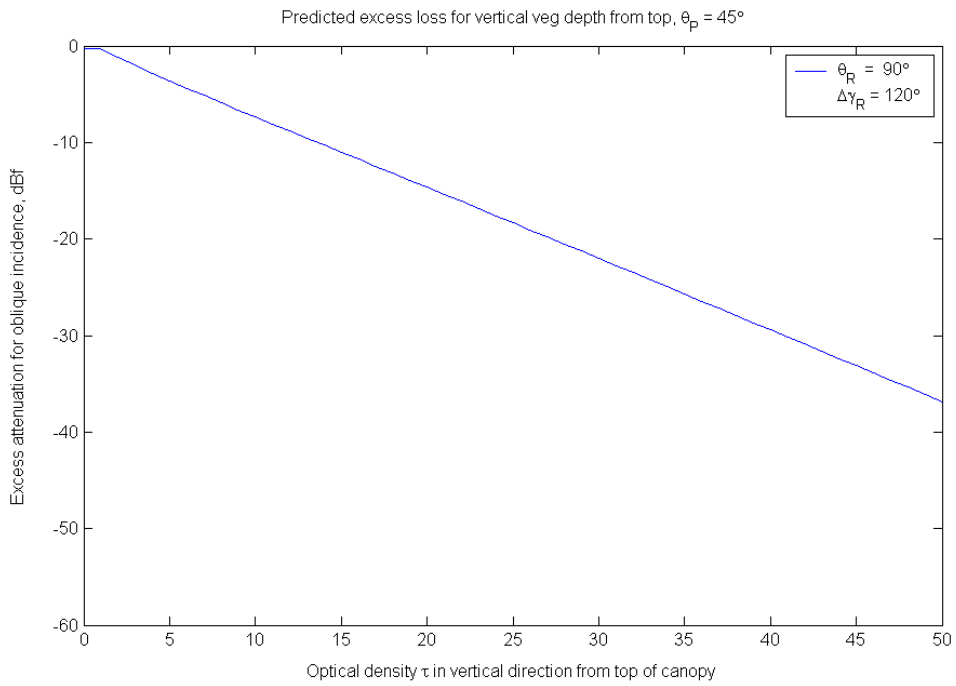

Figure 3-33 Vertical excess attenuation curve for $\Delta\gamma_R = 120°$, $\theta_P = 45°$, $\theta_R = 90°$

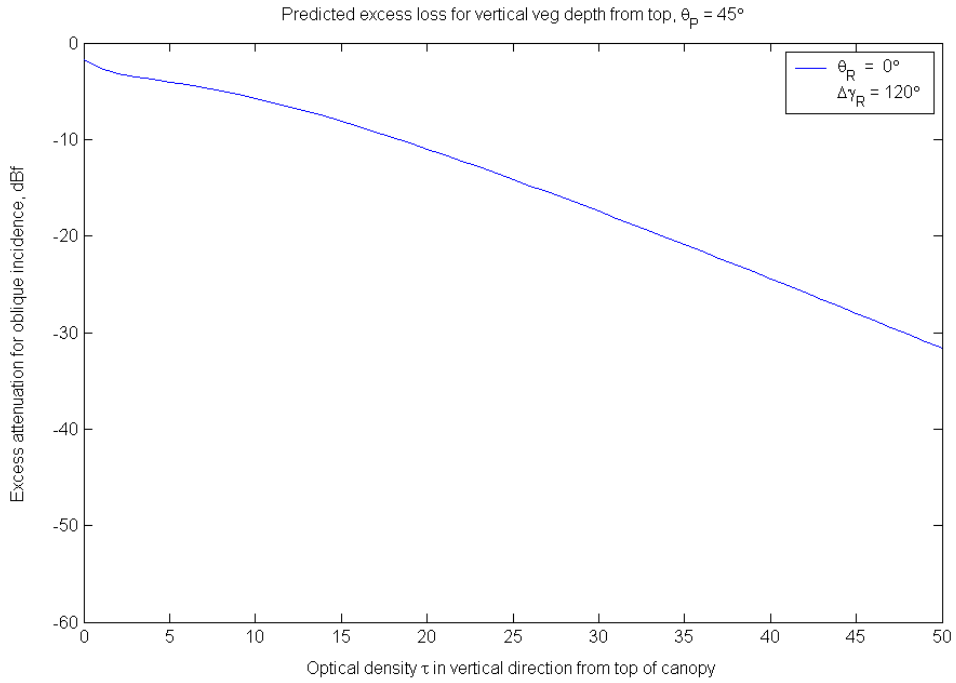

Figure 3-34 Vertical excess attenuation curve for $\Delta\gamma_R = 120°$, $\theta_P = 45°$, $\theta_R = 0°$

3.7 Combination of model elements

1.1.1 Firstly, if any of the components is much larger than any of the others (i.e. the attenuation is much less than the other components), then the other terms may be discarded and this term alone may be taken as giving the received signal value. However, should two or more of the components be of similar order, the question arises as to whether or not a coherent addition of the terms should be made.

3.7.2 For the case of the ground-reflected wave, the following heuristic argument may be applied to limit the need for the addition of this term.

3.7.3 The ground reflected path is relatively clear, by comparison with the direct or through vegetation path, if the foliage is elevated, as shown in Figure 3-35.

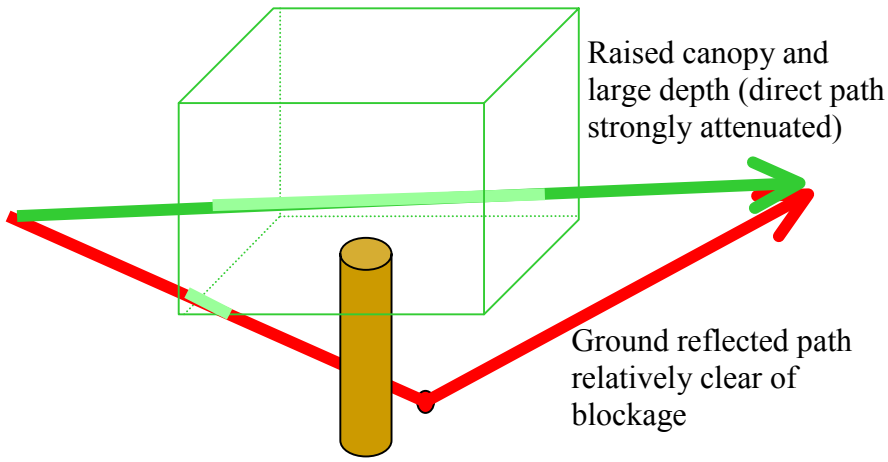

Figure 3-35 Geometry for dominant ground reflection beneath a raised canopy

3.7.4 In this case, if the vegetation depth is sufficiently large, the ground reflected ray may dominate the received field, and the scattered component may be neglected.

3.7.5 For geometries where the transmitter is much further from the vegetation than the receiver, ie where the ground reflection point occurs in front of the vegetation screen, this has the effect that the incident illumination on the vegetation can no longer be considered a plane wave.

3.7.6 For the two cases shown in Figure 3-36, the direct ray and the ground reflected ray may still interfere coherently, and therefore an estimation of the overall attenuation of the vegetation can be given by the summation of the scattered term and the ground reflected term.

3.7.7 For other geometries with larger depths through vegetation, but no clear path beneath the foliage, where both the ground reflected and direct components will have travelled through a similar depth of vegetation, the RET theory predicts that the signal will propagate by a mode of diffuse scatter. This is by nature an incoherent signal, with no single resolvable ray. For this case, any non-uniformity on the wavefront across the incident plane of the vegetation may be assumed to have averaged out at the end of these large depths, and the emerging field is solely a wave due to diffuse scatter. Hence for this case, the two

components will not combine coherently, and the variability of the sum of these two components will then be smaller (i.e. no totally destructive interference).

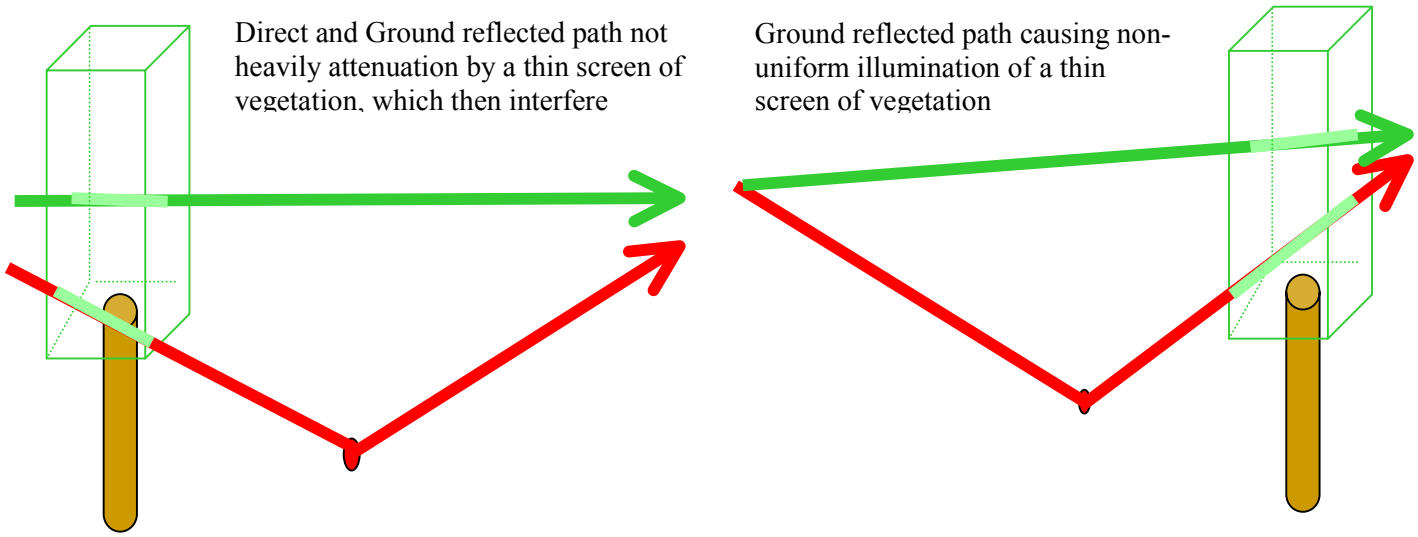

Figure 3-36 Geometry for combination of direct and ground reflected rays through a thin screen

3.7.8 This effect can be seen in Figure 3-37, where the ratio of maxima to minima of the received signal is plotted as a function of vegetation depth (i.e. depth through the foliage), for seven different frequencies.

3.7.9 One can see that the variability with height is, in general, decreasing with vegetation depth for the higher frequencies, and increasing with depth for the lower frequencies. At the higher frequencies the effects of diffuse scatter is stronger with depth, and therefore for the greater depths the received field is the sum of a large number of diffuse components, giving less variability. For the lower frequencies, the effects of the diffuse scatter occur at much larger vegetation depths, since the optical path length is smaller, and the signal variability is not reduced at greater depths. For the smaller frequencies, the change in total path length of the reflected ray is also smaller as the receiver is moved for a fixed distance. In this case 14m height gain corresponded to a change in path length difference of ~ 1 wavelength for 2GHz compared with ~ 40 wavelengths at 18GHz. This effect may also reduce the measured variability at the lower frequencies.

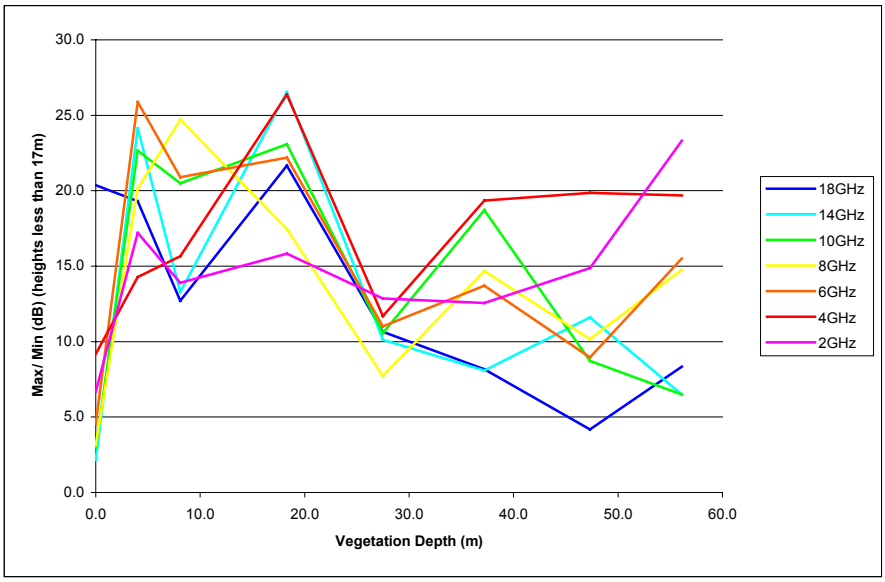

Figure 3-37 Signal variability as a function of vegetation depth

3.8 Method of application

3.8.1 Calculation of the Top diffracted component

3.8.1.1 The diffraction loss, L_{top}, experienced by the signal path diffracted over the vegetation, may be treated as double isolated knife-edge diffraction for the geometry defined in Figure 3-38.

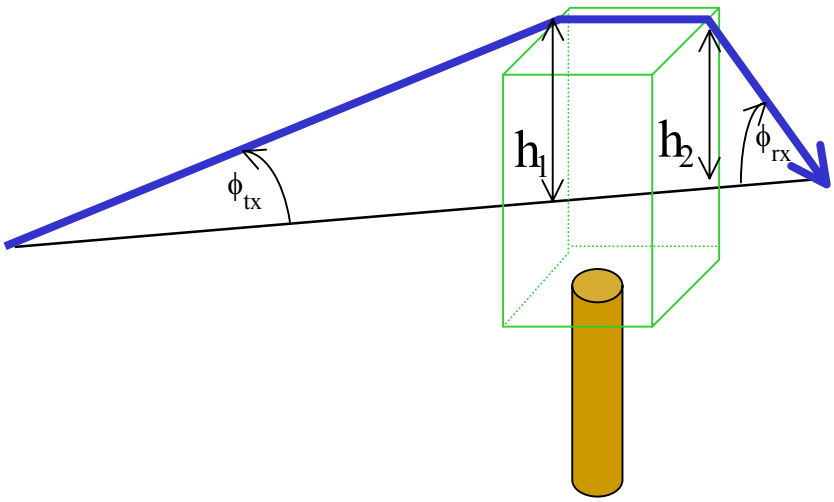

Figure 3-38 Geometry for Top Diffracted wave

3.8.1.2 This calculated as per ITU-R Recommendation 526-3, §4.4:

3.8.1.3

$$L_{top} = 6.9 + 20\log\left(\sqrt{(v(h_1)-0.1)^2+1}+v(h_1)-0.1\right)+G_{Tx}(\phi_{tx}) + 6.9 + 20\log\left(\sqrt{(v(h_2)-0.1)^2+1}+v(h_2)-0.1\right)+L_c+G_{Rx}(\phi_{rx})$$

Equation 3-17

3.8.1.4 where $G_{Tx}(\phi_{Tx})$ and $G_{Rx}(\phi rx)$ are the losses due to angles of the diffracted wave leaving the transmit antenna and coming into the receive antenna, respectively.

3.8.2 Calculation of the Side Diffracted component

3.8.2.1 The diffraction loss, L_{sidea} and L_{sideb}, experienced by the signal diffracted around the vegetation, may be treated as double isolated knife-edge diffraction, for the geometry defined in Figure 3-39.

Edge diffracted components

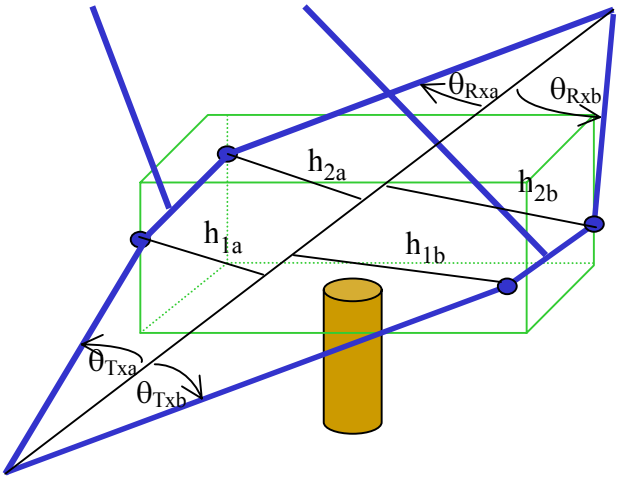

Figure 3-39 Geometry for edge diffracted wave

3.8.2.2 This calculated as per ITU-R Recommendation 526-3, §4.4:

$$L_{sidea} = 6.9 + 20\log\left(\sqrt{(\nu(h_{1a}) - 0.1)^2 + 1} + \nu(h_{1a}) - 0.1\right) + G_{Tx}(\theta_{Txa})$$
$$+ 6.9 + 20\log\left(\sqrt{(\nu(h_{2a}) - 0.1)^2 + 1} + \nu(h_{2a}) - 0.1\right) + L_c + G_{Rx}(\theta_{Rxa})$$

Equation 3-18

and

$$L_{sideb} = 6.9 + 20\log\left(\sqrt{(\nu(h_{1b}) - 0.1)^2 + 1} + \nu(h_{1b}) - 0.1\right) + G_{Tx}(\theta_{Txb})$$
$$+ 6.9 + 20\log\left(\sqrt{(\nu(h_{2b}) - 0.1)^2 + 1} + \nu(h_{2b}) - 0.1\right) + L_c + G_{Rx}(\theta_{Rxb})$$

Equation 3-19

3.8.2.3 where $G_{Tx}(\theta_{Txa,Txb})$ and $G_{Rx}(\theta_{Txa,Txb})$ are the losses due to the angles at which the diffracted waves leave the transmit antenna and enter the receive antenna, for sides a and b of the vegetation, respectively.

3.8.3 Calculation of the ground reflected component

3.8.3.1 It is assumed that the path is sufficiently short that the ground reflected wave may be modelled by the geometry shown in Figure 3-40.

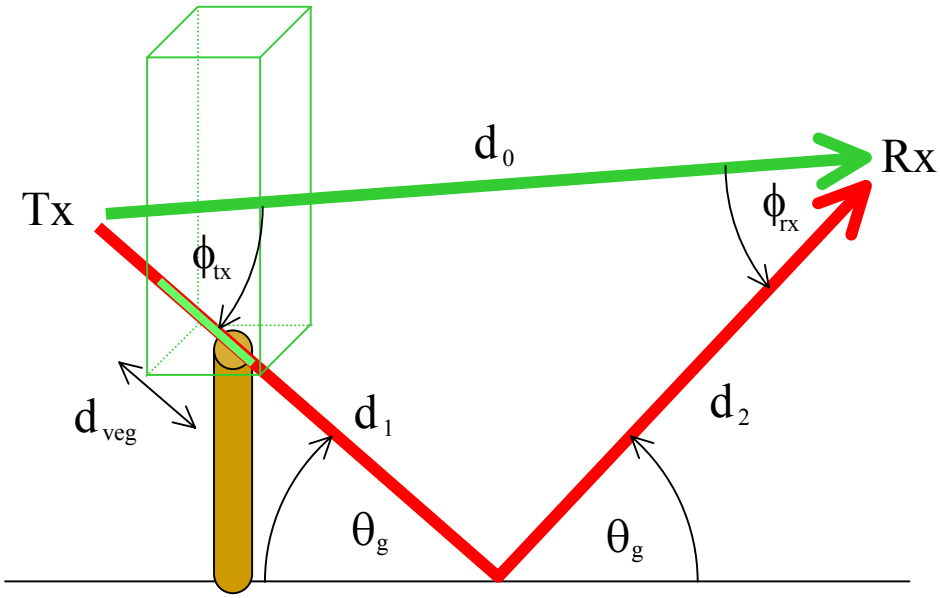

Figure 3-40 Geometry for ground reflected wave

3.8.3.2 To calculate the Loss experienced by the ground reflected wave at the receiver, the reflection coefficient, R_0, of the ground reflected signal may be calculated using the method outlined in CCIR Report 1008-1 [1], with a given grazing angle θ_g. The values for the permittivity and conductance are obtained from ITU-R Rec. 527-3.

3.8.3.3 The loss experienced by the ground reflected wave, L_g , is then given by

$$L_{ground} = L_{gveg}(d_{veg}) + 20\log_{10}\left(\frac{d_1 + d_2}{d_0}\right) - 20\log_{10}(R_0) + G_{Tx}(\phi_{tx}) + G_{Rx}(\phi_{rx}) \qquad \textit{Equation 3-20}$$

3.8.3.4 where $G_{Rx}(\alpha)$ and $G_{Tx}(\beta)$ are the losses due to angles of the reflected wave leaving the transmit antenna and coming into the receive antenna, respectively, and $L(d_{veg})$ is the loss due to the propagation of the ground reflected wave through the total vegetation depth, d_{veg}. This is calculated using the same method as the through vegetation loss presented in Section 3.8.4, with the vegetation depth of the ground reflected wave, d_{veg},, being substituted for d.

3.8.4 Calculation of the "through" or scattered component

3.8.4.1 In order to make accurate predictions of the excess attenuation to vegetation, the user needs to input the following parameters into the RET equation (Equation 3-20):

α , the ratio of the forward scattered power to the total scattered power,

β , the beamwidth of the phase function,

σ_τ , the combined absorption and scatter coefficient,

W, the albedo,

$\Delta\gamma_R$, the beamwidth of the receiving antenna,

d, the distance into the vegetation in metres.

3.8.4.2 Given the input parameters: frequency (in GHz), the typical leaf size of the vegetation to be modelled and the Leaf Area Index (LAI) of the tree species, one can obtain the nearest value of α, β, W and σ_τ from the RET parameter tables (Table 3-1 - Table 3-4). Should these parameters be unavailable, one should assume the nearest match from the species listed to the tables. Alternatively parameters for unknown geometries, species and frequencies can be determined experimentally, using the method outlined for determining these given in the RET phase function measurement recipe. The values of the parameters obtained can then be used to further populate the tables.

	Horse Chestnut *Aesculus hippocastanum L.*	Silver Maple *Acer saccharinum L.*	Silver Maple *Acer saccharinum L.*	London Plane *Platanus hispanica Muenchh*	London Plane *Platanus hispanica Muenchh*	Common Lime *Tilia x europaea*	Common Lime *Tilia x europaea*	Sycamore *Acer pseudoplatanus L.*	Sycamore *Acer pseudoplatanus L.*
	In leaf	In leaf	Out leaf	In leaf	Out leaf	In Leaf	Out Leaf	In leaf	Out leaf
LAI		1.691		1.93		1.475		1.631	0.483
Leaf Size	0.300	0.15		0.250		0.100		0.15	
Frequency (GHz)	α								
1.3	0.9	0.95	0.9	0.95	0.9	0.9	0.95		0.95
2	0.75		0.95	0.95			0.95		0.95
2.2			0.95	0.5					
11	0.85	0.9		0.7	0.95	0.95	0.95		0.95
37				0.95					
61.5		0.8		0.25				0.9	

Table 3-1 Fitted values of α with frequency / species

	Horse Chestnut *Aesculus hippocastanum L.*	Silver Maple *Acer saccharinum L.*	Silver Maple *Acer saccharinum L.*	London Plane *Platanus hispanica Muenchh*	London Plane *Platanus hispanica Muenchh*	Common Lime *Tilia x europaea*	Common Lime *Tilia x europaea*	Sycamore *Acer pseudoplatanus L.*	Sycamore *Acer pseudoplatanus L.*
	In leaf	In leaf	Out leaf	In leaf	Out leaf	In Leaf	Out Leaf	In leaf	Out leaf
LAI		1.691		1.93		1.475		1.631	0.483
Leaf Size	0.300	0.15		0.250		0.100		0.15	
Frequency (GHz)	β								
1.3	21	14	43	42	16	76	50		70
2	80		31	49			60		62
2.2			25	13					
11	69	58		100	19	78	48		44
37				18					
61.5		48		2				59	

Table 3-2 Fitted values of β with frequency / species

	Horse Chestnut *Aesculus hippocastanum L.*	Silver Maple *Acer saccharinum L.*	Silver Maple *Acer saccharinum L.*	London Plane *Platanus hispanica Muenchh*	London Plane *Platanus hispanica Muenchh*	Common Lime *Tilia x europaea*	Common Lime *Tilia x europaea*	Sycamore *Acer pseudoplatanus L.*	Sycamore *Acer pseudoplatanus L.*
	In leaf	In leaf	Out leaf	In leaf	Out leaf	In Leaf	Out Leaf	In leaf	Out leaf
LAI		1.691		1.93		1.475		1.631	0.483
Leaf Size	0.300	0.15		0.250		0.100		0.15	
Frequency (GHz)					**W**				
1.3	0.25	0.95	0.25	0.95	0.95	0.95	0.95		0.85
2	0.55		0.95	0.95			0.95		0.95
2.2			0.95	0.45					
11	0.95	0.95		0.95	0.95	0.75	0.95		0.95
37				0.95					
61.5		0.8		0.5				0.9	

Table 3-3 Fitted values of albedo with frequency / species

	Horse Chestnut *Aesculus hippocastanum L.*	Silver Maple *Acer saccharinum L.*	Silver Maple *Acer saccharinum L.*	London Plane *Platanus hispanica Muenchh*	London Plane *Platanus hispanica Muenchh*	Common Lime *Tilia x europaea*	Common Lime *Tilia x europaea*	Sycamore *Acer pseudoplatanus L.*	Sycamore *Acer pseudoplatanus L.*
	In leaf	In leaf	Out leaf	In leaf	Out leaf	In Leaf	Out Leaf	In leaf	Out leaf
LAI		1.691		1.93		1.475		1.631	0.483
Leaf Size	0.300	0.15		0.250		0.100		0.15	
Frequency (GHz)					σ_τ				
1.3	0.772	0.241	0.139	0.147	0.221	0.22	0.591		0.36
2	0.091		0.176	0.203			0.692		0.249
2.2			0.377	0.244					
11	0.124	0.321		0.75	0.459	0.56	0.757		0.179
37				0.441					
61.5		0.567		0.498				0.647	

Table 3-4 Fitted values of σ_τ with frequency / species

3.8.4.3 These 4 tabled parameters, together with the frequency, and $\Delta\gamma_{3db}$,the 3dB beamwidth of the receive antenna, are then used in the RET Engine. The code provided will convert the 3dB beamwidth provided by the user into Gaussian beamwidth and will calculate the excess attenuation due to vegetation at a given vegetation depth as a loss in dB.

3.8.4.4 The attenuation due to scatter through the vegetation, L_{scat}, is then given by:

$$L_{scat} = -10\log_{10}\left(\frac{P_R}{P_{\max}}\right) \qquad \textit{Equation 3-21}$$

where $\frac{P_R}{P_{\max}}$ is defined in Equation 3-7.

3.8.5 Combination of the individual components

3.8.6 The total loss, L_{total}, experienced by a signal propagating through trees is then given by the combination of loss terms:

$$L_{total} = -10\log_{10}\left\{10^{\left(\frac{-L_{sidea}}{10}\right)} + 10^{\left(\frac{-L_{sideb}}{10}\right)} + 10^{\left(\frac{-L_{top}}{10}\right)} + 10^{\left(\frac{-L_{ground}}{10}\right)} + 10^{\left(\frac{-L_{scat}}{10}\right)}\right\} \qquad \textit{Equation 3-22}$$

3.9 Model Validation

3.9.1.1 The model was tested by comparing the results of the measurement made at Twyning Nursery on a line of London Plane trees (*Platanus hispanica Muenchh*), as depicted in Figure 3-41.

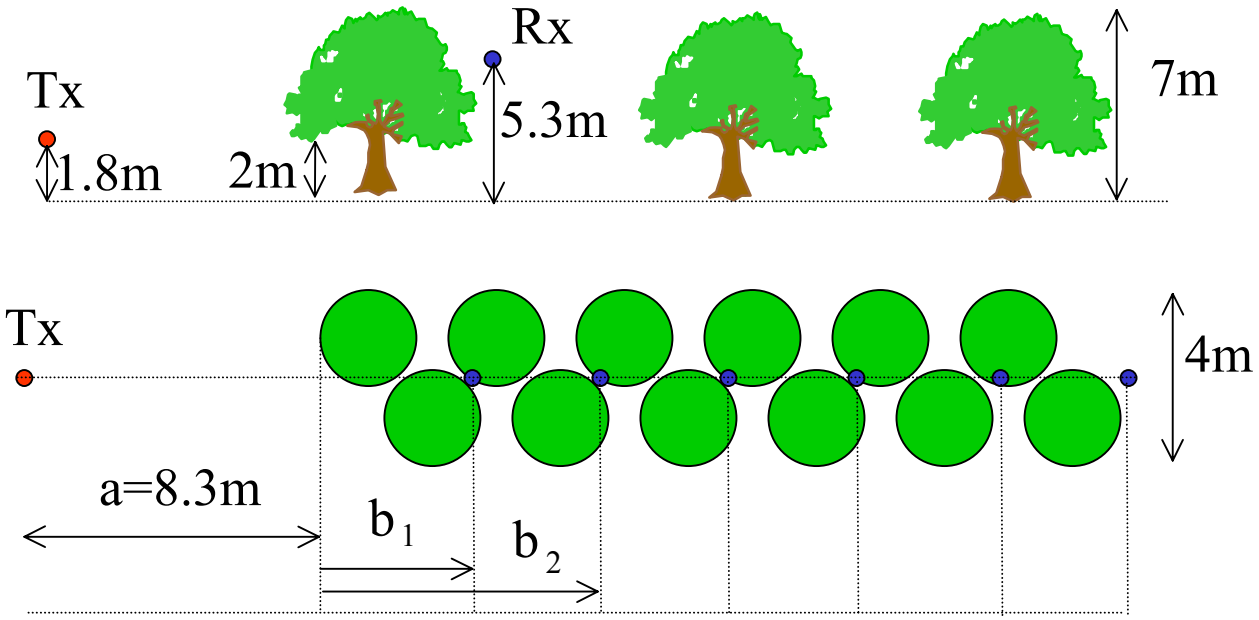

Figure 3-41 Geometry for London Plane measurement

3.9.1.2 The measured results consisted of 490 points, for 10 different vegetation depths at 49 frequencies ranging from 400MHz up to 18GHz. A full implementation of the model described in section 3.11 was made for each of the receiver locations and frequencies, including side-diffracted component, the top-diffracted component, the ground reflected component and the through or scattered component. This data was chosen as a reasonable test set as it had not been used for obtaining the RET parameters, and therefore any fit obtained would not be biased towards the new generic model.

3.9.1.3 Figure 3-42 shows each of these modelled components, compared with the average measured attenuation for the whole record of data. Here the record numbers 1-49 represent the measured attenuation for frequencies 18 – 0.4 GHz after the first tree, record numbers 50-98 represent that for frequencies 18 – 0.4 GHz after the second tree and so on. One can see that the average measured attenuation generally agrees with the total predicted loss, which is for the most part dominated by the scatter term, and occasionally by the ground-reflected term.

3.9.1.4 Figure 3-47 shows the total modelled loss and the modelled side-diffracted component compared with the measured average, maximum and minimum loss. The maximum measured loss is generally between the predicted scatter loss and the predicted ground reflection loss and appears to be capped by the side-diffracted component. One should note that where the maximum measured attenuation rose above the equivalent noise floor attenuation, the attenuation is shown as zero (though these points were then neglected in any further comparisons, such as the calculation of the RMS discrepancy).

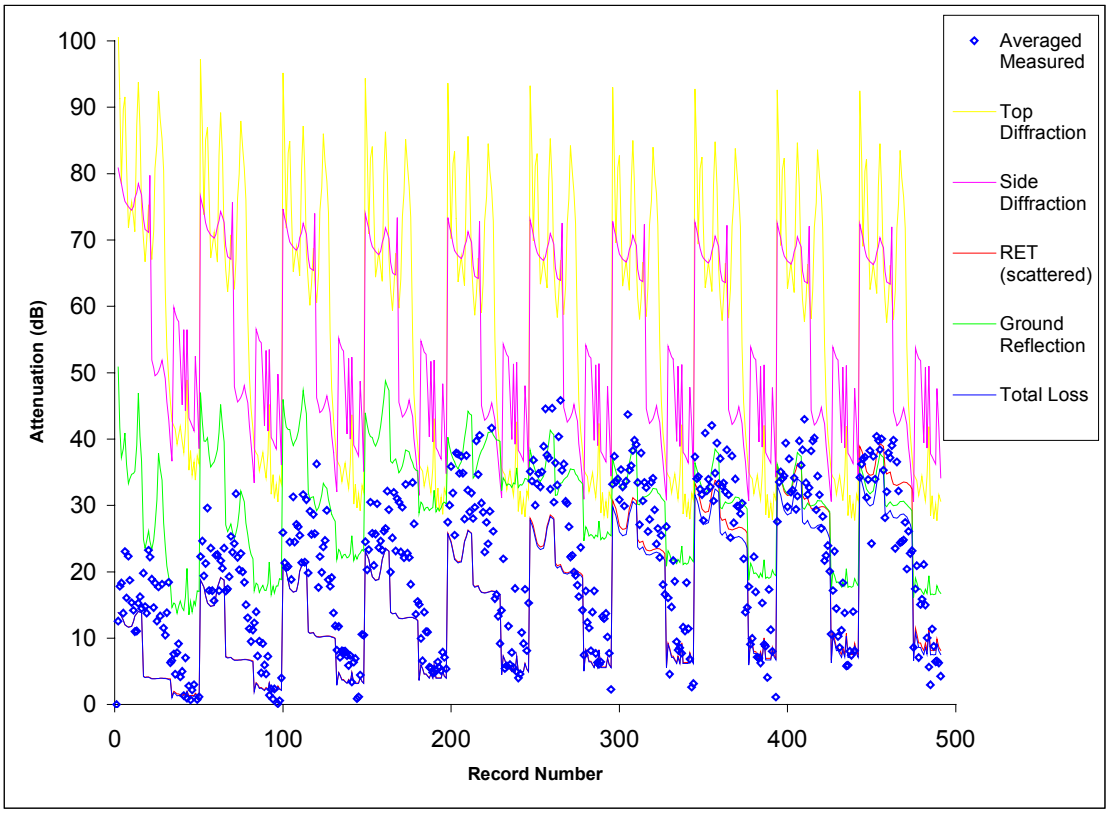

Figure 3-42 Modelled components compared with full measurement record

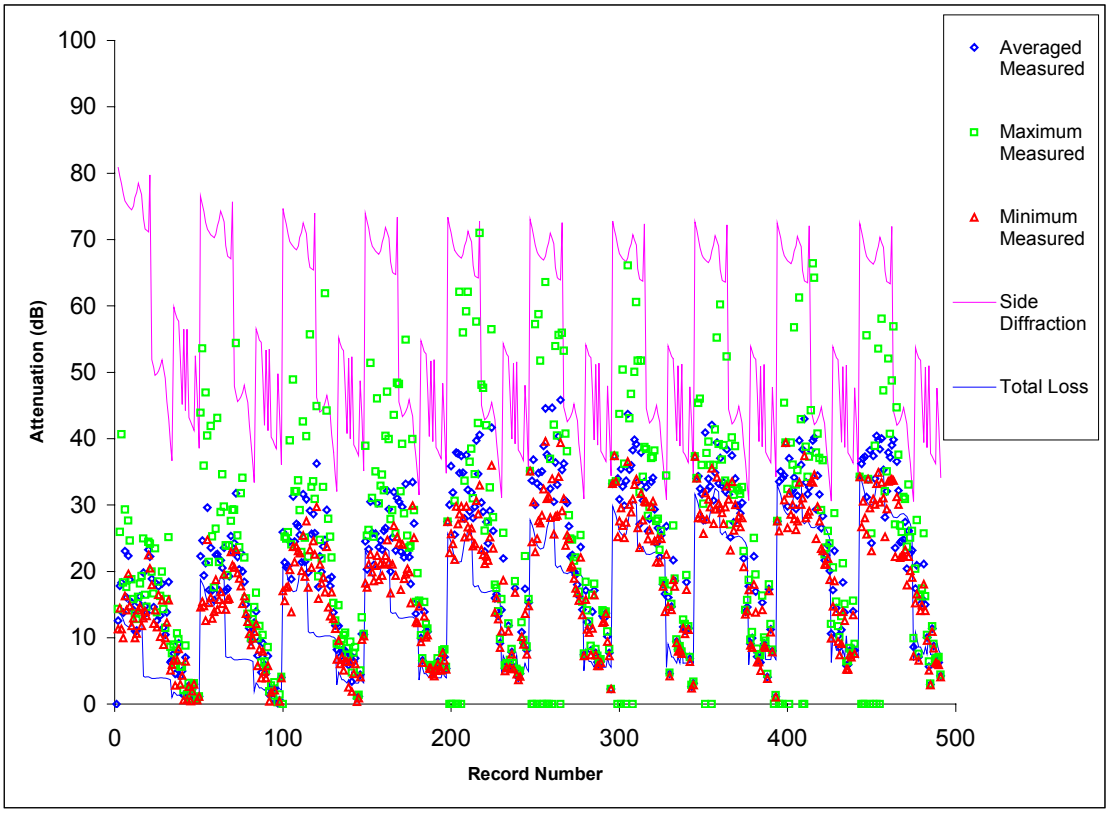

Figure 3-43 Modelled components compared with full measurement record

3.9.1.5 In order to give a comparative test of the performance of the new generic model, the measured results for this dataset were also compared with an implementation of the current

ITU-R Recommendation on vegetation attenuation [ITU-R, 2000]. The results, for the whole series of data, are shown in Figure 3-44.

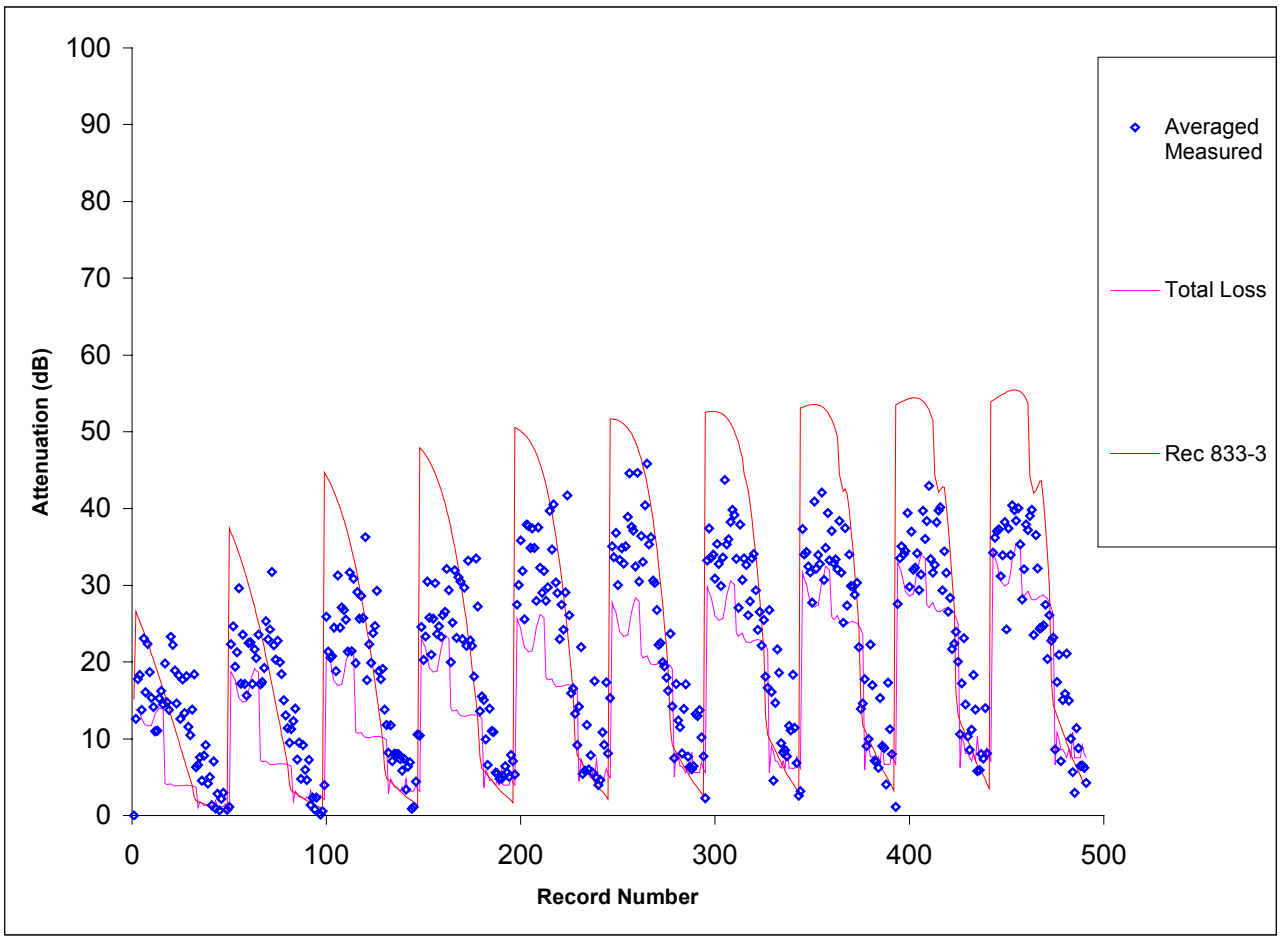

Figure 3-44 Comparison of Generic model fit to data with ITU-R Rec. 833-3

3.9.1.6 One can see that in general, the generic model presented gives a better fit, as the ITU-R model tends to follow the predicted diffraction attenuation, particularly at the higher frequencies. The advantage of the generic model, for this measurement at least, appears to be the inclusion of the ground reflected component. This improvement is borne out by making a comparison of the root mean squared (RMS) discrepancy as a measure of the fit of each model to the data. The RMS discrepancy between the generic model and the 490 measured data points was 8.38 dB, whereas that for the ITU-R 833-3 model was 11.51 dB.

3.10 Discussion

3.10.1 Model limitations and Future work

3.10.1.1 The Generic model presented here is based on data obtained within a limited timescale. Also, in spite of the fact that many measurements were made, it was found during the project that only a subset of these measurements gave usable data in terms of obtaining the scatter function parameters. As a result, the table of RET parameters fitted to the data are limited in extent and further values will be required to cover different species and frequencies with greater accuracy. Where the radio planner wishes to predict the loss through a species not tabled in the RET parameter tables, the required values may be

interpolated from the values present (as was done in the model testing). Where precise input parameters are required and effort is available, an experimental method for obtaining these values has been provided, in which the values obtained can then be used to further populate the tables, and therefore evolve the model.

3.10.2 Channel Dynamics

3.10.2.1 The generic model was developed by fitting to a large database of measurements. Despite the fact that many of these measurements were obtained by using wideband equipment, the model itself was fitted only to narrowband data (ie measured narrowband, or a single bin of wideband data) and the model is therefore strictly valid for the narrowband channel. Some case studies of the wideband effects are presented in Section 4.2, and suggest that the model may yield a reasonable average attenuation for a given path through vegetation, but the attenuation may not necessarily be flat across the wideband channel. Thus, care should be taken when implementing the model to simulate the effects of vegetation on wideband systems.

3.10.2.2 In addition to the wideband effects, the effect of the through-vegetation path on the narrowband signal can vary dramatically with transmitter / receiver location and also with time, since the trees are not static. Indeed, the branches will move to a large extent in windy conditions. Figure 3-45 - Figure 3-52 show the narrowband channel dynamics in terms of several time series for three tree types (one in and out of leaf, the other two in leaf), for the case of a single tree depth and paths through deep vegetation, at a range of frequencies.

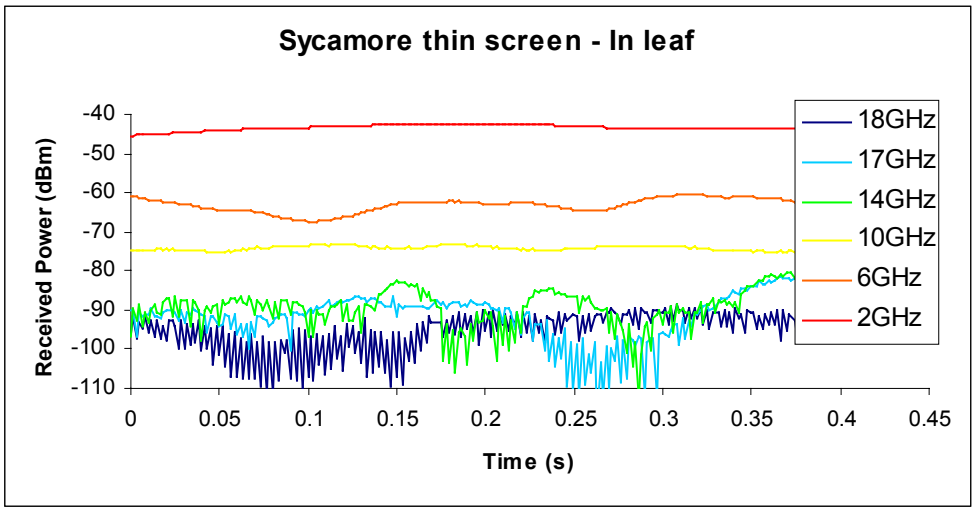

Figure 3-45 Received power as a function of time through 4m of Sycamore (in leaf)

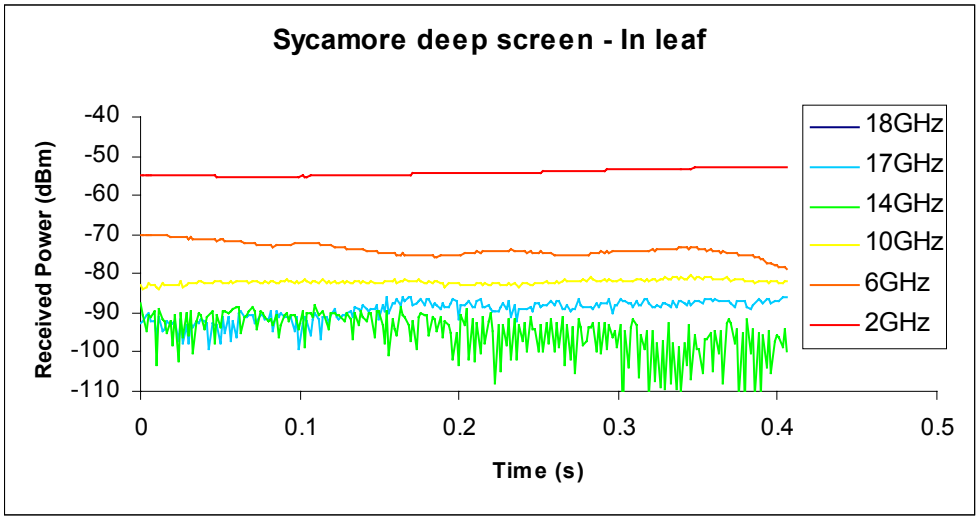

Figure 3-46 Received power as a function of time through 42m of Sycamore (in leaf)

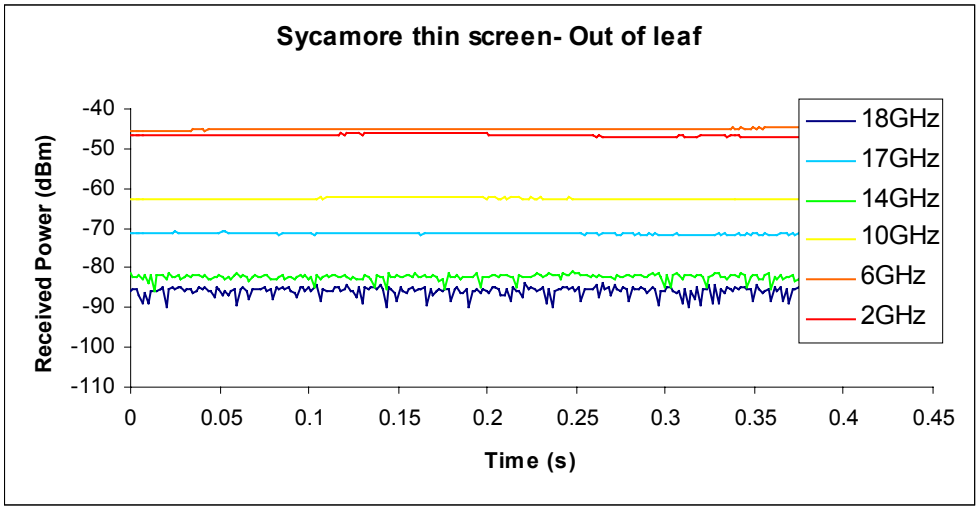

Figure 3-47 Received power as a function of time through 4m of Sycamore (out of leaf)

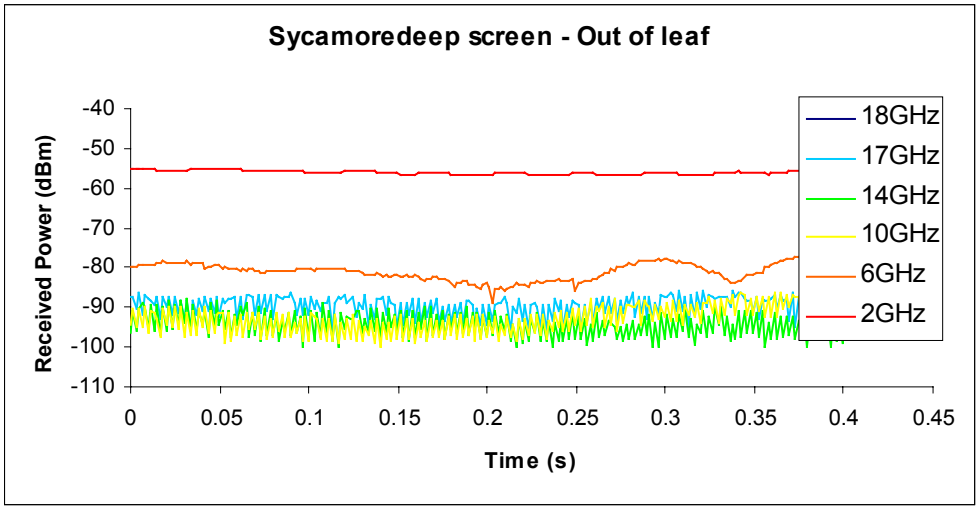

Figure 3-48 Received power as a function of time through 42m of Sycamore (out leaf)

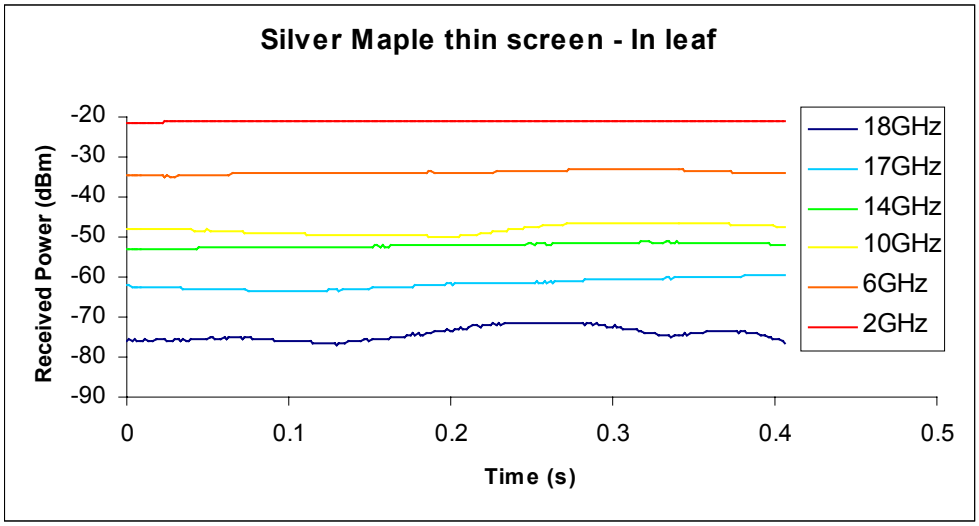

Figure 3-49 Received power as a function of time through 5.2m of Silver Maple (in leaf)

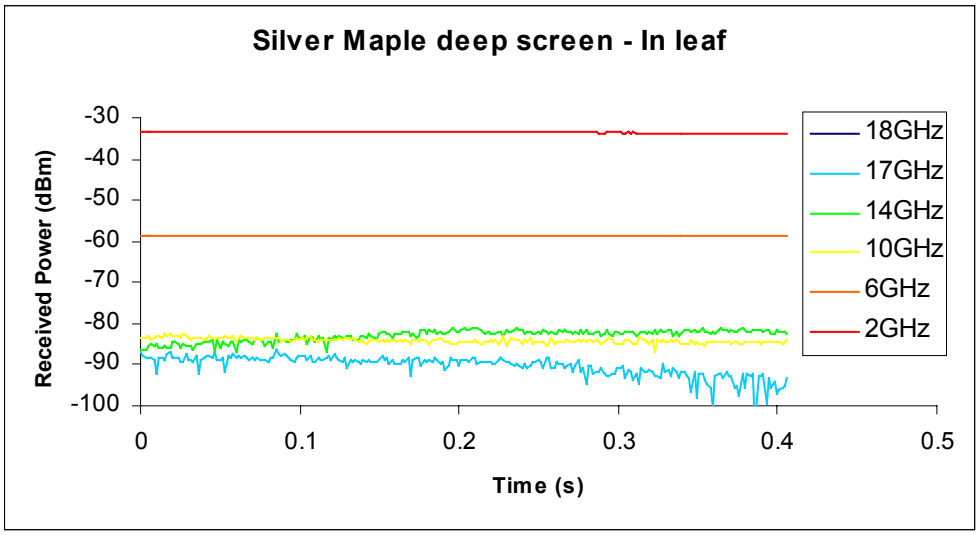

Figure 3-50 Received power as a function of time through 41.1m of Silver Maple (in leaf)

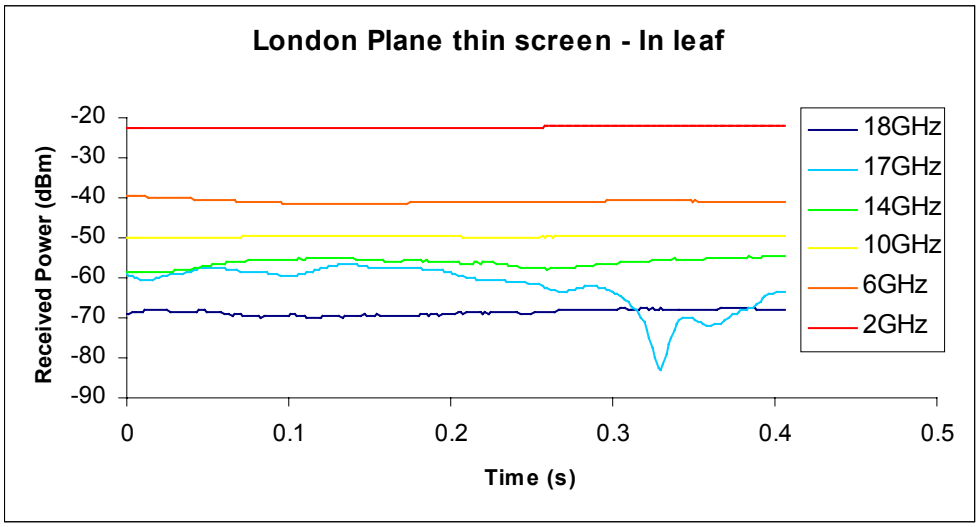

Figure 3-51 Received power as a function of time through 4.9m of London Plane (in leaf)

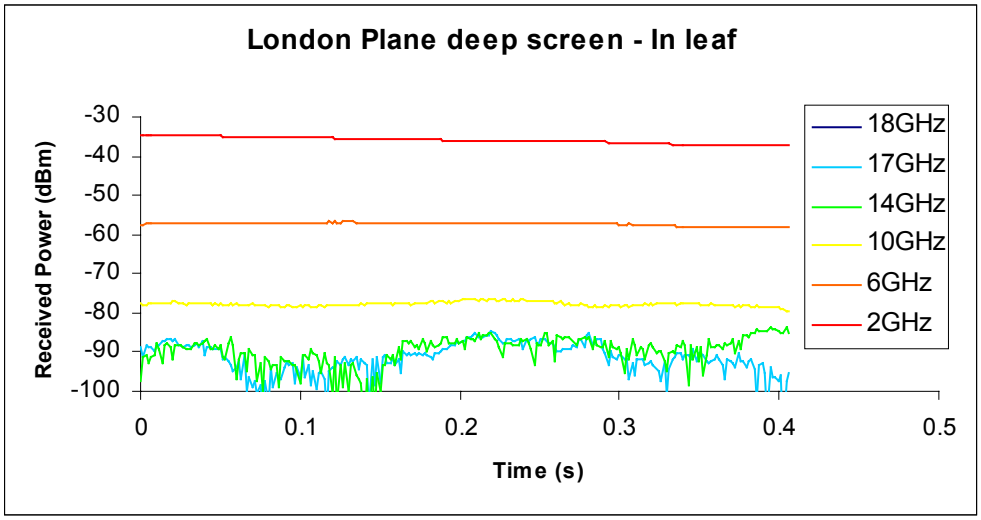

Figure 3-52 Received power as a function of time through 41.7m of London Plane (in leaf)

3.10.3 One can see that the received power can vary quite strongly with time, depending upon the frequency, and vegetation depth. One should note that a value of attenuation predicted by the generic model is given as an average signal level, and the level may well exhibit deep nulls over short timescales (~ 10s of ms) and over seasonal variations.

3.10.4 The measurements database contains some account of this variability, given in terms of measured maxima and minima, together with the standard deviation.

4 Analysis of Wideband Measurements

4.1 Introduction

4.1.1.1 The narrowband model must take into consideration the geometry of the radiowave propagation path. Depending on the geometry, the received signal may be composed of direct or line-of-sight (LOS), scatter, refracted or diffracted components. A combination of these components may result in an enhanced received signal level, although their interaction may also render a signal unintelligible if used for communication purposes. The aim of the wideband measurements in the development of the narrowband model is to identify these multipath components, characterise them (based on the measurement site geometry) and assess their effect on the quality of the received signal.

4.1.1.2 The wideband measurements have also been used to assess the dominant propagation paths at each measurement site. This ensures that the characteristics identified are not unique to that site, which may be caused by interfering multiple waves, but are characteristics of any radiowave propagating through foliage.

4.1.1.3 To date, studies and narrowband development have been based purely on narrowband data, without any wideband analysis conducted at the site. The wideband analysis is necessary to explain any unexpected irregularities that may occur in the measurement data and to verify that what is being measured is the excess attenuation of a radiowave through foliage and not a combination of LOS, diffracted, reflected and scattered waves.

4.1.2 Measurement System, Data Processing and Analysis

4.1.2.1 The channel sounder transmits a 31 MHz bandwidth signal simultaneously at three carrier frequencies; 1.3, 2 and 11 GHz [Austin et al. 1997]. However, only one frequency can be received at any one time. The transmitter and receiver systems are shown in Figure 4-1 and Figure 4-2.

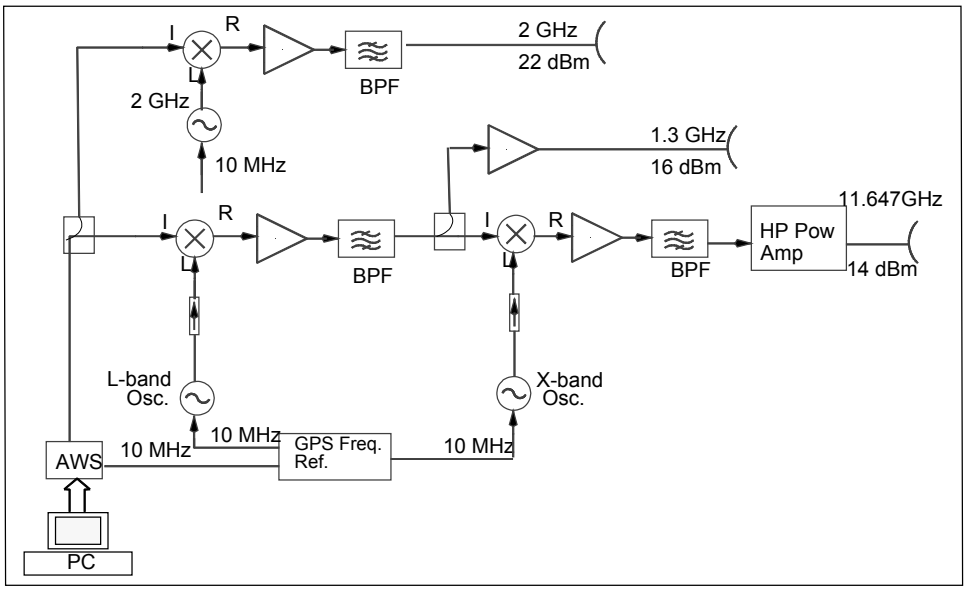

Figure 4-1 Wideband 1.3GHz, 2GHz and 11.647GHz Transmitter

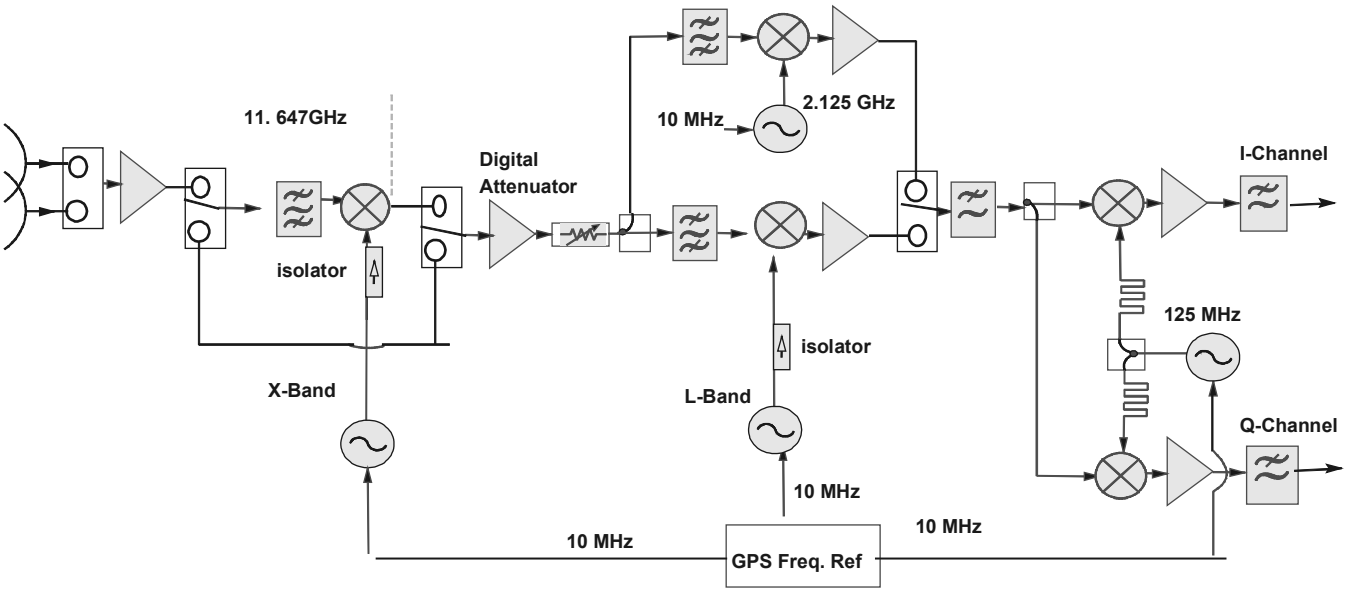

Figure 4-2 Wideband 1.3GHz, 2GHz and 11.647GHz Receiver

4.1.2.2 The University of Portsmouth and RAL shared a common receiver front-end when measurements were done at the same time. At the input, the receiver system was switched depending on frequency to be measured. The receiver sensitivity was approximately -90dBm. The antennas used were all vertically polarised and included:

- An X-band horn (18º beamwidth) for 11GHz transmission and a 20º beamwidth Angus horn for 11GHz reception.
- Patch array antenna with a beamwidth of 40º at 2GHz transmission and the Angus horn (70º beamwidth) at the receiving end.
- Yagi loop array antennas for both transmission and reception at 1.3 GHz (18º beamwidth).

4.1.2.3 The measured channel transfer functions (TF) were averaged 128 times. The averaged 128 TFs were all captured in 1 ms and a channel snapshot was taken at every 33 ms time interval. During processing, the measured transfer function was calibrated to remove the system response. The transfer functions were then fed to the Portsmouth software based on the Singular Value Decomposition–Prony (SVDP) algorithm that fits the multi-ray model and estimates the discrete channel impulse response, Figure 4-3, [Lau et al. 1991]. 128 channel impulse responses measured in 4.29s were super-imposed to obtain the channel delay power spectrum (DPS). The delay spread and the frequency correlation function (FCF), from which the coherence bandwidth is calculated, was then computed from the DPS. The signal levels used in this report is the signal level of a single spectral line that has been extracted from the received signal bandwidth.

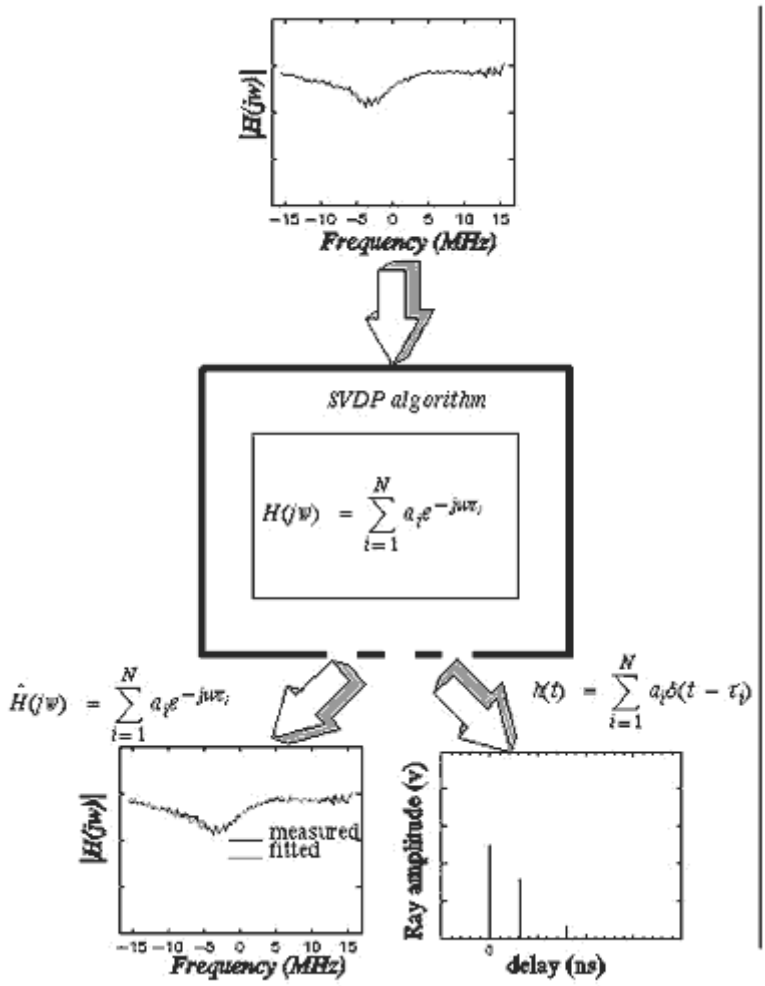

Figure 4-3 Multipath Signal Component Estimation using the SVDP Algorithm

4.1.2.4 The multipath statistic that has been used to give an assessment of the channel quality for a wideband communication system is RMS delay spread. RMS delay spread gives an indication of the time spread of the signal due to multipath propagation, and hence can give an idea of the severity of the intersymbol interference. It is defined as the square root of the second central moment of the delay power spectrum, $\rho(\Delta\tau)$, occupying the range (τ_0, τ_1),

$$T_s = \sqrt{\frac{1}{P}\int_{\tau 0}^{\tau 1}(\iota - \tau_{mean})^2\,\rho(\Delta\tau)d\tau} \qquad \textit{Equation 4-1 Calculation of RMS Delay Spread}$$

where $P = \int_{\tau 0}^{\tau 1}\rho(\Delta\tau)d\tau$ is the total power, $\tau_{mean} = \frac{1}{P}\int_{\tau 0}^{\tau 1}\tau\rho(\Delta\tau)d\tau$ is the average delay and $\rho(\Delta\tau)$ is the delay power spectrum. A rule of thumb is that the bit error rate (BER) of a system will be less than 10^{-3} if the rms delay spread is less than 0.2 of the symbol duration [Rappaport and Sandhu, 1994].

4.1.2.5 The impulse response estimation plots that are presented in this report show the evolution of the impulse response at one position over a period of four seconds, Figure 4-4(a), and the relative amplitudes from one snapshot in that evolution plot, Figure 4-4(b).

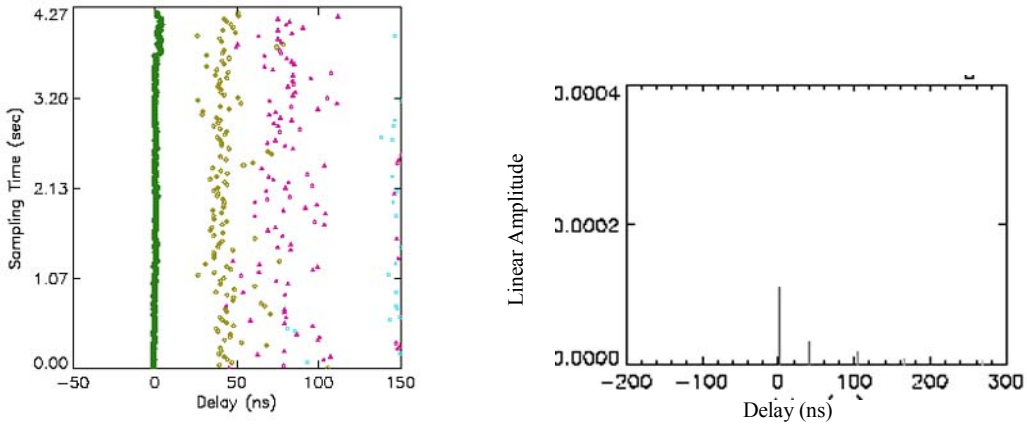

(a) (b)

Figure 4-4 (a) Example of the Evolution of Impulse Response with Time and (b) Single Snapshot of the Estimated Impulse Response at any Site

4.1.2.6 Figure 4-4(a) shows the evolution of the channel impulse responses over a 4-second duration. Each snapshot is estimated from one measured transfer function and the time between each consecutive snapshot is 33ms. Each dot on the graph represents one impulse. The size of the dot indicates the strength of the impulse, the larger the dot the stronger the impulse and the colour indicates the position that the impulse is received. For example in Figure 4-4(a), green indicates the strongest ray received, yellow the second strongest, purple the third and blue the fourth. Figure 4-4(b) shows the relative amplitudes of these impulses. The y-axis represents the linear amplitude of each ray and on both plots the x-axis is the delay time in nanoseconds.

4.2 Case Studies

4.2.1.1 Although wideband measurements were conducted at all of the sites, only four have been chosen for phenomenological analysis. The analysis of the wideband data was done in comparison with the narrowband data that was calculated by extracting a single spectral line from the measured wideband signal. The sites selected were: Twyning Nursery (London Plane, Silver Maple and Common Lime) and Fermi Avenue (Horse Chestnut). In-leaf and out-of-leaf measurements have been conducted at all of the Twyning Nursery sites, but only in-leaf measurements were conducted at Fermi Avenue. *The excess attenuation due to foliage has been calculated by subtracting the free space losses and normalising to zero at zero foliage depth*. Low antenna heights and a short distance between antennas meant that ground reflection were regularly observed which could be identified from the wideband measurements.

4.2.2 Twyning Nursery – London Plane

Tree Type:	London Plane
Tree Height:	6m
TX Height:	3.5m
RX Height:	3.5m
TX Antennas:	X-Band horn(11GHz), patch array(2GHz), loop array(1.3GHz)
RX Antennas:	Angus horn(11GHz and 2GHz), loop array(1.3GHz)

4.2.2.1 The trees at this site were planted in single rows at regular intervals and they were all immature. Due to the shape of the measurement geometry, diffraction over and around the side of the trees was expected to be significant. In addition, scattered power and reflections from adjacent rows of trees of different species was expected too. A picture of the measurement site, Figure 4-5(a), shows the line of trees where the measurements were carried out (the row to the left side of tyre tracks). The measurement site geometry is shown in Figure 4-5(b), the blue line shows the movement of the receiver. At each measurement point the receiver was put in between the trees, in line with the tree trunks.

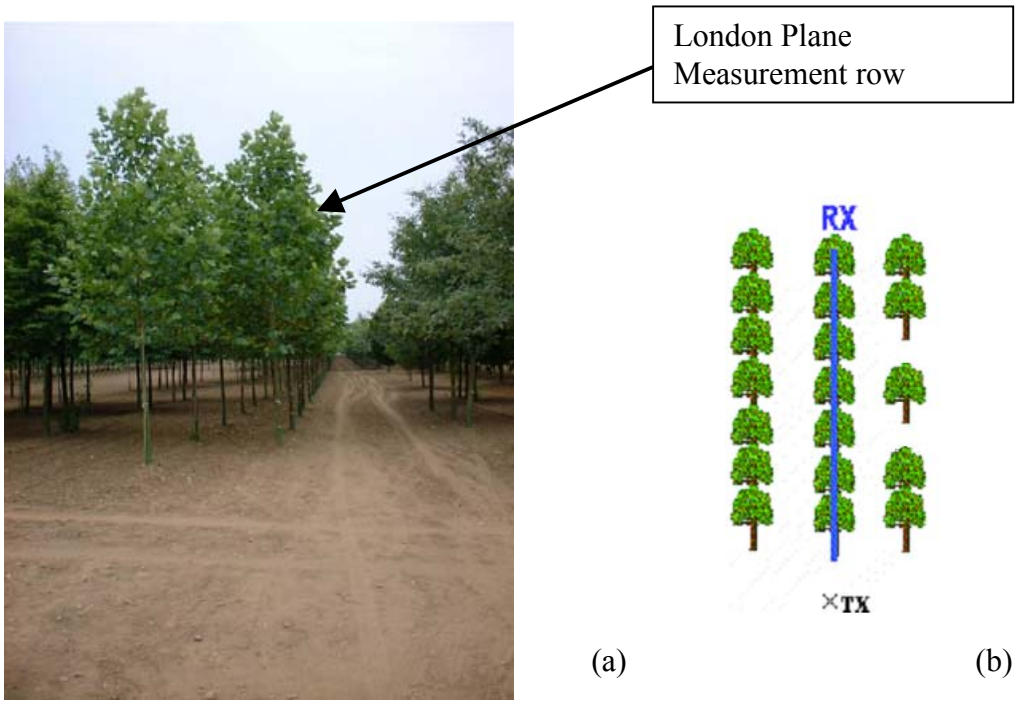

Figure 4-5 London Plane (a) Picture of Experimental Set-up. (b) Measurement Geometry

4.2.2.2 The line of trees to the right hand side of the London plane, had gaps without trees at 30m and 50m. The estimated impulse response showed that the signal power of the second component increased significantly at these points.

4.2.2.3 The graph of excess attenuation as a function of foliage depth, Figure 4-6 and Figure 4-7, shows that excess attenuation due to the presence of foliage increased with frequency. All three frequencies suffered from less excess attenuation in the absence of leaves, indicating that leaves act as an attenuating medium at 1.3GHz, 2GHz and 11.647GHz. It also indicates

that the excess attenuation curve exhibits a dual slope characteristic and the initial slope is steeper with an increase in frequency.

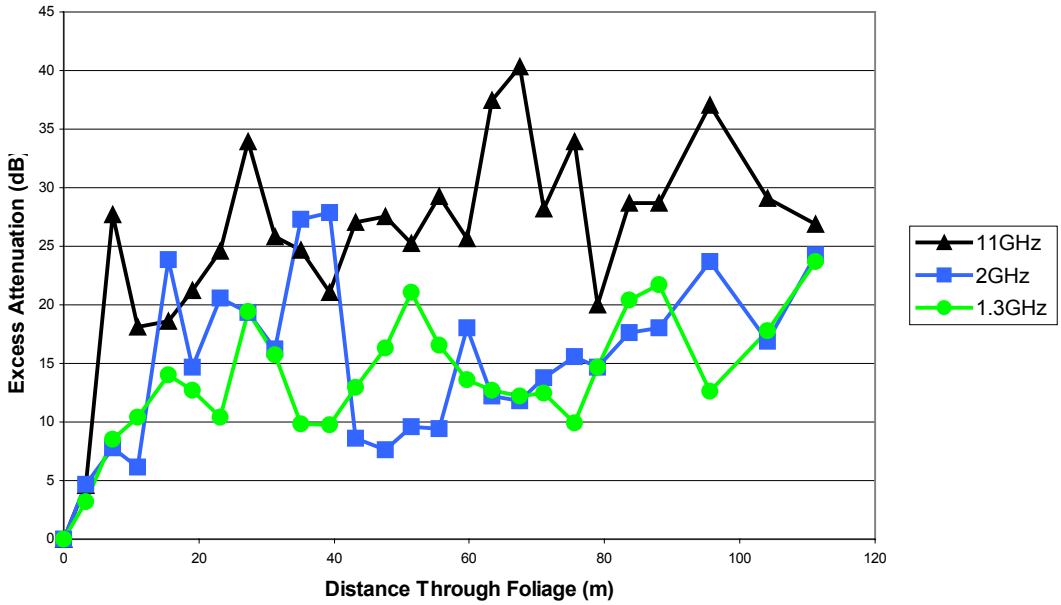

Figure 4-6 Excess attenuation as a Function of Foliage Depth (London Plane) , In-Leaf

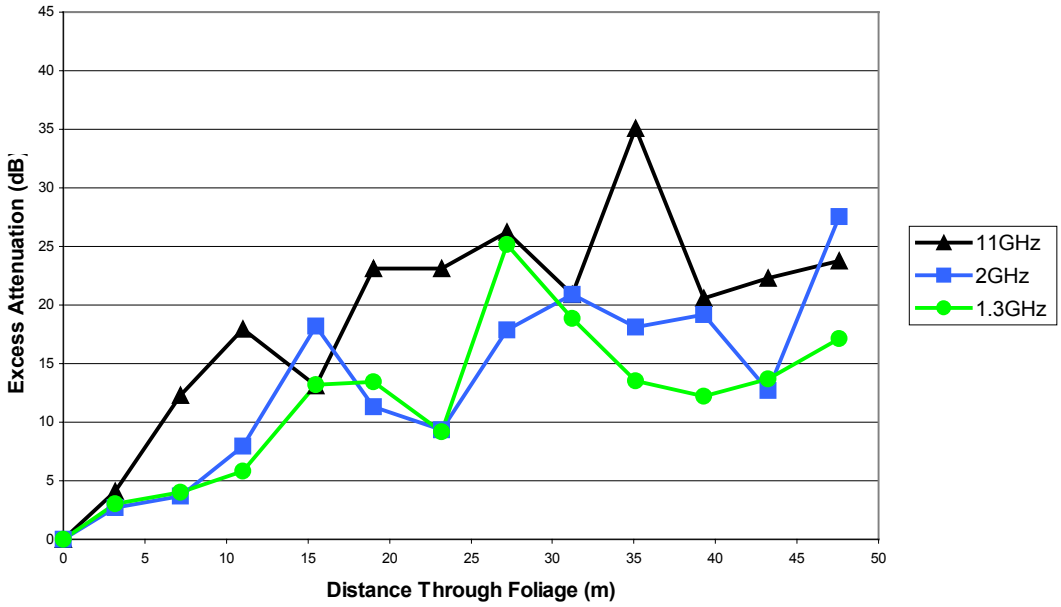

Figure 4-7 Excess attenuation as a Function of Foliage Depth (London Plane), Out-of-Leaf

4.2.2.4 The leaf size of the London plane is large and comparable with the wavelength at 2GHz (15cm), the wavelength at 11.647GHz (2.57cm) was more comparable with the branches of the trees. Although the trees had an almost random orientation of leaves and the experimental set-up was VV polarisation, the leaves had a physical dimension relative to the wavelength at L-band when viewed from any plane, so the orientation of leaves has little effect when considering them as scattering objects.

4.2.2.5 The graph of delay spread (in-leaf), Figure 4-8, shows that the 2GHz signal varies quite significantly in comparison to the other frequencies. This variation is not seen on the out-of-leaf graph, Figure 4-9. The range of time delays used to calculate the RMS delay spread was taken as 30dB below the peak of the DPS. Fluctuations in the amplitude of the strong component, as seen at this site, meant that the 30dB noise floor often goes down to include very small components that may be distributed over a wide delay range and hence explains the large variations seen in the calculated delay spread.

4.2.2.6 There is no apparent correlation between frequencies at each of the points for either delay spread or excess attenuation. The lack of correlation between frequencies for the excess attenuation graphs indicates that the variation in levels on the graphs originates from multiple components being received either in-phase (increasing signal level) or out-of-phase (decreasing signal level). As the multipath components have an amplitude that is quite high relative to the attenuated direct ray, this addition or subtraction to the signal strength can be significant. The lack of correlation between frequencies for the calculated delay spread indicates that the propagation mechanisms responsible for the presence of strong components and the strength of these components are different for each frequency.

4.2.2.7 In-leaf delay spread at 2GHz does not show a high correlation with signal level, whereas at 1.3GHz and 11.647GHz delay spread graphs show a slight correlation with the excess attenuation graphs. Out-of-leaf measurements show a fairly high correlation between excess attenuation and delay spread for all frequencies, but there is no apparent correlation between frequencies for either delay spread or excess attenuation. Delay spread is often used as a parameter for determining the quality of a wideband channel. The apparent lack of correlation between excess attenuation and delay spread indicates that although a narrowband model might predict the signal strength to be sufficient for good transmission, the scattering from leaves and reflection from other objects could render the signal useless for communication purposes.

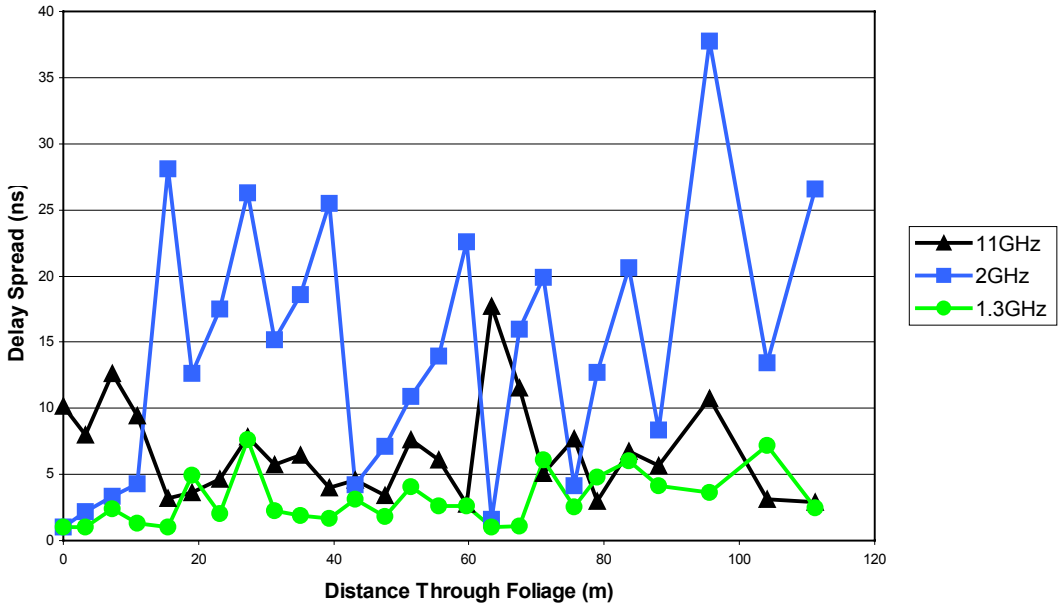

Figure 4-8 Delay Spread as a Function of Foliage Depth (London Plane), In-Leaf

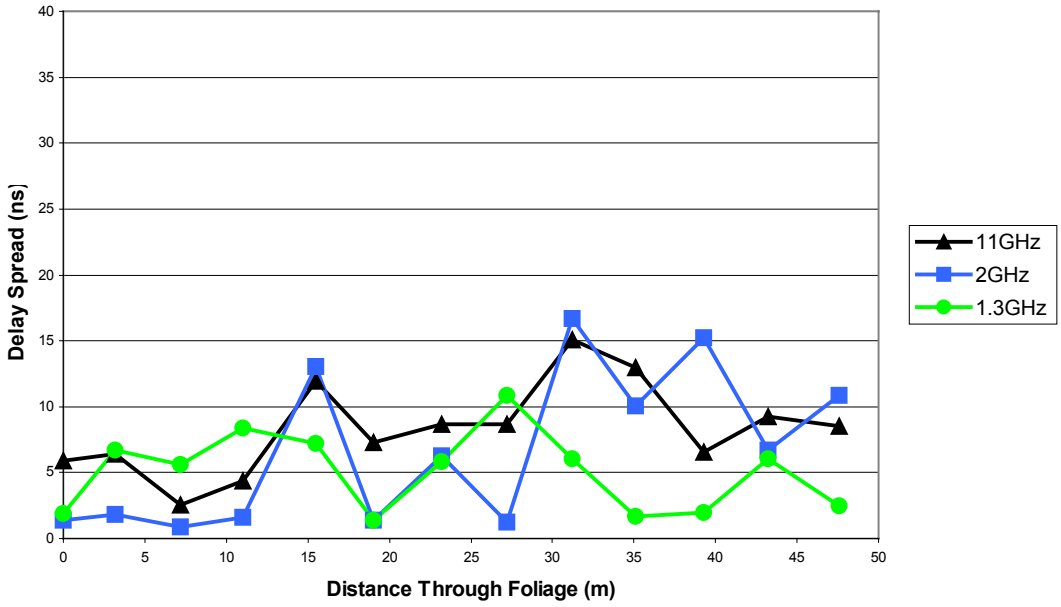

Figure 4-9 Delay Spread as a Function of Foliage Depth (London Plane), Out-of-Leaf

4.2.2.8 The impulse response estimation for the 1.3GHz in-leaf measurements typically gave a very strong second ray at approximately 10ns. In the example shown in Figure 4-10, the second ray is stronger than the first ray. It should be noted that the delay axis is normalised to the strongest component. Where the second component is stronger than the first, the first shows up as having negative delay. The first ray is the propagation of the radiowave through foliage. The second wave is a diffracted component propagating over the top or round the edges of the trees. As these diffracted paths have almost the same length, because the tree canopy is very small, they are received at approximately the same time. The example in Figure 4-10 is an extreme case and generally the first component is stronger than the second. There were also smaller rays received at between 60 and 110ns. These are thought to be scattered components and sometimes system noise. The size of the third ray was insignificant by comparison with the strongest ray and therefore has little effect on the transfer function.

4.2.2.9 A strong second ray at 10ns will give a fade in the transfer function, repeating every 100MHz. The size of the fade depends on the relative amplitudes of the first and second ray. If the first and second rays are of similar strength, the fade will be deep. Since the fading is frequency selective it is possible that measurements used for the narrowband model are sometimes conducted at nulls in the transfer function, causing more excess attenuation to be seen in the measurement and greater variations in signal strength from one position to the next.

4.2.2.10 Out-of-leaf measurements exhibited more excess attenuation of the second component. The wavelength at 1.3GHz is relatively larger in comparison to the size of the trunks and branches for this particular measurement site. Hence the direct path suffered very little excess attenuation due to the trees. A decrease in power reflected by the ground could be due to the roughness of the soil by comparison with the wavelength during the out-of-leaf measurements. It is possible that the diffracted wave over and around the trees does not exist in the out-of-leaf case. As the branches are thin and sparsely distributed, they no longer act as a surface along which a wave can propagate. A third ray was not seen in the out-of-

leaf measurements as it was in the in-leaf measurements. Individual rays were seen (very insignificant in comparison with the strongest ray) above 90 to 100ns. These are thought to be reflections of the tree trunks. In-leaf, the leaves covering the trees act as a reflecting surface (the leafs are comparable to the wavelength at 1.3GHz). Without leaves the trunks reflect the radiowaves, although their shapes and sizes do not make them very efficient reflectors, so the reflected waves are greatly attenuated.

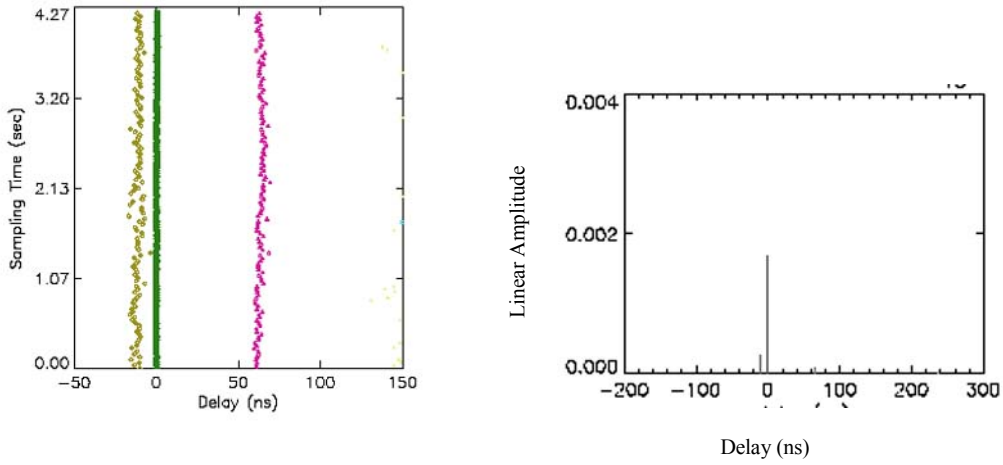

Figure 4-10 1.3GHz London Plane In-leaf at 50.1m (foliage depth 28.7m)

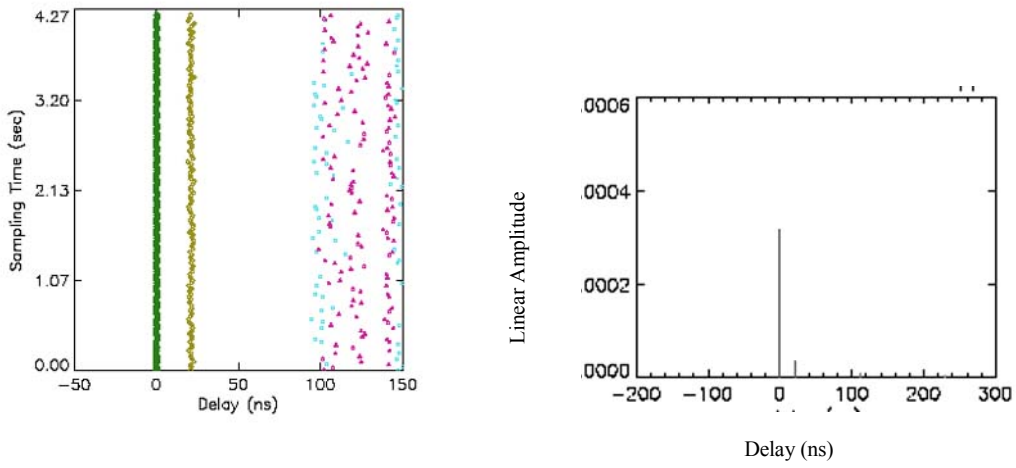

Figure 4-11 1.3GHz London Plane Out-of-leaf at 50.1m (foliage depth 28.7m)

4.2.2.11 In-leaf 2GHz measurements had consistently strong second components, relative to the amplitude of the first component, between 20 and 30ns. This was mirrored in the out-of-leaf measurements, although the out-of-leaf measurements exhibited a more attenuated second component that was less consistent in arrival time. The strong second component caused a deeper null in the transfer function and the interaction with the main ray caused more variations in received signal strength. As can be seen from the excess attenuation graphs, Figure 4-6 and Figure 4-7, especially the in-leaf measurements there are points that exhibit large variations in the received power at 2GHz.

4.2.2.12 The second ray is attributable to the reflection of the row of trees on the left hand side of the row under investigation. This row is closer than the one on the right hand side, accounting

for the smaller delay time. It may not have acted as a good reflecting surface at 1.3GHz or the channel between the two rows might have been too narrow to support propagation of 1.3GHz. The ground reflected/diffracted ray at 10ns is also noticeable for both in- and out-of-leaf, although it is not as strong as at 1.3GHz.

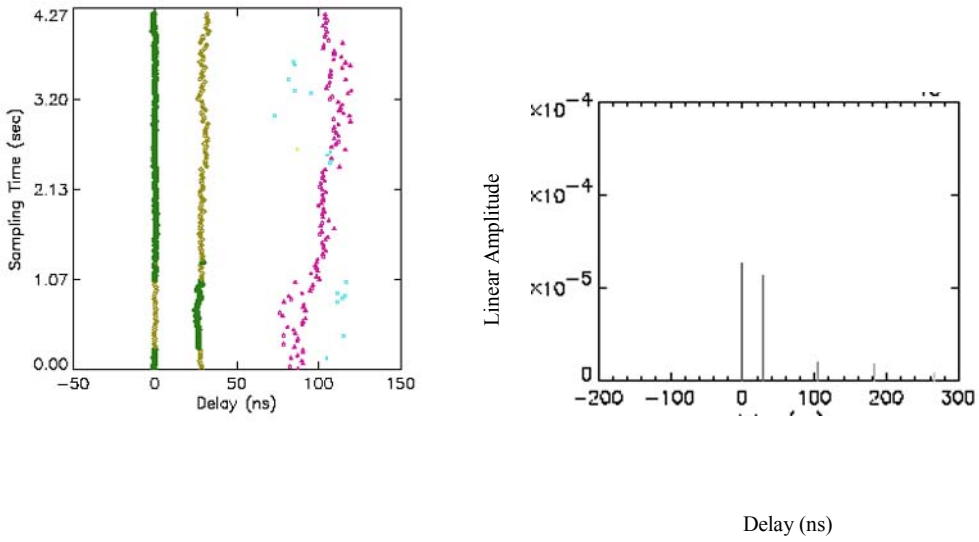

Figure 4-12 2GHz London Plane In-leaf at 50.1m (foliage depth 28.7m)

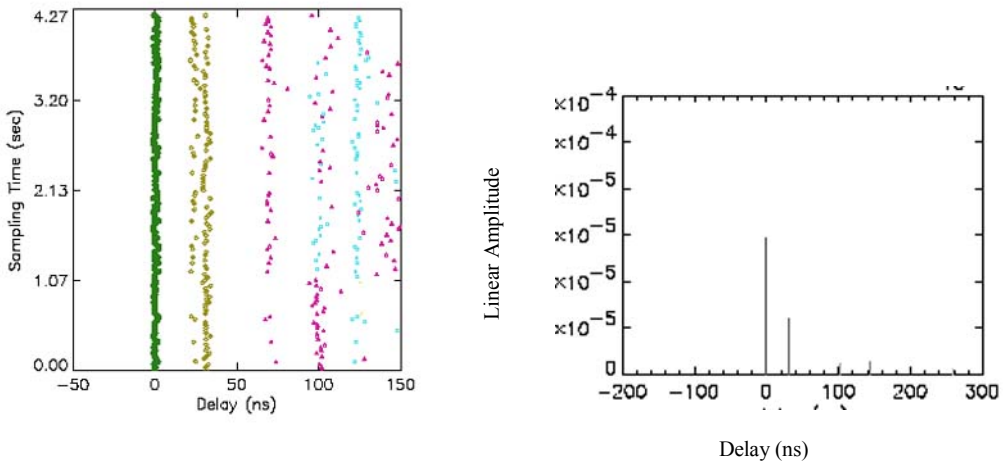

Figure 4-13 2GHz London Plane Out-of-leaf at 50.1m (foliage depth 28.7m)

4.2.2.13 11GHz did show a significant difference between in- and out-of-leaf. From the excess attenuation curves it appears that the in-leaf measurements do give a much higher excess attenuation than out-of-leaf, indicating that the leaves attenuate the 11GHz signal more considerably than 1.3GHz and 2GHz signals. Although the delay spread does not differ very much between in- and out-of-leaf measurements the impulse responses do show some differences. Out-of-leaf measurements show that the delay times and amplitudes of the components vary a lot more than for the in-leaf measurements. Most importantly it should be noted that the out-of-leaf components measured had a relatively small magnitude compared to the strongest component observed in the in-leaf measurements. This suggests

that the strong in-leaf component was due primarily to diffraction around the edge of the trees that was facilitated by the relatively "smooth" contours of these edges. However, in out-of-leaf conditions, propagation was due principally to scattering and hence, the small amplitudes.

4.2.2.14 In the out-of-leaf measurements leaves are no longer present to attenuate the waves that are scattered off the branches and trunks. More scattered waves are received and this scattering varies with wind (almost always present in winter out-of-leaf measurements) and receiver position, so the delay time and amplitudes are constantly varying. The second rays shown in Figure 4-14 and Figure 4-15 show a delay time of between 20 and 25ns, thought to be a reflection off the adjacent row of trees.

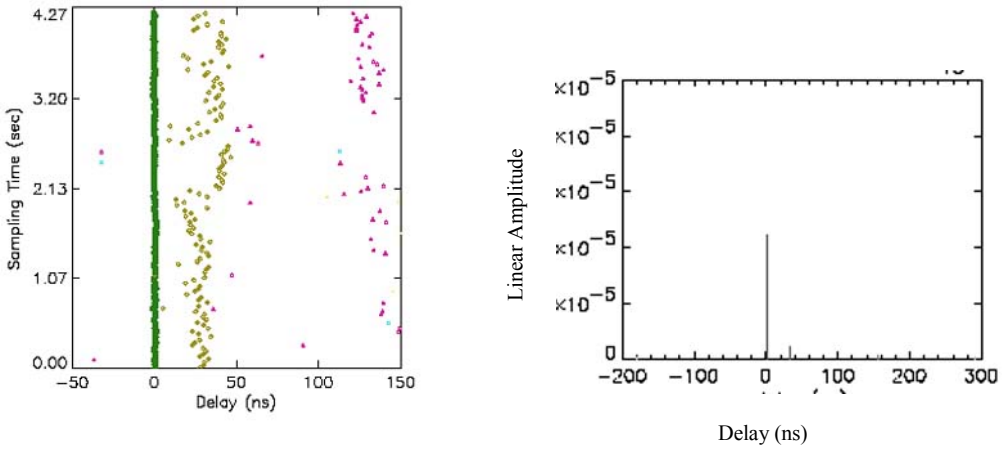

Figure 4-14 11GHz London Plane In-leaf at 50.1m (foliage depth 28.7m)

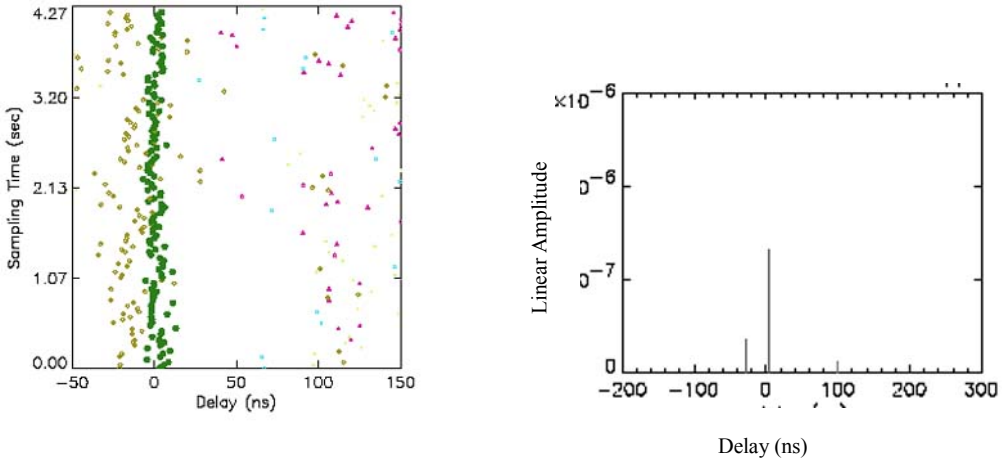

Figure 4-15 11GHz London Plane Out-of-leaf at 50.1m (foliage depth 28.7m)

4.2.3 Twyning Nursery – Silver Maple

Tree Type:	Silver Maple
TX Height:	3.5m
RX Height:	3.5m
TX Antennas:	X-Band horn(11GHz), patch array(2GHz), loop array (1.3GHz)
RX Antennas:	Angus horn(11GHz and 2GHz), loop array(1.3GHz)

4.2.3.1 The trees at this site were planted in single rows at regular intervals and they were all immature. Due to the shape of the measurement geometry diffraction over and around the side of the trees was expected to be significant. In addition, scatter power from adjacent rows of trees of different species was expected. A picture of the measurement site, Figure 4-16(a), shows the line of trees where the measurements were carried out (the row behind the yellow mast). The measurement site geometry is shown in Figure 4-16(b), the blue line shows the movement of the receiver. At each measurement point the receiver was put in between the trees, in line with the tree trunks.

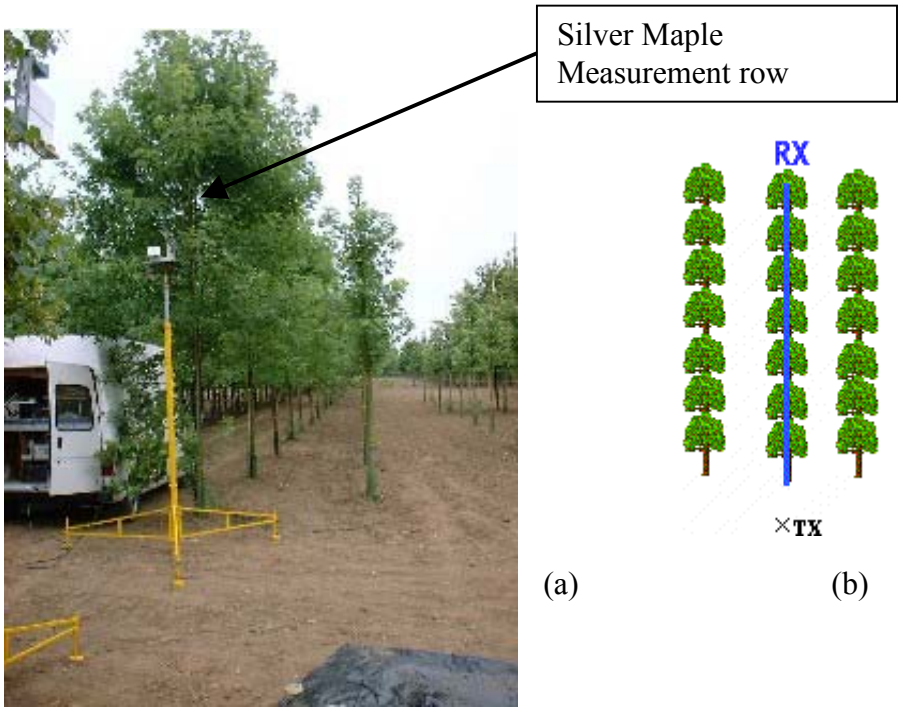

Figure 4-16 (a) Picture of the row of Silver Maple, (b) Measurement Geometry

4.2.3.2 The excess attenuation curves, Figure 4-17 and Figure 4-18, for the silver maple show 11GHz to have a significantly larger excess attenuation than 1.3GHz and 2GHz for the in-leaf measurements. In the out-of-leaf measurements 11GHz suffers from a significant decrease in excess attenuation whereas 1.3GHz and 2GHz appear to suffer an increase in excess attenuation, in comparison to the in-leaf measurements. Both in- and out-of-leaf measurement excess attenuation graphs exhibit a dual slope curve, with out-of-leaf

measurements having a much steeper initial curve than in-leaf for 1.3GHz and 2GHz. The absence of leaves that offer a smooth surface for diffracted components could explain the increased excess attenuation for out-of-leaf measurements at 1.3GHz and 2GHz. As was the case with the London Plane, the received signal is due primarily to scattering. The long branches of the Silver Maple mean that the receiver antenna was often among branches. That meant that the received signal, especially at 11GHz, was composed of scattered components and severely attenuated diffraction path in the presence of leaves. However, in out-of-leaf measurements, any diffracted component was much stronger than in in-leaf measurements resulting in a much lower excess attenuation at 11GHz. At 1.3GHz and 2GHz excess attenuation of the diffracted component was small resulting in much stronger overall signal strength. In the absence of leaves, the diffracted component was absent due to the lack of a dense volume with "smooth" surfaces conducive for diffraction. Hence the received components are primarily due to scatter by tree branches and trunks.

4.2.3.3 This could be due to the fact that the receiver was facing the transmitter in line with the tree trunks and with no reflective surfaces (leaves) the signal was not reflected back towards the receiver. This might be the case as the leaves had a size similar to the wavelengths at 1.3GHz and 2GHz and were therefore going to reflect and scatter some of the radiowave energy. The diffracted wave was not as powerful in the out-of-leaf case so the most significant wave was the LOS wave propagating through the tree trunks. As the receiver was so close to the trunks, they sometimes shadow it. After a few positions the radiowave could be received by diffracted and reflected paths.

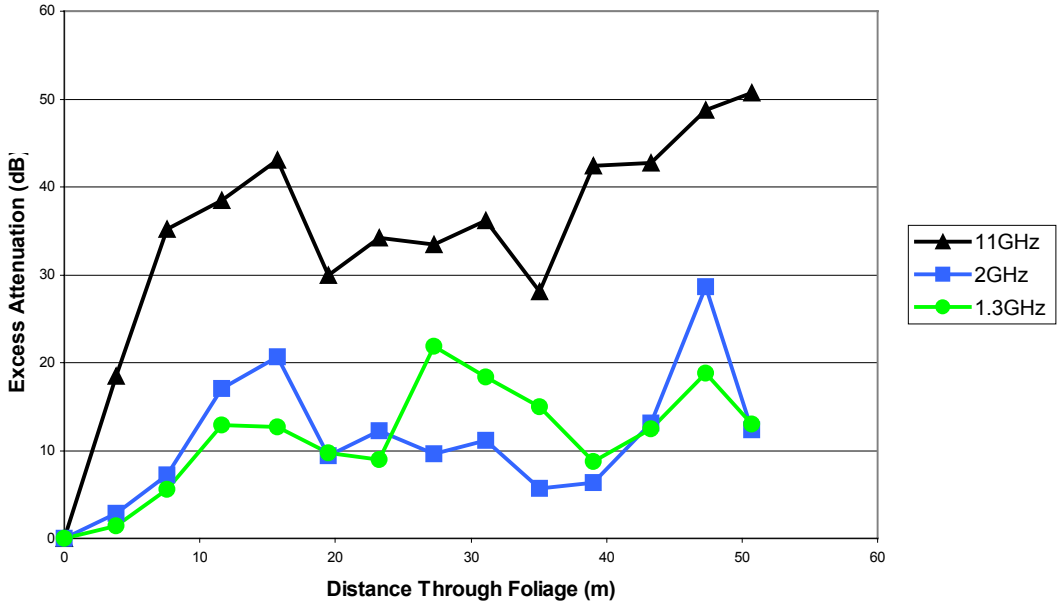

Figure 4-17 Excess attenuation as a Function of Foliage Depth (Silver Maple), In-Leaf

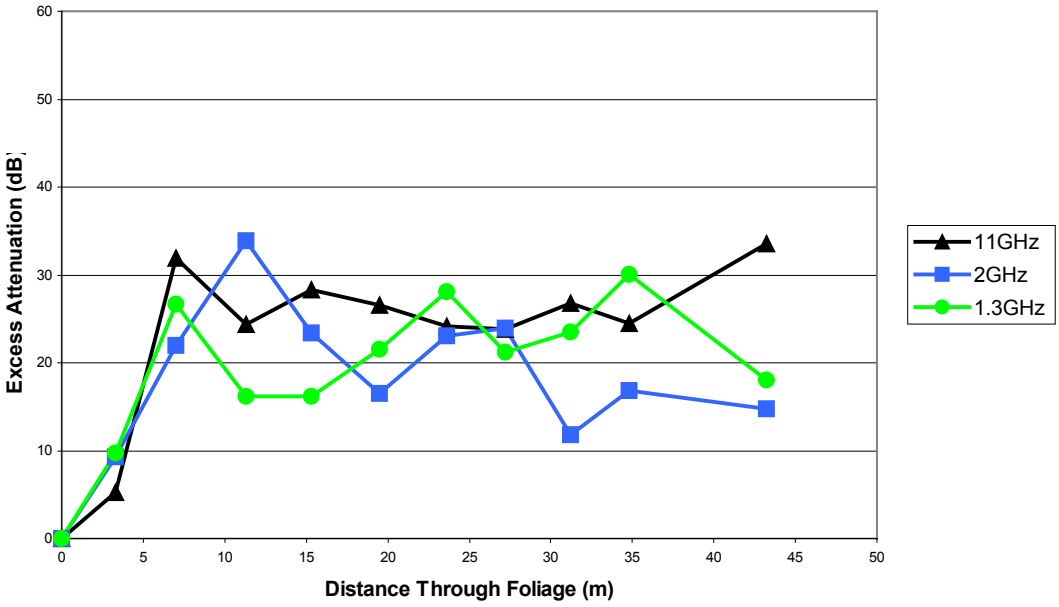

Figure 4-18 Excess attenuation as a Function of Foliage Depth (Silver Maple), Out-of-Leaf

4.2.3.4 There is a large increase in the delay spread, Figure 4-19 and Figure 4-20, for both 2GHz and 11GHz, and a significant change in the amount of variation at these two frequencies, with the out-of-leaf measurements compared with the in-leaf measurements. In the out-of-leaf case there are no leaves to attenuate any scattered or reflected signal, so more scattered power is received increasing the delay spread. At 11GHz and 2GHz there are more objects that are a size relative to the wavelength (branches and trunks). The in-leaf 11GHz measurements also exhibit a large increase in delay spread at the last two points of the measurements, at a large foliage depth. This is when the received components change from coherent to incoherent waves and the received signal is dominated by forward scatter.

4.2.3.5 The peaks in the 2GHz delay spread, Figure 4-20, at 24m and 31m are due to 2 components being received with equal strength at approximately 10ns delay. This would cause a big increase in the delay spread and the possibility of a big increase in excess attenuation. A large increase in excess attenuation is not seen because the frequency spectral line taken as a representation of the signal level was far from the null formed from the reception of the two components.

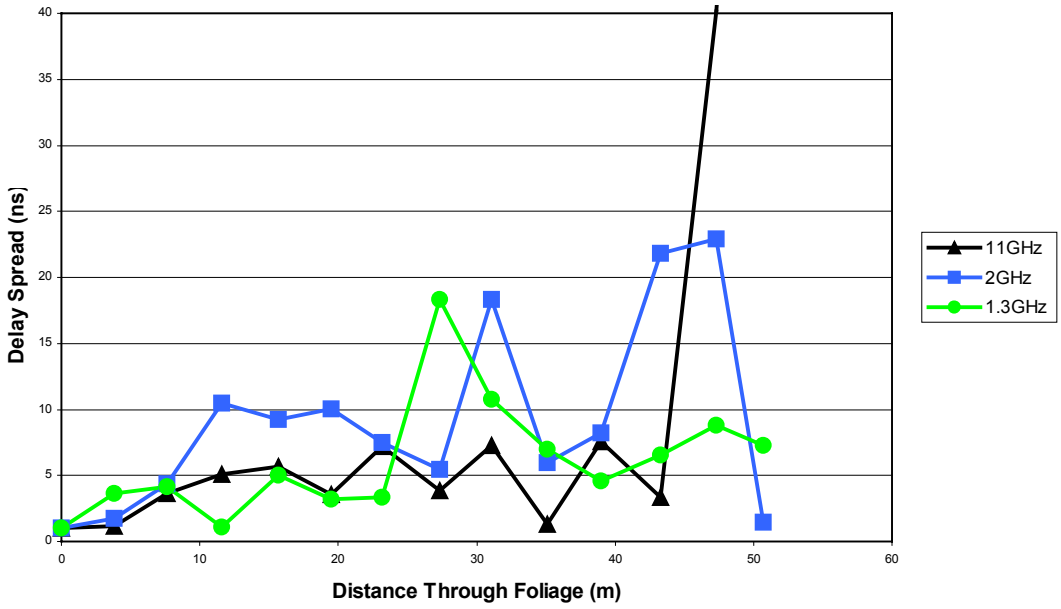

Figure 4-19 Delay Spread as a Function of Foliage Depth (Silver Maple), In-Leaf

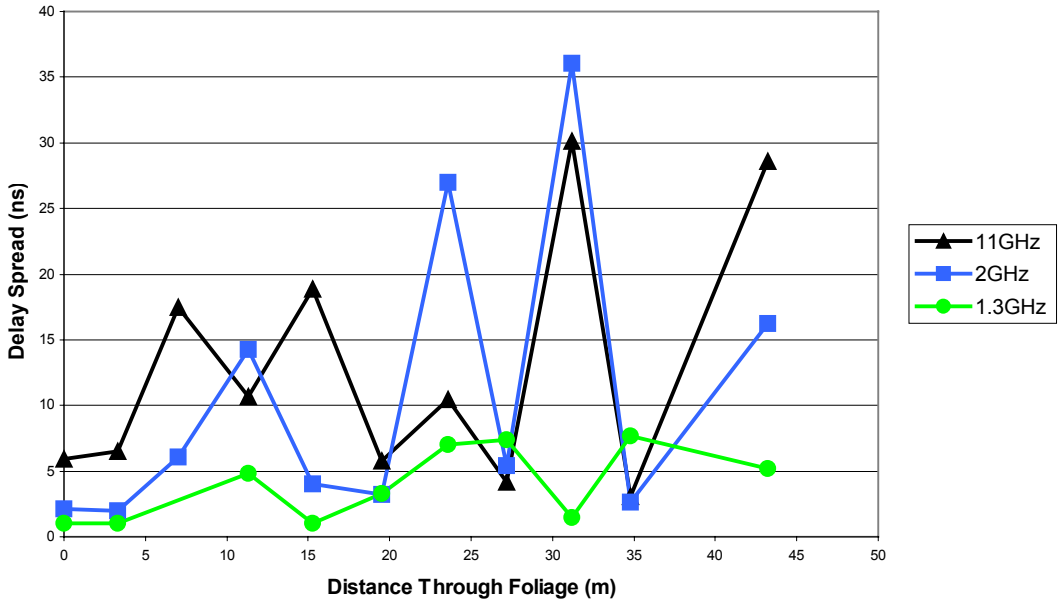

Figure 4-20 Delay Spread as a Function of Foliage Depth (Silver Maple), Out-of-Leaf

4.2.3.6 The ground reflected and diffracted rays are seen in a majority of 1.3GHz in-leaf impulse response estimations of the measurements, although not in the out-of-leaf measurements. The branches of the Silver Maple start at relatively higher heights and grow upwards. That allows ground clearance at the bottom of the tree with little or no branches to attenuate any ground reflected component. Thus the estimated impulse response show three strong components that include the diffracted and the ground reflected paths. In the out-of-leaf measurements, the diffracted component is absent and the measured components have relatively smaller amplitudes, with significant contributions from scatter components.

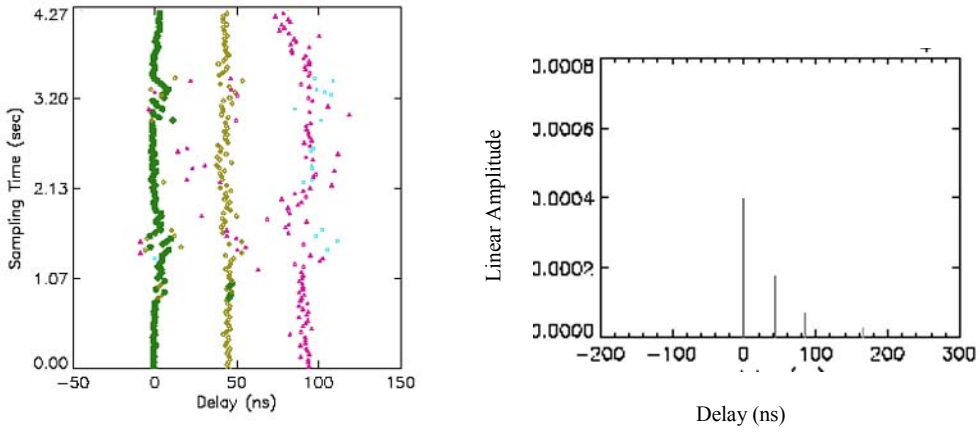

Figure 4-21 1.3GHz Silver Maple In-Leaf at 31.7m (foliage depth 18.2m)

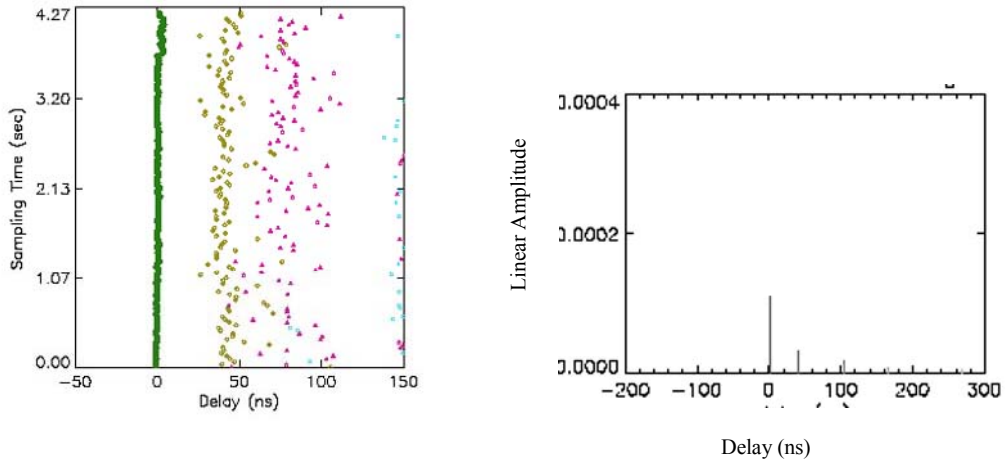

Figure 4-22 1.3GHz Silver Maple Out-of-Leaf at 31.7m (foliage depth 18.2m)

4.2.3.7 The 2GHz in-leaf measurements presented in Figure 4-23 and Figure 4-24 exhibit some similarities with 1.3GHz. There is a strong wave consisting of the ground reflection and diffraction. A reflection at 50ns and 100ns can be seen, although the reflected power is not as great as at 1.3GHz. In the out-of-leaf measurement the ground reflected ray is strong but the diffracted and scatter rays are almost completely insignificant. The upward orientation and close arrangement of branches along the trunk, which is also along the direction that the antennas are pointing, meant that the scattered components were severely attenuated to the point of insignificance.

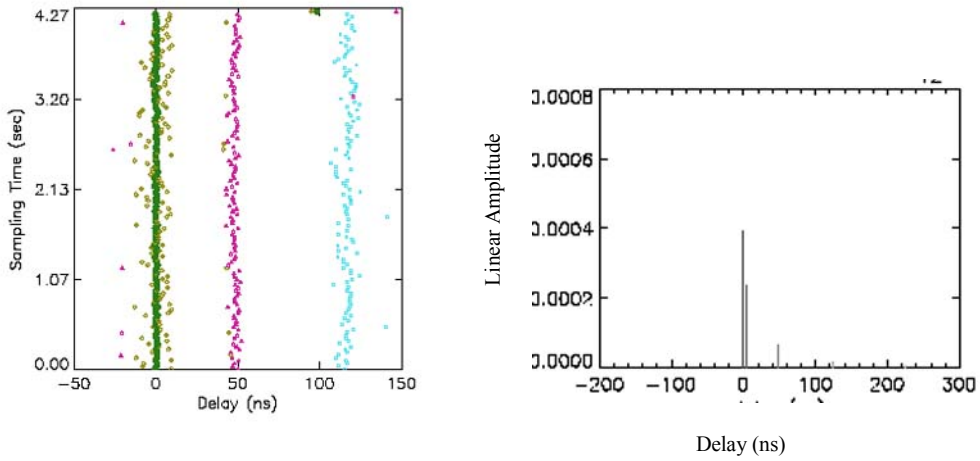

Figure 4-23 2GHz Silver Maple In-Leaf at 31.7m (foliage depth 18.2m)

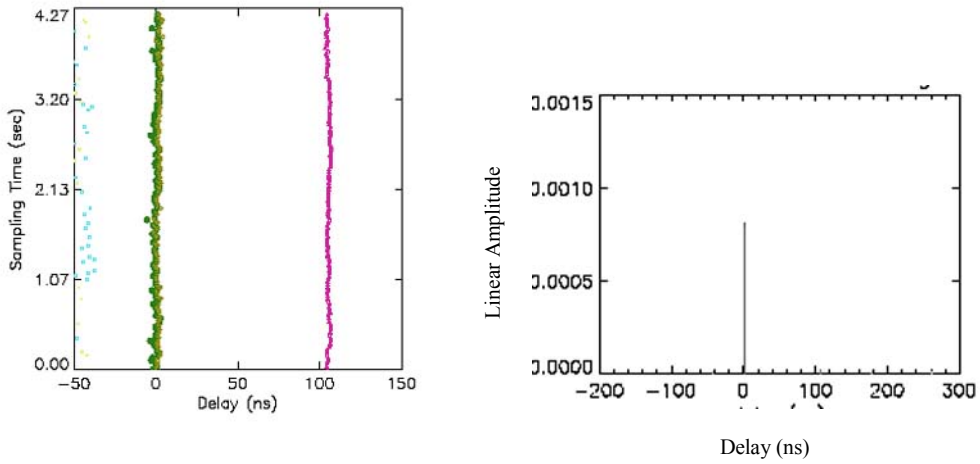

Figure 4-24 2GHz Silver Maple Out-of-Leaf at 31.7m (foliage depth 18.2m)

4.2.3.8 11GHz in-leaf measurements, Figure 4-25, shows one strong component and smaller scattered noise-like components. The strong component is thought to be due to diffraction. The rest of the components, scatter and ground reflected, are severely attenuated because of the distribution of the branches and position of the antenna. However, in out-of-leaf measurements, Figure 4-26, only weak ground reflection and scatter components were observed.

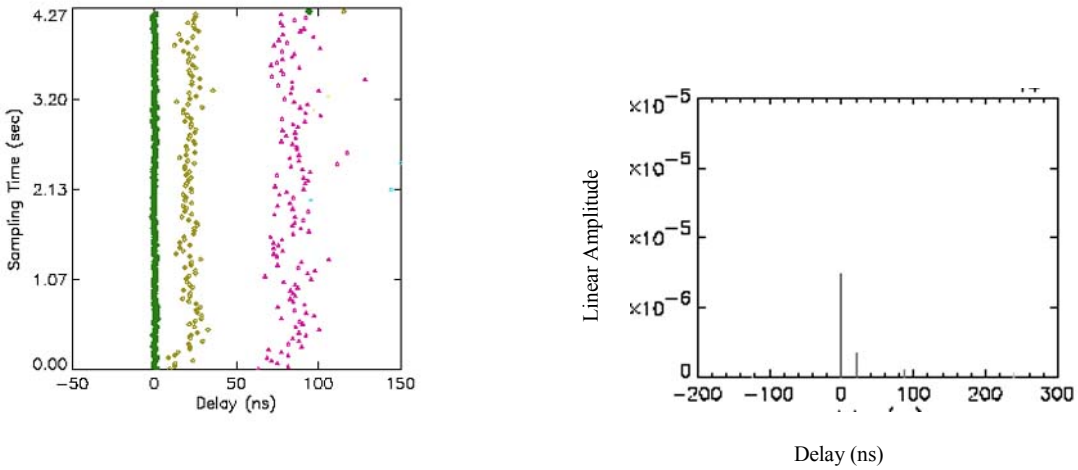

Figure 4-25 11GHz Silver Maple In-Leaf at 31.7m (foliage depth 18.2m)

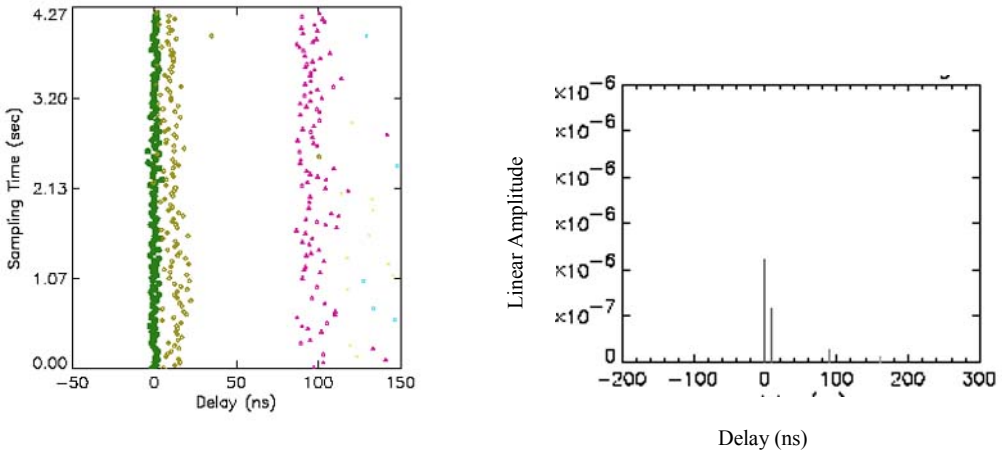

Figure 4-26 11GHz Silver Maple Out-of-Leaf at 31.7m (foliage depth 18.2m)

4.2.4 Twyning Nursery – Common Lime

Tree Type:	Common Lime
Tree Height:	6m
TX Height:	3.5m
RX Height:	3.5m
TX Antennas:	X-Band horn(11GHz), patch array(2GHz), loop array (1.3GHz)
RX Antennas:	Angus horn(11GHz and 2GHz), loop array(1.3GHz)

4.2.4.1 Like all trees at Twyning, the Common Lime were planted in single rows at regular intervals. Due to the shape of the measurement geometry diffraction over and around the side of the trees was expected to be significant. In addition, scatter power from adjacent rows of trees of different species was expected. A picture of the measurement site, Figure 4-27(a), shows the line of trees where the measurements were carried out (the row on the

right hand side). The measurement site geometry is shown on Figure 4-27(b), the blue line shows the movement of the receiver. At each measurement point the receiver is put in between the trees, in line with the tree trunks.

4.2.4.2 The size of leaf of the Common Lime tree is more comparable with half the wavelength of 1.3GHz and 2GHz and the branches of the tree are comparable with the wavelength at 11.647GHz. The Common Lime tree has more branches than either the London plane or the Silver maple and the canopy is much more compact and dense.

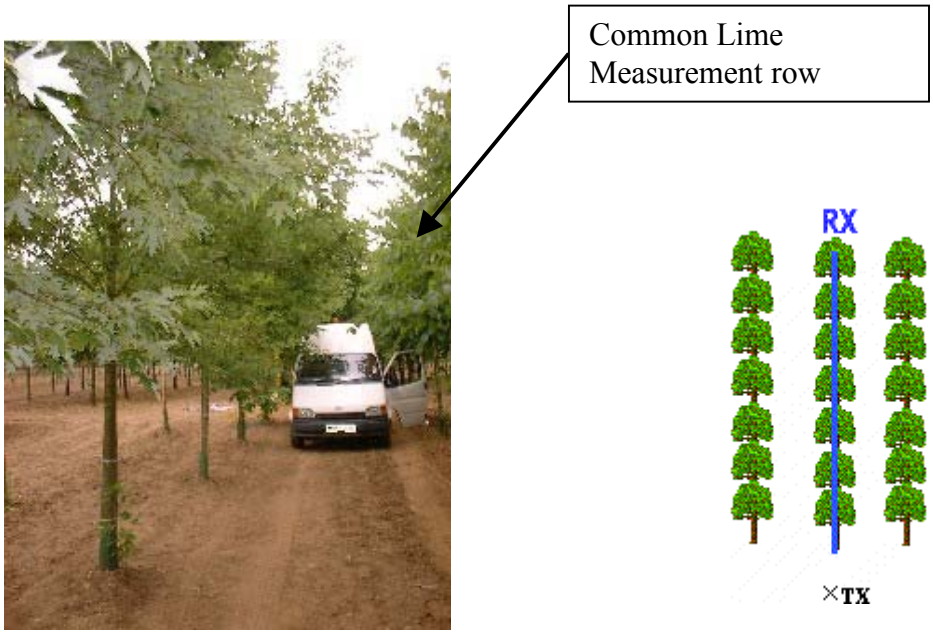

(a) (b)

Figure 4-27 Common Lime (a) Picture of Measurement Set-up (b) Measurement Geometry

4.2.4.3 Both in-leaf and out-of-leaf excess attenuation graphs, Figure 4-28 and Figure 4-29, show an increase in excess attenuation with an increase in foliage depth. Both graphs also show a definite dual slope structure and less excess attenuation in the out-of-leaf measurements when compared to the in-leaf measurements. 11GHz has a very steep second curve, the last 3 points are very nearly into the noise floor of the measurement system, explaining the levelling off of the excess attenuation curve. Analysing the wideband data it is found that after 21m there is only one ray present, all reflected and scattered rays have been severely attenuated and become insignificant. This is thought to be the reason why the signal level doesn't vary very much, as there is not the constructive or destructive effect of multipath nor any nulls in the transfer function that vary from one position to the next. As with other sites the excess attenuation at 11GHz decreases in the out-of-leaf measurements compared to the in-leaf measurements.

4.2.4.4 The out-of-leaf measurements show a large amount of variation in the excess attenuation curves and again 11GHz suffers from a similar amount of excess attenuation as 1.3GHz and 2GHz. The out-of-leaf measurements at 11GHz suffered from a lot more multipath than the in-leaf measurements, the leaves of the trees not absorbing the energy of reflected and scattered waves. 2GHz and 1.3GHz exhibit large variations in excess attenuation as well, possibly due to the scattering effect of the branches.

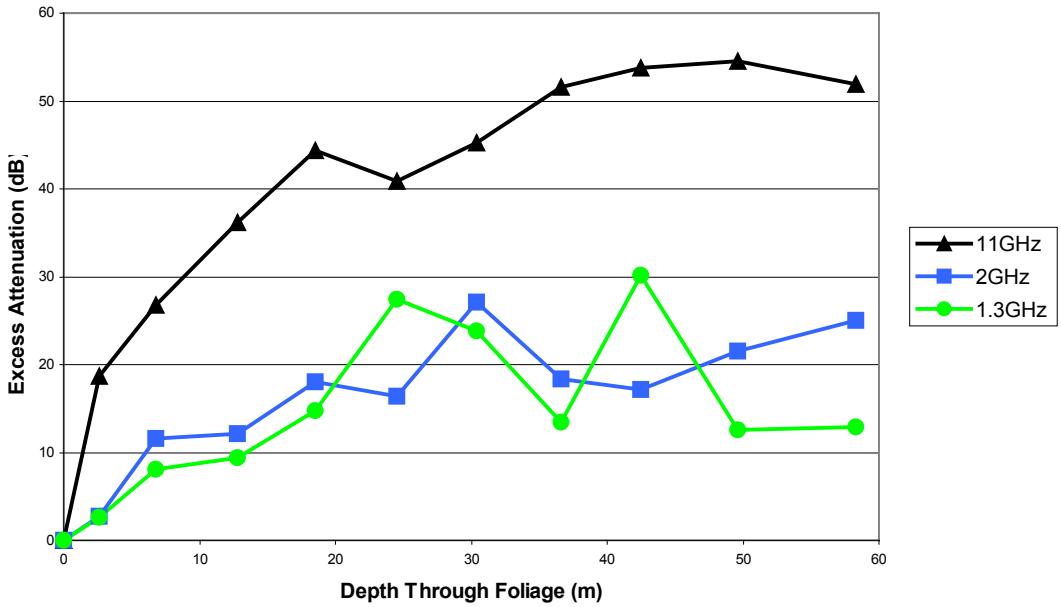

Figure 4-28 Excess attenuation as a Function of Foliage Depth (Common Lime), In-Leaf

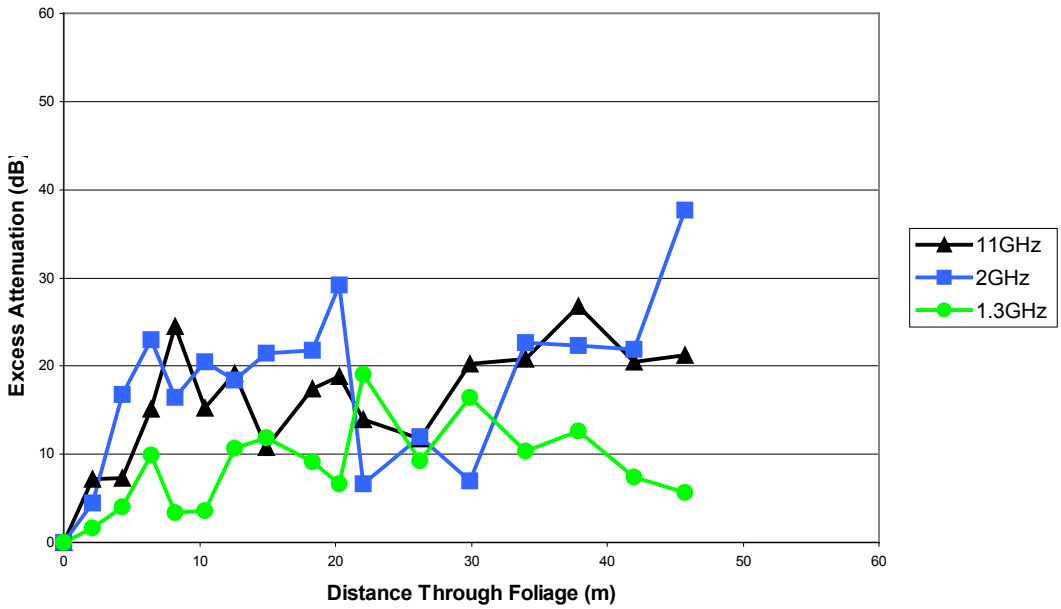

Figure 4-29 Excess attenuation as a Function of Foliage Depth (Common Lime), Out-of-leaf

4.2.4.5 There is a small amount of correlation between delay spread, Figure 4-30 and Figure 4-31 and excess attenuation for both in- and out-of-leaf measurements. The large variations in the excess attenuation values of the out-of-leaf measurements are reflected in the calculated delay spread. The 11GHz in-leaf delay spread values show a very low delay spread for the initial foliage depths, characterised by the single received ray, and then the delay spread increases dramatically as the incoherent wave takes over as the dominant mode of propagation and the measurements approach the noise floor. The in-leaf delay spread graph exhibits a large increase in delay spread at the last four points of the measurements, at a

large foliage depth. This is when the propagation mode changes from a coherent wave to an incoherent wave, where the received signal is dominated by forward scatter. The out-of-leaf delay spreads are all very similar, the delay spread is lower in the out-of-leaf measurements than the in-leaf measurements for both 1.3GHz and 2GHz, although 11GHz delay spread increases.

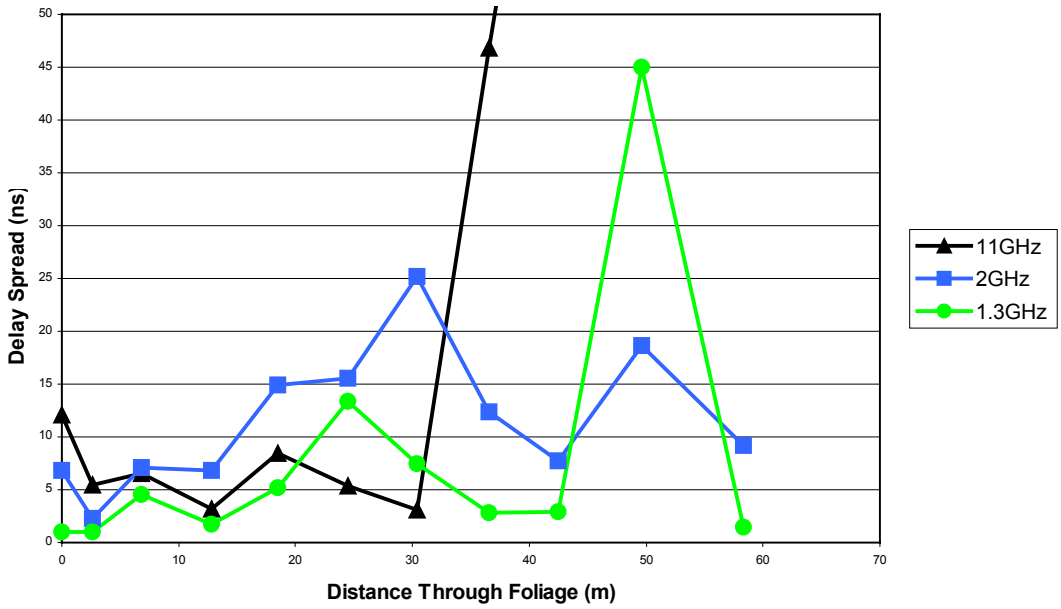

Figure 4-30 Delay Spread as a Function of Foliage Depth (Common Lime), In-Leaf

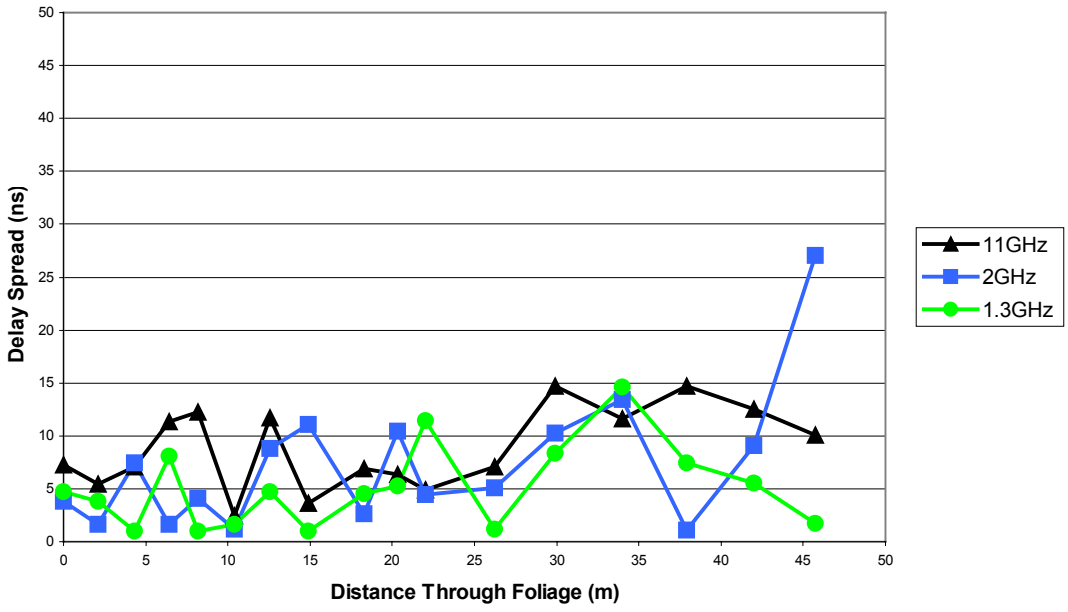

Figure 4-31 Delay Spread as a Function of Foliage Depth (Common Lime), Out-of-Leaf

4.2.4.6 There is a definite ground reflected/diffracted wave for the in- and out-of-leaf impulse response estimations, Figure 4-32 and Figure 4-33. Throughout the measurements both in- and out-of-leaf seem to be equally distributed in their strength of second ray (although the diagram shows out-of-leaf to have a stronger second ray, this is only one snapshot from one

measurement position). The second ray's mean strength is approximately 40% of the main ray, although on occasions both in- and out-of-leaf, it is stronger than the main ray. There is less of a difference between in- and out-of-leaf because of the dense canopy acting as a solid edge in a similar way, with or without leaves. The second rays are attributable to adjacent rows of trees. Throughout the measurements there is a constant third ray at around 80ns.

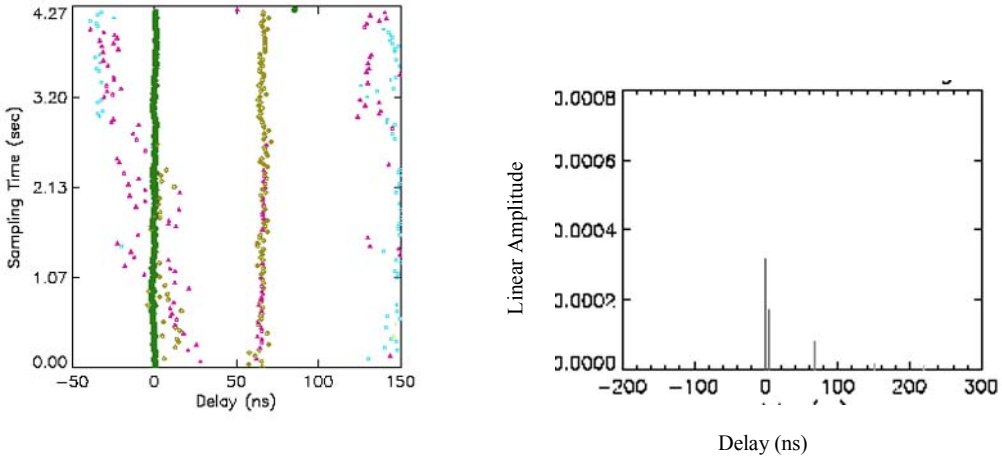

Figure 4-32 1.3GHz Common Lime In-Leaf at 28m (foliage depth 21m)

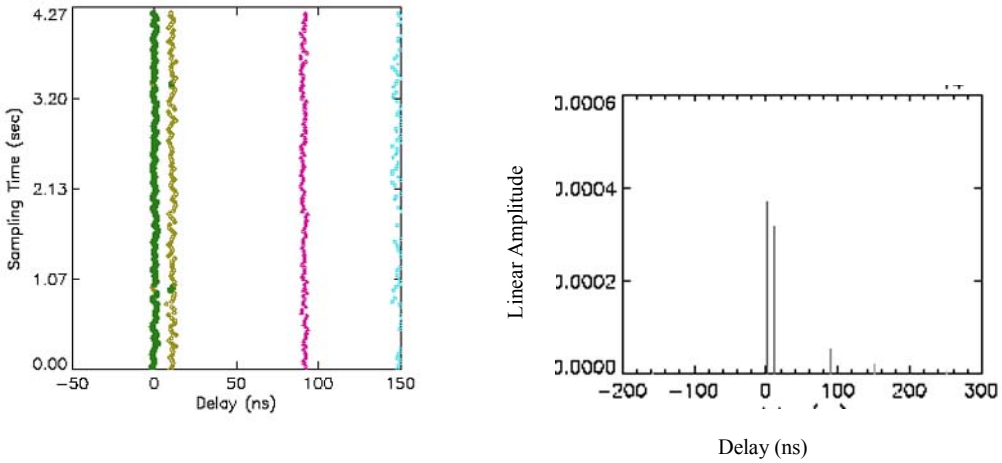

Figure 4-33 1.3GHz Common Lime Out-of-Leaf at 28m (foliage depth 21m)

4.2.4.7 The ground reflected ray was frequently stronger than the main ray in the out-of-leaf and in-leaf 2GHz measurements, indicating that the leafy canopy did not propagate a wave along its edge as well as a branchy canopy, as opposed to the 1.3GHz measurements when it did. At 2GHz the closely packed branches meant that diffracted and reflected components were dominant. In in-leaf measurements, these components were attenuated, but in out-of-leaf measurements these components were much stronger, Figure 4-34 and Figure 4-35. Scattering of these components by branches near the receiver antenna is illustrated by the presence of weaker components around the stronger components.

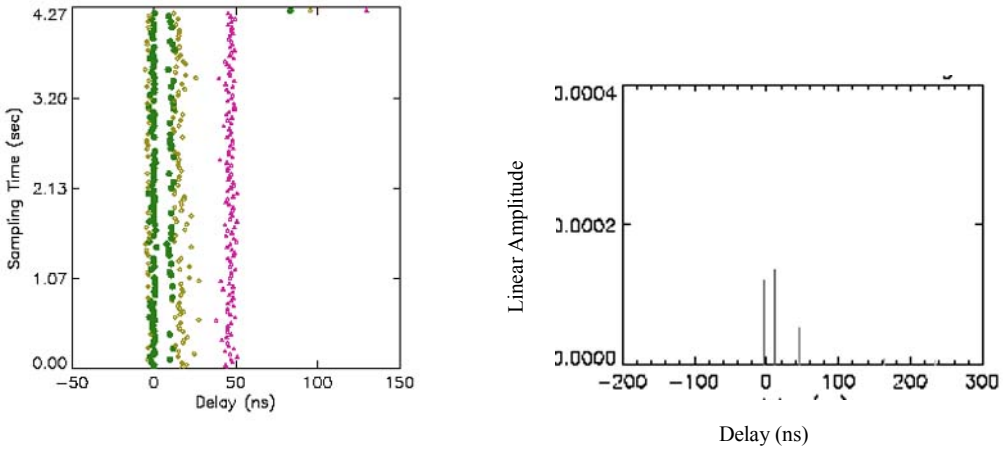

Figure 4-34 2GHz Common Lime In-Leaf at 28m (foliage depth 21m)

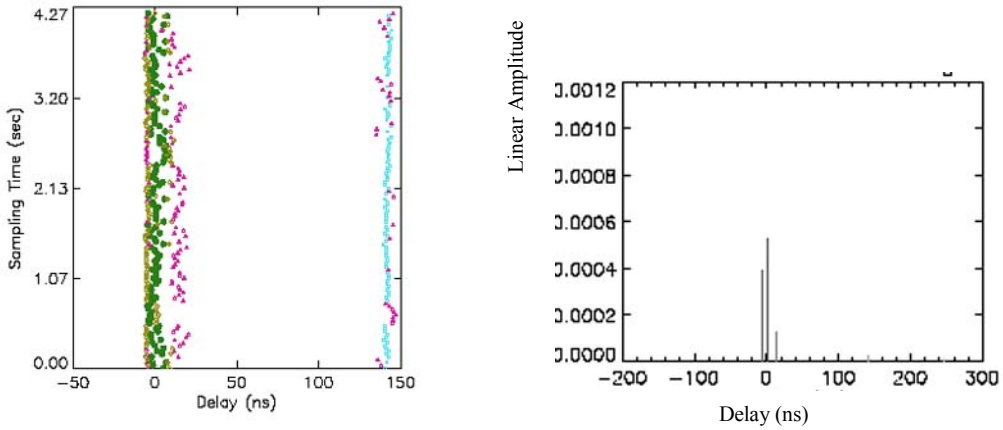

Figure 4-35 2GHz Common Lime Out-of-Leaf at 28m (foliage depth 21m)

4.2.4.8 At 11GHz there is very little multipath in the in-leaf measurements, Figure 4-36, and at larger foliage depths the propagation is dominated by forward scatter. With the out-of-leaf measurements, Figure 4-37, there are a lot more components identified in the impulse response estimation. The dense foliage canopy acts as a scattering medium at 11GHz.

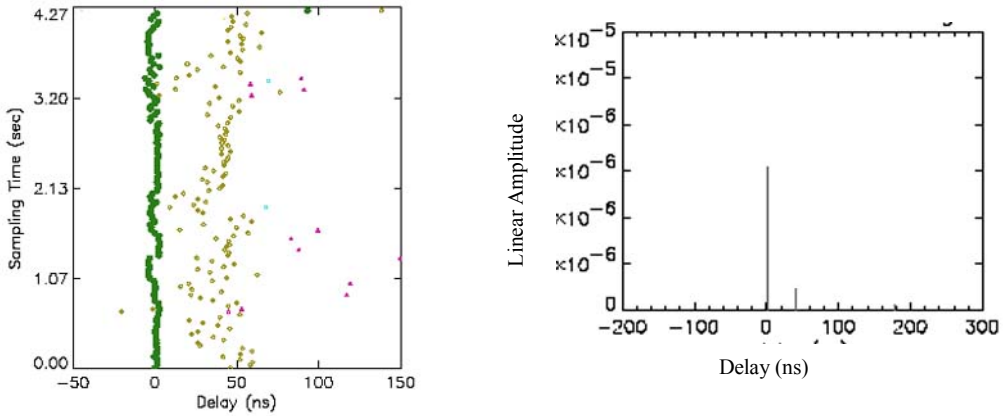

Figure 4-36 11GHz Common Lime In-Leaf at 28m (foliage depth 21m)

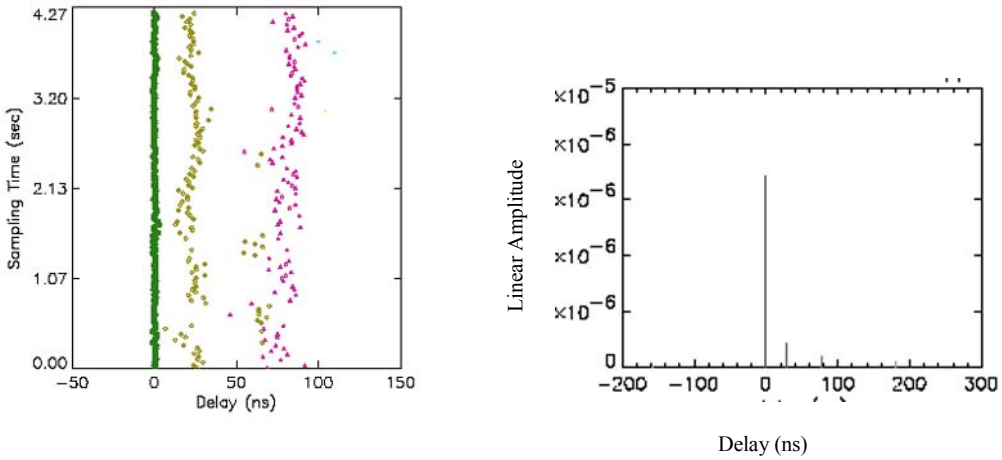

Figure 4-37 11GHz Common Lime Out-of-Leaf at 28m (foliage depth 21m)

4.2.5 Fermi Avenue

Tree Type:	Horse Chestnut
Tree Height:	7-8m
TX Height:	3.5m
RX Height:	5.3m
TX Antennas:	X-Band horn(11GHz), patch array(2GHz), loop array (1.3GHz)
RX Antennas:	Angus horn(11GHz, 2GHz and 1.3GHz)

4.2.5.1 This site was adjacent to a main road leading into an industrial park. The trees were evenly planted and separated from other trees by a fair distance. The measurements at this site suffered from the effects of cars driving past. This was worse at around 5:00pm when people left work. There was also a significant signal component thought to be due to reflections from lampposts. Coaches and buses driving in between the transmitter and receiver also affected the measurements. This site is the same site that was used for measurements that aided the design of the current ITU-R recommendation for radiowave propagation through foliage, so a thorough investigation will assess its usefulness for a narrowband model. The measurement set-up for this particular site is shown in Figure 4-38. Only in-leaf measurements were carried out.

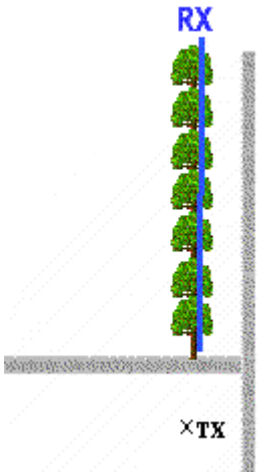

Figure 4-38 Fermi Avenue (a) Picture of Measurement Set-up (b) Measurement Geometry

4.2.5.2 The graph of excess attenuation with foliage depth, Figure 4-39, does not show a large difference in the excess attenuation at different frequencies at the same point. All of the frequencies appear to have similar excess attenuation curves. The dual slope characteristic is also present, although the initial slope is a lot shallower than previously seen. This could be due to the position of the receiver which was not directly in line with the trunks at all times. At 11GHz the excess attenuation is less than for 1.3GHz and 2GHz for a short way into the foliage. Analysing the wideband data shows that at small foliage depths 11GHz multipath components are a lot weaker than at 1.3GHz and 2GHz. The fact that 2GHz has a higher excess attenuation, could be due to the fact that the wide beamwidth antennas receive more of the multipath components being reflected from the lampposts along the road. The more powerful multipath components lead to a deeper fade and a higher probability that the measurement is located somewhere within that fade.

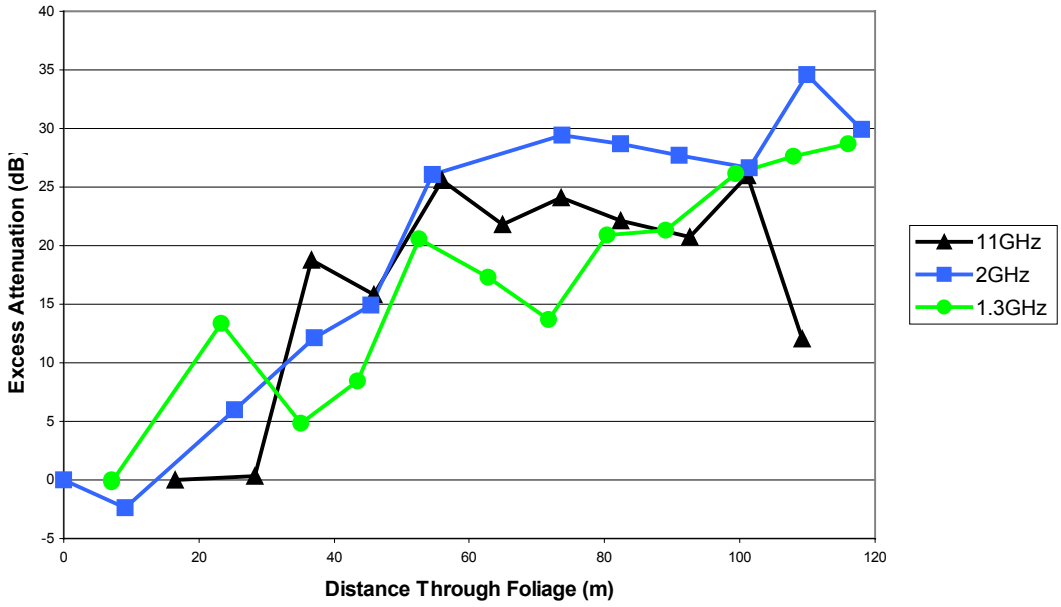

Figure 4-39 Excess attenuation as a Function of Foliage Depth (Fermi Avenue)

4.2.5.3 The delay spread graph, Figure 4-40, does show some correlation with the excess attenuation curves, Figure 4-39. For all three frequencies excess attenuation increases (approximately 30m foliage depth) there is a corresponding increase in delay spread. The final three points of delay spread calculated for 1.3GHz show a rise in the delay spread, not exhibited in the other frequencies. As these measurements were done later in the day, when people were leaving their offices, there was a lot of traffic on the nearby road.

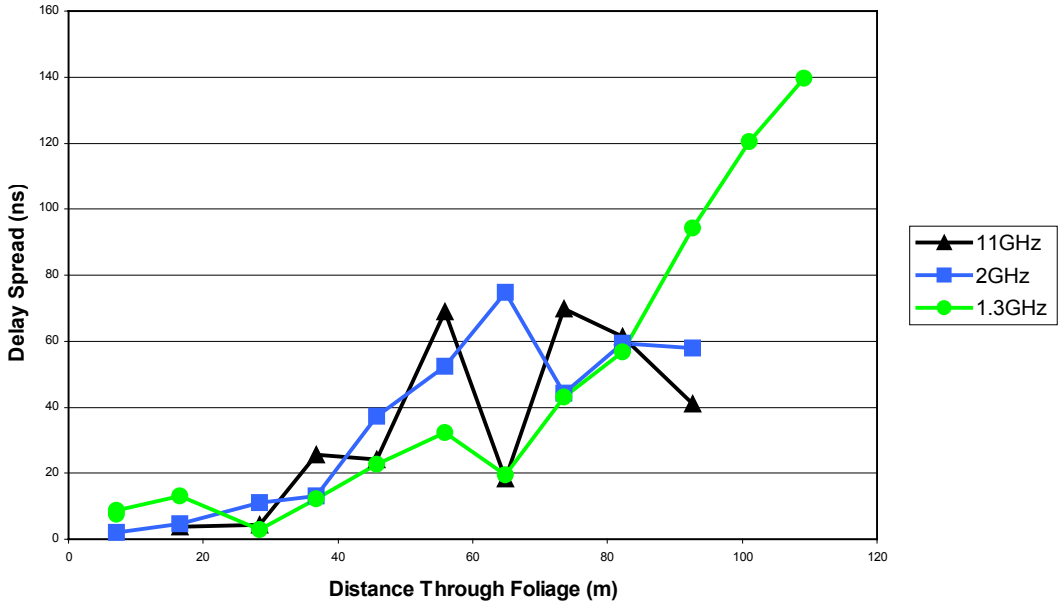

Figure 4-40 Delay Spread as a Function of Foliage Depth (Fermi Avenue)

4.2.5.4 The reflection from lampposts introduced stable and defined ray components as shown in Figure 4-41, Figure 4-42 and Figure 4-43. These reflections are stronger than the scattered and foliage attenuated rays. The presence of strong reflected components from lampposts,

with large separation in time resulted in large calculated values for delay spread at this site. The graphing software plots the strongest ray as being the first ray received, so in Figure 4-41 the delay times of the received rays can be misleading. The ray at –40ns is the first ray received (foliage attenuated component), but that at 0ns is the strongest component.

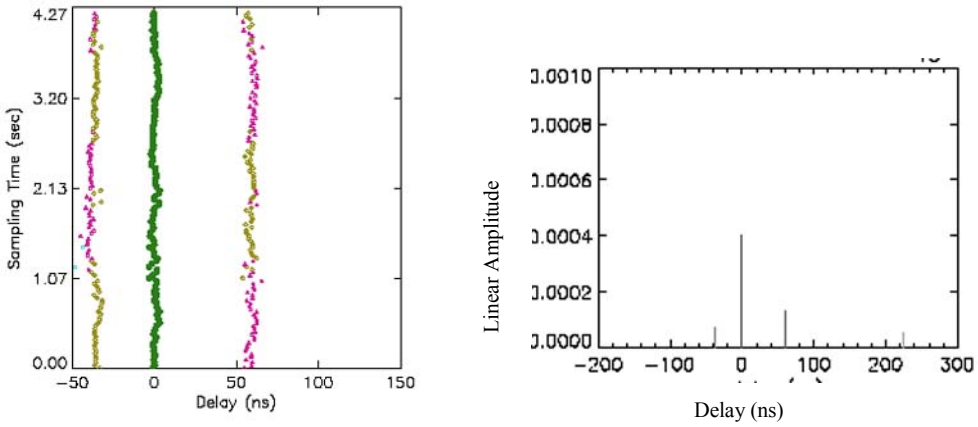

Figure 4-41 1.3GHz Fermi Avenue at 90.9m (foliage depth 49m)

4.2.5.5 The 2GHz wideband data showed that all the received signal paths were strong, Figure 4-42. There were also scatter-components due to vegetation, which are negligible in comparison to the strong reflected components.

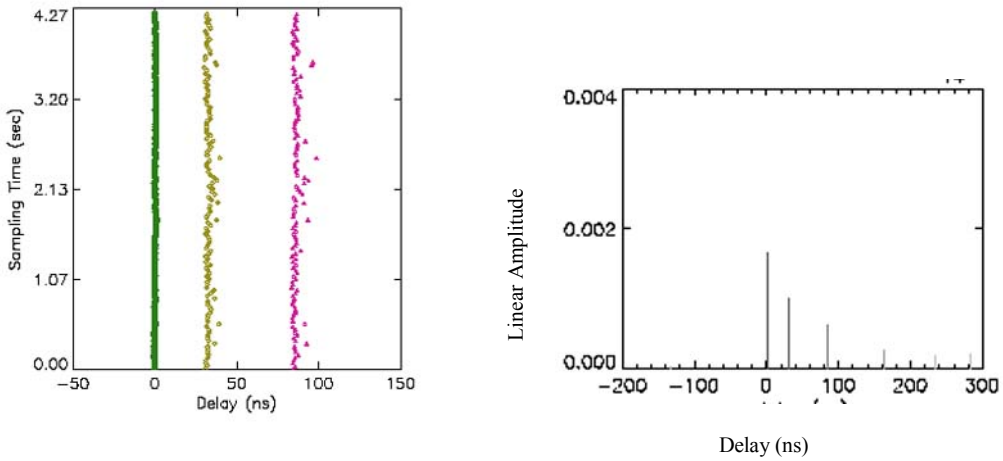

Figure 4-42 2GHz Fermi Avenue at 90.9m (foliage depth 49m)

4.2.5.6 At large foliage depths, as given in Figure 4-43, 11GHz is severely attenuated, including the reflected paths. 11GHz was also more severely affected when a bus passed between the transmitter and receiver. The impulse response plot shows that scatter components were dominant at greater foliage depth.

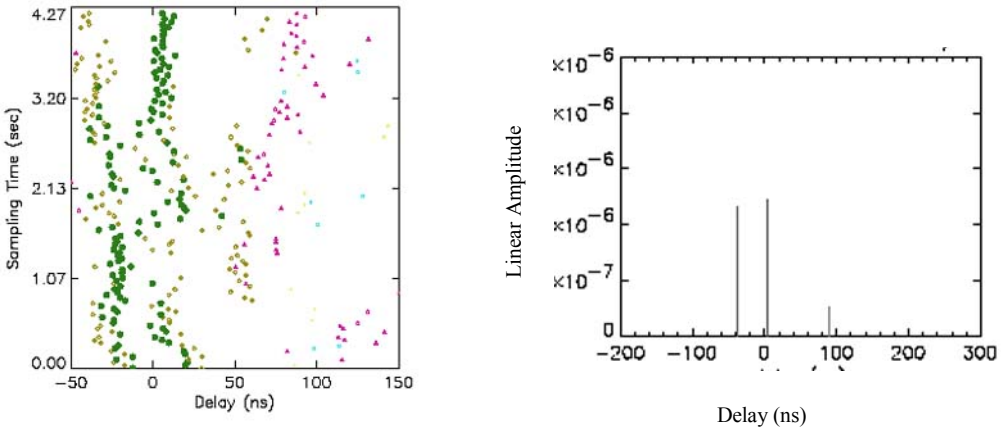

Figure 4-43 11GHz Fermi Avenue at 90.9m (foliage depth 49m)

4.2.6 Ravelin Park – Sycamore, Effect of Wind

4.2.6.1 Measurements were conducted at a site where the trees were susceptible to swaying due to the wind. As shown in Figure 4-44, the trees were immature and had long branches.

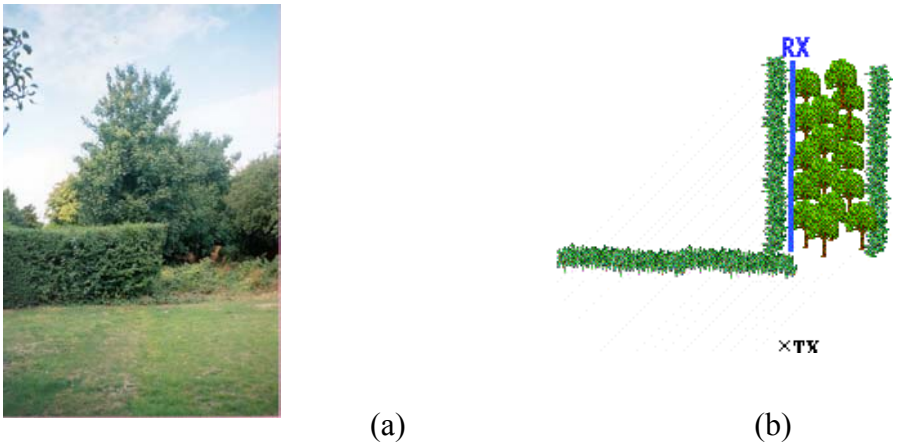

(a) (b)

Figure 4-44 Sycamore (a) Picture of Measurement Set-up (b) Measurement Geometry

4.2.6.2 Figure 4-45 and Figure 4-46 shows the effect of wind on the impulse responses of the channel at 2GHz and 11GHz. In both cases an example of the time varying nature that wind induces is shown alongside an example of a time invariant case. The effect of the swaying branches on the channel could be identified most prominently at 7.5m receiver height, when the receiver antenna is located near the canopy. The wind varies the position of the edge of the canopy, along which a diffracted radiowave can propagate, varying the time of arrival of that wave. This effect causes fast small scale variations in the time and amplitude of the received components which introduces fast variations in the signal envelope and transfer function. In addition to this variation, at 11GHz the twigs and branches are of a size comparable to the wavelength of the signal so the swaying motion causes more scattering.

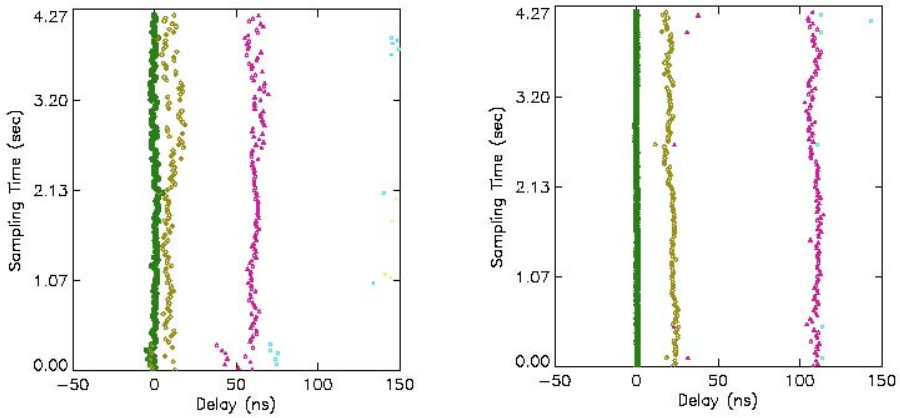

(a) (b)

Figure 4-45 Sycamore 2GHz Estimated Impulse Response (a) With Wind (b) Without Wind

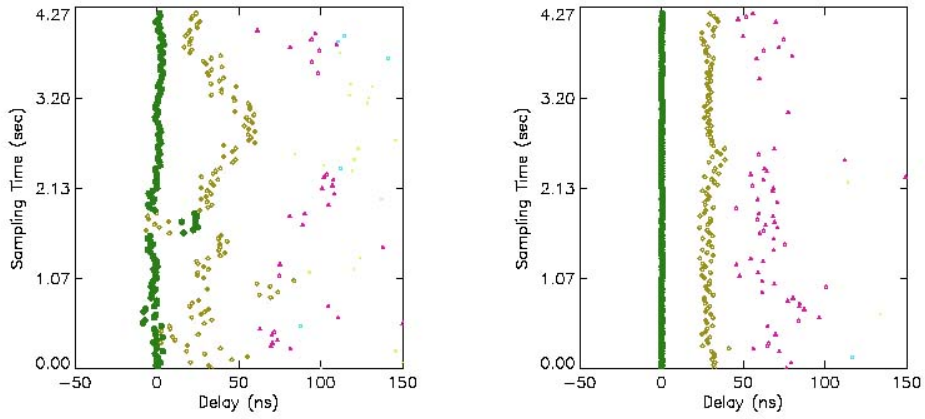

(a) (b)

Figure 4-46 Sycamore 11GHz Estimated Impulse Response (a) With Wind (b) Without Wind

4.3 Discussion

4.3.1 To facilitate the understanding of the general trends, a best "eye" approximation is presented of the earlier figures. With the obvious reservations Table 4-1, Table 4-2 and Table 4-3 summarise those approximations of excess attenuation and delay spread at each site. The values are given at 5, 15, 30 and 50 metres foliage depth. In general, the results show that at 11GHz the signal suffered more excess attenuation in in-leaf condition than in out-of-leaf irrespective of the tree type, shape or measurement geometry. However, the delay spread values were less defined. The results at 2GHz were also less defined for London Plane and Silver Maple. At shallow foliage depths of less than 30m, smaller excess attenuations were measured for London Plane than at greater depth. The reverse is true for Silver Maple. At 1GHz the results show that, with the exception of Silver Maple, greater excess attenuation was obtained for the in-leaf condition. At 1GHz and 2GHz delay spread values were consistently less than 20ns for the foliage depth presented in the tables.

However, larger values were obtained at 11GHz especially at large depths where there were, generally, a lack of dominant signal components. Only in-leaf measurements were carried out on the Horse Chestnut trees. By comparison, the results show that less excess attenuation was measured at the same foliage depth for the Horse Chestnut than for all of the three other species presented in this wideband analysis. This is thought to be the result of signal enhancements by reflections off lampposts and traffic.

Tree Type	Leaf State	Parameter (Eye estimate)	Foliage Depth (m)			
			5m	15m	30m	50m
London Plane	In	Excess attenuation (dB)	5	14	16	18
		Delay Spread (ns)	2	2	3	4
	Out	Excess attenuation (dB)	3	13	19	17
		Delay Spread (ns)	6	8	6	6
Silver Maple	In	Excess attenuation (dB)	2	13	16	16
		Delay Spread (ns)	4	5	10	9
	Out	Excess attenuation (dB)	15	16	22	25
		Delay Spread (ns)	2	2	4	5
Common Lime	In	Excess attenuation (dB)	5	12	20	18
		Delay Spread (ns)	4	4	9	18
	Out	Excess attenuation (dB)	6	12	14	10
		Delay Spread (ns)	3	2	8	4
Horse Chestnut	In	Excess attenuation (dB)	0	5	9	15
		Delay Spread (ns)	10	15	5	23

Table 4-1 1GHz delay spread and excess attenuation for selected foliage depths

Tree Type	Leaf State	Parameter (Eye estimate)	Foliage Depth (m)			
			5m	15m	30m	50m
London Plane	In	Excess attenuation (dB)	4	16	18	16
		Delay Spread (ns)	3	16	16	14
	Out	Excess attenuation (dB)	3	15	20	23
		Delay Spread (ns)	2	10	10	10
Silver Maple	In	Excess attenuation (dB)	5	16	13	19
		Delay Spread (ns)	3	9	11	10
	Out	Excess attenuation (dB)	15	24	19	16
		Delay Spread (ns)	3	7	15	15
Common Lime	In	Excess attenuation (dB)	8	14	26	24
		Delay Spread (ns)	6	12	18	17
	Out	Excess attenuation (dB)	15	17	14	20
		Delay Spread (ns)	5	8	8	20
Horse Chestnut	In	Excess attenuation (dB)	0	0	8	20
		Delay Spread (ns)	0	5	12	40

Table 4-2 2GHz delay spread and excess attenuation for selected foliage depths

Tree Type	Leaf State	Parameter (Eye estimate)	Foliage Depth (m)			
			5m	15m	30m	50m
London Plane	In	Excess attenuation (dB)	5	18	25	26
		Delay Spread (ns)	10	5	6	8
	Out	Excess attenuation (dB)	7	13	21	25
		Delay Spread (ns)	5	10	13	9
Silver Maple	In	Excess attenuation (dB)	20	35	35	40
		Delay Spread (ns)	3	6	6	70
	Out	Excess attenuation (dB)	15	26	26	35
		Delay Spread (ns)	10	16	18	20
Common Lime	In	Excess attenuation (dB)	22	38	45	58
		Delay Spread (ns)	9	8	4	100
	Out	Excess attenuation (dB)	8	11	20	23
		Delay Spread (ns)	10	4	12	14
Horse Chestnut	In	Excess attenuation (dB)	0	0	5	20
		Delay Spread (ns)	4	4	5	40

Table 4-3 11GHz delay spread and excess attenuation for selected foliage depths

4.3.2 The excess attenuation graphs show variations in received signal level that are not correlated between the three frequencies measured. This indicates that the variations are not due to the presence of foliage attenuating the direct component, but are due to multiple components being received that interact with the forward component in differing ways. Analysis of the wideband measurement data indicates that some sites exhibit similar propagation mechanisms for all frequencies, although some frequencies have stronger multiple components than others. Twyning nursery was dominated by reflected and diffracted waves, depending on the tree species. Fermi Avenue was dominated by components reflecting off the lampposts along either side of the road near to the measurement site. The measurements conducted at Fermi Avenue also suffered from blockage due to buses driving in front of the transmitter and from the traffic driving along the nearby road. The reflections from the lampposts were also frequently stronger than the foliage attenuated and scatter components. These gave incorrect values for the excess attenuation through foliage as the signal is primarily made up of reflections off lampposts that are strong enough to render scattered components negligible.

4.3.3 The absence of correlation between excess attenuation and delay spread means that, although a narrowband model may predict the reception of a strong signal, this may be rendered unintelligible for communication purposes by multipath. This was especially the case for the Silver Maple measurements where the delay spread values exhibit a lot of variation, whereas the excess attenuation values appeared fairly stable in comparison. The delay spread variation could be due to different multipath components dominating the propagation path at different positions.

4.3.4 The excess attenuation might be lower for most frequencies at most of the sites for the out-of-leaf measurements, but the wideband characteristics are less favourable for communication purposes. The second rays received in most sites had a higher power, in comparison with the strongest ray, when compared to the in-leaf measurements. A stronger second ray gives a deeper null in the transfer function so that the bandwidth that the signal

occupies is more likely to suffer from more excess attenuation than is predicted from a narrow band model.

4.3.5 The results show that in-leaf, diffraction round the edge or top of trees is the dominant mode of propagation. The scatter components are severely attenuated in comparison to the diffracted component. In general, ground reflected component dominates in out-of-leaf condition. This is especially true for trees with relatively high canopy in comparison to the receiver antenna height. Scatter components are also more pronounced in out-of-leaf than in-leaf because of the absence of leaves that attenuate these components. Measurement results have shown that temporal dynamic variations of signal amplitudes are more pronounced for species of tree that have sparsely distributed branches, and hence leaves. In general the wideband results have illustrated the importance of understanding the prevailing propagation mechanisms in propagation model development. The received signal has been shown to be a combination of scattered, attenuated, reflected and diffracted components where the dominant mechanism is determined by the type of geometry. Further and more detailed studies are required to be able to develop an all-encompassing (generic) model for either narrowband or wideband systems.

5 Conclusions

5.1 Existing Models of 1-60GHz Propagation through Vegetation

5.1.1 Prediction models which estimate the excess attenuation due to vegetation are critical to mobile and terrestrial radio service providers for planning radio networks and optimising cell coverage while minimising intercell interference.

5.1.2 The existing models reviewed in this report contain few parameters relating to the vegetation medium, path geometry and seasonal effects on the radio system performance. They have limited applicability because in their formulation and validation they were based on a limited number of site geometries and relatively few measurements.

5.2 The New Generic model

5.2.1 A generic attenuation model with appropriate parameters, based on knowledge and understanding of the propagation modes arising in vegetation, is clearly both valuable and necessary for radio system planning. The generic model presented in this report accounts for a wide variety of vegetation media, path geometries and frequencies. The model combines an edge diffraction and ground reflection model (based on existing ITU-R Recommendations) with a direct (through vegetation) signal modelled through the application of Radiative Energy Transfer (RET) theory.

5.2.2 The database of measurements on which the model is based (available from the Radiocommunications Agency) includes signal attenuation measurements, propagation geometries and associated vegetation density and RET parameters. The RET parameters were derived empirically by iterative curve fitting to the radio signal strength measurements at varying depths of vegetation.

5.2.3 The RET parameter accuracy may be improved by measuring the phase (or scatter) function of the vegetation directly. Various methods of taking this measurement were conducted and compared. It was concluded that the most practical method for determining the phase function (scatter function) of the vegetation is to fix the location of transmitter and receiver antennas at the same height and rotate a narrow receiver antenna beam azimuthally by ±40°. The receiver should be 2-3 tree depths within the canopy region of the vegetation.

5.3 Model Performance

5.3.1 Initial tests have compared the predictions of the new generic model and the existing ITU-R Rec. 833 model with narrowband signal attenuation measurements from a line of London Plane trees. The new generic model showed a better fit to the measurements, whilst ITU-R Rec 833 showed that the attenuation due to diffraction dominated its predictions, particularly at higher frequencies. A considerable advantage of the generic model lies the inclusion of the ground reflected component. A comparison of the generic model with 490 point measurements of attenuation at a range of vegetation depths yielded an RMS discrepancy of 8.38 dB, whereas that for the existing ITU-R 833-3 model was 11.51 dB. Proposed changes to ITU-R Recommendation 833 are provided in Appendix A, as submitted to the ITU.

5.4 Wideband Channel Characteristics

5.4.1 Vegetation can cause scatter, refraction, diffraction, absorption and reflection of radio waves. Consequently, the radio signals follow multiple paths which arrive at the receiver with a distribution of discrete time delays. Measurements using a wide bandwidth sounder waveform has allowed these multipath components to be resolved and analysed.

5.4.2 The absence of correlation between attenuation and multipath delay spread which has been observed in the wideband measurements means that, although the narrowband model may predict the reception of a strong signal, this may be rendered unintelligible for communication purposes by the intersymbol interference caused by multipath. A variation in delay spread can be due to different multipath components dominating the propagation path at different positions.

5.4.3 The attenuation has been seen to be lower for most frequencies for the out-of-leaf measurements, but the wideband characteristics are less favourable for communication purposes. The second strongest rays received, in out-of-leaf state, generally have a higher power, in comparison with the strongest ray, when compared to the in-leaf measurements. A stronger second ray gives a deeper null in the transfer function so that the bandwidth the signal occupies is highly likely to suffer from more attenuation than is predicted from a narrow band model.

5.4.4 The measurements presented in Section 4 showed that for trees in leaf, diffraction around the edge or top of trees is the dominant mode of propagation. The scatter components are severely attenuated in comparison to the diffracted component. In general, the ground reflected component dominates when the trees are out of leaf. This is especially true for trees with relatively high canopy in comparison to the receiver antenna height. Scatter components are also more pronounced when trees are out of leaf because of the absence of leaves that attenuate these components. Wideband measurement analysis has shown that temporal dynamic variations of signal amplitudes are more pronounced for species of tree that have sparsely distributed branches and leaves.

6 Recommendations

- **Develop a generic wideband (>100MHz) and dynamic model of propagation through vegetation.** The model should account for variations in attenuation for wet and dry conditions, and assess the impact of dynamic variations on the channel due to movement of leaves and branches in the wind. Fast (sub-second) fading dynamics, coherence bandwidths, etc. of signals propagating through, around or scattered from vegetation are critical parameters for quality of service, RF regulation and the assessment of spectrum efficiency. A wideband model would provide a better prediction of the data rates available for broadband services in sub-urban or rural areas. The correlation between wideband system parameters, such as the coherence bandwidth, should be related to the RET parameters. A high value of the RET parameter α indicates strong forward scattering and possibly low RMS delay spread. Conversely, higher values of RMS delay may result from a medium scattering incident energy in directions additional to the forward direction.

- **Investigate vegetation-induced scatter and reflection characteristics for interference predictions.** The scattering and reflection characteristics of vegetation and their impact on interference and co-ordination distances are not fully understood. Further investigation of these processes should be performed through measurement and simulations. The impact on future radio systems should be addressed.

- **Establish a relationship between RET model parameters and differing UK vegetation types.** This will enable the narrowband generic model to be used more efficiently so it gains acceptance in the national and international (ITU) community. The dependence of the RET parameters on frequency, type and density of the vegetation has yet to be fully determined. Further research, verified through further measurements, should be performed to establish these relationships.

- **Extend the database of signal attenuation measurements to include under-represented species and higher frequencies.** Further measurements are required, particularly at higher frequencies (>20MHz) and particularly for shrubs and evergreen trees which are presently under-represented in the database. For accurate parameterisation of the RET model, it is highly recommended that future measurements include measurements of the phase function using the procedure given in this report.

- **Assess the effects of depolarisation of planar radio waves as they propagate through vegetation.** This is particularly important for the efficient utilisation of the spectrum in cellular networks. Since the present campaign measured mainly vertical to vertical (VV) polarisation, a correction for other polarisation combinations is required in future enhancements to the model.

7 Acknowledgements

7.1 The authors would like to acknowledge and thank the UK Radiocommunications Agency for funding this research.

7.2 We would also like to thank the Malvern Hills Conservators, J & J Nurseries Ltd. of Twyning, near Tewkesbury, Gloucestershire, the Management of Queen Elizabeth Country Park, Hampshire and all others who kindly allowed us access to their property during the measurement campaign.

8 References

AL-NUAIMI, M. O., HAMMOUDEH, A. M.: “Attenuation functions of microwave signals propagated through trees”, Electronic Letters, 29, (14), pp. 1307-1308, 1993a.

AL-NUAIMI, M. O., HAMMOUDEH, A. M.: 'Influence of Vegetation on Attenuation of Radiowave Signals in the X-Band Frequency Region', COST 235 TD, CP 149, June 1993b.

AL-NUAIMI, M. O., HAMMOUDEH, A. M., "Measurements and Predictions of Attenuation and Scatter of Microwave Signals by Trees", IEE Proceeding on Antennas and Propagation, Part H, Vol. 141, No. 2, 1994a.

AL-NUAIMI, M.O., HAMMOUDEH, A.M. “Measurements and Predictions of Attenuation and Scatter of Microwave Signals by Trees”, IEE Proc Microw. Antennas Propag., Vol. 141, No. 2, April 1994b.

AL-NUAIMI, M. O., STEPHENS, R. B. L.: “Measurements and prediction model optimisation for signal attenuation in vegetation media at centimetre wave frequencies” IEE Proceedings on Microwave Antennas and Propagation, Vol. 145, No 3, June 1998.

AUSTIN, J., W.P.A. DITMAR, W.K. LAM, E. VILAR, and K.W. WAN, A spread spectrum communications channel sounder, IEEE Trans. Commun., 45(7), 840-847, 1997.

CALDEIRINHA, R. F. S.: “Radio Characterisation of Single Trees at Micro- and Millimetre Wave Frequencies”, PhD thesis, University of Glamorgan, 2001.

CALDEIRINHA, R., AL-NUAIMI, M.: "Co-Polar and Cross-Polar Measurements of the Re-Radiation Signal at 20 GHz from a Tree and their Analysis in the region around the Nulls", IEEE Proceedings of the Sixteenth National Radio Science Conference, Ain Shams University, Cairo, Egypt, INV4, Feb. 23-25, 1999.

CALDEIRINHA, R., AL-NUAIMI, M.: "Analysis of the Re-radiation Functions of Single Trees and Idealised Structures at 20 GHz", AP2000 Millennium Conference on Antennas & Propagation, Davos, Switzerland, Pap. 460, April 11-15, 2000.

CALDEIRINHA, R., AL-NUAIMI, M.: "An Accurate Model for RCS of Single Leaves ", 4th European Personal Mobile Communications Conference, EPMCC2001, Vienna, Austria, February 20th-22nd, 2001a.

CALDEIRINHA, R., AL-NUAIMI, M.: "A Novel FDTD based method for prediction of bistatic RCS of single leaves and trees", 11th International Conference on Antennas & Propagation, ICAP2001, Manchester, UK, April 17-20, 2001b.

CALDEIRINHA, R., AL-NUAIMI, M.: "Modelling of the re-radiation functions of single trees based on wideband measurements at L-band", 11th International Conference on Antennas & Propagation, ICAP2001, Manchester, UK, April 17-20, 2001c.

CAVALCANTE, G. P. S., GIARDOLA, A. J.: “Optimisation of radio communication in media with three layers”, IEEE Antennas and Propagation, Vol. AP-31, January 1983.

CAVALCANTE, G. P. S., ROGERS, D. A. and GIARDOLA, A. J.: “Radio loss in forests using a model with four layered media”, Radio Science, Vol. 18, 1983.

CCIR Report. 1008-1, Reflections from the surface of the earth, §2, 1990.

COST 235, “Radiowave propagation effects on next generation fixed services terrestrial telecommunications systems”, Final Report, ISBN 92-827-8023-6, Commission of the European Union, 1996.

DIDASCALOU, D. et al. “Millimeter-Wave Scattering and Penetration in Isolated Vegetation Structures”, IEEE trans Geoscience and Remote Sensing, Vol. 38, No. 5, Sept. 2000

Draft COST 231 Final Report, "Digital Mobile Radio: COST 231 View on the Evolution towards 3rd Generation Systems", COST 231 TD(96)042-A, Turin, April 17-19, 1996.

DTI, "Multimedia Communications on the move", A Consultation Document from the Department of Trade and Industry, July 1997

EWE, H. T., CHUAH, H. T. “Electromagnetic Scattering from an Electrically Dense Vegetation Medium”, IEEE trans Geoscience and Remote Sensing, Vol. 38, No. 5, Sept. 2000.

FUNG, A. K., FUNG, H. S.: ”Application of first-order renormalisation method to scattering from a vegetation-like half-space”, IEEE Transactions on Geoscience Electronics, Vol. GE-15, No. 4, October 1977.

FUNG, A. K., FUNG, H. S.:”A scatter model for leafy vegetation”, IEEE Transactions on Geoscience Electronics, Vol. GE-16, No. 4, October 1978.

GRAHAM, R.F. “Identification of Suitable Carrier Frequency for Mobile Terrestrial Communication Systems with Low Antenna Height”, http:argeenhouse.com/society /TacCom/milcom_98_paper.html., 1998

HAMMOUDEH, A. M., STEPHENS, R., AL-NUAIMI, M. O.: “Characterisation and Modelling of Scatter, Attenuation and Depolarisation of Millimetre Waves due to Foliage”, 26th EuMC, Prague, Czech Republic, September 1996.

HIU, T., SARABANDI, K.: “Electromagnetic Scattering from Short Branching Vegetation”, IEEE trans Geoscience and Remote Sensing, Vol. 38, No. 2, March. 2000.

ISHIMARU, A: “Wave propagation and scattering in random media”, Academic Press, Vol. 1, 1978.

ITU-R Rec. 526-3, Propagation by Diffraction, §4, Int. Telecom. Union, Geneva, 2000.

ITU-R Rec. 527-3, Electrical characteristics of the surface of the earth, §2, Int. Telecom. Union, Geneva, 2000.

ITU-R Rec. 833-2, “Attenuation in vegetation”, Int. Telecom. Union, Geneva, 1999.

ITU-R Rec. 833-2, Attenuation in vegetation, Int. Telecom. Union, Geneva, 2000.

JOHNSON, R. A., SCHWERING, F.: “A transport theory of millimeter wave propagation in woods and forests”, CECOM-TR-85-1, Fort Monmouth, New Jersey, 1985

KARALIOPOULOS, M.S., PAVLIDOU, F. N.: “Modelling the land mobile satellite channel: a review”, IEE Electronics Communication Engineering Journal, Vol. 11, No. 5, October 1999.

LAU, W.H., J. AUSTIN, A. HEWITT, E. VILAR, and L. MARTIN, Analysis of the time-variant structure of the microwave line-of-sight multipath phenomena, IEEE Trans. Commun., 39(6), 847-855, 1991.

LE-WEI LI et al, “Analysis of Radiowave Propagation in a Four-Layered Anisotropic Forest”, IEEE trans Geoscience and Remote Sensing, Vol. 37, No. 4, July 1999.

LEWENZ, R. “Path loss variation due to vegetation movement”, Proc. IEE National Conference on Antennas and Propagation, pp. 97-100, 1999.

LI, L. W., YEO, T. S.: “Radio wave propagation along mixed paths through a four-layered model of rain forest: An analytic approach”, IEEE Transactions on Antennas and Propagation, Vol. 46, No. 7, July 1998.

MATSCHEK, R., LINOT, B.: “Model for wave propagation in presence of vegetation based on the UTD associating transmitted and lateral waves”, National Conference on Antennas and Propagation, Conference Publication No. 461, 30 March - 1 April, 1999.

MÄTZLER, C.: ”Microwave (1-100 GHz) Dielectric model of leaves”, IEEE Transactions on Geoscience and Remote Sensing, Vol. 32, No. 5, September 1994.

PAULSEN, A., SEVILLE, A.: “Attenuation and distortion of millimetre radio wave propagation through vegetation“ Millennium conference on Antennas and Propagation (AP 2000), April 2000.

RAPPAPORT T.S. and SANDHU S., Radio-wave propagation for emerging wireless personal communication systems, IEEE Antennas and Propagation Magazine, 36(5), 14-23, 1994.

SACHS, D. L., WYATT, P. J.: “A Conducting-Slab Model for Electromagnetic Propagation Within a Jungle Medium”, Radio Science, Vol. 3 (New Series), No. 2, February 1968.

SCHWERING, F. K.: “Millimeter-Wave Propagation in Vegetation: Experiments and Theory”, IEEE Transactions on Geoscience and Remote Sensing, Vol. 26, No. 3, May 1988.

SCHWERING, F.K., ESPELAND, H.: “Millimeter-wave Propagation in Vegetation: Experiments and Theory”, IEEE Trans. Geoscience and Remote Sensing, Vol. 26, No. 3, May 1988.

SEKER, S. S.: “A Simulation of Multi-Components Propagation Model of Lossy Medium”, Proc Millenium Conference on Antennas and Propagation, 2000.

SEKER, S. S.: “Radio pulse transmission along mixed paths in a stratified forest”, Proceedings of Inst. Elect. Eng., Vol. 136, part H, 1989.

SEVILLE, A., YILMAZ,U., CHARRIERE, P.R.V., POWELL, N., CRAIG, K.H., “Building scatter and vegetation attenuation measurements at 38 GHz”, Proceedings of ICAP 95, IEE Conference Publication No. 407, pp. 2.46-2.50, 1995.

SEVILLE, A.: “Vegetation Attenuation: Modelling and Measurements at Millimetric Frequencies”, 10th International Conference on Antennas and Propagation, Conference Publication No. 436, 14-17 April 1997.

STEPHENS, R. B. L., AL-NUAIMI, M. O. and CALDEIRINHA, R.: "Characterisation of depolarisation of radio signals by single trees at 20 GHz", Fifteenth National Radio Science Conference, Helwan, Cairo, Egypt, B12 1-7, Feb. 24-26, 1998.

STEPHENS, R. B. L., AL-NUAIMI, M. O.: “Attenuation measurements and modelling in vegetation media at 11.2 GHz and 20 GHz”, Electron Lett., 31, (20), pp. 1783-1785, 1995.

STEPHENS, R.B.L.: “A study and modelling of the propagation effects of vegetation on radiowaves at cm-wavelength frequencies”, PhD thesis, University of Glamorgan, 1998.

TAMIR, T. “On radio-wave propagation in forest environments”, IEEE Trans. AP-15 (6), pp. 806-817, 1967.

TORRICO, S. A., BERTONI, H. L.: 'Modelling Tree Effects on Path Loss in a Residential Environment', IEEE Transactions on Antennas and Propagation, Vol. 46. No. 6, June 1998.

VOGEL, W. J., GOLDHIRSH, J.: “Fade Measurements at L-band and UHF in Mountainous Terrain for Land Mobile Satellite Systems”, IEEE Transactions on Antennas and Propagation, Vol.AP-36, No. 1, pp. 104-113, 1988.

VOGEL, W. J., GOLDHIRSH, J.: “Tree Attenuation at 869 MHz derived from remotely piloted aircrafted measurement”, IEEE Transactions on Antennas and Propagation, Vol.AP-34, No. 11, pp. 1460-1464, 1986.

WEISSBERGER, M. A.: “An initial critical summary of models for predicting the attenuation of radio waves by trees”, ESD-TR-81-101, EMC Analysis Center, Annapolis, MD, USA, 1982.

A Contributions to the International Telecommunication Union (ITU-R)

A.1 Contents

A.1.1 The following three papers were contributed to the ITU-R as a result of the studies presented in this report. The first contribution is an information paper describing the Generic Model. The second suggests procedures for measuring and determining RET parameters and the third paper describes the Generic Model in detail.

A.1.2 The three papers are reproduced in this appendix in the form they were submitted in May 2002.

INFORMATION PAPER

A Generic Model for Propagation through Vegetation

Introduction

In the case of land mobile systems as well as wireless fixed access systems, the propagation path may encounter single trees, large bushes, forests etc. These obstructions may then give rise to both absorption and scatter of radio signals, both of which must be modelled if radio communications services are to be optimised during the planning or development phase.

To develop a generic vegetation attenuation model, which takes into account aspects such as path geometry (i.e. locations of transmitter and receivers in relation to the vegetation), vegetation density, systems characteristics, etc the UK have developed a generic attenuation model based on an extensive measurement campaign and deterministic modelling.

The work was funded by the UK Radiocommunications Agency and performed by a consortium comprising four parties: The Centre for R.F. Propagation and Atmospheric Research (CPAR) at QinetiQ, Malvern; The Radio Communications Research Unit at the Rutherford Appleton Laboratory, The Microwave Telecommunication Systems Research Group (MTSRG) at the University of Portsmouth and The Radiowave Propagation and System Design (RP&SD) Research Unit at the University of Glamorgan.

The output of the study programme has resulted in three key deliverables:

1 an extensive data base of measurements which comprises the measurement data, diagrams of the measurements scenario, and descriptions of the measurement hardware;

2 a method describing how vegetation depth and phase function measurements can be made in the field and how the data can be used to provide user defined RET information as input to the generic model;

3 a generic vegetation attenuation model.

The generic model is simple to implement and could be integrated into existing GIS databases. For example, when applied to radio-planning type modelling using GIS data or Forestry Commission data, a simple survey of the path through vegetation may be used as input to the vegetation model. If these databases do not have the appropriate input data, such as foliage density, or electrical parameters directly, then these parameters may be interpolated from available information such as species, height, age of planting or photographic data.

Rationale

Much work has been done to date on propagation through vegetation, such as the Radiative Energy Transfer (RET) modelling within the University of Glamorgan [1] and elsewhere [2,3]. However this work has been limited to one particular aspect of the through-vegetation path, namely the scattered component, and is valid for millimetric frequencies. RCRU were previously involved in the development of an empirical model [4], based on a series of measurements of attenuation through vegetation, which was adopted in ITU-R 833 [5]. The ITU model includes some consideration of a component diffracted around the edges of the canopy, but still has many limitations.

The aim of this project was to combine and extend these approaches by increasing the number of measured species, geometries and frequencies giving more separable results for the differing mechanisms of propagation through the vegetation. Furthermore, by the inclusion of vegetation parameters characterising the density of vegetation in the model, a more complete and predictable model could be developed.

Measurement Campaign

A campaign of (wide and narrowband) measurements have been made at over 10 locations, consisting of 10 different tree species (in various states of foliage). Specific measurements were made to identify and separate individual mechanisms for propagation through (or even around) the vegetation, in order to determine which components the general model should include.

In addition to these RF measurements, a characterisation of the density of the vegetation was made by taking hemispherical canopy photographs of the foliage from ground level with a high resolution camera with a Fisheye lens. These photographs were analysed to determine the fraction of sky not obscured by the canopy (the Gap Fraction) and the leaf area index (LAI) using a computer program called HemiView.

Narrowband Measurements

Narrowband Measurements were performed to provide the basic data for the development and frequency scaling of the generic model. The equipment used consisted of “Off the shelf” test equipment and broadband antennas enabling measurements to be made at spot frequencies from 2GHz – 18GHz (at 500MHz intervals). Each measurement consisted of a time series sampled at 1kHz rate in order to provide a study of the dynamic effects of the vegetation. The ease of measurements with the narrowband system enabled a more intensive study of the effects at specific locations. For example, at one location, the receiver height was varied from 5-17m in 2m increments to investigate the possibility of a ‘diffracted’ or ‘surface’ component coming over the top of the foliage.

In addition, phase (or scatter) function measurements have been made and the results used to provide input parameters into the Radiative Energy Transfer model.

Wideband Study

Measurements were also made using two wideband channel sounders at frequencies of 1.3GHz, 2.0GHz, 11.2GHz, 37.5GHz and 60GHz. The results of these measurements were used to augment the development of the narrowband model (ie the latter two frequencies extending the frequency range of the narrowband data), and also to provide wideband characterisation of the channel through vegetation. In addition to this, the data provided further insight into the actual propagation mechanism, in terms of the path delays of individual signal components.

Development of the Generic Model

A database of measured results has been formatted and collated which includes full details of the measurement system used and the measurement geometry. These data, consisting of over 12000 individual measurements, were used to determine in the first instance over which frequency range, and for what geometry, each of the various propagation mechanisms dominate.

The data were compared with a diffraction model (ITU-R Rec 526, as in ITU-R Rec 833). Where the measured attenuation was lower than the diffraction limit, and must therefore be due to the scatter component, the data were used to determine reasonable values of the required input parameters for the modelling of the scattered component.

A first order approximation to the Radiative Energy Transfer (RET) has been adopted and values for the input parameters (such as the scatter function main lobe beamwidth and the albedo) obtained by comparison with the phase function measurements and attenuation rate measurements at different frequencies and for different species. This model is used as the “engine” to determine the scattered component for a given path through vegetation. The attenuation from the scattered component is then combined with the attenuation from other mechanism to determine the total vegetation attenuation for the path.

Outline method of application

Each of the following components are calculated and then power-combined to provide a prediction of the overall attenuation.

Calculation of the Top- and Side-diffracted component

The diffracted field over and around the vegetation is calculated as per ITU-R Recommendation 526 [6], and may be treated as double isolated knife-edge diffraction.

Calculation of the ground reflected component

To calculate the power of the ground reflected wave at the receiver, the reflection coefficient of the ground reflected signal may be calculated using the method outlined in ITU-R Report 1008-1 [7] with values for the permitivity and conductance obtained from ITU-R Rec. 527 [8].

Calculation of the "through" or scattered component

In order to make accurate predictions of the excess attenuation due to vegetation, the user must input the following parameters into the RET equation:

i) α, the ratio of the forward scattered power to the total scattered power

ii) β, the beamwith of the phase function

iii) σ_τ, the combined absorption and scatter coefficient

iv) W, the albedo

v) $\Delta\gamma_R$, the beamwith of the receiving antenna

vi) d, the distance into the vegetation in metres

Given the input parameters: frequency (in GHz), the typical leaf size of the vegetation to be modelled and the Leaf Area Index (LAI) of the tree species, one can obtain the nearest value of α, β, W and σ_τ from the RET parameter tables. These tabled parameters were obtained by fitting to measurements of attenuation as a function of vegetation depth). Should these parameters be unavailable, one should assume the nearest match from the species listed to the tables.

Alternatively parameters for unknown geometries, species and frequencies can be determined experimentally, using a method developed within the consortium. These values of the parameters obtained can then be used to further populate the tables.

These 4 tabled parameters, together with the frequency, and the 3dB beamwidth of the receive antenna, are then used in the RET Engine. The code provided will convert the 3dB beamwidth provided by the user into Gaussian beamwidth and will calculate the excess attenuation due to vegetation at a given vegetation depth as a loss in dB.

Conclusion

A generic vegetation attenuation model has been developed which takes into account differing system geometries and vegetation type/density. The model is based on an extensive measurement campaign and deterministic modelling. The generic model is simple to implement and could be integrated into existing GIS databases. For example, when applied to radio-planning type modelling, GIS data or Forestry Commission data, even a simple survey of the path through vegetation may be used as input to the vegetation model. If these databases do not have the appropriate input data such as foliage density, or electrical parameters directly, then these parameters may be interpolated from available information such as species, height, age of planting or photographic data.

Consideration is being given by UK SG3 whether the method in its present from is suitable for adoption within ITU.

References

1. AL-NUAIMI, M. O. and HAMMOUDEH, A. M., " Measurements and Predictions of Attenuation and Scatter of Microwave Signals by Trees", IEE Proceeding on Antennas and Propagation, Part H, Vol. 141, No. 2, 1994.
2. JOHNSON, R. A. and SCHWERING, F.: 'A transport theory of millimeter wave propagation in woods and forests', CECOM-TR-85-1, Fort Monmouth, New Jersey, 1985
3. ISHIMARU, A: 'Wave propagation and scattering in random media', Academic Press, Vol. 11978.
4. SEVILLE, A.: 'Vegetation Attenuation: Modelling and Measurements at Millimetric Frequencies', 10th International Conference on Antennas and Propagation, Conference Publication No. 436, 14-17 April 1997.
5. ITU-R Rec. 833-2, Attenuation in vegetation, Int. Telecom. Union, Geneva, 2000.
6. ITU-R Rec. 526-3, Propagation by Diffraction, §4, Int. Telecom. Union, Geneva, 2000.
7. CCIR Report. 1008-1, Reflections from the surface of the earth, §2, 1990.
8. ITU-R Rec. 527-3, Electrical characteristics of the surface of the earth, §2, Int. Telecom. Union, Geneva, 2000.

INTERNATIONAL TELECOMMUNICATION UNION
RADIOCOMMUNICATION STUDY GROUPS

Document 3K/UK-XXX
7 May 2002
Original: English only

United Kingdom

MEASURING THE INPUT PARAMETERS FOR THE RET

1 Introduction

The Radiative Energy Transfer Theory (RET) allows an analytical calculation of the attenuation of a scattering medium, such as vegetation. It forms an integral part of a generic model developed as part of a project funded by the UK Radiocommunications Agency and performed by a consortium comprising four parties: The Centre for R.F. Propagation and Atmospheric Research (CPAR) at QinetiQ, Malvern; The Radio Communications Research Unit at the Rutherford Appleton Laboratory, The Microwave Telecommunication Systems Research (MTSRG) Group at the University of Portsmouth and The Radiowave Propagation and System Design (RP&SD) Research Unit at the University of Glamorgan.

2 RET Input Parameters

The RET requires six input parameters, four of which are specific for the scattering medium and two are geometry and system descriptors. The four medium dependent parameters need to be established experimentally and are dependent on the type of vegetation, frequency and state of foliation.

i) α, the ratio of the forward scattered power to the total scattered power
ii) β, the beamwith of the phase function
iii) σ_t, the combined absorption and scatter cross-section
iv) W, the albedo
v) $\Delta\gamma_R$, the beamwith of the receiving antenna
vi) d, the distance into the vegetation in metres

The parameters α and β are best determined by measuring the scatter function usually referred to as the 'phase' function of the vegetation medium. The phase function characterises the scattering behaviour of the medium at short distances after the air vegetation interface. Section 3 describes the phase function measurements in more detail. Parameters σ_t and W can be determined from attenuation curve measurements into the vegetation medium described in section 4.

3 Phase Function Measurements

The phase function (PF) forms an integral part in the determination of the parameters needed for the Radiative Energy Transfer Theory RET. This recommendation presents a guide outlining how to conduct phase function measurements. The main purpose of such measurements will be to extract the parameters α and β required for the derivation of the RET model.

3.1 Choosing the Measurement Site

Phase function measurements are necessary to derive the parameters α and β for the vegetation medium, which in turn enables RET modelling of excess attenuation in the medium. In many cases the phase function measurement will therefore be conducted in conjunction with measurements of the

excess attenuation experienced in the vegetation medium as a function of vegetation depth. An ideal site will comprise of a group of trees, behind which receiver access at various depth locations is possible. The site requires a reasonable foreground clearance to enable the tree group to be illuminated by the transmitter, thus fulfilling the condition of a half space of vegetation, illuminated with an incident plane wave signal. Furthermore, the site needs to be free of objects that can cause spurious reflected signals to interfere with the scattered signal from the trees to the receiver location.
Phase function measurements combined with excess attenuation measurements, performed for a line of trees made up of the same tree species can jointly provide the RET parameters. The results can be used to develop a prediction model for the behaviour of excess attenuation as a function of vegetation depth.

3.2 Measurement Geometry

The RET describes the energy transfer in a medium exhibiting both scattering and absorbing properties. This is treated by the RET as homogenous infinite half space. Both transmit and receive antennas are arranged to have a common volume irradiated in the scattering medium. Under these conditions the RET postulates a phase function with Gaussian shaped forward lobe and an isotropic background. The two parameters α and β, define the exact shape of which for the vegetation medium is depend on factors such as the species and density of vegetation and foliation state. The location at which the phase function is measured is also important. The RET predicts that the forward lobe broadens as the observation point moves inside the medium. This occurs due to the attenuation of the coherent component and the relative increase in the level of the isotropic scatter. This suggests that there is an optimum region within which the measurement should be conducted.

The following conditions are proposed for the measurement geometry.

(i) The region in which the phase function measurement is carried out needs to lie within that defined by the initial predominately linear (dB scale) slope of the excess attenuation curve. A location 2 to 3 trees deep into the medium is recommended. This allows sufficient amount of scattering medium after the interface to be present to result in an isotropic back-scatter coherent forward lobe, without the widening of the forward lobe taking part yet.

(ii) The assumption of homogeneity of the medium in the RET is more easily satisfied in the canopy region of the tree rather than that containing the trunk. A further benefit of largely confining the common volume to the canopy region is accrued from the avoidance of strong diffracted and reflected signal components emanating from trunks and the ground. In single tree measurements of the phase function it was found that illuminating around 70 to 90% of the tree canopy yields good results. When groups of trees are considered, the transmit antenna vegetation distance should be fixed carefully. This distance in combination with the transmit antenna elevation beamwidth are utilised to ensure that ground reflections and diffraction components over the top of the canopy are minimised.

(iii) The phase function forward lobe is aligned with the direction of propagation of the incident signal. It is therefor preferable to place the transmit and receive antennas at the same height. This also ensures normal incidence conditions. If the heights differ the phase function will be tilted with respect to the horizontal and the direction of incidence. The orientation of the receiver antenna as well as that of the axis of rotation needs to be adjusted accordingly. The beamwidth of the phase function is relatively narrow, so that tilts of a few degrees with respect to the receiver alignment will lead to significant reduction of the magnitude of the forward lobe and consequently the determination of α.

3.3 Antenna Characteristics

3.3.1 Transmit Antenna

The beamwidth of the transmit antenna needs to be wide enough to illuminate sufficient width and height of vegetation in order to provide together with the receive antenna sufficient excited common volume for the measurement. However, the beamwidth must be, relatively speaking, narrow as not to

give rise to diffracted and reflected signal components, which will influence the measured phase function pattern.

3.3.2 Receive Antenna

The receive antenna ideally has a very small beamwidth, in order to measure the relatively narrow beamwidth of the phase function itself. In practice a receive antenna of a few degrees beamwidth gives good results.

3.4 Receiver Antenna Displacement

The most practical and most accurate method to measure the phase function is to place the receiver antenna inside the vegetation medium at a distance from the air vegetation interface specified in section 3.2. At this location the receiver antenna needs to be rotated about its vertical axis in discrete increments after each the signal level needs to be recorded. Since the beamwidth of the phase function is considered to be relatively narrow the antenna only needs to be rotated over a section of a circle, e.g. ± 40º with respect to the line receiver – transmitter. The principal set up is sketched in figure 1.

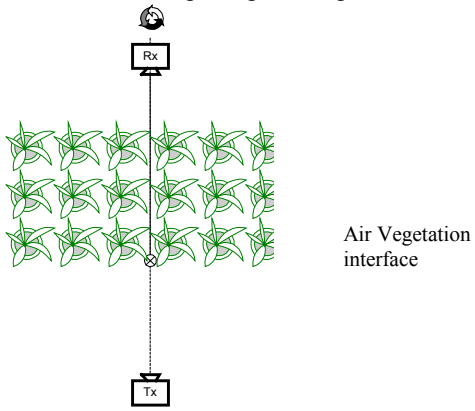

Figure 1: Principal measurement set up for phase function measurement

3.5 Link Budget considerations

Apart from the free space loss due to the distance between transmitter and receiver the excess attenuation of the vegetation as well as the difference between forward lobe and isotropic back-scatter region of the phase function have to be considered. At millimetre and near millimetre frequencies the attenuation resulting from one large dense tree can be considerable, i.e. in the region of a few 10s of dB. Even at 11 GHz a large horse chestnut tree in full leaf was found to give as much 35dB attenuation. The difference between forward lobe and back-scatter regions of the phase function, is expected to be between 20 and 50 dB depending on the values of α. The measurement system must have sufficient dynamic range to overcome the strong initial excess attenuation due to vegetation, and the difference in level between the forward lobe signal and the back-scatter. As a guide the dynamic range of the receiver needs to be about 80 dB to yield the phase function shape and parameters.

4 Excess Attenuation Curve Measurements

Excess attenuation curve measurements are obtained by measuring the signal level at various depth into the vegetation medium. The RET predicts a graph with an initially linear part (in dB) and a transition region into a final attenuation rate. The slope of the initial slope is used to obtain the parameter σ_t. Whereas the transition region and the final attenuation rate are used to find the parameter W (albedo) via best fit curve fitting.

4.1 Determination of parameter σ_τ using initial slope

The first term I_{ri} of the RET equation describes the initial slope of the attenuation function with distance *z* in metres.

$$P = P_0 \cdot e^{-\sigma_\tau z} \quad \textbf{(1)}$$

Where *P* is the measured signal power inside the vegetation and P_0 is the power received at the incident air-vegetation interface. The RET describes excess attenuation due to vegetation, so that the signal decay, due to free space loss, is not included in *P*.
If the attenuation curve is displayed in dB Eq.11 can be written as:

$$10 \cdot \log \frac{P}{P_0} = -10 \cdot \log(\sigma_\tau z \log e) \quad \textbf{(2)}$$

The initial slope of the graph (dB/m) is given by:

$$\frac{\Delta A}{\Delta d} = -4.43 \cdot \sigma_\tau \quad \textbf{(3)}$$

where $A = 10 \cdot \log \frac{P}{P_0}$ is the attenuation in dB.

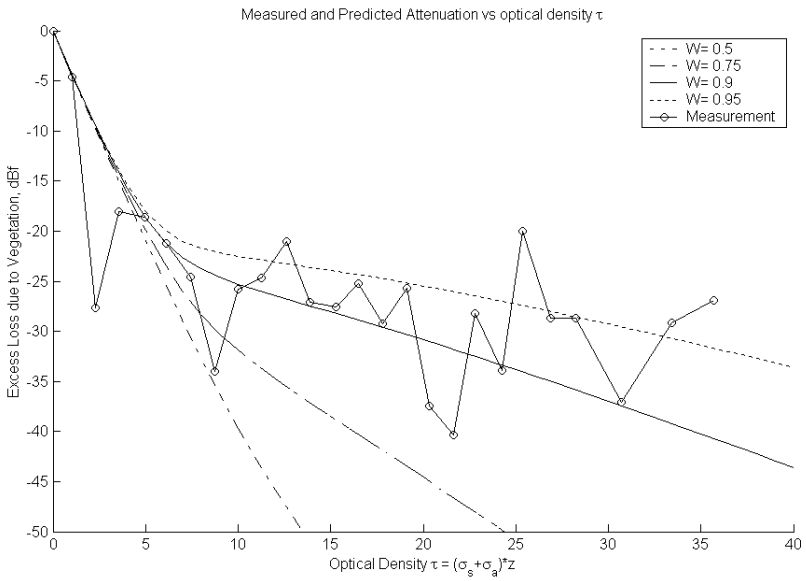

Figure 2: Predicted and Measured Excess attenuation vs optical density τ for different albedos

Figure 2 illustrates the fitting of predicted attenuation curves with different albedos to measured excess attenuation.

In order to model the RET attenuation curves the RET equation needs to be calculated. The RET equation is as follows:

$$\frac{P_R}{P_{\max}} = e^{-\tau} \qquad (I_{ri})$$

$$\left.\begin{aligned} &+\frac{\Delta\gamma_R^2}{4}\cdot\{[e^{-\hat{\tau}} - e^{-\tau}]\cdot\overline{q}_M \\ &+ e^{-\tau}\cdot\sum_{m=1}^{M}\frac{1}{m!}(\alpha W\tau)^m\ [\overline{q}_m - \overline{q}_M]\} \end{aligned}\right\} (I_1) \qquad (4)$$

$$+\frac{\Delta\gamma_R^2}{2}\cdot\{-e^{-\hat{\tau}}\cdot\frac{1}{P_N} + \sum_{k=\frac{N+1}{2}}^{N}[A_k e^{-\frac{\hat{\tau}}{s_k}}\cdot\sum_{n=0}^{N}\frac{1}{1-\frac{\mu_n}{s_k}}]\} \qquad (I_2)$$

where P_R is the received power by the receiving antenna with its gain pattern and $P_{\max}$ is the received signal strength received in the absence of vegetation. $\Delta\gamma_R$ is the beamwidth of the receiving antenna, and *m* is the order of the term I_1. The term I_1 is more accurately evaluated for higher values of *m*, however it will not change significantly for *m* > 10. N in I_2 has to be an odd number larger than 1. A compromise has to be found between accuracy and computing time. Large values for *N* will increase computing time dramatically. Reasonable values were found to be: 11 < N < 21.

The following relations also apply:

$$\tau = (\sigma_a + \sigma_s)\cdot z = \sigma_\tau \cdot z$$

τ defines the optical density and z is the distance in metres

$$\overline{q}_m = \frac{4}{\Delta\gamma_R^2 + m\beta^2}$$

$$\mu_n = -\cos(\frac{n\pi}{N})$$

$$P_n = \sin^2(\frac{\pi}{2N}) \qquad \text{for } n = 0, N \qquad (5)$$

$$P_n = \sin(\frac{\pi}{N})\cdot\sin(\frac{n\pi}{N}) \qquad \text{for } n = 1,2,...,N-1$$

$$\hat{\tau} = (1-\alpha W)\tau$$

$$\hat{W} = \frac{(1-\alpha)W}{1-\alpha W} \qquad \hat{W} \text{ is refered to as the reduced albedo}$$

The first line in the RHS of Eq. 7 represents I_{ri}, which is usually refered to as the *'first'* term, whereas the sum of the second and third line give I_1, refered to as the *'second'* term. These appear in explicit form. The fourth line represents the *'third'* term I_2 of the RET equation , which contains the attenuation coefficients s_k and the amplitude factors A_k. These need to be determined numerically using the following expressions:

The attenuation coefficients s_k are determined by the characteristic equation:

$$\frac{\hat{W}}{2}\cdot\sum_{n=0}^{N}\frac{P_n}{1-\frac{\mu_n}{s}} = 1 \qquad (6)$$

The LHS of eqn. 9 will equal 1 for values of *s*, which represent the roots of this equation. It will yield *N + 1* roots, for which the following applies:

$$s_{0,\ldots,\frac{N}{2}} = -s_{N,\ldots,\frac{N+1}{2}}$$

The amplitude factors A_k are determined by a system of linear equations given by:

$$\sum_{k=\frac{N+1}{2}}^{N} \frac{A_k}{1-\frac{\mu_n}{s_k}} = \frac{\delta_n}{P_N} \qquad \text{for} \qquad n = \frac{N+1}{2} \quad \ldots. \quad N \tag{7}$$

The linear system of equations can be written in matrix form $A \cdot B = C$ as follows:

$$\begin{bmatrix} A_{\frac{N+1}{2}} \\ \vdots \\ A_N \end{bmatrix} \cdot \begin{bmatrix} b_{\frac{N+2}{2},\frac{N+2}{2}} & \cdots & b_{\frac{N+2}{2},N} \\ \vdots & & \vdots \\ b_{N,\frac{N+2}{2}} & \cdots & b_{N,N} \end{bmatrix} = \frac{\delta_n}{P_N}$$

where: **(8)**

$$b_{n,k} = \frac{1}{1+\frac{\mu_n}{s_k}} \qquad \text{with} \quad k,n = \frac{N+1}{2} \quad \ldots \quad N$$

$$\delta_n = 0 \quad \text{for} \quad n \neq N$$

and

$$\delta_n = 1 \quad \text{for} \quad n = N$$

This system of equations can be solved for coefficients A_k using for example Gaussian elimination.

When using antenna beamwiths in these equations, it has to be taken into account that the antenna gain beamwidth and the scatter function beamwidth in Eq. 7 have been assumed to be Gaussian. Using a Gaussian shape the mainlobe of the power radiation pattern is reduced by 1/e. The resulting beamwidth of the Gaussian pattern is related to the 3 dB beamwidth by $\Delta\gamma_R = 0.6 \cdot \Delta\gamma_{3db}$.

INTERNATIONAL TELECOMMUNICATION UNION
RADIOCOMMUNICATION STUDY GROUPS

Document 3K/UK-XXX
7 May 2002
Original: English only

United Kingdom

Proposed Revision to the method for predicting Vegetation Attenuation above 1 GHz in Recommendation ITU-R P.833-3

Summary

This document contains a proposed modification to the recommendation on Attenuation in Vegetation, ITU-R P.833-3.

The existing section 3.2 is a model for the attenuation due to propagation through vegetation for frequencies above 5 GHz that was based on a fit to a database of measured data. This document presents an improved detailed model that fully considers the effects of separate modes of propagation around, over, beneath and through the vegetation. Each of the around vegetation components is calculated using existing ITU-R recommendations, and the through or scattered component is calculated using a model based upon the theory of Radiative Energy Transfer (RET). The components are then combined to estimate the attenuation. The new model extends the frequency coverage down to 1 GHz.

The model has been tested against the results from a campaign of Wideband and Narrowband measurements made at over 10 locations, for 10 different tree species in various states of foliage. Specific measurements were made to identify and separate individual mechanisms for propagation through (or around) the vegetation, in order to determine which components the general model should include. In addition to these RF measurements, a characterisation of the density of the vegetation was made by taking hemispherical canopy photographs of the foliage from ground level with a high-resolution camera with a fisheye lens. The proposed changes are presented in Annex 1.

References

1. ITU-R Rec. 833-3, Attenuation in vegetation, Int. Telecom. Union, Geneva, 2001.
2. ITU-R Rec. 526-7, Propagation by Diffraction, §4, Int. Telecom. Union, Geneva, 2001.
3. CCIR Report. 1008-1, Reflections from the surface of the earth, §2, 1990.
4. ITU-R Rec. 527-3, Electrical characteristics of the surface of the earth, §2, Int. Telecom. Union, Geneva, 2000.

Annex 1

Proposed change to Rec. P.833-3

Change the title of section 3.1 to read:

3.1 At or below 1 GHz

Replace the existing section 3.2 with the following:

3.2 Above 1 GHz.

In order to estimate the total field, the diffracted, ground reflected and through vegetation scattering components are first calculated and then combined.

The diffracted components consist of those over the top of the vegetation and those around the sides of the vegetation and are calculated using existing ITU-R recommendations. The ground reflected component is calculated using ITU-R recommendations and the method of CCIR Report 1008-1. The through or scattered component is calculated using a model based upon the theory of Radiative Energy Transfer (RET).

Calculation of the Top diffracted component

The diffraction loss, L_{top}, experienced by the signal path diffracted over the vegetation, may be treated as double isolated knife-edge diffraction for the geometry defined in Figure 3.

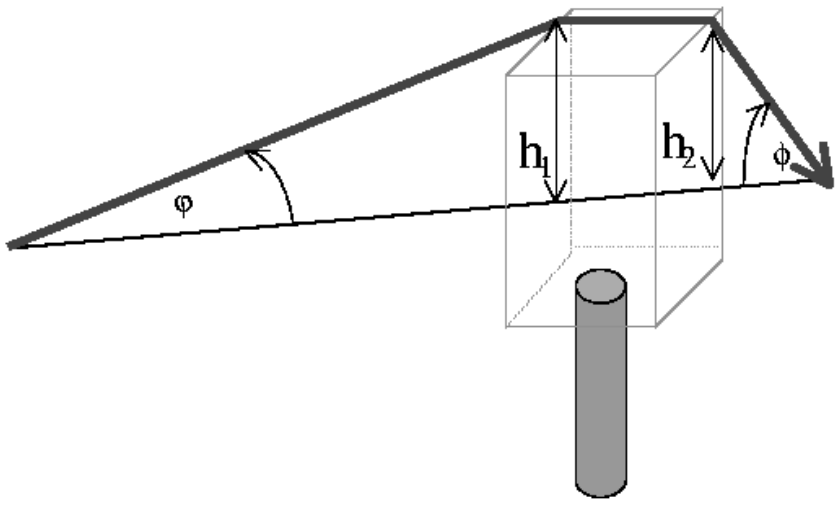

Figure 3

This calculated as per ITU-R Recommendation 526-3, §4.4:

$$L_{top} = 6.9 + 20\log\left(\sqrt{(\nu(h_1)-0.1)^2+1}+\nu(h_1)-0.1\right)+G_{Tx}(\varphi)$$
$$+ 6.9 + 20\log\left(\sqrt{(\nu(h_2)-0.1)^2+1}+\nu(h_2)-0.1\right)+L_c+G_{Rx}(\phi) \quad [4]$$

where $G_{Tx}(\varphi)$ and $G_{Rx}(\phi)$ are the losses due to angles of the diffracted wave leaving the transmit antenna and coming into the receive antenna, respectively.

Calculation of the Side Diffracted component

The diffraction loss, L_{sidea} and L_{sideb}, experienced by the signal diffracted around the vegetation, may be treated as double isolated knife-edge diffraction, for the geometry defined in Figure 4.

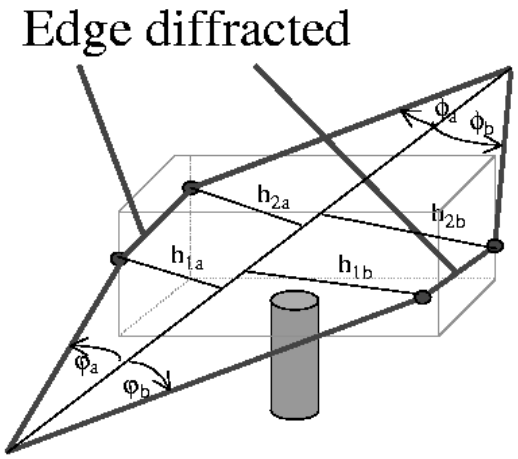

Figure 4

This calculated as per ITU-R Recommendation 526-7, §4.4:

$$L_{sidea} = 6.9 + 20\log\left(\sqrt{(\nu(h_{1a})-0.1)^2+1}+\nu(h_{1a})-0.1\right)+G_{Tx}(\varphi_a)$$
$$+ 6.9 + 20\log\left(\sqrt{(\nu(h_{2a})-0.1)^2+1}+\nu(h_{2a})-0.1\right)+L_c+G_{Rx}(\phi_a) \quad [5]$$

and

$$L_{sideb} = 6.9 + 20\log\left(\sqrt{(\nu(h_{1b})-0.1)^2+1}+\nu(h_{1b})-0.1\right)+G_{Tx}(\varphi_b)$$
$$+ 6.9 + 20\log\left(\sqrt{(\nu(h_{2b})-0.1)^2+1}+\nu(h_{2b})-0.1\right)+L_c+G_{Rx}(\phi_b) \quad [6]$$

where $G_{Tx}(\varphi_{a,b})$ and $G_{Rx}(\phi_{a,b})$ are the losses due to angles of the diffracted wave leaving the transmit antenna and coming into the receive antenna, for side a and b, respectively.

Calculation of the ground reflected component

It is assumed that the path is sufficiently short that the ground reflected wave may be modelled by the geometry shown in Figure 5.

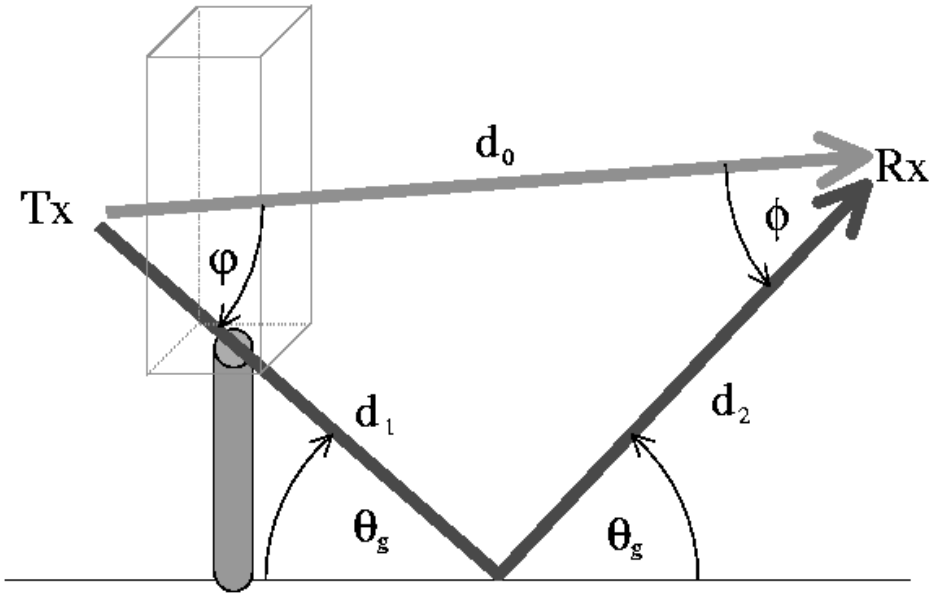

Figure 5

To calculate the Loss experienced by the ground reflected wave at the receiver, the reflection coefficient, R_0, of the ground reflected signal may be calculated using the method outlined in CCIR Report 1008-1, with a given grazing angle θ_g. The values for the permittivity and conductance are obtained from ITU-R Rec. 527-3.

The loss experienced by the ground reflected wave, L_g , is then given by

$$L_{ground} = 20\log_{10}\left(\frac{d_1 + d_2}{d_0}\right) - 20\log_{10}(R_0) + G_{Tx}(\varphi) + G_{Rx}(\phi) \qquad [7]$$

where $G_{Rx}(\varphi)$ and $G_{Tx}(\phi)$ are the losses due to angles of the reflected wave leaving the transmit antenna and coming into the receive antenna, respectively.

Calculation of the "through" or scattered component

In order to make accurate predictions of the excess attenuation to vegetation the user needs to input the following parameters into the RET equation (equation [8]):

i) α, the ratio of the forward scattered power to the total scattered power

ii) β, the beamwidth of the phase function

iii) σ_t , the combined absorption and scatter coefficient

iv) W, the albedo

v) $\Delta\gamma_R$, the beamwidth of the receiving antenna

vi) d, the distance into the vegetation in metres

Given the input parameters: frequency (in GHz), the typical leaf size of the vegetation to be modelled and the Leaf Area Index (LAI) of the tree species, one can obtain the nearest value of α, β, W and σ_τ from the RET parameter tables [tables1-4]. Should these parameters be unavailable, one should assume the nearest match from the species listed to the tables. Alternatively parameters for unknown geometries, species and frequencies can be determined experimentally, using the method outlined for determining these given in the RET phase function measurement recipe. The values of the parameters obtained can then be used to further populate the tables.

These 4 tabled parameters, together with the frequency, and $\Delta\gamma_{3db}$,the 3dB beamwidth of the receive antenna, are then used in the RET Engine. The code provided will convert the 3dB beamwidth provided by the user into Gaussian beamwidth and will calculate the excess attenuation due to vegetation at a given vegetation depth as a loss in dB.

The attenuation due to scatter through the vegetation, L_{scat}, is then given by:

$$L_{scat} = -10\log_{10}\left(\begin{array}{l} e^{-\tau} + \frac{\Delta\gamma_R^2}{4}\cdot\{[e^{-\hat{\tau}} - e^{-\tau}]\cdot\bar{q}_M + e^{-\tau}\cdot\sum_{m=1}^{M}\frac{1}{m!}(\alpha W\tau)^m\ [\bar{q}_m - \bar{q}_M]\} \\ + \frac{\Delta\gamma_R^2}{2}\cdot\{-e^{\hat{\tau}}\cdot\frac{1}{P_N} + \sum_{k=\frac{N+1}{2}}^{N}[A_k e^{\frac{\hat{\tau}}{s_k}}\cdot\sum_{n=0}^{N}\frac{1}{1-\frac{\mu_n}{s_k}}]\} \end{array}\right) \quad [8]$$

where

$\Delta\gamma_R = 0.6\cdot\Delta\gamma_{3db}$ (the 3dB beamwidth of the receiving antenna),

m is the order of the first term I_1 will not change significantly for $m > 10$ (hence for most cases, M=10),

$\tau = (\sigma_a + \sigma_s)\cdot z$ is the optical density τ as function of distance z

$$\bar{q}_m = \frac{4}{\Delta\gamma_R^2 + m\beta_S^2},$$

$$\beta_S = 0.6\cdot\beta$$

$$\mu_n = -\cos(\frac{n\pi}{N}), \quad [9]$$

$$P_n = \sin^2(\frac{\pi}{2N}),$$

$$\hat{\tau} = (1 - \alpha W)\tau ,$$

The attenuation coefficients s_k are determined by the characteristic equation:

$$\frac{\hat{W}}{2} \cdot \sum_{n=0}^{N} \frac{P_n}{1 - \frac{\mu_n}{s}} = 1$$

where: $P_n = \sin(\frac{\pi}{N}) \ \sin(\frac{n\pi}{N})$ and $\hat{W} = \frac{(1-\alpha)W}{1-\alpha W}$ [10]

The amplitude factors A_k are determined by a system of linear equations given by:

$$\sum_{k=\frac{N+1}{2}}^{N} \frac{A_k}{1 - \frac{\mu_n}{s_k}} = \frac{\delta_n}{P_N} \qquad \text{for} \qquad n = \frac{N+1}{2} \ .... \ N \qquad [11]$$

where:

$\delta_n = 0$ for $n \neq N$ and $\delta_n = 1$ for $n = N$

Combination of the individual components

The total loss, L_{total}, experienced by a signal propagating through trees is then given by the combination of loss terms:

$$L_{total} = -10 \log_{10} \left\{ 10^{\left(\frac{-L_{sdev}}{10}\right)} + 10^{\left(\frac{-L_{sdeb}}{10}\right)} + 10^{\left(\frac{-L_{top}}{10}\right)} + 10^{\left(\frac{-L_{ground}}{10}\right)} + 10^{\left(\frac{-L_{stem}}{10}\right)} \right\} \qquad [12]$$

	Horse Chestnut	Silver Maple	Silver Maple	London Plane	London Plane	Common Lime	Common Lime	Sycamore	Sycamore
	In leaf	In leaf	Out of leaf	In leaf	Out leaf	In Leaf	Out of Leaf	In leaf	Out of leaf
LAI		1.691		1.93		1.475		1.631	0.483
Leaf Size	0.300	0.15		0.250		0.100		0.15	
Frequency (GHz)	α								
1.3	0.9	0.95	0.9	0.95	0.9	0.9	0.95		0.95
2	0.75		0.95	0.95			0.95		0.95
2.2			0.95	0.5					
11	0.85	0.9		0.7	0.95	0.95	0.95		0.95
37				0.95					
61.5		0.8		0.25				0.9	

Table 1: Fitted values of α with frequency / species.

	Horse Chestnut	Silver Maple	Silver Maple	London Plane	London Plane	Common Lime	Common Lime	Sycamore	Sycamore
	In leaf	In leaf	Out of leaf	In leaf	Out leaf	In Leaf	Out of Leaf	In leaf	Out of leaf
LAI		1.691		1.93		1.475		1.631	0.483
Leaf Size	0.300	0.15		0.250		0.100		0.15	
Frequency (GHz)	β								
1.3	21	14	43	42	16	76	50		70
2	80		31	49			60		62
2.2			25	13					
11	69	58		100	19	78	48		44
37				18					
61.5		48		2				59	

Table 2: Fitted values of β with frequency / species.

	Horse Chestnut	Silver Maple	Silver Maple	London Plane	London Plane	Common Lime	Common Lime	Sycamore	Sycamore
	In leaf	In leaf	Out of leaf	In leaf	Out leaf	In Leaf	Out of Leaf	In leaf	Out of leaf
LAI		1.691		1.93		1.475		1.631	0.483
Leaf Size	0.300	0.15		0.250		0.100		0.15	
Frequency (GHz)					**W**				
1.3	0.25	0.95	0.25	0.95	0.95	0.95	0.95		0.85
2	0.55		0.95	0.95			0.95		0.95
2.2			0.95	0.45					
11	0.95	0.95		0.95	0.95	0.75	0.95		0.95
37				0.95					
61.5		0.8		0.5				0.9	

Table 3: Fitted values of albedo with frequency / species.

	Horse Chestnut	Silver Maple	Silver Maple	London Plane	London Plane	Common Lime	Common Lime	Sycamore	Sycamore
	In leaf	In leaf	Out of leaf	In leaf	Out leaf	In Leaf	Out of Leaf	In leaf	Out of leaf
LAI		1.691		1.93		1.475		1.631	0.483
Leaf Size	0.300	0.15		0.250		0.100		0.15	
Frequency (GHz)					σ_τ				
1.3	0.772	0.241	0.139	0.147	0.221	0.22	0.591		0.36
2	0.091		0.176	0.203			0.692		0.249
2.2			0.377	0.244					
11	0.124	0.321		0.75	0.459	0.56	0.757		0.179
37				0.441					
61.5		0.567		0.498				0.647	

Table 4: Fitted values of σ_τ with frequency / species

B A Review of Existing Vegetation Attenuation Models

B.1 Background

B.1.1 Wireless Communications are revolutionising personal and telecommunications services and the way in which they are utilised. Overall growth in cellular, fixed and satellite communication system markets in recent years has exceeded expectations. There is a widespread anticipation that customer demand for wireless telecommunication systems will continue to expand in the foreseeable future. In addition to providing a wide range of services, larger bandwidths may be required which is forcing system designers to consider frequencies at higher frequency bands e.g. microwave and millimetric frequencies.

B.1.2 The large number of users, especially mobile users, has resulted in network planners increasing system capacity by locating transmission antennas at heights that are comparable or lower than surrounding trees and buildings [Graham, 1998]. This reduces cell size (picocells) and increases the system capacity within a given area compared to larger cells (micro or macro cells). For successful network planning, and basic system design, propagation algorithms that determine the path loss and the signal coverage are critical to successful deployments. These prediction algorithms are also highly desirable for radio planners in predicting and controlling mutual co-channel interference between existing and new radio links.

B.1.3 In the case of land mobile systems as well as wireless fixed access systems, trees, bushes, hedges, etc. may occur singly or in a group, within the radio cell. These obstructions may then give rise to both absorption and scatter of radio signals. It is these scattering and absorption effects that must be investigated if the accuracy of planning tools, required for mobile and fixed-link radio communication services are to be improved and spectrum utilisation optimised.

B.1.4 To date, most of the interest has been centred at frequencies around the GSM (Groupe Spéciale Mobile) and the Digital Cellular System, DCS-1800 bands. At these frequencies, tree attenuation is considered as one of the dominant effects influencing radio propagation in rural and suburban areas [Cost 231, 1996], [DTI, 1997].

B.1.5 In [Caldeirinha, 2001a] the author performed analytical studies based on experimental measurements, and showed that the presence of trees, singly or as a group, in the radio path of a point-to-point link, could influence the level of the received signal:

a. directly by providing an additional (excess) attenuation to that caused by free space propagation;
b. indirectly by scattering which results in lateral contributions to the received signal;
c. through depolarisation of the incident wave which represents another significant factor influencing radiowave propagation [Al-Nuaimi, Hammoudeh, 1994a], [Al-Nuaimi, Stephens 1998], [Al-Nuaimi, Hammoudeh, 1993a].

B.1.6 The latter is especially significant at higher frequency bands, where the wavelength becomes comparable to the physical dimensions of the scattering elements of the tree [Stephens et al., 1998]. Propagation modes associated with absorption, scatter and

depolarisation are addressed in [Caldeirinha, 2001a], [Caldeirinha, Al-Nuaimi, 1999], [Caldeirinha, Al-Nuaimi, 2000].

B.1.7 Accurate modelling of the propagation of microwaves and millimetre waves through tree foliage, generally requires accurate electromagnetic description of the tree geometry, including its branches and leaves, valid over a wide range of frequencies. Also because of the complex physical processes arising from the propagation modes involved, approximate prediction models appropriately validated are very useful to radio systems planners and designers. At their most basic form, these models, referred to as empirical models, express the excess attenuation (that in addition to free space attenuation) of vegetation media as a function of frequency and path length through vegetation. Ideally, more developed forms of prediction models are required. These could take into consideration more specific details of the vegetation medium such as vegetation density, spatial distribution of trees, size and orientation of branches and leaves, and seasonal factors relating to foliation state and moisture content [Caldeirinha, Al-Nuaimi, 2001b], [Caldeirinha, Al-Nuaimi, 2001c]. In addition to these physical parameters, radio system characteristics, such as frequency, antenna heights, polarisation, azimuth and elevation etc, should (ideally) also be included.

B.1.8 Propagation effects on terrestrial communications systems in the microwave and millimetre wave frequency bands have been the subject of considerable study in the last few years. Measurements available in the literature up to about 1982 are summarised in Weissberger´s report [Weissberger, 1982] and to a lesser extent in Section B.6. In the former, where fifty reports, journal articles, and texts are reviewed, the report falls into two broad categories: the available prediction models and the available measurements data.

B.1.9 Most of the vegetation models found in the literature have been formulated for military purposes for the development of new numerical communication techniques and radar systems. Empirical and theoretical (statistical and analytical) models have been developed to characterise the effects of vegetation on the propagation of radiowaves [Matschek, Linot, 1999]. Empirical modelling has received limited interest over the last six years, though it was very popular in the period of 1985-1995 [Karaliopoulos, Pavlidou, 1999]. Statistical modelling seems to have been the favoured modelling approach over the last 10 years, as well as numerical techniques aimed at solving the relevant wave equations [Caldeirinha, Al-Nuaimi, 2001c].

B.1.10 The different models available outlined below are classified in three categories. These are emperical, semi empirical and analytical models.

B.2 Overview of Empirical Models

B.2.1 The considerable advantage of empirical models is the simplicity of the final mathematical expressions which describe them, and hence, their easy application.

B.2.2 One of the drawbacks of empirical modelling, is that formulated models are strictly related to specific measured data sets and fail to give any indication as to the physical processes involved in the propagation within the channel [Karaliopoulos, Pavlidou, 1999]. Such models usually refer either to the mean attenuation of the propagation signal caused by vegetation or to the calculation of the link budget needed to compensate for propagation losses and deep fades caused by vegetation. Parameters in these models, e.g. frequency,

incident angles, path length through vegetation and other parameters associated with the specific environment under which measurements were performed, are usually computed through regression curves fitted to measurement data.

B.2.3 It should also be stressed that the semi-empirical vegetation models have a problem shared with other models (e.g. RET) in that they give little account of the dynamic effects of the channel [Paulsen, Seville, 2000], [Lewenz, 1999] and no account of the wideband effects of the vegetation medium.

B.3 The Modified Exponential Decay Model (MED)

B.3.1 Weissberger developed a Modified Exponential Decay model (MED) after reviewing several exponential decay models. These expressed the specific attenuation [dB per meter] of path length, and were based on several sets of available measured attenuation data carried out in different environments in the United States at frequencies from 230 MHz to 96 GHz. He concluded that an exponential decay model was appropriate for those situations where the propagation occurred through a body (grove) of trees rather than by diffraction. The model is described by Equations B-1 and B-2,

$$L = 1.33 f^{0.284} d^{0.588} \quad \text{for } 14m \le d \le 400m \qquad \textit{Equation B-1}$$

$$L = 0.45 f^{0.284} d \quad \text{for } 0m \le d < 14m \qquad \textit{Equation B-2}$$

where L is the loss in dB, f is the frequency in GHz, and d is the depth of trees in meters.

B.3.2 The difference in path loss for trees with and without leaves reported in [Weissberger, 1982] is 3 to 5 dB in the frequency range of 450-950 MHz. The model shown in Equations B-1 and B-2, for prediction of attenuation caused by vegetation, was assessed in [Al-Nuaimi, Hammoudeh, 1993b] and was found to offer a very poor fit to measured data at higher frequencies (11.2 - 20 GHz) compared to that obtained at UHF and VHF frequencies. It is desirable that an empirical model should also consider other factors, such as tree type, density of trees and moisture contents of leaves in the canopy. However, the inclusion of these factors in such a model cannot be readily achieved, and further research supported by measured data is necessary.

B.4 The ITU-R Model and its Derivatives

B.4.1 The International Telecommunications Union of Radio sector (ITU-R) model and its derivatives can be found within the published literature for predicting the attenuation of vegetation media. These empirical models, as presented in [Stephens, 1998], have been optimised for different geometries and types of vegetation, providing quick and general estimates of the amount of excess attenuation caused by a particular vegetation medium.

B.4.2 The model proposed in COST 235 [Cost 235, 1996] takes the form of Equations B-3 and B-4, for the case of vegetation in both foliated states; in-leaf and out-of-leaf.

$$L = 15.6 f^{-0.009} d^{0.26} \quad \text{[dB]} \quad \textit{In-leaf} \qquad \textit{Equation B-3}$$

$$L = 26.6 f^{-0.2} d^{0.5} \quad \text{[dB]} \quad \textit{Out-of-leaf} \qquad \textit{Equation B-4}$$

where frequency f and distance d are expressed in MHz and m respectively.

B.4.3 Further optimisation of the three numerical values of the ITU-R model has resulted in the Fitted ITU-R (FITU-R) model. The optimisation was carried out using measurement data at 11.2 and 20 GHz for each of the foliation states [Stephens, Al-Nuaimi, 1995] and this has resulted in the following formulas:

$$L = 0.39 f^{0.39} d^{0.25} \quad \text{[dB]} \quad \textit{In-leaf} \qquad \textit{Equation B-5}$$

$$L = 0.37 f^{0.18} d^{0.59} \quad \text{[dB]} \quad \textit{Out-of-leaf} \qquad \textit{Equation B-6}$$

where frequency f and distance d are expressed in MHz and m respectively.

B.4.4 The COST235 and FITU-R models indicate that the signal level received with a small number of trees obstructing the signal path decays at a considerably faster rate relative to that obtained with a larger number of trees. This is in good agreeement with the predictions obtained from a theoretical model described in [Al-Nuaimi, Hammoudeh, 1994a], [Johnson, Schwering, 1985] based on the radiative energy transfer theory. It can be explained by the interplay between the coherent (direct path) component, which dominates at short distances into the vegetation depth but is strongly attenuated, and the incoherent (multipath scattered) component, which is less attenuated and takes over at relatively large depths. The foliage attenuation is shown to be higher for trees with leaves, due to the higher absortion per unit volume, and at higher frequencies, where the wavelength becomes comparable to the dimensions of leaves and small branches.

B.5 Semi-Empirical Models

B.5.1 Semi-empirical models [Seville, 1997], [Paulsen, Seville, 2000] are usually very simple to employ and by definition give the best fit to measured data, but do not do well in highlighting the underlying mechanisms. Most of the above models consider only the scattered component, and not other mechanisms of propagation, such as diffracted fields

over the top, or around the sides of the vegetation. This particular mechanism was partially included in one of the empirical models for very specific geometries [ITU-R Rec 833-2]. This model includes the beginnings of separable mechanisms for the determination of vegetation loss. It determines for a given frequency and vegetation depth whether

i) "common volume" scattering or

ii) diffraction around the edges and over the top, is likely to give the highest propagated component of the received signal.

B.5.2 However, it currently lacks any information on the density and structure of the vegetation, and suffers from a lack of available data for more general measurement geometries.

B.6 Non Zero Gradient Model

B.6.1 The attenuation of trees as a function of vegetation depth has been shown in the literature to be more accurately represented by dual slope attenuation functions [Al-Nuaimi, Hammoudeh, 1993b]. The nonzero gradient (NZG) model has been developed by researchers at Rutherford Appleton Laboratory (RAL) to accommodate this dual slope attenuation function seeking to follow the dual gradient of the measured attenuation curve. The initial slope describes the loss experienced by the coherent component, whilst the second slope describes that mainly experienced by the incoherent component, which occurs at a much reduced rate. This empirical model considers both of these components and optimise the parameters to give the best fit with measurement data obtained recently at 11.2 and 20 GHz. The model can be expressed as Equation B-7, where L is the excess attenuation in dB, R_0 and R_∞ are the initial and final specific attenuation values in dB/m, respectively, d is the vegetation depth in metre and k the final attenuation offset in dB. The values for these three parameters were estimated and are given in Table B-1 [Stephens, 1998].

$$L = R_\infty d + k\left(1 - e^{-\frac{(R_0 - R_\infty)d}{k}}\right) \qquad \textit{Equation B-7}$$

Constant Parameter	In-Leaf	Out-of-Leaf
R_∞ (dB/m)	0.33	0.24
R_0 (dB/m)	19.82	6.25
k (dB)	37.87	6.45

Table B-1 NZG model parameters

B.7 Dual Gradient Model

B.7.1 The NZG model was further developed by researchers at RAL to accommodate the difference in the received signal levels, when using antennas of different beamwidths,

resulting in the Dual Gradient (DG) model. In [Cost 235, 1996] and [Seville, 1997], the site geometry is taken into account, which considers the extent of illumination of the vegetation medium. This is characterised by the illumination width, W, the maximum effective coupling width resulting from the interaction between the transmit and receive antenna beamwidths inside the vegetation medium, as shown in Figure B-1. The DG model also includes the frequency of the propagation as a parameter and takes the form shown in Equation B-8,

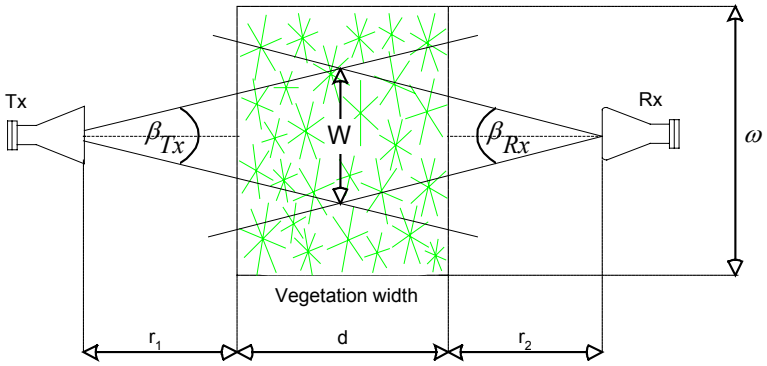

Figure B-1 Vegetation measurement geometry

$$L = \frac{R\infty}{f^a W^b} d + \frac{k}{W^c}\left(1 - e^{\left(-\frac{(R_0 - R_\infty)W_c}{k} d\right)}\right) \qquad \textit{Equation B-8}$$

where a, b, c, k, R_0 and R_∞ are constants described in [COST 235, 1996], [Seville, 1997], and given in Table B-2.

B.7.2 The frequency f is given in GHz and W is the maximum effective coupling width between the two antennas and is defined by Equation B-9.

B.7.3 The DG model expresses a frequency dependance in its equation, which, unlike the NZG, seems to contradict that in the ITU-R models [Stephens, 1998]. The inverse relationship with frequency (f^a and $a > 0$) suggests a decreasing attenuation as frequency increases, which appears to contradict both the anticipated behaviour and that observed in the measured data. Preliminary testing of this model by *Stephens* [Stephens, 1998] have revealed certain shortcomings and inaccuracies. It was concluded that further work on this model is needed in order to eliminate these inconsistencies.

Constant Parameter	In-Leaf	Out-of-Leaf
a	0.7	0.64
b	0.81	0.43
c	0.37	0.97
k	68.8	114.7
R_0	16.7	6.59
R_∞	8.77	3.89

Table B-2 Constant values for Equation B-8

$$W = \min\begin{pmatrix} \dfrac{(r_1 + d + r_2)\tan(\beta_{Tx})\tan(\beta_{Rx})}{\tan(\beta_{Tx}) + \tan(\beta_{Rx})} \\ (r_1 + d)\tan(\beta_{Tx}) \\ (d + r_2)\tan(\beta_{Rx}) \\ \omega \end{pmatrix} \qquad \textit{Equation B-9}$$

B.7.4 Furthermore, *Schwering* [Schwering, 1988] has conducted similar propagation measurements in vegetation with CW signals at 9.6, 28.8 and 57.6 GHz. His results show a clear trend for the vegetation loss to increase with frequency, which seems to occur in a consistent but not necessarily uniform fashion. In particular, for trees in leaf, the foliage loss is shown to increase substantially as the frequency is raised from 9.6 to 28.8 GHz, but that increase occurred at a much slower rate between 28.8 and 57.6 GHz.

B.8 Performance of models based on Measured Data

B.8.1 The models described in the preceding sections have been validated with measured data, conducted at various frequencies and in various outdoor environments [Al-Nuaimi, Hammoudeh, 1994], [Al-Nuaimi, Stephens, 1998], [Al-Nuaimi, Hammoudeh, 1993a], [Al-Nuaimi, Hammoudeh, 1993b], [Stephens, 1998], [Seville, 1997], [Hammoudeh et al, 1996]. A highly relevant paper by *Al-Nuaimi* and *Stephens* [Al-Nuaimi, Stephens, 1998], describes the models' performance analysed against measured data at two frequencies. Results obtained by the authors are given in Table B-3, where it can be seen that the FITU-R model results in the smallest *RMS* error, for both in-leaf and out-of-leaf generic cases. The DG model was not included in this study, due to the inconsistencies outlined above.

	Model *RMS* Error , *dB*		
Foliage State	ITU-R	FITU-R	NZG
In-leaf	9.85	9.42	16.31
Out-of-leaf	15.36	8.98	12.74

Table B-3 Performance of empirical models

B.9 Analytical (theoretical) Modelling

B.9.1 In contrast to empirical models, analytical models offer an insight into the physical processes involved in the propagation of radiowaves through vegetation. However, they usually require the use of numerical analysis methods to provide solutions to the intractable analytical formulations [Caldeirinha, Al-Nuaimi, 2000].

B.9.2 In [Matschek and Linot, 1999], two different types of theoretical models are presented. The first type is based on the consideration that the vegetation medium is homogeneous and should be treated as an isotropic dielectric material with constant permittivity and conductivity [Cavalcante, Giardola, 1983], [Calvalcante et al, 1983], [Seker, 1989], [Li, Yeo, 1998]. In the second, the material is considered to be heterogeneous, where vegetation is described as a mixture of trunks, branches, leaves and air [Torrico, Bertoni, 1998], [Fung, Fung, 1977], [Fung, Fung, 1978], [Mätzler, 1994]. In the latter case, each material is represented by a simple geometrical shape and characterised by its complex permittivity, the effective volume it occupies and by the statistical distribution of the spatial orientation of its elements. The radiative energy transfer model is another type of theoretical modelling, which is based on a more accurate representation of the propagation modes, but requires a rather precise and extensive database.

B.10 Geometrical and Uniform Theories of Diffraction (GTD/UTD)

B.10.1 Various ray-based models can be found in the literature, e.g. [Matschek, Linot, 1999], [Li, Yeo, 1998]. Ray methods are high-frequency methods and are not applicable to objects with dimensions less than a few wavelengths. The geometrical theory of diffraction (GTD) provides equations for the interactions of rays with specific geometries. The definition of ray-tracing interactions also means that the illuminated object must be placed in the far field region of the source.

B.10.2 For the frequency range 300 MHz – 90 GHz, the mechanisms by which the wave propagates can vary dramatically. The scattering has been modelled deterministically in many different ways depending on the electrical density of the vegetative medium. At lower frequencies, where individual components of the vegetation (trunks, branches, twigs and leaves or needles) and their separations are small by comparison with the radio wavelength, the propagation has been modelled in terms of a lateral wave [Tamir, 1967], and vegetation is considered as a single homogeneous dielectric slab. At frequencies above 200MHz or so, a single slab becomes inadequate. As the scale of the changes in density and structure of the vegetation become greater than the order of a wavelength, and layered representations of the vegetation should be used [Le-Wei Li et al, 1999]. This gives a good model for complex loss due to vegetation, but appears to be valid only up to around 2 GHz.

B.10.3 In [Sachs, Wyatt, 1968], a simple dielectric slab model of a jungle was shown to be capable of explaining the experimental propagation data over a wide range of parameters. The model, which considered only vertical polarisation with both antennas placed in the jungle, is applicable to frequencies of up to 100 MHz. Recently, *Li and Yeo* [Li, Yeo, 1998] have proposed a novel full-wave analysis of the radiowaves propagating along mixed paths inside a four-layered forest model, as shown in Figure B-2, applicable to frequencies up to 3 GHz. The model proposed initially in [Cavalcante, Giardola, 1983] consists of four dielectric regions (or layers), which are isotropic and homogeneous. The first layer is the semi-infinite

free-space, whereas the second layer represents the forest canopy. The third and fourth layers model the trunk and the semi-infinite ground plane, respectively. As the distance between the transmitter and the receiver is very long, the radio wave propagation through the stratified forest is characterised by the lateral wave that mainly propagates on top of the canopy along the air-canopy interface. For short distances, however, such a propagation is denominated by the direct or coherent component.

B.10.4 Another ray-based model has been proposed in the literature [Matschek, Linot, 1999], based on the Uniform Theory of Diffraction (UTD). The model associates a double-diffracted component over the canopy and a transmission component which includes the exact calculation of refraction angles. This model has been validated with propagation measurements taken at 1.9 GHz, in a wooded cross road configuration, and gives an mean error of -0.27 dB and a standard deviation σ of 2.03 dB.

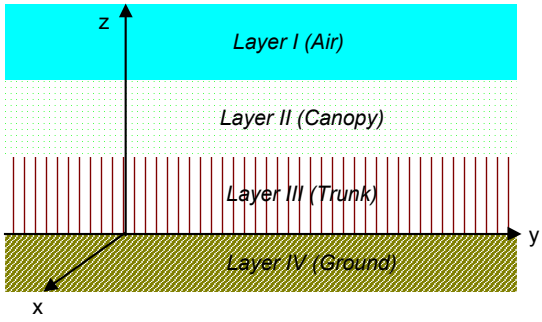

Figure B-2: Four-layered model of a typical forest

B.11 The Radiative Energy Transfer Theory

B.11.1 An analytical model based on the theory of radiative energy transfer may be used to predict the attenuation curves and directional spectra due to propagation of a microwave signal through vegetation [Al-Nuaimi, Hammoudeh, 1994a], [Johnson, Schwering, 1985], [Ishimaru, 1978]. The vegetation medium is modelled as a statistically homogeneous random medium of scatterers ds which is characterised by the absorption cross section per unit volume σ_a, the scatter cross-section per unit volume σ_s and the scatter function of the medium $p(\hat{s},\hat{s}')$. The scatter function (phase function) is characterised by a narrow forward lobe and an isotropic background, where the unit vectors $\hat{s}'$ and $\hat{s}$ indicate, for each event, the incidence direction and the scatter direction, respectively, as shown in Figure B-3.

B.11.2 The model considers a plane wave incident from an air half space upon the planar interface of a vegetation half space. The basic equation of the radiative energy transfer theory is expressed in terms of the specific intensity I and is given in Equation B-10.

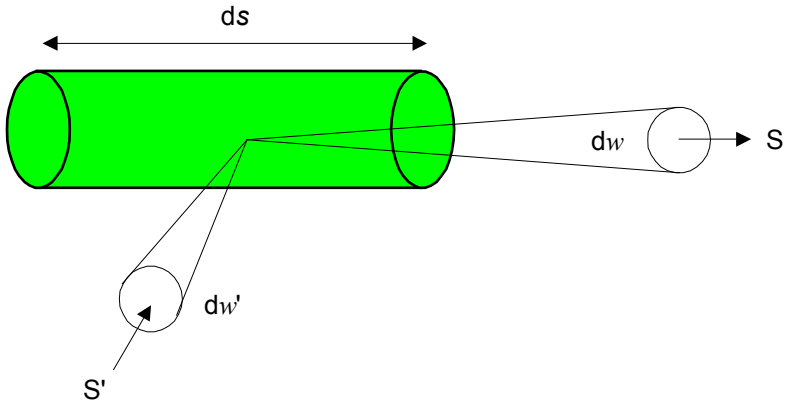

Figure B-3: Scattering from a homogeneous random medium of scatterers ds

$$s.\nabla I(\hat{r},\hat{s}) + (\sigma_A + \sigma_s) I(\hat{r},\hat{s}) = \frac{\sigma_s}{4\pi} \int_{4\pi} p(\hat{s},\hat{s}') I(\hat{r},\hat{s}') d\Omega' \qquad \textit{Equation B-10}$$

B.11.3 The theory gives the specific intensity at a given point within the vegetation medium I as a sum of a coherent component I_{ri}, which is reduced in intensity due to absorption and scatter of the incident wave, and an incoherent (diffuse) component I_d due to the scattered wave. Each scatterer is assumed to have a directional scatter profile, or phase function. As the constituents of the tree are relatively large relative to the wavelength at micro- and millimetre wave frequencies, the scatter function is assumed to consist of a strongly scattering forward lobe, which can be assumed to be Gaussion of width β_s, with an isotropic background level. The forward lobe takes the form in Equation B-11,

$$f(\theta) = \left(\frac{2}{\beta_s} \right)^2 e^{-(\theta/\ \beta_s)^2} \qquad \textit{Equation B-11}$$

where $\theta = \cos^{-1}(\hat{s},\hat{s}')$ and β_s is the beamwidth of the forward lobe, both in radians.

B.11.4 The scattering pattern shown in Figure B-4 is given by Equation B-12, where α is the ratio of the forward scattered power to the total scattered power.

$$p(\theta) = \alpha . f(\theta) + (1 - \alpha) \qquad \textit{Equation B-12}$$

B.11.5 The parameters σ_a, σ_s, α and β_s are specific to a vegetation medium and may be estimated for the medium under study by comparison of experimental and predicted results

[Al-Nuaimi, Hammoudeh, 1994a], [Hammoudeh et al, 1996]. The relative magnitudes of σ_a and σ_s are described in terms of the albedo w which is given in Equation B-13.

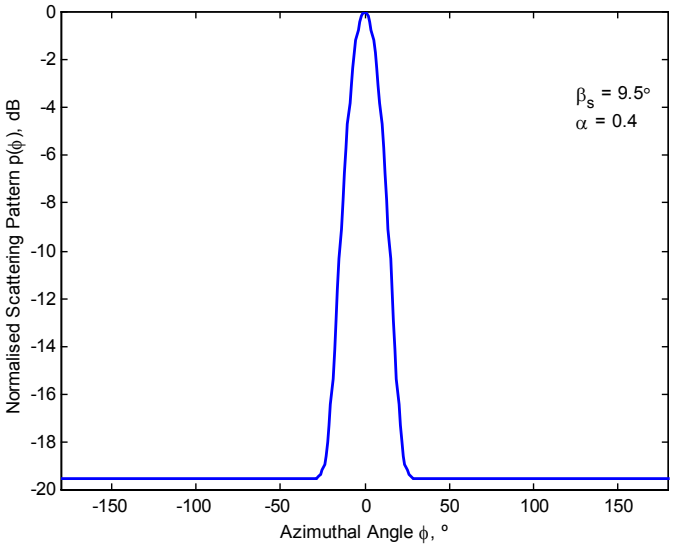

Figure B-4: Typical normalised scattering pattern of a vegetation medium

$$w = \frac{\sigma_s}{(\sigma_s + \sigma_a)} \qquad \textit{Equation B-13}$$

B.11.6 The implementation of this deterministic approach using numerical techniques gives a good understanding of the physical processes affecting propagation through vegetation. Indeed, this theory predicts the dual slope nature of the measured attenuation versus vegetation depth curves and provides a physical interpretation. The equation based on the RET theory that allows the prediction of the attenuation curve is given in [Stephens, 1998] and [Hammoudeh et al, 1996], and takes the form of Equation B-14:

$$P = P_0\left(e^{-\sigma_T d} + qe^{-\sigma_T d}\left[e^{\sigma_s \alpha . d} - 1\right]\right) \qquad \textit{Equation B-14}$$

where P is the received signal power, P_0 is the free space signal power, σ_T is the extinction cross section and is related to σ_a and σ_s by $\sigma_T = \sigma_a + \sigma_s$, q is a weighting factor related to the scattering pattern $p(\theta)$ and the radiation patten of the receive antenna [Stephens, 1998].

B.11.7 For the initial part of these curves, the received signal is reduced linearly by scatter and absorption of the incident signal. As the receiver is moved deeper into the vegetation, and the direct coherent component is reduced further still, the isotropically scattered component becomes significant. Due to the increasing scatter volume as we move deeper into the medium, the scatter signal level tends to be maintained, leading in turn to an attenuation rate which is significantly reduced at these depths.

B.11.8 Solution of the RET Equation (B-10) is explained in Section 3.

B.12 Full wave solutions

B.12.1 Full wave scatter modelling at these frequencies has been performed with geometric models of trees (leaves as disks, needles / trunks / branches as cylinders) [Seker, 2000], [Ewe, Chuah, 2000] and [Hiu, Sarabandi, 2000] with some success. However such methods are computationally expensive. It is also to be noted that the input parameters such as distributions of individual scattering types may be difficult to obtain in practice.

B.12.2 The paper [Hiu, Sarabandi, 2000] makes some interesting points on the scale of vegetation by comparing the wavelength in terms of near field scattering and electrical density. This seems to come to a transition at just the frequency range of interest in this project. Though the paper is primarily concerned with backscatter, associated with SAR remote sensing, this particular type of modelling may be useful in determining the wideband effects. This maybe achieved by slightly varying the distributions of 3-D tree models, iteratively, and using these iterative, deterministic results to provide generic trends.)

B.12.3 At millimetric frequencies, where the vegetation medium can be thought of as electrically sparse, the theory of Radiative Energy Transfer (RET) has proved good for modelling the bulk properties of vegetation [Ishimaru, 1978], [Schwering, Espeland. 1988], [Al-Nuaimi, Hammoudeh, 1994b]. The paper [Didascalou et al, 2000] shows a method of employing RET which is much less computationally expensive than the full wave models at millimetric frequencies. RET, however, needs input parameters such as the albedo or phase function of the scattering components, which are derived from measurements, so in one way could be seen as a “fitted” model. The strength of the RET lies in its truer representation of the propagation modes arising in vegetation media.

B.13 Physical Optics

B.13.1 Another theoretical model has been presented in [Torrico, Betroni, 1998] to include the effects of trees on the propagation loss in residential areas. In this model, the properties of a tree are characterised by the mean field, the attenuation, and phase delay. Physical Optics (PO) are then used to evaluate the diffracting field at the receiver by using a multiple Kirchhoff-Huygens integration for each absorbing/phase half-screen combination. Trees are

represented as an ensemble of leaves and branches, all having prescribed location and orientation statistics, as shown in Figure B-5. Leaves are modelled as flat, circular, lossy-dielectric discs, and branches as finitely long, circular, lossy-dielectric cylinders.

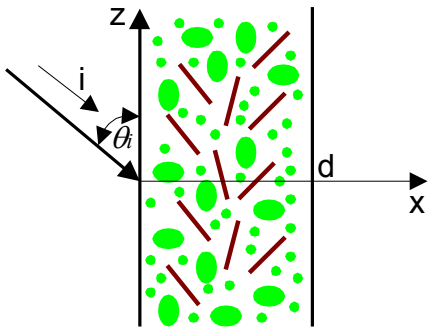

Figure B-5: Incident plane wave on slab with thin discs and cylinders.

B.13.2 In solving the wave equation for the mean scattered field propagating through a tree, it was found that the wave propagation constant has both real and imaginary components [Torrico, Betroni, 1998]. The implication of the loss due to the scatterers is that the mean field in the canopy decays in the respective direction of propagation. *Torrico and Bertoni* [Torrico, Betroni, 1998] have concluded that the specific attenuation for vertically polarised radio waves is higher than that for horizontal polarisation. The reason lies in the statistical distribution of leaves and branches with respect to the incidence angle of the incident plane wave. In their particular example, the distribution of branches was more vertical than horizontal. The model shows the effects of trees on the propagation loss and identifies those physical properties of the trees that are significant in computing their propagation constants. These properties include the probability density functions of the scatterers, the electromagnetic characteristics of the scatterers, and their dimensions.

B.13.3 Numerical calculation of both the specific attenuation and the skin depth of a tree becomes rather difficult to implement, when considering the randomness of the scatterers within the canopy. In addition, the model requires a full wave analysis of the scattered signal in order to obtain the mean-field and subsequently the propagation constant in the canopy. Their derivations are based on the determination of the scattering amplitude tensor elements of arbitrarily orientated branches and leaves.

B.14 Other Prediction Models for Vegetation Attenuation

B.14.1 Other prediction models available in the literature have been developed to characterise signal attenuation as a function of vegetation depth. These models are mainly applicable at frequencies lower than those addressed in this report. A brief summary of related work is included below.

B.14.2 *Vogel* and *Goldhirsh* [Vogel, Goldhirsh, 1986], [Vogel, Goldhirsh, 1988] carried out an extensive tree attenuation measurements for Land Mobile Satellite Systems (LMSS). Their results were derived from an experiment performed using a helicopter and remotely piloted aircraft as the source platform at L-band (1502 MHz) and UHF (870 MHz). Much information was generated by this set of field experiments in a variety of situations such as line of trees in a road scenario, mountain regions, various types of trees etc. The attenuation

was calculated by comparing the power changes for a scenario in which the receiving antenna was placed in front and behind a particular tree. A summary of static single tree attenuation results at 870 MHz using circularly polarised antennas is given in Table B-4.

	Attenuation in *dB*		**Attenuation Coef. *(dB/m)***	
Tree Type	Largest	Average	Largest	Average
Burr Oak	13.9	11.1	1.0	0.8
Holly	19.9	12.1	2.3	1.2
Pin Oak	18.4	13.1	1.85	1.3
Pine Grove	17.2	15.4	1.3	1.1
Sassafras	16.1	9.8	3.2	1.9
Scots Pine	7.7	6.6	0.9	0.7
White Pine	12.1	10.6	1.5	1.2
Overal Average	14.3	10.6	1.8	1.3

Table B-4 Summary of a static single tree attenuation at UHF (870 MHz)

B.14.3 Based on their measurements for attenuation due to roadside trees, the authors introduced the model given in Equations B-15 and B-16, which predict the attenuation, L, due to a single tree as a function of elevation angle θ, for both in-leaf and out-of-leaf cases [Matschek, Liniot, 1999]. The attenuation L is given in decibels (dB) and θ is the elevation angle in degrees. The model is valid for elevation angles from 15° to 40°, which shows that foliage increases the attenuation of the signal by several dB, which can rise by 15 dB or more at higher frequencies [Al-Nuaimi, Hammoudeh, 1994a], [Al-Nuaimi, Hammudeh, 1993a], [Stephens, 1998].

$$L(\theta) = 0.48\theta + 26.2 \quad \text{[dB]} \quad \textit{In-leaf} \qquad \textit{Equation B-15}$$

$$L(\theta) = 0.35\theta + 19.2 \quad \text{[dB]} \quad \textit{Out-of-leaf} \qquad \textit{Equation B-16}$$

B.15 Depolarisation

B.15.1 One of the important aspects of radio wave propagation in terrestrial links is the change of polarisation of the incoming signal. Models are available for predicting depolarisation from backscattered signal, crop and forest type recognition in the field of remote sensing. However little research on the prediction of the signal that has been depolarised as a result of passing through a volume of vegetation, has been reported in the literature. This was reported by *Caldeirinha* [Caldeirinha, 2001] to be the case when a radio signal propagates through a single tree, which was shown to have a considerable influence on the level of signal received, as a result of tree re-radiation. The depolarisation degree depends strongly on wavelength and on the medium structure, i.e. size and density of leaves, orientation and number of branches. The intensity of the received signal is the sum of the fields re-radiated by such individual scatterers having random orientations and variable electromagnetic properties [Caldeirinha, Al-Nuaimi, 2001c].

B.15.2 Change in polarisation state was reported in this study to vary from well defined elliptical polarisation states in the forward scattering region to randomly polarised (depolarisation) in the back and side scattering regions (see Figure B-6). The depolarisation of the incident plane wave passing through the vegetation medium is closely linked to the structure of the tree and orientation of its constituent elements and the currents induced in these components. Results from depolarisation measurements show that depolarisation is a highly significant propagation process in vegetation media. The re-radiated signal from the side and back of the tree contains a considerably enhanced cross-polar signal component, which can assume comparable levels to that of the co-polar component. Enhancement of the cross polar component observed in the forward region, which was accompanied by a consequent reduction of the co-polar component causes the XPD to reduce considerably. This resulted in a relatively high value of the cross-polar component, with a consequent reduction of the co-polar component level. This can also explain the significant reduction of signal level observed in the co-polarised component which could not simply be explained by local blockage of the incident signal [Caldeirinha, Al-Nuaimi, 2000].

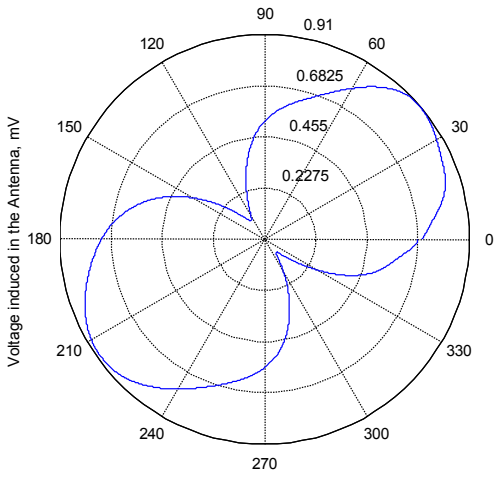

Figure B-6: Typical polarisation pattern of the re-radiated signal from a ficus *tree.*

B.15.3 Clearly depolarisation and the reduction of the XPD have important implications on the design of both terrestrial and satellite radio links whose paths include vegetation. The results

also show that depolarisation, in addition to absorption and scatter, is an important factor in prediction models for propagation in vegetation.

B.16 Conclusion

B.16.1 Prediction models which estimate the excess attenuation due to vegetation are critical to mobile and terrestrial radio service providers for not only planning radio networks but also for optimising spectrum utilisation by accurately predicting cell coverage, and minimising intercell interference.

B.16.2 A number of propagation prediction models are available and these have been summarised in this report. These can be used to provide estimates of the excess attenuation at specified frequency bands. The models, although simple, contain few parameters relating to the vegetation medium, path geometry and seasonal effects on the radio system performance.

B.16.3 Disadvantages of these models stem from their limited applicability because in their formulation and validation, they were based on a limited number of site geometries and relatively few measurements.

B.16.4 The applicability of the models maybe extended through consideration of further measurements carried out for a variety of vegetation media, path geometries and frequencies. A generic attenuation model with appropriate parameters, based on the knowledge and understanding of the propagation modes arising in vegetation is clearly both valuable and necessary for radio system planning.

B.17 References for Section B

AL-NUAIMI, M. O., HAMMOUDEH, A. M.: “Attenuation functions of microwave signals propagated through trees”, Electronic Letters, 29, (14), pp. 1307-1308, 1993a.

AL-NUAIMI, M. O., HAMMOUDEH, A. M.: 'Influence of Vegetation on Attenuation of Radiowave Signals in the X-Band Frequency Region', COST 235 TD, CP 149, June 1993b.

AL-NUAIMI, M. O., HAMMOUDEH, A. M., "Measurements and Predictions of Attenuation and Scatter of Microwave Signals by Trees", IEE Proceeding on Antennas and Propagation, Part H, Vol. 141, No. 2, 1994a.

AL-NUAIMI, M.O., HAMMOUDEH, A.M. “Measurements and Predictions of Attenuation and Scatter of Microwave Signals by Trees”, IEE Proc Microw. Antennas Propag., Vol. 141, No. 2, April 1994b.

AL-NUAIMI, M. O., STEPHENS, R. B. L.: “Measurements and prediction model optimisation for signal attenuation in vegetation media at centimetre wave frequencies” IEE Proceedings on Microwave Antennas and Propagation, Vol. 145, No 3, June 1998.

CALDEIRINHA, R. F. S.: “Radio Characterisation of Single Trees at Micro- and Millimetre Wave Frequencies”, PhD thesis, University of Glamorgan, 2001.

CALDEIRINHA, R., AL-NUAIMI, M.: "Co-Polar and Cross-Polar Measurements of the Re-Radiation Signal at 20 GHz from a Tree and their Analysis in the region around the

Nulls", IEEE Proceedings of the Sixteenth National Radio Science Conference, Ain Shams University, Cairo, Egypt, INV4, Feb. 23-25, 1999.

CALDEIRINHA, R., AL-NUAIMI, M.: "Analysis of the Re-radiation Functions of Single Trees and Idealised Structures at 20 GHz", AP2000 Millennium Conference on Antennas & Propagation, Davos, Switzerland, Pap. 460, April 11-15, 2000.

CALDEIRINHA, R., AL-NUAIMI, M.: "An Accurate Model for RCS of Single Leaves ", 4th European Personal Mobile Communications Conference, EPMCC2001, Vienna, Austria, February 20th-22nd, 2001a.

CALDEIRINHA, R., AL-NUAIMI, M.: "A Novel FDTD based method for prediction of bistatic RCS of single leaves and trees", 11th International Conference on Antennas & Propagation, ICAP2001, Manchester, UK, April 17-20, 2001b.

CALDEIRINHA, R., AL-NUAIMI, M.: "Modelling of the re-radiation functions of single trees based on wideband measurements at L-band", 11th International Conference on Antennas & Propagation, ICAP2001, Manchester, UK, April 17-20, 2001c.

CAVALCANTE, G. P. S., GIARDOLA, A. J.: “Optimisation of radio communication in media with three layers”, IEEE Antennas and Propagation, Vol. AP-31, January 1983.

CAVALCANTE, G. P. S., ROGERS, D. A. and GIARDOLA, A. J.: “Radio loss in forests using a model with four layered media”, Radio Science, Vol. 18, 1983.

COST 235, “Radiowave propagation effects on next generation fixed services terrestrial telecommunications systems”, Final Report, ISBN 92-827-8023-6, Commission of the European Union, 1996.

DIDASCALOU, D. et al. “Millimeter-Wave Scattering and Penetration in Isolated Vegetation Structures”, IEEE trans Geoscience and Remote Sensing, Vol. 38, No. 5, Sept. 2000

Draft COST 231 Final Report, "Digital Mobile Radio: COST 231 View on the Evolution towards 3rd Generation Systems", COST 231 TD(96)042-A, Turin, April 17-19, 1996.

DTI, "Multimedia Communications on the move", A Consultation Document from the Department of Trade and Industry, July 1997

EWE, H. T., CHUAH, H. T. “Electromagnetic Scattering from an Electrically Dense Vegetation Medium”, IEEE trans Geoscience and Remote Sensing, Vol. 38, No. 5, Sept. 2000.

FUNG, A. K., FUNG, H. S.: ”Application of first-order renormalisation method to scattering from a vegetation-like half-space”, IEEE Transactions on Geoscience Electronics, Vol. GE-15, No. 4, October 1977.

FUNG, A. K., FUNG, H. S.:”A scatter model for leafy vegetation”, IEEE Transactions on Geoscience Electronics, Vol. GE-16, No. 4, October 1978.

GRAHAM, R.F. “Identification of Suitable Carrier Frequency for Mobile Terrestrial Communication Systems with Low Antenna Height”, http:argeenhouse.com/society /TacCom/milcom_98_paper.html., 1998

HAMMOUDEH, A. M., STEPHENS, R., AL-NUAIMI, M. O.: “Characterisation and Modelling of Scatter, Attenuation and Depolarisation of Millimetre Waves due to Foliage”, 26th EuMC, Prague, Czech Republic, September 1996.

HIU, T., SARABANDI, K.: “Electromagnetic Scattering from Short Branching Vegetation”, IEEE trans Geoscience and Remote Sensing, Vol. 38, No. 2, March. 2000.

ISHIMARU, A: “Wave propagation and scattering in random media”, Academic Press, Vol. 1, 1978.

ITU-R Rec. 833-2, “Attenuation in vegetation”, Int. Telecom. Union, Geneva, 1999.

JOHNSON, R. A., SCHWERING, F.: “A transport theory of millimeter wave propagation in woods and forests”, CECOM-TR-85-1, Fort Monmouth, New Jersey, 1985

KARALIOPOULOS, M.S., PAVLIDOU, F. N.: “Modelling the land mobile satellite channel: a review”, IEE Electronics Communication Engineering Journal, Vol. 11, No. 5, October 1999.

LE-WEI LI et al, “Analysis of Radiowave Propagation in a Four-Layered Anisotropic Forest”, IEEE trans Geoscience and Remote Sensing, Vol. 37, No. 4, July 1999.

LEWENZ, R. “Path loss variation due to vegetation movement”, Proc. IEE National Conference on Antennas and Propagation, pp. 97-100, 1999.

LI, L. W., YEO, T. S.: “Radio wave propagation along mixed paths through a four-layered model of rain forest: An analytic approach”, IEEE Transactions on Antennas and Propagation, Vol. 46, No. 7, July 1998.

MATSCHEK, R., LINOT, B.: “Model for wave propagation in presence of vegetation based on the UTD associating transmitted and lateral waves”, National Conference on Antennas and Propagation, Conference Publication No. 461, 30 March - 1 April, 1999.

MÄTZLER, C.: ”Microwave (1-100 GHz) Dielectric model of leaves”, IEEE Transactions on Geoscience and Remote Sensing, Vol. 32, No. 5, September 1994.

PAULSEN, A., SEVILLE, A.: “Attenuation and distortion of millimetre radio wave propagation through vegetation“ Millennium conference on Antennas and Propagation (AP 2000), April 2000.

SACHS, D. L., WYATT, P. J.: “A Conducting-Slab Model for Electromagnetic Propagation Within a Jungle Medium”, Radio Science, Vol. 3 (New Series), No. 2, February 1968.

SCHWERING, F. K.: “Millimeter-Wave Propagation in Vegetation: Experiments and Theory”, IEEE Transactions on Geoscience and Remote Sensing, Vol. 26, No. 3, May 1988.

SCHWERING, F.K., ESPELAND, H.: “Millimeter-wave Propagation in Vegetation: Experiments and Theory”, IEEE Trans. Geoscience and Remote Sensing, Vol. 26, No. 3, May 1988.

SEKER, S. S.: “Radio pulse transmission along mixed paths in s stratified forest”, Proceedings of Inst. Elect. Eng., Vol. 136, part H, 1989.

SEKER, S. S.: “A Simulation of Multi-Components Propagation Model of Lossy Medium”, Proc Millenium Conference on Antennas and Propagation, 2000.

SEVILLE, A.: “Vegetation Attenuation: Modelling and Measurements at Millimetric Frequencies”, 10th International Conference on Antennas and Propagation, Conference Publication No. 436, 14-17 April 1997.

SEVILLE, A., YILMAZ,U., CHARRIERE, P.R.V., POWELL, N., CRAIG, K.H., “Building scatter and vegetation attenuation measurements at 38 GHz”, Proceedings of ICAP 95, IEE Conference Publication No. 407, pp. 2.46-2.50, 1995.

STEPHENS, R.B.L.: “A study and modelling of the propagation effects of vegetation on radiowaves at cm-wavelength frequencies”, PhD thesis, University of Glamorgan, 1998.

STEPHENS, R. B. L., AL-NUAIMI, M. O.: “Attenuation measurements and modelling in vegetation media at 11.2 GHz and 20 GHz”, Electron Lett., 31, (20), pp. 1783-1785, 1995.

STEPHENS, R. B. L., AL-NUAIMI, M. O. and CALDEIRINHA, R.: "Characterisation of depolarisation of radio signals by single trees at 20 GHz", Fifteenth National Radio Science Conference, Helwan, Cairo, Egypt, B12 1-7, Feb. 24-26, 1998.

TAMIR, T. “On radio-wave propagation in forest environments”, IEEE Trans. AP-15 (6), pp. 806-817, 1967.

TORRICO, S. A., BERTONI, H. L.: 'Modelling Tree Effects on Path Loss in a Residential Environment', IEEE Transactions on Antennas and Propagation, Vol. 46. No. 6, June 1998.

VOGEL, W. J., GOLDHIRSH, J.: “Tree Attenuation at 869 MHz derived from remotely piloted aircrafted measurement”, IEEE Transactions on Antennas and Propagation, Vol.AP-34, No. 11, pp. 1460-1464, 1986.

VOGEL, W. J., GOLDHIRSH, J.: “Fade Measurements at L-band and UHF in Mountainous Terrain for Land Mobile Satellite Systems”, IEEE Transactions on Antennas and Propagation, Vol.AP-36, No. 1, pp. 104-113, 1988.

WEISSBERGER, M. A.: “An initial critical summary of models for predicting the attenuation of radio waves by trees”, ESD-TR-81-101, EMC Analysis Center, Annapolis, MD, USA, 1982.

C The Measurements Database

C.1 Introduction

C.1.1 The measurements database consists of over 21000 measurements made during the course of the project. These consisted of various depth measurements at 12 different locations, covering 8 species of trees including some winter measurement being made with the trees out of leaf. Wideband measurements were made at 6 frequencies: 1.3, 2, 2.2, 11.6, 37 and 61.5 GHz and narrowband measurements made over 32 frequencies from 2-18GHz in 0.5GHz steps (plus narrowband measurements from 0.4 - 2 GHz in 100 MHz steps for two cases). Table C.1 shows an outline of the measured data.

C.2 Format of the measurements database

C.2.1 The database consists of a measurement database, which includes the average measured attenuation (in excess of free space loss) and variability in terms of maximum and minimum of the measured attenuation, a specification of the system parameters (frequency, antenna beamwidths, etc), transmitter location and receiver location. Each measurement is assigned a measurement geometry number which is tabled in the measurement geometry file, along with full definitions of the vegetation geometry for each location.

C.2.2 The database is presented in two forms. The Microsoft Excel spreadsheet: vegetation_measurement.xls, has the measurement data contained on sheet 1 and the geometry information listed on sheet 2. The data is also presented as two separate tab-delimited text files: vegetation_measurement_data.txt and vegetation_measurement_geometry.txt.

Location	Vegetation Geometry	Tree Species	Measurement Frequency	Foliage State	Measurement Type
Fermi Ave (RAL)	Line of trees	Horse Chestnut (*Aesculus hippocastanum*)	1.3, 2 & 11.6GHz wideband	In leaf	Depth
Mound (RAL Tx to north of trees)	Triangular wedge	Sycamore / Beech (*Acer pseudoplantanus / Fagus sylvatica)*	2-18GHz narrowband 10-15GHz narrowband 1.3, 2, 2.2, 11.6, and 61.5GHz wideband 2-18GHz narrowband	In leaf Out of leaf	Depth (+Rx Height) Phase function Depth Depth (+Rx Height)
Mound (RAL Tx to West of trees)	Triangular wedge		1.3, 2, 11.6GHz 1.3, 2, 11.6GHz	In leaf Out of leaf	Depth Depth
Guarlford Road, Malvern	Slices through 1 tree	Turkey Oak (*Quercus cerris)*	2.2 and 61.5GHz wideband	In leaf	Depth
R58 (RAL)	Line of trees	Beech (*Fagus sylvatica*)	2-18GHz narrowband 10-15GHz narrowband	In leaf	Depth Phase function
QEC Park (Roebuck)	Track into forest		37 and 61.5GHz wideband	In leaf	Depth
QEC Park (Brow Barrows)	Track into forest		1.3, 2 and 11.6GHz wideband	In leaf	Depth
QEC Park	Track into forest		2-18GHz narrowband	Half in leaf	Depth (+Rx Height)
QEC Park	Rectangular wedge	Lawson Cypress (*Chamaecyparis lawsoniana*)	2-18GHz narrowband 1.3, 2, and 11.6GHz wideband	Conifer	Depth
J.&J. Nurseries, Twyning	Line of trees	Silver Maple (*Acer saccharinum*)	0.4-18GHz narrowband 1.3, 2, 2.2, 11.6 and 61.5GHz wideband 1.3, 2, and 11.6GHz wideband	In leaf Out of leaf	Depth
J.&J. Nurseries, Twyning	Line of trees	London Plane (*Plantanus x hispanica*)	0.4-18GHz narrowband 1.3, 2, 2.2, 11.6, 37 and 61.5GHz wideband 1.3, 2 and 11.6GHz wideband	In leaf Out of leaf	Depth
J.&J. Nurseries, Twyning	Line of trees	Common Lime (*Tilia x Europaea*)	1.3, 2 and 11.6GHz wideband	In and Out of leaf	Depth
RAL (near 12.5m dish)	Group of Potted trees	Weeping Fig (*Ficus naomi)*	10-15GHz and 18-23GHz narrowband	In leaf	Phase function
Glebelands Park, Newport	Line of trees	Sycamore (*Acer pseudoplantanus*)	20GHz narrowband	In leaf	Phase function

Table C.1: Contents of the measurement database

C.2.3 Each file is given with the fields in the following order.

- Mean Attenuation (dB) normalised to free space for measurement path length as per normalisation Equation C-6. NB the data presented does not include any account of the excess attenuation due to antenna pointing effects)
- Maximum Attenuation (dB)
- Minimum Attenuation (dB)
- Standard deviation (dB)
- Noise floor attenuation (dB) ie Attenuation that corresponds to system noise floor at each specific location (includes path loss)
- Measurement type (Phase function / Depth / Other)

- Frequency (in GHz)
- Bandwidth (in kHz)
- Sampling Interval (in milliseconds)
- Number of samples

System Parameters

- Tx 3dB Beamwidth (az)
- Tx 3dB Beamwidth (el)
- Rx 3dB Beamwidth (az)
- Rx 3dB Beamwidth (el)

Beamwidths

- Tx Polarisation (H/V)
- Rx Polarisation (H/V)

- TX x eastings (m)
- TX y northings (m)
- TX z height of ground above sea level (m)
- Tx h height above ground (m)
- Tx pointing theta (az) [θtx]
- Tx pointing phi (el) [ϕtx]
- Rx x
- Rx y
- Rx h height above ground (m)
- Rx pointing theta (az) [θrx]
- Rx pointing phi (el) [ϕrx]
- Total Direct Path (m)
- Total path through vegetation (m)
- Geometry identifier number

Path geometry (as in Figures C-1 to C-3)

- Angles in degrees
- Pointing angles relative to Tx-Rx line
- Positive angles for up in elevation
- Positive angles for clockwise rotation in azimuth
- Tx X, Y Co-ordinates in 6 figure NGR
- Tx Z Co-ordinate height in metres above sea level.
- Rx co-ordinates relative to Tx ground level (x eastings, y northings, z height)

C.2.4 For this case the details of tree groups 1 and 2 are listed in the database but not tree group 3.

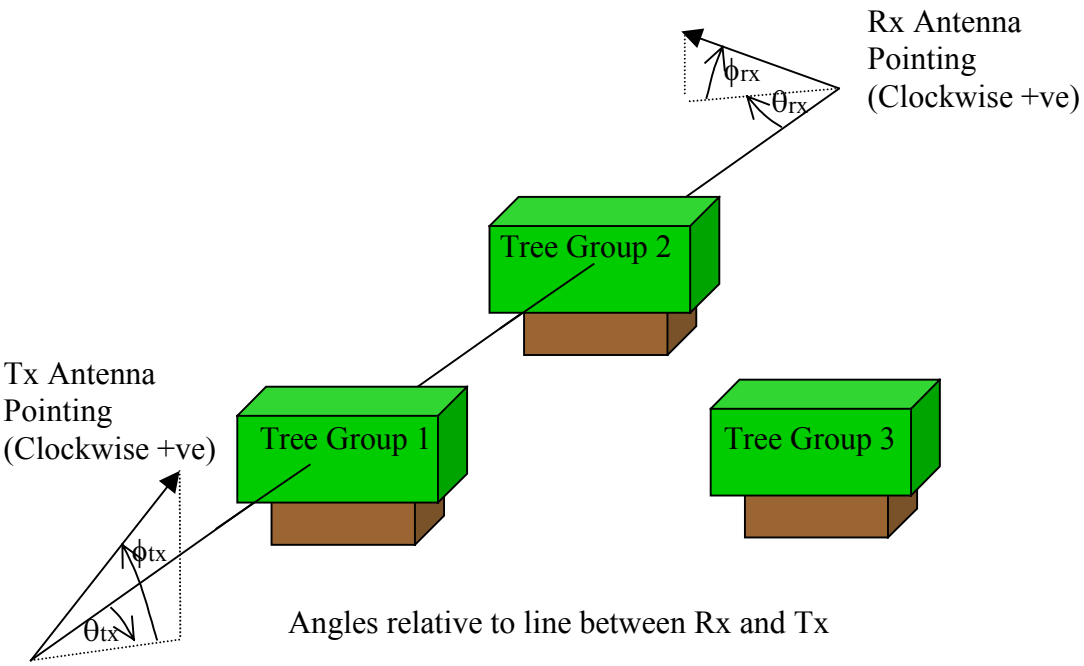

Figure C-1 Antenna pointing Geometry

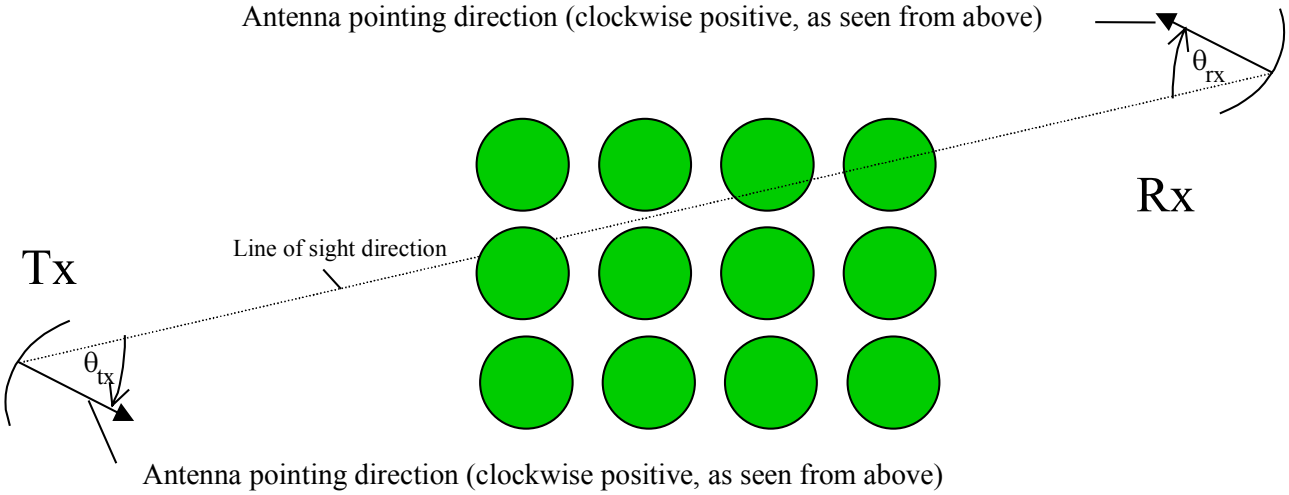

Figure C-2 Antenna pointing Geometry- plan view

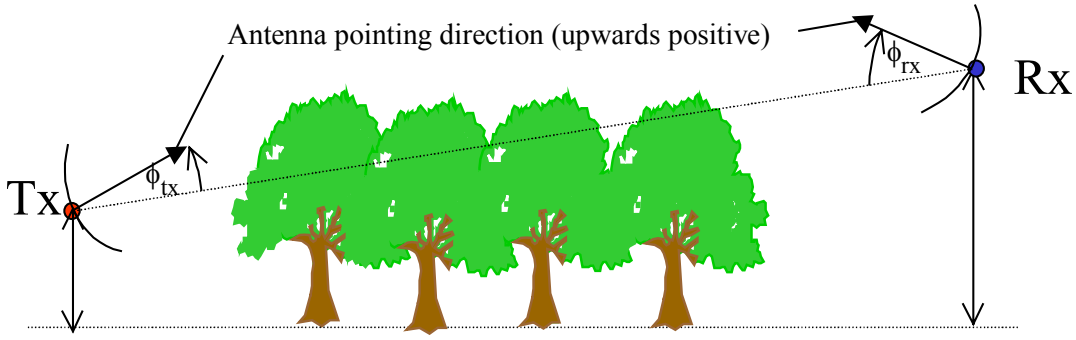

Figure C-3 Antenna pointing Geometry- side view

C.3 Vegetation Geometry file format

C.3.1 The records of the vegetation geometry file are as follows:

- Geometry identifier number
- General comment on site geometry
- Tx Easting (6 figure easting)
- Tx Northing (6 figure northing)
- Tx ground height (height of ground of Tx coordinate above sea level)
- Number of tree groups along path N (individual block when spacing between adjacent foliage is ~ foliage width for 1 tree)

- N blocks of:

  - Tree Species
  - Leaf State (in / out of leaf)
  - Leaf Area Index
  - Gap Fraction
  - Trunk spacing
  - Max Leaf Dimension (m)
  - Min Leaf Dimension (m)
  - Maximum leaf dimension
  - Minimum leaf dimension

  } Species and density parameters for each group of trees that lie between transmitter and receiver

  - $N_{vertices}$
  - x_1
  - y_1
  - z_{1a}
  - z_{1b}
  - z_{1c}
  - …
  - …
  - x_N
  - y_N
  - z_{Na}
  - z_{Nb}
  - z_{Nc}

  } Projected polygon defined by N vertices (3 minimum)

  Co-ordinate points in metres relative to Tx (co-ordinates relative to Tx ground level {x eastings, y northings, z height})

  defining geometry of each group of trees, as in figure C.4 ($N_{vertices}$ =4)

C.3.2 Figures depicting the details of the experimental setups for all of the locations presented in the measurement database are given in the files: vegetation_measurement_figures.ppt and vegetation_measurement_figures.pdf.

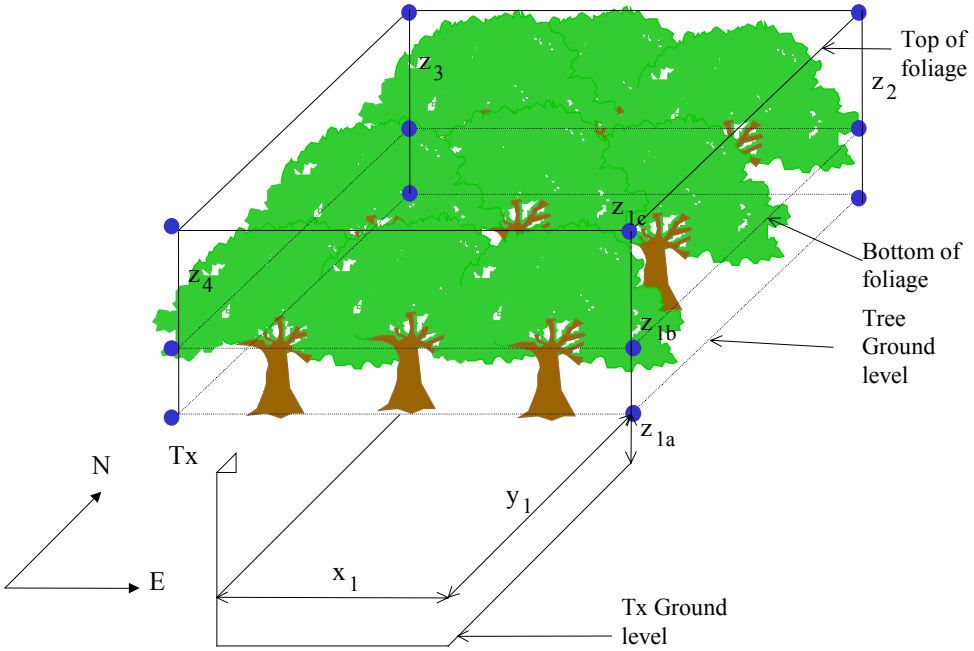

Figure C.4: Specification of the vegetation geometry

C.4 Instructions for adding measurements to complement the database

C.4.1 Calculation of Vegetation Attenuation

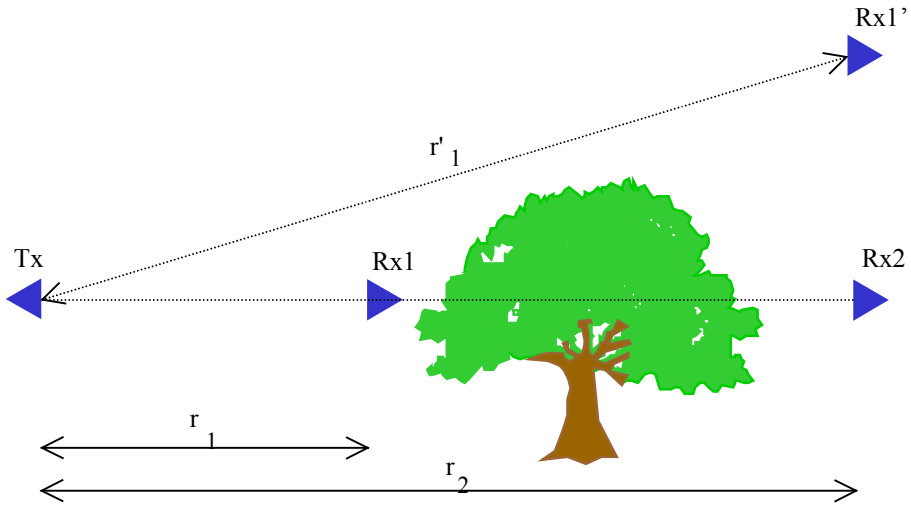

Figure C.5: System calibration and measurement geometry

C.4.1.1 For the line of sight (los) calibration measurement with the receiver placed at position Rx1 in Figure C-1, the averaged received power, P(Rx1) will be:

$$P(Rx1) = P_{tx} + G_{sys} - L_{fs}\,(r_1) \qquad \textit{Equation C-1}$$

C.4.1.2 (For the case of LOS calibration being made by raising the receiver above the tree top to give a line of sight, ie at Rx1' rather than Rx1, r_1' can be substituted for r_1.)

C.4.1.3 Where G_{sys} = Measured system gain (dB) [this is a blanket term for the sum of the individual gains / losses of all the system components and includes the Tx and Rx antenna gains, Rx amplifier gain and all cabling losses]

L_{fs} = Free space loss (dB)

P_{tx} = Transmitted power (dBm).

C.4.1.4 The free space loss is calculated by using the following formula.

$$\textit{Free Space Loss } (L_{fs}) = 20\{\log_{10}(4\pi r_1 f/c)\} \qquad \textit{Equation C-2}$$

Where r_1 = distance between the transmitter (Tx) and receiver (Rx).

f = frequency in Hz

c = velocity of light in a vacuum. (2.998×10^8m/s).

C.4.1.5 Therefore, the received power that would be seen at position Rx2 on Figure C-1 if the trees were not present*, P_{eff}(Rx2), is then

$$P_{eff}\,(Rx2) = P_{tx} + G_{sys} - L_{fs}\,(r_2) \qquad \textit{Equation C-3}$$

C.4.1.6 Or, when we substitute for G_{sys} and L_{fs} (r_2)

$$P_{eff}\,(Rx2) = P(Rx1) + 20\{\log_{10}(4\pi r_1 f/c)\} - 20\{\log_{10}(4\pi r_2 f/c)\} \qquad \textit{Equation C-4}$$

* NB this is neglecting the effects of ground reflections, which may very well be significant. A full inclusion of ground effects may be necessary by the use of terrain data.

C.4.1.7 The Excess Attenuation due to vegetation, A, is then:

$$A = P_{eff}(Rx2) - P(Rx2) \qquad \textit{Equation C-5}$$

or

$$A = P(Rx1) - P(Rx2) - 20\{\log_{10}(r_2 / r_1)\} \qquad \textit{Equation C-6}$$

C.5 Calculation of Signal Maxima, Minima and Noise Floor Attenuation

C.5.1 Procedure

C.5.1.1 This procedure can be duplicated by substituting the system noise floor, the maximum received power and the minimum received power (in dBm, for each specific frequency) in the above procedure for the measured average power to produce the noise floor attenuation, minimum attenuation and maximum attenuation, respectively. One should note that by definition, this noise floor attenuation will vary by location (as it is the attenuation in excess of free space seen when the system noise floor is reached). The average given is a temporal average (where the average is made in dB, not converted to linear power / amplitude). The number of samples and sampling interval were different for each of the organisations performing the measurements, the data-acquisition procedures were different, and the pre-processing of the data to provide measured attenuation averages, maxima, minima and standard deviations were correspondingly different.

C.5.2 RAL measurements and averaging procedure

C.5.2.1 For each measurement location, and for each frequency sampled in sequence, a spectrum analyser was used to perform a frequency sweep (bandwidth 5kHz, resolution bandwidth 1kHz, sweep time 200ms) and the peak identified, in order to account for frequency drift of the transmit – receive equipment. Where the received power of this peak was greater than –90dBm, the spectrum analyser was triggered to sweep through a time series measurement of 1s, with the spectrum analysers "zero span" option. This time series of 601 points was then transferred to the controlling PC and an average attenuation calculated by taking the mean of these 601 values and subtracting this from the calibration measurement value as in equation 6 above (less the path difference term). Where the initial measurement peak was less than –90dBm, the spectrum analyser resolution bandwidth was reduced to 30Hz, and the frequency sweep repeated (the sweep time was changed to 969ms accordingly). The peak of this frequency sweep was then taken as the power measurement value, with only one measured value (set equal to the mean, min and max, giving a standard deviation of 0), and the attenuation calculated as before.

C.5.3 University of Portsmouth measurements and averaging procedure

C.5.3.1 For each measurement location, and for each frequency sampled in sequence, 4 data blocks were captured in 2.4 minutes. Each data block is captured in 4.29 seconds. (the additional time is taken to transfer data into the control PC storage). Each data block consists of 128 Transfer functions (across the wideband measurement channel), each (recorded) transfer functions is an average of 128 (measured) transfer functions. Each data block is therefore a temporal average of 16384 (measured) transfer functions over a sampling period of 4.29 seconds and each measurement point is an average of 65536 (measured) transfer functions, sampled over four 4.29 second intervals spread over a total period of 1.8 minutes. After the data averaging procedure has been performed, a single line is selected to give the time-averaged narrowband attenuation as in equation 6.

C.5.4 QinetiQ measurements and averaging procedure

C.5.4.1 For each measurement location, and for each frequency sampled in sequence, the number of impulses collected is given in the data files as "Number of samples", typically 10000 collected at an interval of 12 milliseconds, ie. ~83 measurements per second. Each impulse response is the FFT of the frequency response across the whole 120 MHz bandwidth. The averaged attenuation is obtained by taking the average of the peak power value of each impulse response, and using this to calculate the measured attenuation as in Equation C-6. This is the same as summing all of the peak value of successive impulse responses, and dividing by the number of total number of impulse responses.

C.5.5 University of Glamorgan measurements and averaging procedure

C.5.5.1 For each measurement location, the received power was sampled by taking a 1MHz frequency sweep on the spectrum analyser with a resolution bandwidth of 100kHz (sweep time 50ms). The peak of the frequency response was taken and this peak averaged over 100 iterations (taking a total time of around 30 seconds, with a total sampling interval of 5s per point). This averaged measured power was then used to calculate the time averaged measured attenuation as in Equation C-6.

Distribution list

Name	Institution	Copy number(s)
D. Eden	Radiocommunications Agency	1-5
A. Shukla	QinetiQ, Malvern	6-10
K. Craig	Rutherford Appleton Laboratory	11-13
M. Al-Nuaimi	University of Glamorgan	14-16
E. Vilar	University of Portsmouth	17-19
Project File	QinetiQ, Malvern	20
	QinetiQ, Malvern Information Centre	21-22

Report documentation page

1. Originator's report number:	QINETIQ/KI/COM/CR020196/1.0		
2. Originator's Name and Location:	Neil Rogers D714, QinetiQ Ltd., Malvern Technology Park, St. Andrews Rd., Malvern, Worcs., WR14 3PS.		
3. RA Contract number and period covered:	AY3880/510005719 Dec 00 - Apr 02		
4. RA Sponsor's Name and Location:	D. Eden, Manager – National Radio Propagation Programme, South Quay 3, 189 Marsh Wall, London, E14 9SX		
5. Report Classification and Caveats in use:	6. Date written:	Pagination:	References:
UNMARKED (UNLIMITED)	May 2002	xvi + 134	55
7a. Report Title:	A Generic Model of 1-60 GHz Radio Propagation through Vegetation - Final Report		
7b. Translation / Conference details (if translation give foreign title / if part of conference then give conference particulars): N/A			
7c. Title classification:	UNMARKED (UNLIMITED)		
8. Authors:	NC Rogers, A Seville, J Richter, D Ndzi, N Savage, R Caldeirinha, AK Shukla, M Al-Nuaimi, K Craig, E Vilar and J Austin		
9. Descriptors / Key words:	RADIO RADIOWAVE PROPAGATION ATTENUATION VEGETATION MILLIMETRE-WAVE MICROWAVE RET		

10a. Abstract. (An abstract should aim to give an informative and concise summary of the report in up to 300 words).

This is the final report of a 15-month project to develop a generic model of 1-60 GHz narrowband radio signal attenuation in vegetation. The report provides a summary of previous modelling of millimetre-wave propagation through vegetation. The new generic model, which combines edge diffraction, ground reflection and a direct (through vegetation) signal (modelled using Radiative Energy Transfer (RET) theory) is described. RET is used to predict the attenuation *vs*. foliage depth using parameters to describe the absorption and scatter cross-section, albedo, and scatter function of the vegetation. The generic model is based on measurements made at twelve locations in England, including eight different species of trees, both in-leaf and out-of-leaf. A wide variety of geometries were included in the measurements, including propagation through single trees, lines of trees, and dense woodland. The vegetation density and structure was characterised by computerised analysis of hemispherical-aperture photographs of the canopy, together with measurements of tree spacing, heights and leaf dimensions. A variety of antenna beamwidths, heights, and angular geometries were measured. Narrowband measurements were made between 2 and 18 GHz (at 0.5 GHz intervals) and wideband measurements (up to 120 MHz bandwidth) were made at 1.3, 2.2, 11.2, 37.5 and 61.5 GHz. The wideband measurements were made to inform the analysis process (for example, to identify multipath components). Several case studies of the wideband data have been performed. The model is ideally suited to micro- and picocellular radio service planning, and with the aid of databases of forest dimensions, locations and tree types, the model may be used on a macrocellular scale.

10b. Abstract classification: UL	

This page is intentionally blank